1-2022

Adipose-derived stromal vascular fraction therapy improves age-related adrenergic mediated microvascular dysfunction and increases revascularization potential following injury.

Gabrielle Brown
University of Louisville

ADIPOSE-DERIVED STROMAL VASCULAR FRACTION THERAPY IMPROVES AGE-RELATED ADRENERGIC MEDIATED MICROVASCULAR DYSFUNCTION AND INCREASES REVASCULARIZATION POTENTIAL FOLLOWING INJURY

By

Gabrielle Brown
B.A., Carson-Newman University, 2016
M.S., University of Louisville, 2019

A Dissertation
Submitted to the Faculty of the
School of Medicine of the University of Louisville
in Partial Fulfillment of the Requirements
for the Degree of

Doctor of Philosophy
in Physiology and Biophysics

Department of Physiology
University of Louisville
Louisville, Kentucky

May 2022

ADIPOSE-DERIVED STROMAL VASCULAR FRACTION THERAPY IMPROVES AGE-RELATED ADRENERGIC MEDIATED MICROVASCULAR DYSFUNCTION AND INCREASES REVASCULARIZATION POTENTIAL FOLLOWING INJURY

By

Gabrielle Brown

Dissertation Approved on:

April 12, 2022

By the following Dissertation Committee:

_____

Thesis Chair - Dr. Amanda Jo LeBlanc

_____

Committee Member - Dr. Dale Schuschke

_____

Committee Member - Dr. Claudio Maldonado

_____

Committee Member - Dr. Cynthia Metz

_____

Committee Member - Dr. Kyung Hong

DEDICATION

To all aspiring thinkers and doers:

astra inclinant, sed non obligant - the stars incline us, they do not bind us.

ACKNOWLEDGEMENTS

I would like to begin by thanking all those who have helped and guided me along the way. To my mentors at Carson-Newman University, Drs. Patsy Boyce, Matthew Wilkerson, and Stephen Wright, you all contributed to me finding my career path and encouraged me to pursue it unshakably. To my dissertation committee at the University of Louisville, Drs. Dale Schuschke, Claudio Maldonado, Cynthia Metz, and Kyung Hong, beyond being exceptional educators in the classroom you all have provided guidance in my research and training as a future educator. In the coming years as I step into the classroom, I hope to embody you all as esteemed educators. To my mentor and dissertation chair, Dr. Amanda J. LeBlanc, thank you for welcoming me into your lab and under your guidance five years ago. I will always cherish the time I have spent in your lab and all the things I have learned.

Not only do I have my mentor to thank but all of those with whom I have worked closely with and that I call dear friends: Natia Kelm, Fangping Yuan, Jason Beare, Evan Tracy, Nolan Boyd, and Kelly Fredericksen. Thank you all for your continuing support and for always willing to lend a hand.

To my family, thank you to my mom and my dad. Thank you for teaching me to chase my dreams. Thank you for helping me chase my dreams. None of this would be possible without your love and support so thank you. Finally, thank you to my husband,

Brandon S. Brown. You have been my solid ground since high school. Through all the challenges in life you have always been by my side lending a hand to hold. Thank you for being my greatest fan.

ABSTRACT

ADIPOSE-DERIVED STROMAL VASCULAR FRACTION THERAPY IMPROVES AGE-RELATED ADRENERGIC MEDIATED MICROVASCULAR DYSFUNCTION AND INCREASES REVASCULARIZATION POTENTIAL FOLLOWING INJURY

Gabrielle Brown

May 14, 2022

The role of the microcirculation is to balance blood flow and oxygen delivery to meet local metabolic and oxygen demands. With advancing age, the health of the endothelium declines leading to improper augmentation of the microcirculation; decreasing vasoreactivity and angiogenic potential which can further increase the risk of ischemia. The multiple contributing factors that drive the decline in endothelial health with age make traditional pharmacological interventions challenging whereas cell-based therapies can exert multifactorial gains. Adipose-derived stromal vascular fraction (SVF) is an emerging therapeutic for its easily accessible, autologous, anti-inflammatory, and angiogenic properties. It is a heterogenous population comprised of leukocyte and vascular cell populations as well as a small population of mesenchymal stem cells. Coronary perfusion and isolated coronary microvessels from young, old, and old treated with young SVF, female Fisher-344 rats were examined for health and functionality to beta-adrenergic receptor agonists (β-AR). Advancing age decreases coronary perfusion and vasoreactivity to β1-AR agonist norepinephrine (NE). A one-time tail vein injection

of 10 million SVF cells 4 weeks prior reversed the age-related impairment in coronary microvascular dysfunction. Furthermore, isolated coronary microvessels from young, old, and old treated with SVF rats were examined for age- and SVF-related alterations in β1-AR cell signaling. Advancing age reduced the expression of β1-ARs on coronary microvessels and increased the expression of vasodilatory inhibitors, GRK2 and Gαi. While SVF fully restored the β1-AR population it only marginally mitigated the inhibitor expression back to young control levels. Advancing age altered the cellular composition of SVF promoting a more pro-inflammatory phenotype with increased M1 macrophages and various types of T cells with a reduced mesenchymal stem cell population. Intravenously injected SVF can disseminate and engraft into the microcirculation of mesenteric windows; connective tissues located along the small intestines. SVF from young donors can significantly increase vascularized area of an aged mesenteric window subjected to a hypoxic-like injury compared to aged SVF which only marginally improves vascular area. Advancing age can drive a decline in the functionality of the microcirculation. SVF therapy offers a promising vascular therapeutic reversing the age-related dysfunction, increasing organ perfusion, and promoting revascularization following injury.

TABLE OF CONTENTS

LIST OF TABLES

LIST OF FIGURES

CHAPTER 1

INTRODUCTION

The cardiovascular system is comprised of the heart and all the blood vessels of the body. The vascular portion of the circulation can be divided into several categories based upon anatomical structure: conducting arteries, resistance arterioles, capillaries, venules and veins. The large conducting arteries such as the aorta and carotids have multiple thick layers consisting of vascular smooth muscle, elastin, and collagen, all contributing to their distensibility property. These components allow the large vessels to dampen the pulse pressure derived from the left ventricle (LV) [1]. The vascular wall of arterioles is primarily composed of smooth muscle cells which allow the vessels to dilate or constrict over a considerable range in response to agonists and antagonists. These vessels range from 20-100 μm in diameter [2, 3]. Capillaries are vessels consisting of a single layer of endothelium and <10 μm in luminal diameter, which facilitate the exchange of gases and metabolites [4]. Arterioles and capillaries are part of the microcirculation (in addition to venules) [5] whose role it is to regulate blood flow to tissues in response to tissue metabolites and neural innervation [6].

Sympathetic Control of the Microcirculation

The myocardium and microcirculation are innervated and respond to norepinephrine (NE), an adrenergic catecholamine released by the sympathetic nervous system. NE initiates its effect by binding to G-protein coupled adrenergic receptors (ARs) resulting in activation of the receptor through conformational change [7]. Families and subcategories of ARs are grouped based upon their structure, associated intracellular proteins, and elicited effect [8]. The expression of ARs varies based upon tissue and in the case of the vasculature, expression can differ with branching order [9]. In the myocardium, there is 4:1 ratio of beta-1 (β1-AR) to beta-2 AR (β2-AR), with minimal expression of the beta-3 AR (β3-AR) [10, 11]. In the vasculature, β2-AR is more abundant in the vascular smooth muscle cells (VSMCs) than on the endothelium of the arterioles. In the coronaries, specifically, the endothelial cells predominantly express β1-ARs while the VSMCs express β1-AR as well as alpha-1 ARs (α1-ARs) [12-14]. As branching order increases, relative expression of β1- and α1-AR decreases whereas β2-, β3-, and alpha-2 (α2-AR) adrenergic receptors increase [9]. While there is some β3-AR expression in the vasculature, expression is minimal but, interestingly, it is found most abundantly in white and brown adipose tissue [15, 16].

The major role of these receptors in the heart is to increase altering inotropy, lusitropy, and chronotropy [17, 18] or to mediate vasorelaxation (β-ARs) or vasoconstriction (α-ARs) via agonism. In the vasculature, all three β-ARs are associated with a stimulatory G-protein (Gs) to activate adenylate cyclase which in turn converts ATP into cyclic AMP (cAMP), leading to activation of protein kinase A to phosphorylate the myosin light chain kinase, resulting in inactivation of the myosin light chain and

inducing vasodilation [19, 20]. The α1-ARs activate a Gq alpha subunit and phospholipase C to hydrolyze phosphatidylinositol 4,5-bisphosphate into diacylglycerol and inositol triphosphate, which in turn activates its receptor in the endoplasmic reticulum to release calcium and induce vasoconstriction. On the other hand, α2-ARs induce vasoconstriction via activation of an inhibitory G-protein (Gαi), thereby inhibiting AC. In healthy vessels, there is a favoring of β-AR mediated vasodilation to α-AR mediated vasoconstriction. The stimulatory proteins of β-ARs that induce vasodilation are the main intracellular second messengers of this signaling cascade, though inhibitory and regulatory proteins are also associated with the β-ARs. Of note, β2- and β3-ARs are functionally distinct from β1-AR by their ability to also deactivate ACs by coupling to a Gαi subunit [8].

Another regulatory protein in the β-AR signaling cascade belongs to a family of proteins called G-protein receptor kinases (GRKs). Upon catecholamine-receptor binding, GRK2 causes phosphorylation of internal tail of the β-AR thereby sterically hindering the Gs protein coupling [21]. In addition, GRK-mediated phosphorylation recruits β-arrestin to the receptor-GRK complex, further causing steric hindrance and desensitization [17]. β-arrestin primes the β-receptor for dynamin-mediated internalization into clathrin-coated endosomes for storage, trafficking to lysosomes for degradation, or eventual recycling to the plasma membrane [22-25]. These pro-desensitization and internalization processes exist in a homeostatic balance with the process of resensitization, where β-AR receptors are dephosphorylated at the plasma membrane or predominantly in the endosome, then trafficked back to the plasma membrane ready to receive agonistic signals and induce vasodilation again [20, 26-29].

Resensitization is mediated by phosphatases, namely protein phosphatase 2A [30]. While adrenergic-mediated vasorelaxation is one mechanism microvessels use to augment blood flow, vasodilation can also be achieved through other adrenergic receptor agonists such as dobutamine [31], or through endothelium-independent mechanisms such as nitric oxide (NO) being produced in response to increased intraluminal flow [32, 33].

New Microvessel Development

The oxygen needs of a tissue are met through the regulation of blood flow, but also through angiogenesis, or growth of new blood vessels, if more blood flow is needed. The formation of new blood vessels stems from hypoxic regions of a given tissue generating hypoxia inducing factor-α, followed by local endothelial cells producing vascular endothelial growth factor (VEGF) and plasma derived growth factor (PDGF) in response. This stimulates the differentiation of an endothelial cell into a tip cell which forms a stalk, ultimately leading to the generation of a capillary sprout from existing vasculature [34]. Not only does this process occur in areas of hypoxia but also in areas of healing following injury. Microvascular regeneration or repair is a multistage process involving progressive changes in microvessel phenotypes and microvascular networks. Importantly, repairs leading to effective perfusion involve not only deriving new microvessels and vessel segments, but the coordinated organization of these elements into a new or existing network that now meets the perfusion, metabolic, and functional needs of the tissue [35-37]. Adaptation of the neovessels in the context of this network re-organization is a dynamic, multi-cell process involving neovessel pruning or remodeling into arterioles, capillaries, or venules [38]. Critically important to the vascularization

outcomes is the establishment of vasoactive regulation of the new microvasculature to enable proper physiological responses to tissue function [39-42].

Microvascular Pathologies and Aging

Pathologies of the vasculature and microvasculature are often complex in nature, leading to loss of physiological homeostatic regulation of patency and adequate perfusion to match tissue metabolic demands. Contributing pathological factors include endothelial dysfunction, oxidative stress, mitochondrial dysfunction, endoplasmic reticular stress, loss of angiogenic potential and vascular density, and greater senescence and apoptosis. In the setting of advanced age, many of the factors listed have already initiated and pushed the tissue environment into a pathophysiological outcome when a remodeling stimulus arises [43]. Aging has long been considered an unmodifiable risk factor for the development of vascular pathologies [44, 45]. The age-related impairment in vascular remodeling is most apparent in the microvascular networks and is caused by a decline in the health of the endothelium [46].

As early as age 40, a decline in endothelial function can develop, with most clinical manifestations apparent around 50 years of age followed by a steep decline in function as age continues to advance [47]. With the world's population of aged individuals ever increasing, peripheral vascular disease (PVD) is a major cause of ischemic injury and mortality [48, 49]. PVD is a broad disease that encompasses large artery atherosclerotic plaque obstructions to non-occlusive microvascular disease (MVD). In the periphery, MVD can lead to organ perfusion/demand mismatch and ultimately organ failure or loss of limb [50, 51]. With advancing age, coronary perfusion is compromised by ~43% which correlates negatively with myocardial flow reserve, all of

which exacerbate coronary microvascular dysfunction (CMD) [52, 53]. To assess the structure and functionality of the coronary microcirculation, a coronary flow reserve (CFR) can be measured and obtained through non-invasive echocardiography testing. CFR is calculated via dobutamine (Dob, β1-AR agonist) or adenosine infusion which increases blood flow (BF) velocity through the left anterior descending (LAD) artery. CFR is calculated as a ratio of LAD velocity during stress (Dob or adenosine) compared to LAD velocity during rest, highlighting the adrenergic ties in CMD [54, 55]. Clinically, CMD is defined as CFR $\leq$ 2.5, endothelial dysfunction with constriction to acetylcholine (Ach), or <20% coronary dilation to nitroglycerin [56]. CMD represents significant societal economic cost burden, similar to that of obstructive disease (~$750,000 vs. ~$1,000,000 lifetime cost burden), driven by repeat angiography, increased anti-ischemic therapy costs and increased hospitalization, thus showcasing the significance of this pathology and need for comprehensive management strategies [57].

Mechanisms of Microvascular Disease

Oxidative Stress. The decline in the health of the vasculature in advancing age occurs through several mechanisms, including increased systemic oxidative stress [58], cellular senescence [59], and inflammation [60], all of which drive endothelial dysfunction and subsequent development of MVD [43, 61]. Oxidative stress is an increase in reactive oxygen species (ROS) which can rapidly combine with NO producing a reactive peroxynitrite [62] and reducing the bioavailability of NO. Furthermore, the expression levels of endothelial nitric oxide synthase decrease as aging progresses [63]. Cellular senescence refers to the limited number of cell divisions one cell can undergo due to genetic and morphological changes [64, 65] which can be brought

about through loss of telomeres, then DNA from repeated cellular divisions [66]. In endothelial cells, cellular senescence can present as decreased endothelial cell proliferation and impaired migration and dysfunction [67] which can be reversed through induction of telomerase [68]. Cellular senescence is also characterized by the senescence-associated secretory phenotype, whereby cells exhibit increased secretion of interleukins, chemokines, growth factors, matrix metalloproteinases, insoluble proteins and extracellular matrix [65]. This leads to a pro-inflammatory state with feedforward mechanisms that further increase oxidative stress.

Inflammation. The term "inflammageing" refers to a pro-inflammatory state associated with aging and is defined by increased blood markers of inflammation without a triggering event, with simultaneous reduction of capacity to launch an appropriate inflammatory response when a triggering event does occur [65, 69]. Inflammageing is a dynamic process occurring with age as each individual cytokine increases at different ages and with different slopes, and can vary greatly by individual [70]. At some unknown point in the aging process, the increases of various cytokines/factors culminate in pathological effects, thereby setting a pathological threshold. This threshold is lowest for individuals 60-80 years old leading to a decline in vascular health. Chronic inflammation has been shown to drive cellular senescence and increased apoptosis [71], decreasing endothelial cell proliferation [72] which can lead to diminished tissue repair following an injury [73, 74]. Specifically, normal aging-related increases include: interleukins (IL), IL-1, IL-6, IL-8, IL-13, IL-15, IL-18, C-reactive protein, interferon α and β, transforming growth factor β (TGFβ), tumor necrosis factor α (TNFα), monocyte chemoattractant protein-1 (MCP-1), along with decreases in VEGF and IL-2 [65, 75-81]. The factors

described above are part of the multifaceted pathologies of age-related generators of endothelial dysfunction.

Endothelial Dysfunction. Age-related endothelial dysfunction can impact the health of the microvasculature and regulation of blood flow through feed forwards mechanism involving adrenergic receptor desensitization and impairments in revascularization following injury. Aging leads to an overload of catecholamines released from the sympathetic neurohormonal system; while initially protective against a declining cardiac output, excess catecholamines can cause compensatory receptor degradation after prolonged stimulation [82-85]. The β-AR has been shown to decrease in sensitivity and density with age in the myocardium, aorta, mesentery, and coronary vasculatures [39, 86-90]. The catecholamine mediated desensitization can reduce the population of the β1-AR from 77% to 60% in the myocardium [10, 91-93] and results in a shift away from coronary vasodilation and toward vasoconstriction as the α-ARs remain unchanged with age [9, 92, 94-96]. Improper augmentation of blood flow in response to vasodilatory stress can lead to poor perfusion and increased risk of ischemic injury [97, 98]. A therapeutic that restored the beta-receptor sensitivity (**Chapter 2**) and population (**Chapter 3**) back to youthful levels would be a desirable therapy in reducing the ischemic risk of this aged population.

Angiogenic potential. Endothelial health parallels the capacity of a microvascular network to sprout new vessels via angiogenesis and collateralization, the process of forming vessels around ischemic areas. Thus, microvascular growth and network remodeling are crucial for the maintenance of the overall health and functionality of an organ [99]. Advancing age and endothelial dysfunction impairs angiogenesis by

compromising endothelial cell proliferation, inducing endothelial cell apoptosis, dampening cell migration, increasing endothelial cell senescence, and reducing levels of VEGF and PDGF needed for stalk formation [100-103]. This results in the older population being more susceptible to injury and illness [104], while also taking up to twice as long to heal as measured by time for re-epithelization of subcutaneous wounds [105]. Increasing the density of the microcirculation could serve as a preemptive measure to increase blood flow to a tissue decreasing the ischemic risk and enhancement of angiogenesis following an injury would serve as a valuable therapeutic for aged patients (**Chapter 4**). Currently, no drug regimen of this nature exists as aberrant and uncontrolled vascular growth is a hallmark within a tumor environment.

Collateralization, or the growth of new blood vessels to service a tissue because existing networks cannot sufficiently supply blood flow, is significantly reduced after injury in patients >70 years old [106]. Proper collateral vessel development is dependent upon upregulation of PDGF on infiltrating cells [107] and endothelial function. PDGF stimulates maturation of blood vessels by smooth muscle cell and pericyte recruitment [108], as immature, uncoated vessels die in a process called rarefaction, a phenomenon that is increased in aged vascular beds [109, 110]. Plasma samples from healthy individuals showed that there is a reduction in basal levels of PDGF as early as 25 years of age [111]. Taken together, those of advanced age experience endothelial dysfunction which increases the risk of ischemic injury, exacerbated by reduced capacity to revascularize the ischemic area, and once ischemia and cell death occur there is aberrant repair. However, the rate of age-related deterioration can differ substantially across sub-populations and individuals [112]. This leads to a question for future consideration: do

specific aging-related changes explain why some sub-populations are more prone to certain CMDs, and can this association be amenable to manipulation in terms of therapeutic targeting?

Post-menopausal Women and Coronary Microvascular Disease

A population at risk for aberrant cardiovascular remodeling are post-menopausal women. Normally with advancing age, ovarian production of estrogen drops by 90%; the conversion of androgens in adipose tissue then becomes the predominant source of estrogen after menopause [113]. Post-menopausal women are at higher risk for CMD compared to their age-matched male counterparts [74]. Furthermore, CMD manifest differently in the sexes. Unlike men who predominately present with large vessel atherosclerosis, as many as 50% of women referred for cardiac evaluation do not have obstructive coronary disease but present with coronary microvascular dysfunction/ischemia [114] representing ~ 90,000 cases per year, a lifetime cost burden of $1 million, and up to an 8% 5-year mortality rate [57, 115]. Women presenting with CMD show signs of heart failure with preserved ejection fraction [116]. This unique presentation of microvascular mediated heart failure is also common in oophorectomized young women, suggesting that estrogen plays an important role in the vitality of blood vessel function [117]. Vascular dysfunction in postmenopausal women is prominent in the resistance vessels of the heart [118]. Further, decreased CFR [119] and impaired angiogenesis become apparent when circulating estrogen declines due to decreased VEGF signaling from the estrogen receptor-2 [120]. Given the importance of the microvasculature in tissue health, it is not surprising that compromised or dysfunctional microvessels contribute to many disease conditions. In many instances, microvascular

repair or regeneration to restore microcirculatory health are necessary components to treating the disease. For example, instances of microvascular insufficiency, i.e. situations of reduced perfusion due to low vascular densities and/or compromised vasodynamics, contribute to or cause tissue ischemia, non-healing ulcers, limited tissue metabolism and health, and further complications related to aging [39, 40, 43, 121-125].

Treating Coronary Microvascular Disease

Therefore, therapeutics to improve microvascular function target a tightly controlled multi-cell process, and in the context of advancing age, pathophysiological remodeling has taken hold. Unfortunately, the traditional pharmaceuticals currently available for vascular diseases are targeted at mitigating one aspect of multifactorial pathologies [126]. While helpful in preserving myocardial β-AR sensitivity by reducing the workload of the myocardium, first-generation beta-blockers are non-specific [127] and little is known of their consequence to the vasodilatory function of coronary microvessels [128]. Although nitrates may provide acute relief of symptoms, there is little evidence of reduced major adverse cardiac events or mortality [129, 130]. Further, nitrates cause rebound angina and increase oxidative stress, and are difficult to manage. Despite these limitations, they are still the recommended treatment for CMD focusing on anti-ischemic protection via reduced inotropism and oxygen conservation [131].

Not only are the current treatments aimed at improving vascular function superficial in their therapeutic capacity; targeting the age-related chronic inflammation impairing revascularization following injury are unfavorable as well. Although pharmacologic anti-inflammatories are used clinically, caution is warranted, as a robust increase in inflammatory markers is the first critical step in tissue healing following

injury. However, in older patients, this inflammatory spike is blunted [69]. Current anti-inflammatory pharmacologics have shown no efficiency in improving age-related microvascular endothelial dysfunction [132] and have also been shown to delay wound healing by inhibiting angiogenesis [133]. In an acute setting of MI, nonsteroidal anti-inflammatory agents such as ibuprofen may lead to delayed necrosis yet ultimately yield expanded infarct regions, increased tendency for ventricular rupturing, and overall worse clinical outcome including increased incidents and recurrent myocardial infarction (MI) [134]. As a preemptive measure, hormone replacement therapy has been utilized to stave off the declining effects from a lack of estrogen, but many clinical trials showed little to no vascular benefit and even adverse effects of hormone replacement therapy in aged females [135]. A novel strategy that can holistically treat each facet of CMD pathophysiology by mending the pathologic microvessels themselves, rather than merely treating their symptomatic consequences, is of significant clinical interest which parallels the multi-faceted gains seen in cell-based therapies [126].

Cell-based Therapeutics

Potential Mechanisms. Initially used to treat leukemia in the 1950's, cell-based therapeutics are currently being utilized in 5,000 active clinical trials [136], with 900 focused on treating cardiovascular diseases (according to a search on March 2022 on grants.gov). While stem cell therapies have been around for more than 70 years, the scientific field is still exploring their enigmatic nature. They are thought to act by cellular engraftment into the host tissues and/or delivering paracrine factors that promote angiogenesis and modulate inflammation within the treated tissue [137-143]. The "paracrine hypothesis" suggests stem cells exert much of their beneficial effect on

damaged tissue through the paracrine action of their secretome (i.e. exocytosed contents or vesicles) rather than engraftment of stem cells into damaged tissue [144]. Using cell culture systems that prevent direct contact while allowing exchange of factors in the shared media, it is established that stem cells can exert regenerative, differentiation induction and pro-angiogenic effects via paracrine mechanisms [145, 146]. Exosomes are membrane-bound vesicles ranging from 30-150 nm released from cells that function in a paracrine manner transporting proteins, lipids, RNAs, microRNAs, mitochondria and more between cells [144, 147, 148]. Although the majority of the field has moved to identify the paracrine hypothesis as the prevailing theory for the majority of stem cell mediated vascular regeneration, there is still relevance for the direct mechanism, i.e. engraftment, such as differentiation and direct transfer of cellular contents which should not be wholly discounted.

Ideal Donor. Given the biological complexity intrinsic to microvascular regeneration, repair and tissue vascularization, many cell-based approaches are showing great promise in regenerating or improving microvascular form and function. Here, these cell therapies act mostly in a paracrine factor through secreted factors or exosomes, or through direct cell interactions such as differentiation, or also through multiple cell interactions such as interactions of donor perivascular niche with endothelial cells [148-151]. There is current discussion about which strategy is most appropriate for stem cell therapy, either using allogeneic cells that can be more readily obtained, or autologous cells that better match host biologic and immunologic dynamics. This debate is often referred to as “self or shelf”. If one were to imagine the “ideal stem cell donor candidate”, its properties would include a young person with no prior disease history, healthy

lifestyle habits whose stem cells would be at no risk for causing rejection/immune response, maximum potential for engraftment, survival, and proliferation, as well as maximal and consistent secretion of therapeutic factors. Likewise, the ideal stem cell recipient for most successful therapeutic benefit would be someone with minimal disease progression (preventative care) with limited co-morbidities and healthy lifestyle habits. In reality, patients often have multiple co-morbidities and progressive disease presentation. Similarly, donor stem cells, even from an ideal stem cell donor candidate, can still potentially elicit immune responses [152]. How would one choose the universal stem cell donor that these allogeneic cellular therapeutics are based on?

Allogeneic stem cells are derived from a non-self-donor of the same species. Potentially, allogeneic stem cells could be produced in enormous quantities and readily available on a large pharmaceutical scale for clinical use, i.e. “off the shelf.” Issues of collection, aging, and disease states can be avoided with use of an ideal donor, who may be a young individual without chronic disease history and a healthy lifestyle [153]. The challenges of allogeneic stem cell sources include immune reactions to the human leukocyte antigens on donor cells, infection transmission from donor to patient, and ethical concerns if the cells are isolated from an embryological source [153]. Pivoting to autologous stem cells, their use dismisses the immunological concerns of non-self-tissue and the ethical concerns that may come with use of embryological tissue. There is greatly decreased risk of transmitting infection from donor to recipient. However, autologous stem cell use can be complicated by cell age and disease states that cause cellular dysfunction [154, 155]. Patients with disease caused by gene defects may not receive any benefit via therapy with autologous cells. The vast number of cells necessary to collect

for expansion *ex vivo* makes collection from autologous donors challenging especially in aged or diseased states [153].

Mesenchymal Stem Cells

Due to the challenges presented above, mesenchymal stem cells (MSCs) are a highly sought-after cell source as an allogeneic or autologous vascular therapeutic. MSCs are relatively hypo-immunogenic [156] with approximately half of international clinical trials from 2004-2018 using allogeneic MSCs as their source [157, 158]. These MSCs exhibit a hypo-immunogenic property due to their capacity to be conditional antigen presenting cells in the early phase of an immune response [159, 160] then immunomodulate through secretion of soluble factors [161, 162]. Preclinical and clinical trial evidence shows MSC therapy to have a multifactorial effect in immune modulated reduction in fibrosis, reduction of hypoxia and oxidative stress, and non-pathological extracellular matrix remodeling. In a setting of MI, MSCs have been shown to reduce scar formation and improve cardiac functions as measured by echocardiography [163, 164]. However, there are conflicting results in MSC efficacy due to variable such as autologous vs allogeneic, dose, and route of administration [165]. On the other hand, MSCs have been shown to increase angiogenesis to further reduce hypoxia and hypoxia-induced oxidative stress [166-168]. A pre-clinical study utilizing a mouse model of MI showed that administration of isogenic MSCs 3-hours post-ischemia resulted in a reduced infarct size, improved LV function, and increased capillary density 4-weeks later [169]. These results were corroborated in a similar study but at a 12-week-endpoint [170].

Initially, the therapeutic mechanism behind some of the gains seen following MSC therapy was due to their differentiation potential, as MSCs can differentiate beyond

their biological blood/bone niche into various cells such as hepatocytes, epithelial cells, or neural cells generated by co-culturing with cytokines during *in vitro* expansion for cell therapy applications [171-173]. However, engraftment and direct differentiation does not always lead to recovery of cardiovascular function. For instance, amnion-derived MSCs can differentiate to cardiomyocyte and endothelial-like cells in a rat model of heart failure, but this came without recovery of cardiac function or reduction in fibrosis [174]. The lack of long-term cell retention, low efficacy, and laborious task of harvest and culture of bone marrow-derived cells led to the use of other sources of cell-based therapies notably adipose-derived stromal vascular fractions (SVF).

Adipose-derived Stromal Vascular Fraction as a Therapeutic Candidate

SVF can be harvested from lipo-aspirate utilizing mechanical or enzymatic digestion of the biological matrix [175]. Recently, medical equipment has been designed and developed that perform this isolation in the operating suite [176]. With the ability to leverage a real-time point-of-care therapeutic approach, specifically through ease of isolation and the availability of autologous sources, SVF has become an ideal candidate in vascular therapeutics [177, 178]. The isolation of adipose stromal cells with multi-lineage differentiation potential was first reported in the peer-reviewed literature in 2001 [179]. In recent years, the use of SVF has emerged as an alternative therapeutic strategy with clinical trials for arthritis, stroke, pulmonary disease, inflammatory bowel, and ischemic cardiomyopathy [180-183]. Further, SVF's use in clinical trials aimed at vascular therapies and vascular regeneration is growing exponentially [184].

SVF is inherently a heterogeneous cell population comprised of mostly endothelial cells, smooth muscle cells, pericytes, fibroblasts, hematopoietic cells such as

macrophages, B cells, and T cells, natural killer, and dendritic cells, and a small number of MSCs [176, 185]. These various cell types are theorized to be an optimal milieu of environmental cues to stimulate SVF engraftment or release of paracrine factors within a tissue to enhance vascular function [186-188]. Further, the benefit of multiple anatomical locations for harvesting and yielding more cell populations gives adipose tissue a greater autologous benefit. Bone marrow-MSCs were initially hailed as the superior autologous cell source to treat MI because of their differentiation potential [171, 172], but recent studies have shown equal efficacy of adipose-derived SVF in improving cardiac function after MI and *in vitro* induction into cardiomyocyte-like-cells, promoting angiogenesis and reducing inflammation [189-195]. This greater efficacy was shown to be in part due to SVF having greater cytokine production, secreting anti-inflammatory and angiogenic growth factors [196-199]. Continuously, a single administration of SVF has been shown to persist as far out as 8 weeks [200], and a single intravenous (i.v.) administration also results in a wide biodistribution [42]. Interestingly, SVF cells can incorporate into the vascular wall long-term [42] and are associated with normalization of inflamed large vessels [201]. The significant potential of microvascular cell-based therapies is being realized in ongoing and recently completed clinical trials, building on current levels of understanding and highlighting future directions for investigation.

Despite these benefits of cell-based therapies, there are few studies conducted using advanced age as the model of pathology. The studies presented in this dissertation describe the use a female rat model of advanced age to understand how aging alters microvascular function (**Chapter 2-3**) and vascular growth (**Chapter 4**). While these clinical trials have shown beneficial effects of SVF administration, to date it is not

approved by the Food and Drug Administration due to questions regarding therapeutic mechanism along with treatment timing, cell dose, and duration. Regardless of the growing number of studies proving SVF's therapeutic efficacy in promoting healing as described above, there is a gap in understanding SVF's therapeutic contribution to an aging vasculature. There is also a need to better understand how SVF cells spatially and temporally contribute to neovascularization and blood flow within a vascular bed. The ultimate goal is to deliver cells to influence and promote microvascular growth and function. These intriguing questions discussed above frame the context of the studies conducted in this dissertation.

The overall hypothesis of this proposal is that advancing age impairs vascular function by reducing vasodilatory sensitivity and decreasing angiogenesis; both of which are improved following SVF therapy. The knowledge of how age affects the cardiovascular system is ever growing but the anatomic limitations of the microvasculature have made examining it in situ/in vivo a challenge. Additionally, this faction of the cardiovascular system is often overlooked in studies examining SVF's efficacy as a therapeutic. Here, we utilize an aged rat model in combination with adipose-derived SVF therapy to examine the microvascular reactivity effects in the coronary microcirculation, as well as the angiogenic and incorporation potential of SVF in the mesenteric microcirculation for the reasons detailed above. The goals of this project were the following:

1. **To determine if there is an age-related impairment in coronary microvascular vasodilation that can be reversed with SVF therapy (Chapter 2).** Coronary microvascular function in young (3 mo), old (24 mo),

and old treated with a 1-time tail vein injection of 10 million SVF cells (O+SVF, 24 mo) female Fisher 344 rats was assessed using echocardiography, pressure-volume loops, and isolated coronary microvascular preps. The impact of age and SVF therapy on microvascular health and subsequent impairment in left ventricular function was measured by pressure-volume loops and blood flow through the LAD during rest and stress trial (coronary flow reserve, CFR). Individual isolated and pressurized coronary microvessels were used to determine sensitivity to beta-adrenergic agonists and antagonists.

2. **To determine where in the intracellular beta-adrenergic signaling cascade age-related impairment and SVF-related improvement occurs (Chapter 3).** Coronary microvascular function in young (3 mo), old (24 mo), and old treated with a 1-time tail vein injection of 10 million SVF cells (O+SVF, 24 mo) female Fisher 344 rats was assessed using isolated coronary microvessels subjected to immunofluorescence, pressure myography, and Next Gen RNA sequencing. Multiple proteins involved in the beta-adrenergic mediated signaling cascade were probed for expression, functionality in contributing to vasodilation, and transcriptional changes in response to age or SVF therapy.
3. **To determine the effect of donor age on SVF's angiogenic potential in an aged and injured vascular bed (Chapter 4).** The cellular populations of SVF were examined for changes due to donor age in female Fisher 344 rats. Mesenteric windows from old (24 mo) female Fisher 344 rats were examined for SVF integration following i.v. injection with and without exteriorization

injury. The administered SVF was from young (4-9 mo) or old (24 mo) donors to examine age-related changes to angiogenic potential in revascularization. The T cell population was isolated or depleted from SVF to determine if T cells are a main cell type needed for promoting revascularization following injury and responsible for SVF's angiogenic gain.

Much of this chapter is from the published works referenced as follows:

Tracy, E. P., G. Rowe, and A.J. LeBlanc, *Cardiac Tissue Remodeling in Healthy Aging: The Road to Pathology.* Am J Physiol Cell Physiol, 2020.

Tracy, E.P., et al., *Aging Induced Impairment of Vascular Function - Mitochondrial Redox Contributions and Physiological/Clinical Implications.* Antioxid Redox Signal, 2021.

Tracy, E.P., et al., *State of the Field: Cellular and Exosomal Therapeutic Approaches in Vascular Regeneration.* Am J Physiol Heart Circ Physiol, 2022

CHAPTER 2

ENHANCED BETA-1 ADRENERGIC RECEPTOR RESPONSIVENESS IN CORONARY ARTERIOLES FOLLOWING INTRAVENOUS STROMAL VASCULAR FRACTION THERAPY IN AGED RATS

Overview

Our past study showed that a single tail vein injection of adipose-derived stromal vascular fraction (SVF) into old rats was associated with improved dobutamine-mediated coronary flow reserve. We hypothesize that intravenous (i.v) injection of SVF improves coronary microvascular function in aged rats via alterations in beta adrenergic microvascular signaling. Female Fischer-344 rats aged young (3 months, n=32) and old (24 months, n=30) were utilized, along with two cell therapies i.v. injected in old rats four weeks prior to sacrifice: $1x10^7$ green fluorescent protein (GFP+) SVF cells (O+SVF, n=21), and $5x10^6$ GFP+ bone-marrow mesenchymal stromal cells (O+BM, n=6), both harvested from young donors. Cardiac ultrasound and pressure-volume measurements were obtained, and coronary arterioles were isolated from each group for microvessel reactivity studies and immunofluorescence staining. Coronary flow reserve decreased with advancing age, but this effect was rescued by the SVF treatment in the O+SVF group. Echocardiography showed an age-related diastolic dysfunction that was improved with SVF to a greater extent than with BM treatment. Coronary arterioles isolated from

SVF-treated rats showed amelioration of the age-related decrease in vasodilation to a non-selective β-AR agonist. I.v. injected SVF cells improved β-adrenergic receptor dependent coronary flow and microvascular function in a model of advanced age.

This chapter is from the published work referenced as follows:

Rowe, G., et al., *Enhanced beta-1 adrenergic receptor responsiveness in coronary arterioles following intravenous stromal vascular fraction therapy in aged rats.* Aging (Albany NY), 2019. **11**(13): p. 4561-4578.

Introduction

Coronary perfusion, reflective of coronary vascular function, is compromised by as much as 43% in advanced age [52] and can contribute to the prevalence of cardiovascular diseases (CVDs) such as heart failure (HF) and coronary microvascular disease (CMD). There are several neurohormonal mechanisms that are activated in order to maintain resting cardiac output (CO) in aging and HF, including sympathetic overdrive [83]. As a result of this overactivation, a desensitization/downregulation of cardiac β-adrenergic receptors (β-AR) occurs over time which leads to decreased cardiac contractility and inotropic reserve [202, 203]. This age-related decrease in catecholamine-responsiveness in the elderly, as well as a decrease in β-AR vasorelaxation in both animals and humans [94, 204, 205], results in a shift away from coronary vasodilation and toward vasoconstriction [94].

In a healthy human heart, there is a 4:1 ratio of β1:β2-AR, with minimal expression of β3-AR [10, 11]. All three β-ARs are associated with the stimulatory G protein (Gs) activation and can have both stimulatory and inhibitory effects on the heart by altering inotropy, lusitropy, and chronotropy [17, 18]. While β1-AR is present in all cardiomyocytes, β2-AR is more abundant in endothelial cells and vascular smooth muscle cells (VSMC) throughout the body [13, 14], while β3-AR is primarily expressed in white and brown adipose tissue [15, 16]. Small coronary resistance arterioles, which determine appropriate increases in vascular blood flow (BF) and can lead to CMD when dysfunctional, exhibit a predominance of β2-AR [12]. Regardless, an age-associated decrease in β-AR sensitivity and density, which is consistent across the species, has been shown in cardiac muscle [87] and has mostly been attributed to a downregulation of β1-

AR [206]. However, it is unknown if β1- and β2-AR signaling in coronary microvessels is altered with age. Since β-AR signaling is abnormal in failing hearts as well as in aged hearts, this pathway is a desirable diagnostic and therapeutic target.

Cell therapies such as mesenchymal stem/stromal cells (MSCs) are thought to act by delivering paracrine factors that promote angiogenesis and modulate inflammation within the treated tissue [137-140]. Our laboratory has described how an intravenous (i.v.) injection of adipose-derived stromal vascular fraction (SVF) was associated with improved dobutamine-mediated coronary flow reserve (CFR) and diastolic function in aged rats in vivo compared to old control rats and those injected with an endothelial cell population [42]. Even though we identified incorporated green fluorescent protein (GFP+) SVF cells in the cardiac and coronary vascular tissue upon explant, isolated coronary vasoreactivity to endothelin, bradykinin, and increases in pressure did not reveal group differences in this study, which led us to explore changes in adrenergic-specific signaling following SVF injection. Previously, MSCs have been shown to influence adrenergic signaling in two models. In 2006, intramyocardial injection of bone-marrow MSC (BM-MSC) led to β-AR upregulation and improved cardiac contractility in a model of non-ischemic HF in rabbits [207], while a more recent study described the rescue of cardiac function under adrenergic challenge in diabetic rats after i.v. injection of BM-MSCs with concomitant restoration of β1-AR mRNA expression in the left ventricle (LV) [208]. However, it is not known if either BM-MSC or SVF cell therapies restore adrenergic signaling in the heart and coronary microvasculature in a model of advanced age, and if this occurs through similar mechanisms.

Therefore, based on the gaps in conclusions from the aforementioned studies, our purpose was to determine if SVF and/or BM-MSC improve beta-adrenergic signaling in the aged heart. Our hypothesis was that cell therapy (either BM-MSC or SVF) will improve β1- and β2-AR-mediated vasodilation in coronary arterioles and this will be associated with improved CFR in aged rats. We tested this hypothesis by comparing young, old, and old rats injected intravenously with either BM-MSC or SVF and evaluated cardiac and microvascular function using ultrasound, pressure-volume (PV) loops, pressure myography, and immunofluorescence focused on adrenergic-specific signaling.

Materials and Methods

Animal model, groups, and endpoint procedures.

All animal surgeries were performed in accordance with protocols approved by the University of Louisville Institutional Animal Care and Use Committee and the NIH *Guide for the Care and Use of Laboratory Animals* [209]. Young (3 mo) and old (22 mo) female Fischer-344 rats (Harlan Laboratories, Indianapolis, IN, USA and National Institute on Aging, Bethesda, MA, USA, respectively) were housed in groups with free access to food and water and were maintained on regular 12-hour light/dark cycles. Rats were acclimated to facility conditions for a minimum of one week prior to endpoint procedures. The remaining old rats were divided randomly into two cell injection groups: old + GFP+ bone marrow stem cells (O+BM) and old + GFP+ SVF cells (O+SVF). Four weeks later, old cell-injected rats were 23-24 months of age at endpoint. All animals were utilized for PV loop data acquisition as well as isolated coronary arteriole experiments. A

subset of animals from each group were utilized for echocardiography and immunofluorescence. Animals were anesthetized deeply with a ketamine/xylazine injection before euthanasia via removal of the heart.

Rat bone marrow cell isolation and culture.

BM-MSC were isolated from femur and tibia bones of young female and male Fischer-344 GFP+ rats (colony maintained in house) using a protocol modified from Barbash et al. [210] and Lennon et al. [211]. Briefly, 3-4 donor animals were anesthetized deeply with 5% inhaled isoflurane balanced with 1 L/min O_2 and then euthanized via removal of the heart. Using sterile technique, femur and tibia bones were exposed and disarticulated at the associated joints, and extraneous muscle and tissue removed leaving only the bones of interest. Care was taken to obtain whole intact bones from each animal. After removal of muscle and connective tissue, bones were stored in DMEM + Penicillin/Streptomycin on ice. Bone cutters were used to remove the proximal and distal end from each bone just below the marrow cavity. Whole bone marrow was then flushed with 10mL sterile Complete Medium (DMEM + 15% fetal bovine serum + Glutamine + Penicillin/Streptomycin) per bone using a 10 mL syringe and 27g needle; bone marrow was collected into a sterile 70 μm filter screen fitted onto a sterile 50 mL conical tube. After filtration, cells were centrifuged at 1400 rpm for 8 min at room temperature and counted with a hemocytometer. Freshly isolated BM-MSC were cultured with an initial seeding density of $7.5x10^7$ cells per T75 culture flask in 10 mL Complete Medium; flasks were placed in a 37°C incubator with 5% CO_2 for 3 days, after which medium was changed every 2-3 days until 95% confluence. Cells were then treated with 0.25% trypsin at 37°C for 2 minutes and passaged into T75 culture flasks ($1.5x10^6$ cells/flask). Media

was changed every 2-3 days and flasks passaged at 95% confluence; this method was repeated until cells were harvested at passage 3 or 4 for infusion into O+BM rats.

SVF isolation.

SVF cells were isolated from a GFP+ Fischer-344 rat colony (maintained in house) as previously described [41, 42]. Briefly, ovarian or epididymal fat pads from young female and male rats respectively (3-6 mo) were harvested, washed, finely minced, and digested in 0.75 mg/mL Type I collagenase solution (Vitacyte). Buoyant adipocytes were removed via centrifugation, and the SVF cell pellet resuspended in 0.1% BSA-PBS as previously described [41, 42]. Freshly isolated SVF cells were then prepared for injection into O+SVF rats.

Cell injections.

BM-MSC populations were trypsinized. BM-MSC and SVF isolate were then washed and filtered separately through a 20 μm screen to eliminate large cell and tissue aggregates. Cell count was determined with a hemocytometer, and GFP+ fluorescence of the cell population confirmed via fluorescence microscopy prior to injection. Old female rats were randomly divided into the two cell injection groups, then injected intravenously with either 10^7 GFP+ SVF cells or $5x10^6$ GFP+ BM-MSC in 1 mL Lactated Ringer's solution (warmed to 37°C) via the tail vein.

Echocardiography.

Systolic and diastolic parameters.

LV systolic and diastolic function were evaluated by transthoracic echocardiography using a Vevo 3100 with MS250D transducer with a frequency of 13-24

MHz as previously described [42] (FUJIFILM VisualSonics Inc., Toronto, Ontario, Canada). Briefly, rats were anesthetized and maintained with isoflurane (induction chamber at 5% with 1.5–2.0 L/min O2 flow followed by 1.5% with 1.5 L/min O2 flow). Rats were then placed in a supine position and the thorax was shaved. Body temperature was maintained at 37–38°C, and heart rate was monitored using Vevo Imaging Station. Variables that represent diastolic function - IVRT, E/A and E/e' ratios - were obtained during resting condition utilizing an apical four chamber view with conventional pulsed wave Doppler and tissue Doppler. E/A ratio was calculated from the peak velocity flow in early diastole (the E wave) to peak velocity flow in late diastole caused by atrial contraction (the A wave) during resting conditions [42]. Results from five cardiac cycles during expiration were averaged together and used for between-group and within-group comparisons.

Coronary flow reserve measurements.

In addition to the standard echocardiographic imaging of cardiac function, a modified parasternal short-axis projection was used for Doppler recording of the LAD during rest while animals were anesthetized with 1.5% inhaled isoflurane, and again during two cardiac stress states induced via dobutamine (Dob, 20 μg/kg/min) and adenosine (140 μg/kg/min) in a random order. The tail vein was cannulated with a 27-gauge butterfly needle for drug administration. Dob and adenosine were infused for a maximum of 5 minutes using an automated perfusion pump (KD Scientific, Holliston, MA), with a recovery period between drugs to allow the heart to return to baseline LAD velocity and heart rate. LAD BF velocity pre-stress and during the stress challenge were

averaged from three consecutive cardiac cycles and CFR was calculated as the ratio of the mean peak LAD BF velocity values during each stress condition and rest [212].

Hemodynamic measurements.

Rats were anesthetized with an intraperitoneal injection of ketamine (50 mg/kg) / xylazine (12.5 mg/kg) / acepromazine (2.0 mg/kg) mix. Conductance readings were made for ~35–60 min prior to harvesting heart tissue. Briefly, the rat was placed in a supine position on a 37 °C pad, tracheotomized and connected to a ventilator to control breathing. The right carotid artery was isolated using silk sutures. The cranial aspect of the carotid artery was ligated, and a microsurgical clip was placed on the proximal carotid artery for hemostasis. The chest cavity was opened between the right 5th and 6th intercostal area and retracted to expose the inferior vena cava (IVC) near the diaphragm; saline-soaked silk suture was placed under the IVC and left for later use during occlusion measurements. An arteriotomy was performed with microsurgical scissors, and a 1.9 F PV 6.00 mm conductance catheter (Transonic, London, ON, Canada) calibrated to current atmospheric pressure was introduced into the carotid artery. The catheter was then secured into the carotid artery with sutures and advanced retrograde across the aortic valve into the LV; continuous hemodynamic monitoring insured proper catheter placement in the LV. PV loops were recorded in the steady state with the ventilator off for 8-10 seconds to reduce loop variability. The ventilator was turned on immediately following baseline recording. After 2-3 minutes of recovery, the ventilator was again turned off and the silk suture under the IVC was gently lifted to induce occlusion of the IVC. Immediately following occlusion recording, catheter was removed, and the animal

was humanely euthanized via vital organ removal. Data recording and analyses of both baseline and occluded PV loops were performed using LabChart Pro software (ADInstruments, Colorado Springs, CO).

Subepicardial arteriole isolation experiments.

The heart was removed from each animal and coronary arterioles from the LAD artery distribution isolated and transferred to a vessel chamber. Arterioles were then cannulated on both ends, pressurized to 45 mmHg [213], and allowed to develop spontaneous tone (> 20% constriction from initial diameter) [42].

The following experiments were randomized in each vessel. Concentration-response curves to isoproterenol (non-specific β-AR agonist, Sigma-Aldrich I6504), dobutamine (primarily a β1-receptor agonist with lower β2 activity, Sigma-Aldrich D0676), NE (α1-, α2-, β1-, and β2-AR agonist, Sigma-Aldrich A9512), and salbutamol (β2-AR agonist, Sigma-Aldrich S8260). Following the agonist responses, some vessels were incubated in the β1-receptor antagonist CPG20712A (Sigma-Aldrich C231) prior to a second concentration-response curve of isoproterenol or NE. Other vessels were incubated in the β2-receptor antagonist ICI118551 (Sigma-Aldrich I127) prior to a second concentration-response curve of isoproterenol. A third subset of vessels received both CPG20712A and ICI118551 simultaneously prior to an additional concentration-response curve of isoproterenol. Upon completion of all response curves, vessels were washed 2x15 min in Ca2+-free physiological salt solution followed by a single dose of sodium nitroprusside (1e-^{4} [M]). Maximum diameter was determined as the largest

diameter achieved throughout the experiment. Tone was calculated as 1-(initial diameter/maximum diameter) x 100.

Immunofluorescence staining.

Coronary arterioles (750 μm-1 mm in length, < 250 μm in diameter) were isolated and fixed in 2% paraformaldehyde in 48- well plates for 1-hour, washed 2x10 min in DCF-PBS, and placed in 0.5% Triton-X/DCF-PBS for 20 minutes at room temperature (RT). After treating with blocking solution for 1 hour at RT, arterioles were incubated in a primary β1-AR antibody (Abcam, ab3442, 1:150) or β2-AR (Abcam, ab182136, 1:100) solution in blocking solution at 4°C overnight with gentle rocking. Normal rabbit serum replaced primary antibody solution for negative control tissues. A donkey anti-rabbit IgG-Alexa Fluor 594 (Invitrogen, A21207, 1:300) blocking solution was added to the tissues and incubated for 1-hour at RT. Nuclei were stained with Dapi. Tissues were placed on slides with anti-fade mounting media, coverslip added, and imaged using a Nikon ECLIPSE confocal microscope system (Nikon, Tokyo, Japan) with a 405 and 562 nm laser. Images were captured at 1024X1024 pixel density and 2 μm Z-step (minimum 10 stacks) with a 40X oil immersion objective. Immunofluorescence intensity of β1- or β2-AR in the region of interest (ROI) boxes were determined by the Nikon NIS Elements AR Analysis software (Nikon) using 20 μmx100 μm area and at least 8 μm in depth [214]. ROI boxes were placed on the vascular wall overlapping both the endothelial and smooth muscle cell layers but excluding the cardiomyocytes.

Statistical analysis.

Statistical analyses were performed with SigmaPlot 14 (Systat), and the significance level was set at $p \leq 0.05$. Animal characteristics, catecholamine levels, echocardiography and hemodynamic measurements, and immunofluorescence intensity were analyzed using one-way ANOVA followed by Holm-Sidak or Dunn's post hoc tests where appropriate. When normality tests failed, one-way Kruskal-Wallia ANOVAs were performed where appropriate. Concentration-response comparisons for between group differences were analyzed with two-way repeated measures ANOVA. Pre- and post-inhibition data were paired for analysis and inhibition of the concentration-response comparisons for within group differences were analyzed with two-way repeated measures ANOVA. All significant interactions were further investigated using Bonferroni post hoc testing. Tone acquired pre- and post-inhibition were analyzed using a paired t-test for within group difference. Between the groups, tone acquired pre- or post-inhibition were analyzed using one-way ANOVA. Data are represented as means±SD or SEM as indicated.

Results

Animal characteristics and circulating catecholamines.

To determine if systemic i.v delivery of SVF or BM-MSC affected fundamental animal characteristics and circulating plasma catecholamine levels, we collected gross anatomical measurements and sampled right ventricular blood; these data are presented in **Table 2.1**. All aged groups (OC, O+SVF, and O+BM) exhibited increased body weight (BW), total ventricular weight, and LV weight compared to YC (**Table 2.1**). There is a

trend of increasing higher circulating plasma levels of norepinephrine (NE) and epinephrine (EPI) in OC rats than in YC and O+SVF; although there is not significant differences between groups (**Table 2.1**). The O+BM group has significantly lower NE (0.2±0.03, n=6) and EPI (0.05±0.01, n=6) levels compared to OC (NE 3.32±0.96; EPI 2.12±0.5, n=15) (**Table 2.1**). There was no difference in plasma levels of serotonin (5HT) between the groups. The OC (0.12±0.02, n=15) showed significantly higher dopamine (DA) levels compared to YC (0.04±0.01, n=10) (**Table 2.1**).

Echocardiography and hemodynamic measurements.

Echocardiography.

To determine whether a cell therapy (SVF or BM-MSC) had any effect on cardiac parameters in aged animals compared to control, echocardiography was performed during rest and summarized in **Table 2.2**. OC rats exhibited a slight increase in stroke volume (SV) due to increased LV end systolic and diastolic volumes (LVVs/d) and dimensions (LVDs/d), but ejection fraction (EF) and CO were preserved, however these differences are not statistically significant (**Table 2.2**). The O+SVF (2.58±0.44, n=10) and O+BM (3.32±0.47, n=6) treated groups showed a significant increase in LVDs when compared to OC (2.17±0.33, n=9, $p < 0.05$) but only the SVF treated group had a significant increase in LV mass (500.49±46.39, n=10) when compared to YC (418.92±46.44, n=10) (**Table 2.2**). Both cell treated (O+SVF and O+BM) groups demonstrated a statistical difference when compared to YC in the following parameters: LVDs, LVDd, LVVs, and LVVd (**Table 2.2**). The O+BM group had a significant decrease in EF and fractional

shortening (FS) when compared to YC (**Table 2.2**). Additionally, the O+BM group had significantly reduced SV, EF, and FS compared to OC and O+SVF (**Table 2.2**).

Hemodynamic measurements.

To determine whether a cell therapy (SVF or BM-MSC) had any effect on hemodynamic variables in aged animals compared to control, PV loop experiments were performed and summarized in **Table 2.2**. There were no significant differences regarding a majority of the PV loop measurements. This is likely due to the differential anesthetic effects of ketamine used for the PV loop measurements (ketamine is a known cardiac depressor [215]) vs. isoflurane used during echocardiography. During periods of vena cava occlusion, preload recruitable stroke work (PRSW) was measured as an index of myocardial contractility. The O+BM (569.06±149.59, n=6) group showed a significant loss in PRSW when compared to YC (-2127.74±865.62, n=13) (**Table 2.2**). Notably, there were no differences in PRSW between the O+SVF (-1111.31±305.77, n =12) treated group and YC (-2127.74±865.62, n=13).

Coronary flow reserve.

In order to evaluate the ability of the heart to respond to a stressor, Doppler recordings of peak left anterior descending (LAD) artery BF velocity were measured during a Dob or an adenosine infusion (**Fig 2.1 A** and **B**). The OC (1.77±0.4, n=9) group had diminished Dob-induced CFR compared to YC (2.31±0.36, n=10) (**Fig 2.1 A**). Treatment with SVF therapy (O+SVF) significantly improved Dob (2.7±0.68, n=10) and adenosine- (2.6±0.41, n=10) induced CFR when compared to OC (Dob 1.77±0.4; adenosine 1.61±0.26, n=9), achieving levels similar to YC (Dob 2.31±0.36; adenosine 2.08±0.55, n=10) (**Fig 2.1 A** and **B**). Adenosine-induced CFR was significantly lower in

the O+BM (2.27±0.27, n=6) group when compared to O+SVF treated but was still significantly higher than OC (**Fig 2.1 B**).

Diastolic function.

Echocardiographic measures of diastolic function are displayed in **Figure 2.2**, including isovolumic relaxation time (IVRT), E/A ratio – representing the ratio of peak velocity of blood flow from gravity in early diastole (the E wave) to peak velocity flow in late diastole caused by atrial contraction (the A wave) – and E/e' – representing the ratio of mitral peak velocity of early filling (E) to early diastolic mitral annular velocity (e'). All measures showed an age-related deterioration in diastolic function when compared to YC (**Fig 2.2 A-D**). The O+SVF treated rats showed a statistically significant improvement in E/A and E/e' ratios when compared to OC (**Fig 2.2 B C**). The O+BM group was similar to OC in that it had significantly decreased E/A and E/e' ratios as compared to YC, and E/A when compared to O+SVF (**Fig 2.2 B** and **C**). There is a significant increase in the time constant of left ventricular relaxation measured by PV relationship (tau) when comparing OC (19.16±0.83, n=16) and O+BM (19.01±0.74, n=6) to YC (15.61±0.48, n=13) (**Fig 2.2 D**).

Subepicardial arteriole isolation experiments.

Arterioles under 150 μm in luminal diameter from the LAD distribution were dissected and isolated to assess whether cell therapy or adrenergic inhibition altered basic vessel characteristics such as spontaneous tone. Neither age (OC) nor a cell therapy (O+SVF and O+BM) significantly altered the maximum diameter or average spontaneous tone reached (**Table 2.3**). Average tone after incubation with ICI118551, CPG20712A, or

both ICI118551+CPG20712A was not significantly different between the groups or when compared to pre-inhibition (**Table 2.3**). β-AR agonists and antagonists were used to assess if cell therapy altered microvascular reactivity to adrenergic stimuli.

Vasodilation to dobutamine (β1-AR) and salbutamol (β2-AR).

Dobutamine and salbutamol were used to examine if cell therapy alters β1- (dobutamine) or β2-AR (salbutamol) responsiveness; data is represented in **Figures 2.3 A** and **B**. At the highest concentrations (1e-^{6} and 1e-^{5} [M]), vasorelaxation to dobutamine is significantly lower with age (OC) and in the O+BM group when compared to YC. At concentration 1e-^{6} [M], O+SVF (26.96±4.7, n=11) vasorelaxation is significantly higher when compared to O+BM (6.98±2.74, n=6) (**Fig 2.3 A**). There is no difference between the groups at any dose of salbutamol (**Fig 2.3 B**).

Isoproterenol-induced vasodilation (non-selective β-AR agonist).

Isoproterenol alone or combined with a β1- or β2-AR antagonist (or both) was used to examine whether receptor activity pre- and post-inhibition is altered with age, and if receptor activity is restored with cell treatment; this data is summarized in **Figures 2.4 A-D**. The complete concentration response of isoproterenol-induced relaxation in O+BM is significantly lower when compared to O+SVF ($p < 0.05$) (**Fig 2.4 A**). Pre-incubation with ICI118551 (a β2-AR antagonist) revealed no difference between the groups. There is a statistically significant reduction in isoproterenol relaxation after inhibition with ICI118551 when compared to the uninhibited isoproterenol dose response for the YC, O+SVF, and O+BM groups at various doses (^) (**Fig 2.4 B**). Preincubation with CPG20712A (β1-AR antagonist) revealed no difference between the groups (**Fig 2.4 C**), but there was a significant attenuation of the 1e-^{8} [M] response in YC and O+SVF

compared to their isoproterenol response (^). For concentrations 1e-^{7} through 1e-^{4} [M], all four groups showed a significant attenuation in relaxation when compared to their corresponding pre-inhibitor isoproterenol concentration response (^) (**Fig 2.4 C**). **Figure 2.4 D** used both ICI118551 and CPG20712A to show potential β3-AR activity. There was no difference between the groups, and every group showed a significant attenuation in relaxation when compared to the corresponding isoproterenol concentration response (^) (**Fig 2.4 D**).

Norepinephrine-induced vasodilation (β1-, β2-, α1-, α2-AR agonist).

NE and the β1-AR antagonist CPG20712A were used to show vasoreactivity to a circulating catecholamine; data is represented in **Figures 2.5 A** and **B**. NE-induced relaxation is significantly decreased in the OC group compared to YC and O+SVF (**Fig 2.5 A)**. It is notable that there is no difference between YC and the O+SVF groups. When CPG20712A was used to attenuate NE-induced relaxation, there was a significant reduction in relaxation post-inhibition at concentrations 3e-^{7} through 1e-^{4} [M] for YC and O+BM (^) (**Fig 2.5 B**).

Immunofluorescence staining.

To assess changes in populations of β1- or β2-AR with advancing age or cell therapy treatment, immunofluorescence was performed on a subset of microvessels from explanted hearts. Representative images from each group were used to show the fluorescence intensity measured on the endothelial-vascular smooth muscle wall of each microvessel (**Fig 2.6 A**). Quantification of β1- or β2-AR fluorescence is shown in **Figure 2.6 B**. Although not statistically significant, there is a slight decrease in both the β1- and

β2-AR with advancing age. Both cell therapies increased levels of β1-AR compared to OC, while treatment with BM-MSC, but not SVF, increased levels of β2-AR.

Table 2.1

Animal Characteristics	**YC (n=26)**	**OC (n=26)**	**O+SVF (n=20)**	**O+BM (n=6)**
Age (months)	4.24±0.09	24.99±0.17	24.66±0.22	25.42±0.26
Body weight (g) (n)	179.95±3.26 (21)	250.04±4.95 * (24)	246.35±9.84 *	264.8±7.39 * (5)
Total Ventricular weight (mg) (n)	49.61±1.39 (18)	65.62±1.38 * (22)	63.59±0.97 * (18)	68.4±3.34 *
LV weight (mg) (n)	38.97±1.39 (18)	54.55±1.81 * (22)	49.73±2.4 * (18)	53.97±1.18 *
Plasma Catecholamine Levels (ng/mL)	**YC (n=10)**	**OC (n=15)**	**O+SVF (n=5)**	**O+BM (n=6)**
Norepinephrine (NE)	0.5±0.14	3.32±0.96	0.27±0.04	0.20±0.03 #
Epinephrine (Epi) (n)	0.52±0.16	2.12±0.5	0.05±0.01	0.05±0.01 #
Serotonin (5HT) (n)	35.99±12.23	139.39±43.38	69.07±35.9	44.02±15.34
Dopamine (DA) (n)	0.04±0.01	0.13±0.02 *	0.05±0.01	0.07±0.01

Table 2.1: Animal characteristics and plasma catecholamine levels.

Gross anatomical measurements and catecholamine levels were measured and averaged. $p < 0.05$ vs. Young Control (*), vs. Old Control (#), and vs. Old+SVF ($); data are presented as means±SEM (n) and analyzed with one-way ANOVA followed by *post hoc* tests where appropriate.

Table 2.2

Ultrasound Parameter	**YC (n=10)**	**OC (n=9)**	**O+SVF (n=10)**	**O+BM (n=6)**
Heart Rate (BPM)	334±19	342±39	322±21	325±21
LVDs (mm)	1.92±0.2	2.17±0.33	2.58±0.44 * #	3.23±0.47 * # $
LVDd (mm)	4.85±0.34	5.2±0.31	5.49±0.38 *	5.50±0.25 *
LVVs (µL)	11.89±3.26	16.51±5.99	25.74±9.88 *	43.61±14.64 * #
LVVd (µL)	111.48±17.35	130.83±17.9	148.29±23.11 *	148.23±15.73 *
Stroke Volume (µL)	99.58±16.49	114.33±17.26	122.56±17.10 *	104.63±15.49 # $
Ejection Fraction (%)	89.31±2.93	86.16±4.41	85.042±3.86	75.25±6.08 * # $
Fractional Shortening (%)	60.51±3.96	56.99±6.08	56.21±4.65	44.68±5.21 * # $
Cardiac Output (mL/min)	36.31±4.57	38.75±4.54	39.35±5.02	37.37±1.86
LV Mass (mg)	418.92±46.44	460.53±89.22	500.49±46.39 *	498.04±27.31
Hemodynamic Parameter	**YC (n=13)**	**OC (n=16)**	**O+SVF (n=12)**	**O+BM (n=6)**
Heart Rate (BPM)	223±11	175±7	184±9	192±10
Systolic BP (mmHg)	109±5	120±8	98±6	122±10
Diastolic BP (mmHg)	88±4	89±4	79±5	91±4
Cardiac Output (mL/min)	21.83±1.20	18.87±1.39	18.74±1.22	18.00±1.96
ESP (mmHg)	90.64±2.91	96.62±5.65	87.93±3.55	97.15±6.56
EDP (mmHg)	6.33±0.51	7.62±1.03	5.48±0.65	8.38±0.89
ESV (µL)	26.76±3.80	28.13±3.37	27.68±3.91	18.03±2.97
EDV (µL)	114.81±5.77	127.37±5.94	130.76±8.37	103.14±11.28
Stroke Volume (µL)	99.18±5.20	107.38±5.49	102.07±5.27	92.72±6.06
Ea (mmHg/µL)	0.95±0.06	0.95±0.08	0.89±0.06	1.08±0.12
.±dp/dt (mmHg/s)	6817.38±366.47	5818.13±305.96	5808.83±318.09	5466.00±230.07
.-dp/dt (mmHg/s)	-5215.69±314.67	-4227.13±256.39	-4173.17±263.75	-4565.17±205.80
Ejection Fraction (%)	75.91±2.42	75.35±1.87	73.79±2.25	79.59±1.38
Occlusion Parameter	**YC (n=13)**	**OC (n=10)**	**O+SVF (n=12)**	**O+BM (n=6)**
Emax (mmHg/µL)	2.09±0.25	1.73±0.19	1.87±0.24	1.19±0.13
EDPVR slope (mmHg/µL)	2.12±0.39	1.46±0.31	1.06±0.25	3.35±0.67
PRSW slope	104.51±9.38	79.54±3.60	81.13±3.95	78.76±7.59
PRSW intercept	-2127.74±865.62	-305.43±358.75	-1111.31±305.77	569.06±149.59 *

Table 2.2: Summary of cardiac functional parameters during echocardiography and pressure-volume loop recordings.

Data are presented as means±SEM, analyzed with one-way ANOVA followed by post hoc test where appropriate. $p < 0.05$ vs. Young Control (*), vs. Old Control (#), and vs. Old+SVF ($)

Figure 2.1

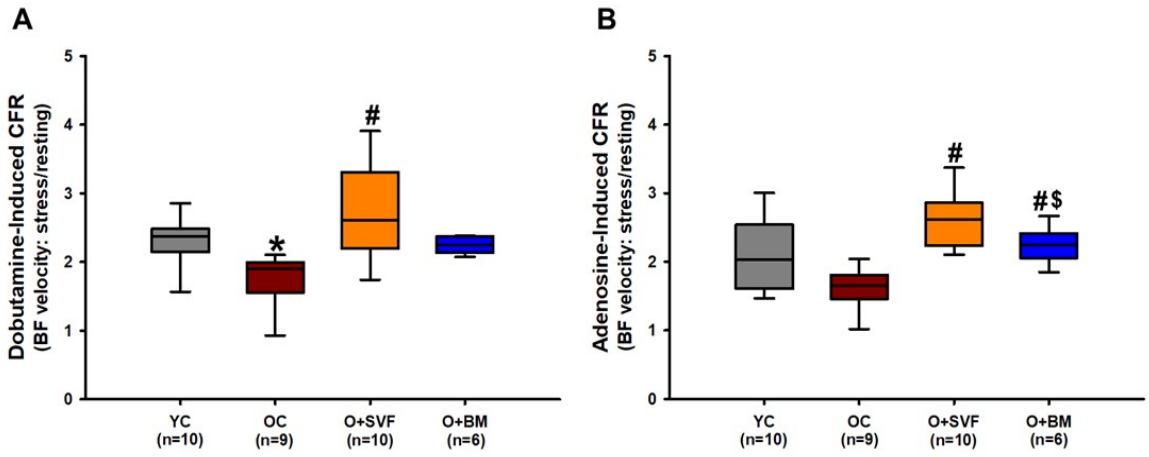

Figure 2.1: Coronary flow reserve using doppler echocardiography in rats.

Stress test was performed on experimental groups using dobutamine (**A**) or adenosine (**B**) and CFR was calculated. O+SVF group exhibited increased CFR vs. OC in both adenosine and dobutamine conditions. $p < 0.05$ vs. Young Control (*), vs. Old Control (#), and vs. Old+ SVF($); Data are presented as means±SDEV, analyzed with one-way Kruskal-Wallis ANOVA followed by *post-hoc* Dunn's (**A**) or with one-way ANOVA followed by Holm-Sidak *post-hoc* analysis (**B**).

Figure 2.2

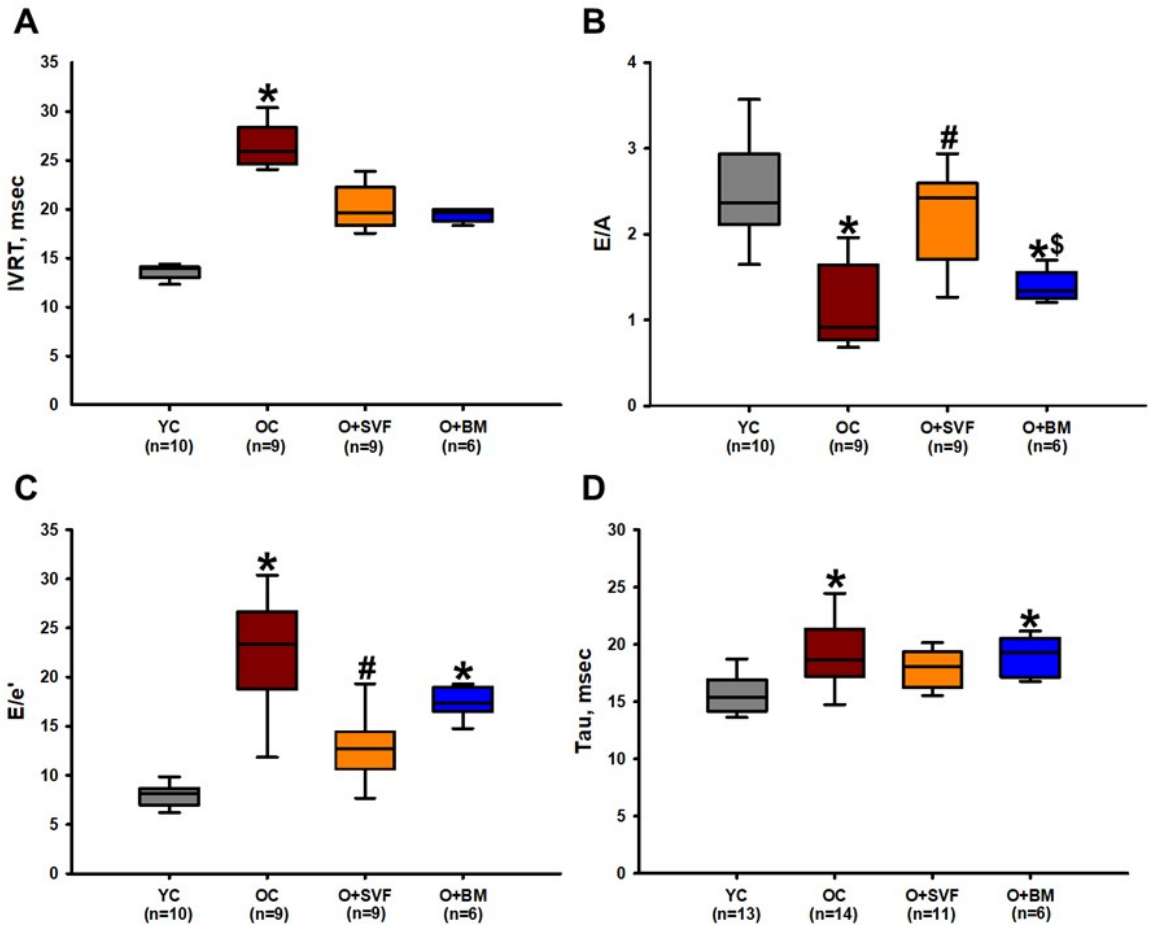

Figure 2.2: Diastolic function assessment using echocardiography and pressure-volume loops.

Compared to YC rats, there was an age-related deterioration in diastolic function as measured echocardiographically by IVRT (**A**), E/A ratio (**B**), E/e' ratio (**C**), and hemodynamically by Tau (**D**). Old rats treated with SVF significantly reversed this dysfunction in measures of E/A ratio (**B**) and E/e' ratio (**C**) compared to OC and normalized diastolic function to YC levels in IVRT (**A**) and Tau (**D**). $p < 0.05$ vs. Young Control (*), vs. Old Control (#), and vs. Old+SVF ($); Data are presented as

means±SDEV, analyzed with one-way Kruskal-Wallis ANOVA followed by *post-hoc* Dunn's (**A,C**) test or one-way ANOVA followed by *post-hoc* Holm-Sidak (**B, D**) test.

Table 2.3

Isolated Vessel Characteristics	YC (n=31)	OC (n=38)	O+SVF (n=32)	O+BM (n=16)
Maximum Diameter	141.1±5.99	144.97±4.61	144.56±4.62	151.19±11.4
Average % Tone	28.77±5.51	29.59±1.19	30.1±1.73	25.87±1.83
Average % Tone after Incubation with ICI118551 (n)	25.43±1.2 (5)	31.05±2.94 (7)	27.04±2.69 (8)	29.45±15.57 (4)
Average % Tone after Incubation with CPG207212A (n)	26.94±2.26 (9)	29.52±1.97 (14)	34.25±3.59 (9)	38.42±4.05 (6)
Average % Tone after Incubation with ICI118551 + CPG207212A (n)	27.86±1.7 (9)	27.24±2.22 (9)	32.78±4.47 (6)	30.78±11.68 (5)

Table 2.3: Isolated vessel characteristics.

Luminal diameters were measured. Tone was calculated as a percent of the maximum diameter for pre- and post-incubation with an inhibitor. $p < 0.05$ vs. Young Control (*), vs. Old Control (#), and vs. Old+SVF ($); data are presented as means±SEM (n) and analyzed with paired t-tests for within group difference while between group difference were analyzed using one-way ANOVA.

Figure 2.3

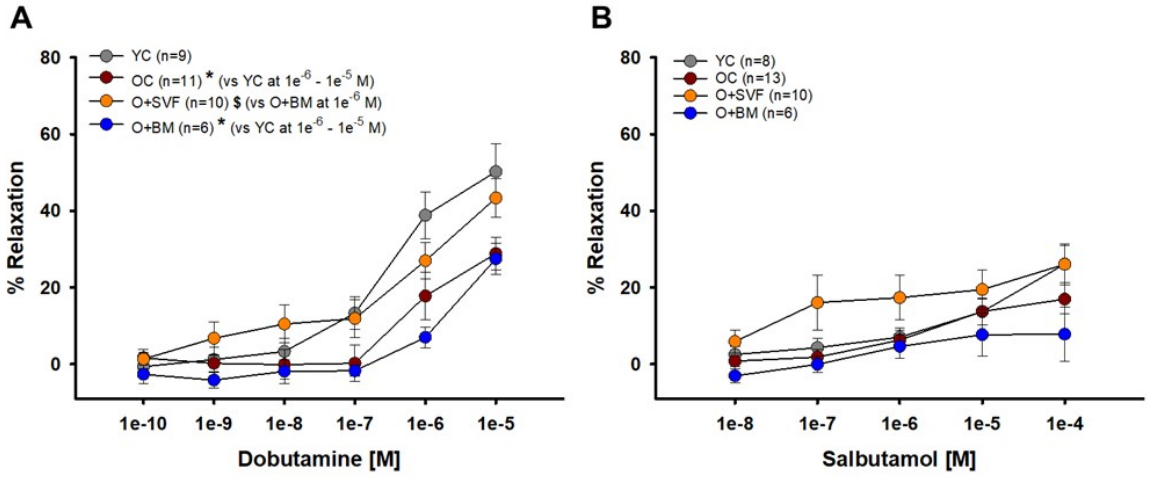

Figure 2.3: Isolated coronary arteriolar vasoreactivity to β1- and β2-AR agonists.

Dobutamine, primarily a β1-AR agonist, induced vasorelaxation in all groups (**A**). Coronary arterioles from YC animals exhibited a significantly greater dilation compared to OC and O+BM at concentrations $1e^{-6}$ and $1e^{-5}$ [M] (*) (**A**). Salbutamol, a β2-AR agonist, induced mild vasorelaxation that was similar between all the groups (**B**). $p <$ 0.05 vs. Young Control (*) or vs Old+SVF ($); data are presented as means±SEM and analyzed with two-way repeated measures ANOVA followed by *post-hoc* Bonferroni test.

Figure 2.4

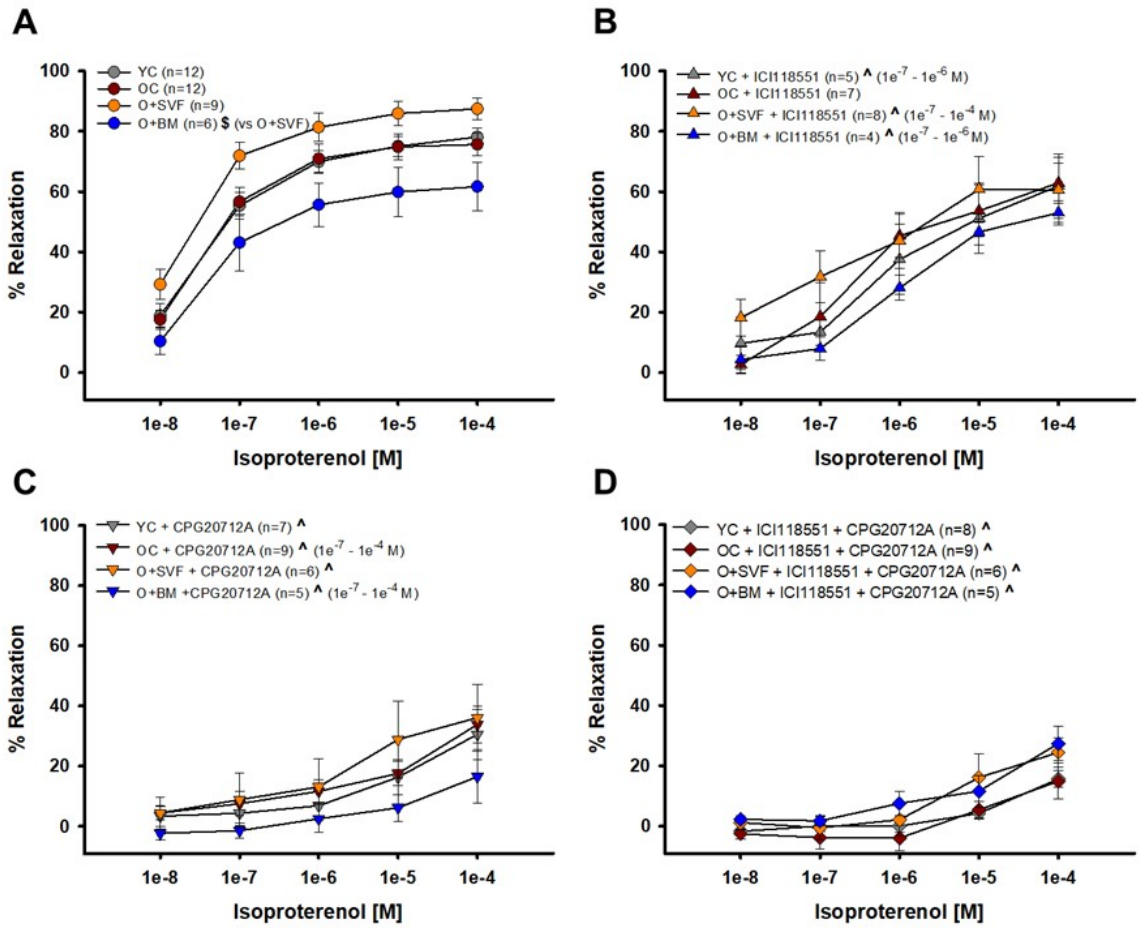

Figure 2.4: Contribution of β1- and β2-AR to isoproterenol-induced vasodilation from isolated coronary arterioles.

Vasorelaxation to isoproterenol, primarily a non-selective β1-, β2-, and β3-AR agonist, was significantly impaired in the O+BM group compared to O+SVF ($) (**A**). Isoproterenol with ICI118551, a β2-AR antagonist, eliminated differences between the groups. Compared to pre-incubation, all groups except OC (YC, O+SVF, and O+BM) had significant attenuation in the inhibited dose response (^) at several concentrations (**B**). Isoproterenol with CPG20712A, a β1-AR antagonist, also eliminated differences

between the groups, and all groups exhibited significant attenuation in the response compared to pre-inhibition (^) (**C**). No group differences to isoproterenol were noted following inhibition with both ICI118551 and CPG20712A, and all groups exhibited significant attenuation in the response compared to pre-inhibition (^) at every concentration (**D**). $p < 0.05$ vs. Young Control (*), vs. Old Control (#), vs. Old+SVF, and pre- vs. post-inhibition (^); data are presented as means±SEM and analyzed with two-way repeated measures ANOVA, paired for inhibitor analysis, followed by *post-hoc* Bonferroni test.

Figure 2.5

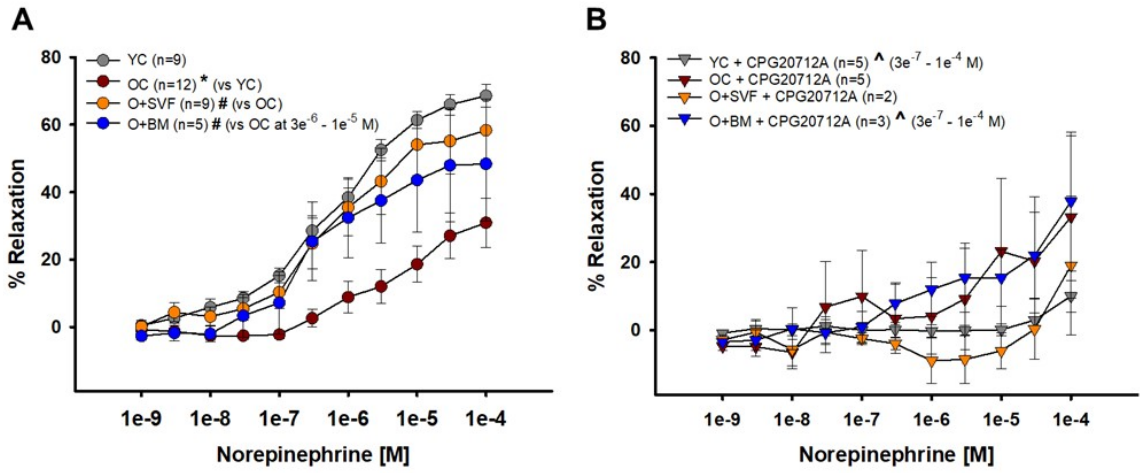

Figure 2.5: Contribution of β2-AR to norepinephrine-induced vasoreactivity in isolated coronary arterioles.

Relaxation to NE was significantly impaired in OC animals compared to YC and O+SVF groups at all concentrations (**A**). NE with CPG20712A, a β1-AR antagonist, attenuated (^) the majority of the vasodilation response ($3e^{-7}$ – $1e^{-4}$ [M]) in YC and O+BM treated groups (**B**). $p < 0.05$ vs. Young Control (*) or vs. Old Control (#) and pre- vs. post-inhibition (^); data are presented as means±SEM and analyzed with two-way repeated measures ANOVA, paired for inhibitor analysis, followed by *post-hoc* Bonferroni test.

Figure 2.6

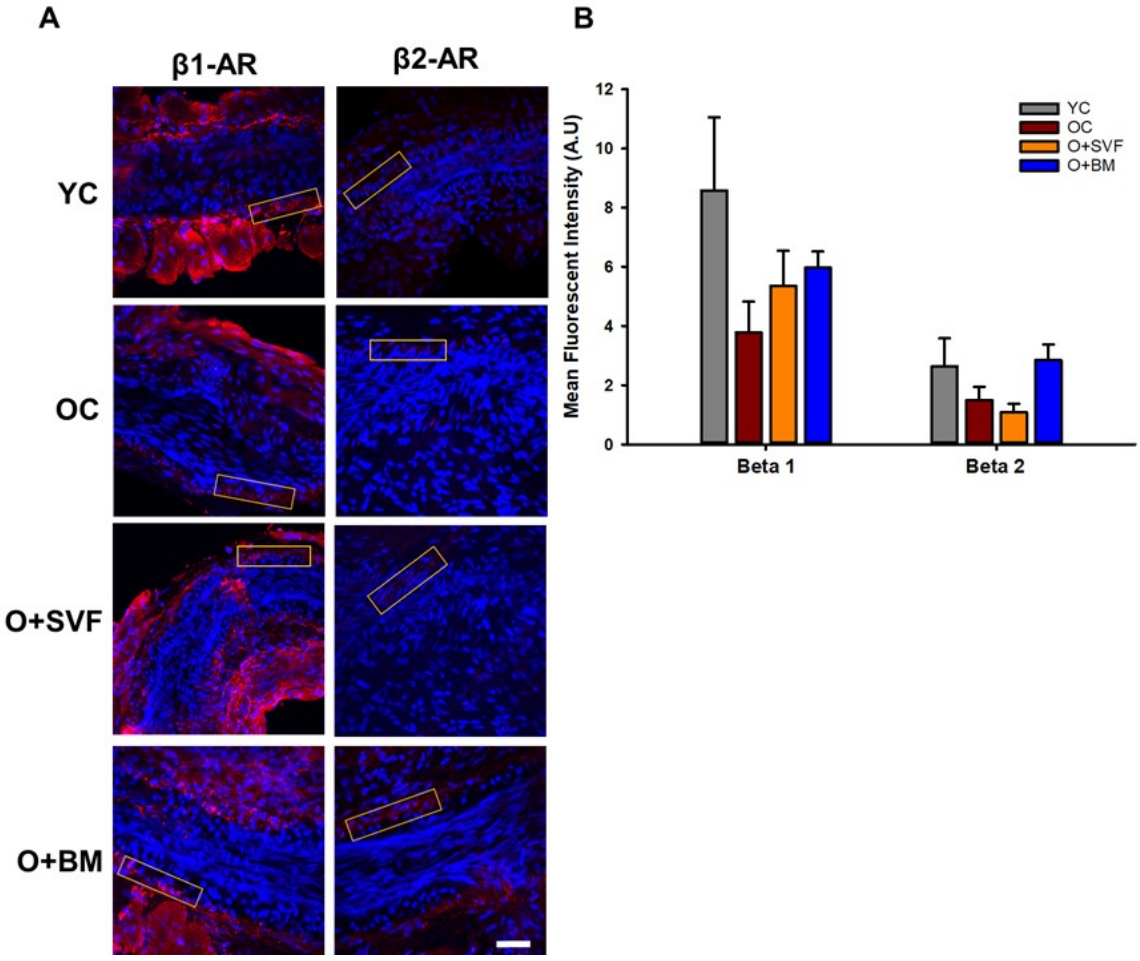

Figure 2.6: β1- and β2-AR immunofluorescence in isolated coronary arterioles. Representative images with ROI boxes used for fluorescent intensity analysis are shown on isolated coronary arterioles stained for β1- or β2-AR (**A**). There is no significant difference between the groups in the expression of β1- or β2-AR as measured by quantification of fluorescent intensity (**B**). Data are represented as means+SEM and analyzed with one-way ANOVA ($n \geq 4$).

Discussion

The major finding from this study is that aged rats treated with intravenous SVF exhibit a restoration of cardiac β-AR responsiveness compared to untreated old controls. This was realized four weeks following SVF treatment by improved CFR, diastolic function, and coronary microvascular reactivity to adrenergic agonists, isoproterenol and norepinephrine. Part of our original hypothesis was supported by the findings in this study, as both SVF and BM-MSC cell therapies were associated with improved arteriolar vasodilation to NE (a non-selective adrenergic agonist), but the BM-MSC group did not show improvements in CFR, diastolic function, or vasodilation to isoproterenol or dobutamine as described in the O+SVF group.

Although still controversial [216], the majority of evidence supports a beneficial effect of cell therapy in treating ischemic and/or dysfunctional cardiac tissue, and this is likely due to still not well-defined paracrine factors released by or in response to the injected cells. Previous studies have shown that MSCs and adipose-derived SVF can be anti-inflammatory and immune-modulatory [198, 199], possibly via influence from the sympathoadrenal system [217]. Additionally, our past studies have shown that SVF cells can incorporate into the vascular wall long-term [42] and are associated with normalization of inflamed large vessels, possibly via alteration in reactive oxygen species (ROS) signaling [201]. It's well known that HF leads to enhanced release of catecholamines [93, 218] and these levels are correlated to the severity of HF [219], resulting in a desensitization of β-ARs which can ultimately promote more cardiac dysfunction [93]. Catecholamine excess has also been demonstrated in advancing age [85], shown to be partially consequent on ROS generation [220], and inversely linked to

vascular endothelial function [221]. In 2006, Dhein and colleagues [207] demonstrated for the first time that intramyocardial injection of BM-MSC normalized both circulating catecholamine levels and β-AR density in the heart after four weeks in a model of non-ischemic cardiomyopathy in rabbits. Although this was not statistically significant, our data supports this trend, as we show an age-related increase in plasma catecholamines that was decreased following BM-MSC or adipose-derived SVF injection (**Table 2.1**).

BM-MSCs were initially hailed as the superior autologous cell source to treat myocardial infarction (MI) because of their differentiation potential [171, 172], but recent studies have shown equal efficacy of adipose-derived SVF in improving cardiac function after MI and in vitro induction into cardiomyocyte-like-cells and vascular elements [189-192]. The present study shows that SVF but not BM-MSC therapy improved diastolic function in aged rats, as measured by E/A, E/e', and tau (**Fig 2.2 B-D**). It is worth mentioning that some group differences observed by ultrasound (EF and SV) were not present for hemodynamic outcomes, but this is likely due to the use of ketamine anesthesia during hemodynamic measurements, which has been associated with depressed LV function (**Table 2.2**) [215]. Regardless, our data stands in contrast to the Monnerat-Cahli [208] study where $5x10^6$ BM-MSCs improved left ventricular developed pressure (LVDP) four weeks after injection in a diabetic rat model. Although we purposefully utilized the same concentration and timeline of BM-MSC treatment in the present study, we did not observe improved cardiac function in the O+BM group compared to the O+SVF group (**Fig 2.2 B-D**), possibly due to the streptozotocin-model of diabetes, use of young male Wister rats, or the method of LVDP measurement in an isolated working heart as performed by Monnerat-Cahli and colleagues [208].

Dobutamine and adenosine both increase cytosolic cAMP production [31] in the coronary circulation to achieve hyperemic flow, but this occurs through different receptor activation (β-AR and adenosine receptors, respectively). The age-related decrease in dobutamine-induced CFR was significantly reversed after SVF treatment (**Fig 2.1 A**), indicating SVF cell therapy improved cardiac β-AR responsiveness. Although age-related deficits were not revealed during adenosine-induced CFR, both cell therapies (SVF and BM-MSC) significantly improved CFR compared to OC (**Fig 2.1 B**). These disparate results may be explained by the fact that β-AR-mediated accumulation of cAMP has been shown to decrease with age, but alternate induction pathways of cAMP appear to be preserved. To this end, relaxation to forskolin - a direct activator of adenylyl cyclase (AC) - are normal in whole vessels [222] while basal levels of AC are increased with age in rat aorta [223], suggesting that the AC enzyme and events distal to cAMP formation are intact with age. Ross et al. [224] showed in vivo that infusion of propranolol (a β1- and β2-AR inhibitor) decreased peak coronary blood flow in response to isometric handgrip exercise in young men, whereas old men (67±4 years) exhibited no effect. These studies support that SVF cell therapy in aged hearts increase CFR through improvements in β-AR-cAMP signaling.

We found that there is a significant age-related decrease in β1-AR-mediated vasodilation, as YC demonstrated increased vasodilation to dobutamine (**Fig 2.3 A**) vs. OC. In this study, we believe SVF therapy worked by improving β-AR, specifically β1, in the coronary microcirculation because vasodilation to dobutamine was increased following SVF treatment vs. the O+BM group. Further, when β1-AR was inhibited using CPG20722, age- and group-related differences were eliminated in the vasodilation to NE

(**Fig 2.5 B**). Dobutamine can elicit differential effects depending on the tissue; in the cardiac tissue it acts mostly via β1-AR stimulation versus in the vascular system it stimulates β1- and β2-AR vasodilation, and also some minor α1-AR vasoconstriction [225]. But the importance of β1-AR stimulation prevails, as Abdelkrim and colleagues [226] demonstrated that immunization against the β1-AR in young rats produced significant decreases in dobutamine and isoproterenol relaxations in small isolated mesenteric arteries, and impaired endothelial-dependent nitric oxide (NO) signaling pathways. As mentioned previously, there is decreased β-AR responsiveness with age [86] and in HF [10, 93] and our findings support this conclusion.

Pretreatment with ICI118551, a β2-AR antagonist, abolished the difference in vasodilation to isoproterenol between the cell-treated groups (**Fig 2.4 A** and **B**), suggesting that there is some contribution of β2-AR activity and/or signaling following SVF but not BM-MSC therapy. This link between SVF treatment and heightened β2-AR activity is supported by the age-related decrease in relaxation to NE in coronary arterioles, which was restored in the SVF cell-treated group (**Fig 2.5 A**). Historically, NE effects on adrenergic receptors have been difficult to study because of the multifaceted/opposing effects on vascular and cardiac tissues. Vasodilation to NE has been previously shown to be primarily mediated through β2-AR on the VSMC of human coronary arterioles [227]. However, we did not find a significant difference in vasodilation between the groups using the selective β2-AR agonist, salbutamol (**Fig 2.3 B**). While β2:β1-AR ratio increases in failing human hearts [218] and in senescent hearts [202, 228], we have a novel observation that the opposite occurs in β2-AR staining in arterioles from OC, and this wasn't altered with SVF treatment (**Fig 2.6**).

If β1-AR undergoes prolonged stimulation, similar to chronic catecholamine spillover in the elderly [229], β2-AR can undergo a cross-desensitization [85]. Schutzer et al. [230] suggested that β2-AR actually achieves maximal desensitization with age, resulting in β2-AR switching from Gstimulatory to Ginhibitory. To that end, β2-AR stimulation with concomitant β1-AR inhibition has been shown to improve cardiac function and myocardial O_2 consumption post-operatively in aged male rats [231]. Of note, β2- and β3-AR are functionally distinct from β1-AR by their ability to deactivate ACs by coupling to the inhibitory G protein (Gαi). Cardiac Gαi levels and activity have been shown to be increased with age in humans and in rodent models [232-234]. It's likely that aging may have a direct influence on β2-AR activity through indirect receptor cross-desensitization due to circulating catecholamines and/or an increase in Gαi activity, and that SVF cell therapy reverses this, but further studies are required to explore this possibility.

Conclusion

It's important to consider the limitations of the present study: 1) radioligand binding would be a more direct method of measuring β1- and β2-AR density and ratio in isolated coronary arterioles compared to our immunofluorescence method, 2) catecholamine levels were analyzed in plasma collected at the conclusion of PV loop experiments while anesthetized with ketamine. Ketamine has been proven to decrease plasma catecholamines whilst inhibiting the uptake of NE, resulting in a transient increase [235]. This may have caused a dampening in the true catecholamine levels. 3) In order to be consistent with a previous study [208], the concentration of cells between the

two cell groups were not the same. 4) This study only utilized female rats as recipients. Our rationale for this is because as age progresses in humans, CMD manifests in the sexes differently. As many as 50% of women referred for evaluation of MI do not have obstructive coronary disease, like most men, but are frequently associated with coronary microvascular dysfunction/ischemia [236]. Follow-up studies suggest that CFR is a better predictor of future adverse events compared to traditional angiographic methods in older women [237]. 5) The present study utilized SVF and BM-MSC from young donor rats only. Our lab and others have previously shown that the age of the donor significantly depresses the angiogenic, vasculogenic, and overall mesenchymal potential of isolated cells [238-240], but it's unknown whether these factors would alter the outcomes in the present study. Lastly, β3-AR plays a key role in the development of LV diastolic dysfunction as recently shown by Yang et al. using a knockout mouse model [241]. The role of β3-AR wasn't directly explored in the current study but warrants investigation to determine if aging and/or cell therapy alter its activity and/or expression.

Our previous study showed SVF incorporation into the cardiac and vascular space four weeks post-injection in an aged rat [42].The field is still unsure if the beneficial effects of injected cells are mediated via secreted factors being released from the cells or if it is the incorporated cells themselves remaining in the circulation and populating the peripheral tissue [242]. Regardless, this new data provides exciting evidence that SVF cell treatment can improve vasodilation to adrenergic agonists and increase CFR compared to old controls rats, providing a new strategy in managing sympathetic desensitization that occurs in advancing age as well as diastolic dysfunction. These

results lay significant groundwork into future studies on cell therapy and resultant sympathoadrenal and β-AR signaling.

CHAPTER 3

CELL THERAPY RESCUES AGING-INDUCED BETA-1 ADRENERGIC RECEPTOR AND GRK2 DYSFUNCTION IN THE CORONARY MICROCIRCULATION

Overview

Our past study showed that coronary arterioles isolated from adipose-derived stromal vascular fraction (SVF)-treated rats showed amelioration of the age-related decrease in vasodilation to β-adrenergic receptor (β-AR) agonist and improved β-AR dependent coronary flow and microvascular function in a model of advanced age. We hypothesized that intravenously (i.v.) injected SVF improves coronary microvascular function in aged rats by re-establishing the equilibrium of the negative regulators of internal adrenergic signaling cascade, G-protein receptor kinase 2 (GRK2) and G-alpha inhibitory (Gαi) proteins, back to youthful levels. Female Fischer-344 rats aged young (3 months, n=24), old (24 months, n=26) and old animals that received $1x10^7$ green fluorescent protein (GFP+) SVF cells (O+SVF, n=11) four weeks prior to sacrifice were utilized. Overnight urine was collected prior to sacrifice for catecholamine measurements. Cardiac samples were used for western blotting while coronary arterioles were isolated for pressure myography studies, immunofluorescence staining, and RNA sequencing. Coronary microvascular levels of the β1 adrenergic receptor are decreased with advancing age, but this decreased expression was rescued by SVF treatment. Aging

led to a decrease in phosphorylated GRK2 in cardiomyocytes vs. young control with restoration of phosphorylation status by SVF. In vessels, there was no change in genetic transcription (RNA sequencing) or protein expression (immunofluorescence), however, inhibition of GRK2 (paroxetine) led to improved vasodilation to norepinephrine in old control (OC) and O+SVF, indicating greater GRK2 functional inhibition of β1-AR in aging. SVF works to improve adrenergic-mediated vasodilation by restoring the β1-AR population and mitigating signal cascade inhibitors to improve vasodilation.

This chapter is from the published work referenced as follows:

Rowe, G., et al., *Cell therapy rescues aging-induced beta-1 adrenergic receptor and GRK2 dysfunction in the coronary microcirculation.* Geroscience, 2021.

Introduction

The coronary microvasculature of aged individuals is unable to properly augment blood flow (BF) in response to vasodilatory stressors [97], leading to poor coronary perfusion and increased risk of heart failure (HF) [98]. In the aging heart, increased circulating catecholamines combined with decreased sensitivity to adrenergic stress [229] can lead to a loss in number and/or function of cardiac beta-adrenergic receptors (β-AR), resulting in decreased cardiac contractility [87, 206]. Since β-AR in the heart and vasculature primarily lead to vasodilation, this age-related decrease results in a microvascular phenotypic shift from a dilatory state to a state of vasoconstriction [94]. It is likely that the overactivation of the sympathetic neurohormonal system that occurs in both advancing age and HF may share common signaling mechanisms [83]. In a failing heart, the population of the β1-AR is reduced from 77% to 60% [91, 92] while the other adrenergic receptors seem to be unaffected or even upregulated in the case of the alpha-adrenergic receptors (α-AR) [92]. However, the status of β-AR-mediated signaling in the coronary microvasculature in advanced age is currently unknown, as well as how this signaling relates to coronary microvascular dysfunction.

Beta-blockers are the preferred treatment for HF to block the inotropic and chronotropic effects of the sympathetic nervous system on the β1-AR [127], but chronic beta-blockade to alleviate HF may be detrimental to the microvasculature [243]. Additionally, the myocardium and microvessels have β2- and β3-AR which are functionally distinct from β1-AR as they both deactivate adenylyl cyclase (AC) by coupling to the inhibitory G-protein (Gαi) compared to a stimulatory G-protein (Gs) for β1-AR signaling [39]. The activity and level of Gαi increases in the myocardium in aging

humans [232], in HF [244, 245], and in rodent models [233, 234]. Aging is also associated with decreased AC activity and cAMP levels in the myocardium [246], but little is known about the role these factors play in the aging microvasculature of the heart.

The age-related decrease in β-AR-mediated vasorelaxation is thought to be due to desensitization of the receptor, but the initial cause of desensitization has been identified at various points of the adrenergic signaling cascade in myocardial tissue [127]: either following a decrease in receptor density from transcriptional downregulation [247] and/or due to the uncoupling of the Gs/AC unit from the adrenergic receptor [248]. In the myocardium, uncoupling of the adrenergic receptor is protective against the increased catecholamine onslaught and shown to be dependent upon G-protein receptor kinases (GRK) [249] and Gαi [250] which both increase with age [251, 252]. GRKs are unique in their kinase function, controlling the affinity of the β-AR for its ligand and initiating receptor internalization through phosphorylation of the internal tail [253]. However, it is unknown if the age-related increase in these negative regulators of adrenergic signaling also occurs in the coronary microcirculation. How GRK and Gαi contribute to the overall age-related decrease in catecholamine-responsiveness is also undetermined. The involvement of β-AR signaling in aging hearts offers a unique diagnostic and therapeutic opportunity to better understand this important pathway and the implications of age within the coronary microcirculation.

Our laboratory has shown that a single intravenous (i.v.) injection of adipose-derived stromal vascular fraction (SVF) improved β-AR-mediated coronary flow reserve (CFR) and restored the vasodilatory capacity of isolated coronary microvessels to β-AR agonists compared to old control rats [39, 42]. The purpose of the current study was to

determine whether SVF cell therapy restores β-AR function in the coronary microcirculation in aged females through reversal of the negative regulators of β-AR signaling, resulting in improved sensitivity and vasodilatory responses to β-adrenergic agonists. Our hypothesis was that cardiac β-adrenergic dysfunction in aging is due to increased GRK2-dependent receptor phosphorylation that can be reversed through SVF cell therapy, leading to increased receptor sensitivity to its ligand and decreased internalization of the receptor, ultimately improving β-adrenergic function in the coronary microcirculation.

Materials and Methods

Animals and experimental groups.

The Institutional Animal Care and Use Committee of the University of Louisville approved this study, and all procedures followed the NIH *Guide for the Care and Use of Laboratory Animals* [254]. Young control (YC, 4 months, equivalent to a 20-year-old human [255], n=24) and old (23 months) female Fischer-344 rats (Envigo Laboratories, Indianapolis, IN, USA and National Institute of Aging, Bethesda, MD, USA, respectively) were group housed with free access to food and water and maintained on regular 12-hour light/dark cycles. Young rats were acclimated to facility conditions for a minimum of one week prior to endpoint procedures. Following one week acclimation, old rats were randomly divided into old control (OC, equivalent to >70-year-old human [255], n=26 or injected with green fluorescent protein positive (GFP+) SVF (O+SVF, n=11) groups. Endpoint procedures were performed four weeks later (aged 24 months).

SVF isolation and cell injections.

SVF cells were isolated from a GFP+ Fischer-344 rat colony (maintained in house) as previously described [39, 41, 42]. Briefly, ovarian or epididymal fat pads from young female and male rats respectively (3-6 months) were harvested, washed, finely minced, and digested in 0.75 mg/mL Type I collagenase solution (Vitacyte 011-1030) and 1 mg/mL Deoxyribonuclease-1 (Sigma DN25). Buoyant adipocytes were removed via centrifugation, and the SVF cell pellet resuspended in 0.1% BSA-PBS as previously described [39, 41, 42]. Freshly isolated SVF were then washed and filtered through a 20-μm screen to eliminate large cell and tissue aggregates. Cell count was determined with a hemocytometer, and GFP+ fluorescence of the cell population confirmed via fluorescence microscopy prior to injection. Old female rats were injected intravenously with 10^7 GFP+ SVF cells in 1 mL Lactated Ringer's solution (warmed to 37°C) via the tail vein as previously described [39, 42].

Urine collection and catecholamine analysis.

Prior to endpoint procedures, a subset of animals (n=6 per group) were individually placed in metabolic cages with free access to food and water for overnight collection of urine (18.5 hours). Frozen samples were sent to the University of Louisville Bioanalytical Core for mass spectrometry analysis of excreted catecholamine levels as previously described [256].

Subepicardial arteriole isolation experiments.

For endpoint procedures, animals were deeply anesthetized with inhaled 5% isoflurane with 1.5-2.0 L/min O_2 flow in induction chamber. After confirming lack of

tactile reflex, the heart was removed and coronary arterioles from the left anterior descending (LAD) artery distribution were isolated, cannulated on both ends and pressurized to 45 mmHg in a 37°C bath containing physiological salt solution (PSS) plus albumin [39, 42, 213]. Upon developing spontaneous tone (≥ 20% constriction from initial diameter), arterioles were treated with β-AR- and/or intracellular signaling-agonist/inhibitor protocols so that stimulation of the β-adrenergic signaling cascade progressed from upstream to downstream. Vessels unable to initially establish spontaneous tone were discarded and some arterioles did not reestablish tone following one or more treatments. The drug/inhibitor protocols were randomized to the isolated vessels:

- Protocol 1 – BRL-37344 (β3-AR agonist, Sigma B169), Norepinephrine (NE)(α1-2, and β1-2 AR agonist, Sigma-Aldrich A9512), and NE following 30 min incubation with Paroxetine HCl (NE+Parox)(GRK-selective antagonist, VWR 89160-896), Sodium Fluoride (NaF)(Gs activator, Sigma-Aldrich S6776).
- Protocol 2 – NE, NE following 20 min incubation with CPG20712A (NE+CPG)(β1-AR antagonist, Sigma C231), Forskolin (AC activator, VWR 89156-986).
- Protocol 3 – Dobutamine (Dob)(primarily a β1-AR agonist with lower β2-AR activity, Sigma-Aldrich D0676), NE, Dob following 20 min incubation with ICI118551 (Dob+ICI)(β2-AR antagonist, Sigma I127), NE+ICI, 8-bromo-cAMP (cAMP-dependent protein kinase activator, VWR 89157-000).

At the end of the protocol, arterioles were washed 2x15 min in calcium-free PSS followed by a single high dose of sodium nitroprusside (SNP $1e^{-4}$ [M]) at the end of

experiment. Maximal dilation for each vessel was determined as the largest diameter achieved throughout the experiment. Data for spontaneous tone was calculated as (1-[luminal diameter]/[max diameter])*100 while percent relaxation was calculated as ([luminal diameter-initial diameter]/[max diameter-initial diameter])*100.

Immunofluorescence staining.

Coronary arterioles (750 μm-1 mm in length, < 250 μm in diameter) were isolated from each heart and fixed in 2% paraformaldehyde in 48-well plates for 1-hour, washed 2x10 min in DCF-PBS, and placed in 0.5% Triton-X/DCF-PBS for 20 minutes at room temperature (RT) for permeabilization. After treating with blocking solution (10% normal donkey serum/0.5% bovine serum albumin/0.1% Triton-X/DCF-PBS) for 1 hour at RT, arterioles were incubated in a primary β1-AR (Abcam ab3442, 1:100), β2-AR (Abcam ab182136, 1:100), β3-AR (Abcam ab59685, 1:200), α1-AR (Invitrogen PA1-30159, 1:100), α2-AR (Abcam ab3462, 1:100), GRK2 (Santa Cruz sc-13143, 1:100), Gs (ThermoFisher PA5-115303, 1:100), Gαi1 (Invitrogen MA5-12800, 2 ug/mL), or beta-arrestin 2 (Invitrogen PA1-732, 2 ug/mL) antibody in blocking solution at 4°C overnight with gentle rocking. Normal rabbit serum replaced primary antibody solution for isotype control tissues. Donkey anti-rabbit IgG-Alexa Fluor 594 (Invitrogen A21207, 1:300 for β1, β2, α1, α2, Gs, and beta-arrestin 2, 1:400 for β3 staining) and/or donkey anti-mouse IgG-Alexa Fluor 647 (Abcam ab150207, 1:300 for GRK2 and Gαi1 staining) antibody in blocking solution were added to the tissues and incubated for 1-hour at RT. Arterioles were washed 2x15 min in DCF-PBS, and nuclei were stained with DAPI. Samples were placed on slides with anti-fade mounting media, coverslipped, and imaged using an

Olympus FluoView 1000 confocal microscope (Olympus America, Center Valley, PA, USA) with 405, and 543, and 635 nm lasers. Images of the adrenergic receptors were captured with a 20X water immersion objective for β-ARs or a 40X objective for α-ARs vessels at 1024x1024 pixel density and 1-1.92 μm Z-step with 6-18 slices (10.68-33.84 μm total image depth) being used for analysis. Immunofluorescence images of GRK2, Gs, Gαi1, and beta-arrestin 2 stained vessels were captured with a 20X water immersion objective at 1024x1024 pixel density and 3.71 μm Z-step size with 3 slices (11.13 μm total image depth) being used for analysis. Immunofluorescence intensity of the stained protein in the region of interest (ROI) boxes were determined by the Nikon NIS Elements AR Analysis software (Nikon Instruments, Melville, NY, USA) using at least 20 μm x 100 μm area and at least 8 μm of depth [39]. ROI boxes were placed on the left and right vascular walls overlapping both the endothelial and smooth muscle cell layers but excluding any cardiomyocytes, then averaged and normalized to the total image depth.

Western blotting.

Following subepicardial arteriole isolation, hearts were flash frozen and stored for protein isolation. Protein was isolated from 3-mm sections of hearts of the LV regions of the heart near the apical LAD by tissue homogenization in RIPA lysis buffer, 1X protease inhibitor (Sigma P8340), and phosphatase inhibitor solution containing 1 mM sodium orthovanadate (Sigma S6508) and 7.5 mM sodium fluoride (Sigma S6776). The homogenate solution incubated at 4°C with gentle rocking for 30 min before being sonicated on ice at 40% power 3 x10 sec each. Homogenate was then centrifuged at 4°C and 12,000 rpm for 20 min. The supernatant was transferred to new tubes for protein

concentration using BioRad DC protein assay (5000111) and a Biotek Synergy 4 spectrophotometer (Biotek Instruments, Highland Park, VT, USA). Protein stocks were sampled and diluted 1:100 prior to concentration assay. BSA (Sigma A6003) from 0.1875 to 1.5 mg/mL in RIPA was used to generate a standard curve. Loading samples were made at 50 µg of protein in 4X Lammelli (BioRad 161-0747) and RIPA buffers then boiled at 95°C for 5 min. Samples were run on 4-20% gradient precast gels (BioRad, 4561095) at 200V for 30 min. Gels were placed in a wet tank transfer cassette with a nitrocellulose membrane (BioRad, 1620112) for transfer at 100V for 1 hour surrounded in ice. Membranes where then blocked in a 5% non-fat dry milk/1X TBS-T solution for 1 hour at RT with gentle rocking. The following primary antibodies were diluted 1:1000 in a 5% non-fat dry milk/1X TBS-T solution and incubated with gentle rocking at 4°C overnight to probe for: β1-AR (Abcam ab3442), β2-AR (Abcam ab182136), β3-AR (Abcam ab59685), phosphorylated GRK2 (Abcam ab58520), GRK2 (Santa Cruz sc-13143), Gs (ThermoFisher PA5-115303), Gαi1 (Invitrogen MA5-12800), beta-arrestins 1&2 (Cell Signaling 4674S), beta-arrestin 2 (Invitrogen PA1-732), and GAPDH (Cell Signaling 8884S, 1:3000). Secondary anti-rabbit (Cell Signaling 7074S) (β2-3-AR, phospho-GRK2, Gs, beta-arrestins 1&2, and GAPDH) or anti-mouse (Cell Signaling 7076S) (GRK2 and Gαi1) HRP conjugated antibodies were diluted in 5% non-fat dry milk/1X TBS-T solution at 1:3000 for all the blots except the β1-AR, in which the anti-rabbit secondary was diluted 1:10,000 and incubated at RT for 1 hour with gentle rocking. Chemiluminescence was performed using BioRad's ECL clarity max solutions (1705062) and imaged using a Chemidoc MP (BioRad, Hercules CA, USA). Intensity of the bands was measured using ROI boxes in ImageJ (NIH). The band intensity of the

protein of interest was normalized to its GAPDH band intensity, then the mean of this ratio was calculated by group. For the phospho-GRK2 to total GRK2 analysis, band intensity normalization was done using the following formula: ([phospho-GRK2/GAPDH]/[GRK2/GAPDH]).

RNA sequencing.

Coronary arterioles (750 μm-1 mm in length, <250 μm in diameter) were flash frozen and stored at -80°C until samples from all groups were collected. Six isolated vessels were pooled from two animals in the same group for an n=3 of biological replicates/group. RNA was harvested with RNAqueous Micro kit (Invitrogen AM1931) and quantified on a NanoDrop (ThermoFisher, Waltham MA, USA). Samples were sent to the University of Louisville Genomics Core for quality control analysis using the Agilent Bioanalyzer 2100 system (Agilent Technologies, Santa Clara, CA) and quantified using a Qubit fluorometric assay (Thermo Fisher Scientific, Waltham, MA) as previously described [257]. Poly-A enrichments, barcoding, and Illumina Next-Gen sequencing for library preparation was performed as previously described [257, 258]. Gene transcripts were analyzed by the University of Louisville Bioinformatics Core for differential expression analysis between group comparisons as previously described [259].

Statistical analysis.

Statistical analyses were performed in SigmaPlot 14.0 (Systat, San Jose, California, USA) with $p < 0.05$ as the significance level. One-way ANOVA was performed on animal characteristics, plasma catecholamine levels, and

immunofluorescence intensity measurements of β-adrenergic receptors; either Holm-Sidak or Dunn's *post hoc* analyses were performed where appropriate. One-way Kruskal-Wallis ANOVAs were utilized in instances of failed normality. Concentration-response curves as well as pre- and post-inhibition responses were analyzed via two-way repeated measures ANOVA followed by Bonferroni *post hoc* analyses. Western blot data were analyzed using One-way ANOVA with Holm-Sidak *post hoc* analysis or a Kruskal-Wallis followed by Dunn's method of *post hoc* analysis where appropriate. RNA sequences were analyzed using Cufflinks-Cuffdiff2 with an absolute $|\log2FC| \geq 1$ to determine differential expression as previously described [259].

Results

Animal characteristics and catecholamine metabolism.

To determine if systemic i.v. delivery of SVF altered animal characteristics and/or excreted catecholamines in the urine, we collected gross anatomical characteristics and sampled urine from overnight collection chambers; these data are presented in **Table 3.1**. All aged groups exhibited increased body weight (BW), total ventricular weight, and left ventricular (LV) weight when compared to YC animals (**Table 3.1**). With aging (OC, 138.31±10.09 ng/mg creatinine, n=6), significantly higher levels of NE excreted in the urine were observed when compared to young animals (YC, 76.53±7.84 ng/mg creatinine, n=6); this was not reversed by SVF treatment (O+SVF, 151.02±14.96 ng/mg creatinine, n=6) (**Table 3.1**). In contrast, there were no age-related or group differences in

urine levels of epinephrine (Epi), serotonin (5HT), dopamine (DA), or a metabolite of serotonin (5-HIAA) between the groups (**Table 3.1**).

Myocardial and microvascular expression of β-adrenergic receptors.

To determine whether age (OC) or SVF cell-based therapy (O+SVF) affected the β-adrenergic receptor population in the myocardium, western blotting was performed (**Fig 3.1**). Measuring band intensity normalized to GAPDH, there was no significant difference in the β1-AR or β2-AR levels in the myocardium across the groups (**Fig 3.1**).

To assess changes to the populations of all the adrenergic receptors (β1-3 ARs and α1-2 ARs) within coronary microvessels with advancing age or following SVF administration, immunofluorescence was performed on a subset of microvessels isolated from explanted hearts. Images from each group were used to analyze the fluorescence intensity measured on the endothelial/smooth muscle cell layer of each microvessel (**Fig 3.2 A**), and quantification of β1-3 ARs or α1-2 ARs fluorescence is shown in **Figure 3.2 B**. There was a significant decrease in the β1-AR with age, but the β1 receptor expression is restored to young levels following SVF cell therapy ($p < 0.05$, n=9/group, **Fig 3.2 B**). No other group differences were observed in β2-3 ARs or α1-2 ARs.

Isolated subepicardial vessel characteristics and β1-AR mediated vasodilation.

Arterioles under 150 μm in luminal diameter from the LAD distribution were dissected and isolated to assess whether cell therapy or adrenergic inhibition altered basic vessel characteristics such as spontaneous tone. Aged groups (OC, 16.50 ±0.73 μm, n=50 and O+SVF, 15.67±0.96 μm, n=27) had increased wall thickness compared to

microvessels isolated from young animals (YC, 12.02±0.56 μm, n=40) (**Table 3.2**). Maximum diameter (Dmax) achieved was significantly higher in OC vessels (154.35±3.61 μm, n=55) when compared to YC (137.6±3.51 μm, n=42) and O+SVF cell therapy (140±4.3 μm, n=31) (**Table 3.2**). Spontaneous tone at the beginning of the experiment, post-GRK2 inhibition with Paroxetine HCl, post-β1-AR inhibition with CPG20712A, and post-β2-AR inhibition with ICI118551 exhibited no significant differences among the groups (**Table 3.2**).

The adrenergic agonist NE and β1-AR antagonist CPG20712A were used to show β1-AR contribution to vasoreactivity via pressure myography; data is represented in **Figures 3.3 A-C**. Following CPG20712A incubation, there was a significant attenuation of NE-induced relaxation when compared to pre-inhibition at doses $1e^{-6}$ - $1e^{-4}$ [M] for all groups (**Fig 3.3 A-C**).

GRK2 regulatory kinase expression in cardiac tissues.

To examine if age or SVF cell therapy alters the expression and/or functionality of GRK2 in the myocardium and coronary microvessels, western blotting, IHC, and pressure myography studies were performed (**Fig 3.4 A-E**). Myocardial samples from each group were probed for phosphorylated and total GRK2 proteins (**Fig 3.4 A**). The ratio of phosphorylated GRK2 (P-GRK2) to total GRK2 was significantly reduced in the myocardium of OC animals compared to YC (**Fig 3.4 A**). In contrast, there was no significant difference in the P-GRK2:GRK2 ratio comparing O+SVF to YC (**Fig 3.4 A**). There was no difference in GRK2 protein expression in the OC group as measured by immunohistochemistry on isolated coronary microvessels compared to vessels from YC

and O+SVF (**Fig 3.4 B**). There was no significant difference in the vasorelaxation of YC vessels to NE following GRK2 inhibition with Paroxetine HCl compared to the pre-inhibition response (n=10, **Fig 3.4 C**), but both the OC (**Fig 3.4 D**) and O+SVF (**Fig 3.4 E**) exhibited significant increases in vasorelaxation response to NE at lower doses when compared to pre-inhibition response curves.

Intracellular signaling components and second messengers.

To determine if age or SVF therapy modifies intracellular transduction and/or second messenger proteins of the β1-AR signaling cascade western blotting, immunofluorescence, and pressure myography experiments were performed (**Fig 3.5**). Myocardial samples from OC and O+SVF showed a significant reduction is Gs protein when compared to YC (**Fig 3.5 A**). Coronary arterioles from each group were isolated and immunofluorescently labeled for the Gs protein; ROI boxes were used to measure fluorescent intensity, but staining showed no significant differences between the groups (**Fig 3.5 C**). Using pressure myography on isolated coronary microvessels and direct Gs activation with NaF, O+SVF exhibited significantly reduced relaxation when compared to YC and OC (**Fig 3.5 D**). Western blotting of myocardial tissue showed a significant increase in the amount of Gαi protein in OC when compared to YC (**Fig 3.5 B**). There was no difference in Gαi protein expression between the groups when measured in the coronary microvasculature (**Fig 3.5 C**). Using Forskolin on isolated vessels via pressure myography, there were no differences between the groups when AC was directly activated (**Fig 3.5 E**).

Receptor endocytic proteins.

To determine if proteins mediating β-AR endocytosis and internalization were altered with age or following SVF therapy, western blotting was performed on myocardial tissue while IHC was done on isolated coronary microvessels (**Fig 3.6**). Probing for beta-arrestins 1&2 via western blotting of myocardial tissues showed a significant increase in the amount of beta-arrestins in the O+SVF group when compared to YC samples (**Fig 3.6 A**). Probing the blot for just beta-arrestin 2 produced no significant differences between any of the groups, although both aged groups (**Fig 3.6 B**). Immunofluorescence of beta-arrestin 2 on isolated coronary arterioles showed no difference between the groups (**Fig 3.6 C**).

Next-Gen RNA sequencing.

RNA sequencing was performed on isolated coronary microvessels, and transcripts identified for adrenergic signaling and catecholamine processing; these data are represented in a heat map (**Fig 3.7**). Catecholamine degradation enzyme monoamine oxidase A was significantly increased with aging ($log_2FC(YC/OC) = -0.45$, $p < 0.001$) but not reversed by SVF therapy ($log_2FC(OC/O+SVF) = -0.24$, $p = 0.16$). However, there is reduced expression of catechol-o-methyltransferase (responsible for catecholamine degradation) in O+SVF when compared old ($log_2FC(OC/O+SVF) = 0.22$, $p = 0.046$). There was a significant increase in the β2-ARs in O+SVF vs. OC ($log2FC(OC/O+SVF) = 0.43$, $p = 0.03$) with no significant differences between groups for β1- and β3-ARs or α1-2 ARs (**Fig 3.7**). Transcription of GRK2 or GRKs 4-6 was not different between YC and

OC (log_2FC(YC/OC) = -0.08, p = 0.57) (**Fig 3.7**). Analysis revealed inhibitory G-protein subunit αo1 (Gnαo1) was increased in aging compared to youth (log_2FC(YC/OC) = -0.41, p = 0.024). There was no significant difference in Gnαo1 between YC vs. O+SVF. G-protein subunit αi2 (Gnαi2) trended towards significance with aging relative to young (log_2FC(YC/OC) = -0.17, p = 0.054). In addition, positive regulation of GTPase activity due to small G-protein signaling modulator 2 (Sgsm2) was downregulated with aging (log_2FC(YC/OC) = 0.34, p = 0.054). There was no significant difference between O+SVF vs. YC or vs. OC for Gnαi2 or Sgsm2 (**Fig 3.7**). However, AC isoform 6 (AC6) was significantly downregulated in aging compared to youth (log_2FC(YC/OC) = 0.28, p = 0.016). AC6 expression was not restored to youthful levels following SVF therapy (log_2FC(YC/O+SVF) = 0.43, $p < 0.001$) (**Fig 3.7**). RNAseq analysis revealed a significant increase in beta-arrestin 2 with aging compared to young (log_2FC(YC/OC) = -0.47, p = 0.02) but no change in beta-arrestin 1 (log_2FC(YC/OC) = 0.119, p = 0.55). Beta-arrestin 2 was not significantly different in O+SVF vs. YC or vs. OC. On the other hand, dynamin (responsible for endocytosis in concert with beta-arrestin) was upregulated in O+SVF vs. old, but not young (log_2FC(OC/O+SVF) = -0.46, p = 0.022) (**Fig 3.7**).

Table 3.1

Animal Characteristics	**YC (n=24)**	**OC (n=26)**	**O+SVF (n=11)**
Age (months)	4.71±0.24	24.7±0.1 *	24.36±0.13 *
Body Weight (g) (n)	188.41±2.06	266.18±4.89 (23) *	255.27±4.77 *
Total Ventricular Weight (mg) (n)	493.62±7.14 (22)	677.95±9.44 (24) *	659.55±26.72 *
LV Weight (mg) (n)	395.14±7.16 (22)	563.67±9.66 (24) *	531.20±22.67 *
Urine Catecholamine Levels (ng/mg creatinine)	**YC (n=6)**	**OC (n=6)**	**O+SVF (n=6)**
Norepinephrine (NE)	76.53±7.84	138.31±10.09 *	151.02±14.96 *
Epinephrine (Epi)	8.18±2.95	13.26±1.47	10.18±2.69
Serotonin (5HT)	734.57±205	776.25±154.32	792.01±168.73
Dopamine (DA)	409.53±121.75	557.04±165.4	557.44±186.96
5-HIAA	4927.54±179.22	4606.3±100.09	4826.25±138.43

Table 3.1: Animal characteristics and urine catecholamine levels.

Gross anatomical measurements and catecholamines levels in the urine from overnight collection were measured and one-way ANOVAs followed by *post hoc* tests run where appropriate. Urine catecholamine levels were normalized to mg creatinine. Data are presented as means±SEM (n), $p < 0.05$ vs. YC (*).

Figure 3.1

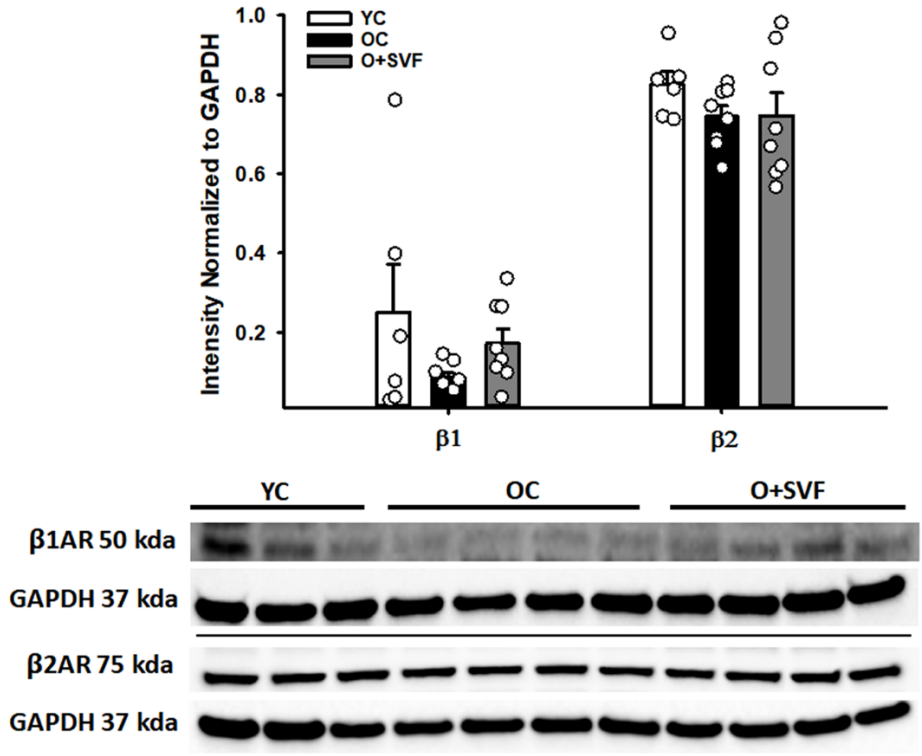

Figure 3.1: Expression of myocardial β1- & β2-AR with aging and following SVF therapy.

Myocardial β1-AR protein expression is reduced (albeit not significantly) in aging and not reversed by SVF therapy (**A, B**). There is no significant change in myocardial β2-AR protein expression with age or with SVF therapy. Protein quantification for expression is measured by band intensity normalized to GAPDH and data presented as means±SEM. Significance determined by One-way ANOVA with Holm-Sidak *post hoc* analysis.

Figure 3.2

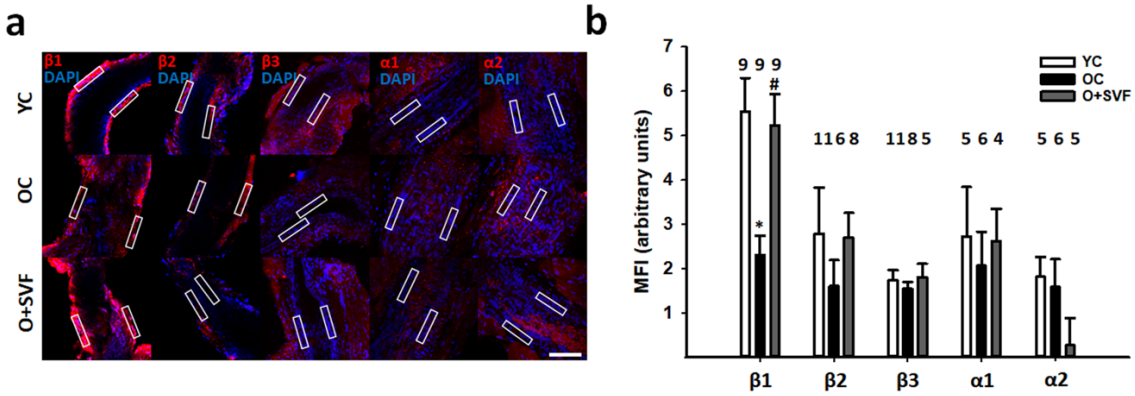

Figure 3.2: Immunofluorescence detection of adrenergic receptors in coronary microvessels.

In coronary microvessels, the β1-AR is significantly reduced in aging and reversed to youthful levels by SVF therapy as measured by Mean Fluorescence Intensity (arbitrary units) while β2-3 ARs and α1-2 ARs remain unchanged (**A, B**). Data is presented as means±SEM, n's above corresponding bar, and significance determined by One-way ANOVA with Bonferroni *post hoc* testing, $p < 0.05$ vs. YC (*) and vs. OC (#). ROI boxes are 10x100 µm. Scale bar equals 100 µm for the β-AR panels and 50 µm α-AR panels.

Table 3.2

Isolated Vessel Characteristics	YC (n=42)	OC (n=55)	O+SVF (n=31)
Wall Thickness (µm) (n)	12.02±0.56 (40)	16.50±0.73 (50) *	15.67±0.96 (27) *
Maximum Diameter (Dmax) (µm)	137.60±3.51	154.35±3.61 *	140±4.3 #
Average % Tone (n)	30.52±2.02 (17)	30.36±1.62 (22)	29.94±2.32 (12)
Average % Tone after Incubation with Paroxetine HCl (n)	28.68±2.46 (12)	29.87±2.18 (16)	26.07±2.8 (9)
Average % Tone after Incubation with CPG20712A (n)	30.1±2.67 (9)	34.59±3.28 (10)	33.56±3.16 (10)
Average % Tone after Incubation with ICI118551 (n)	27.58±1.95 (9)	35.17±3.46 (8)	35.05±2.53 (11)

Table 3.2: Isolated vessel characteristics.

Luminal diameters were measured. Tone was calculated as a percent of the maximum diameter for pre- and post-incubation with an inhibitor. Data are presented as means±SEM (n) and significance determined by One-way ANOVA followed by *post hoc* tests where appropriate. $p < 0.05$ vs. YC (*) and vs. OC (#).

Figure 3.3

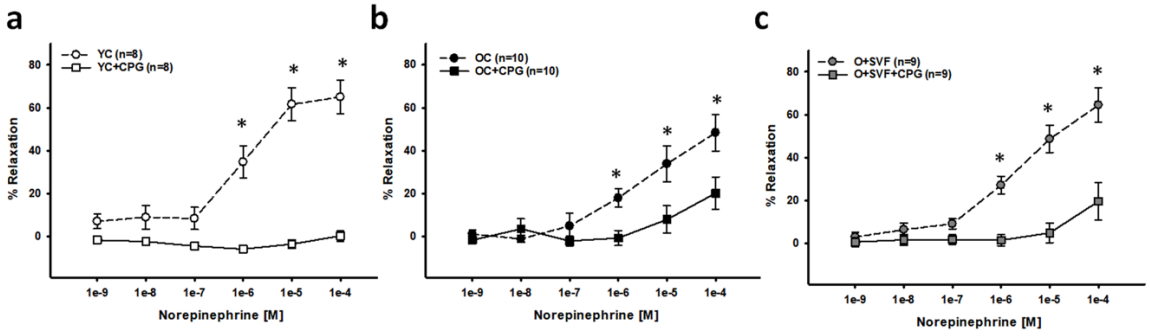

Figure 3.3: Contribution of β1-AR to NE-induced vasorelaxation in isolated coronary microvessels.

NE-mediated vasorelaxation is significantly attenuated by β1-AR inhibition with CPG20712A at $1e^{-6}$ to $1e^{-4}$ [M] doses in YC (**A**), OC (**B**), and O+SVF (**C**). Data are matched pre- to post-inhibition and presented as means±SEM. Significance determined by Two-way Repeated Measures ANOVA with Bonferroni *post hoc* analysis. $p < 0.05$ when pre- vs. post-inhibition (*).

Figure 3.4

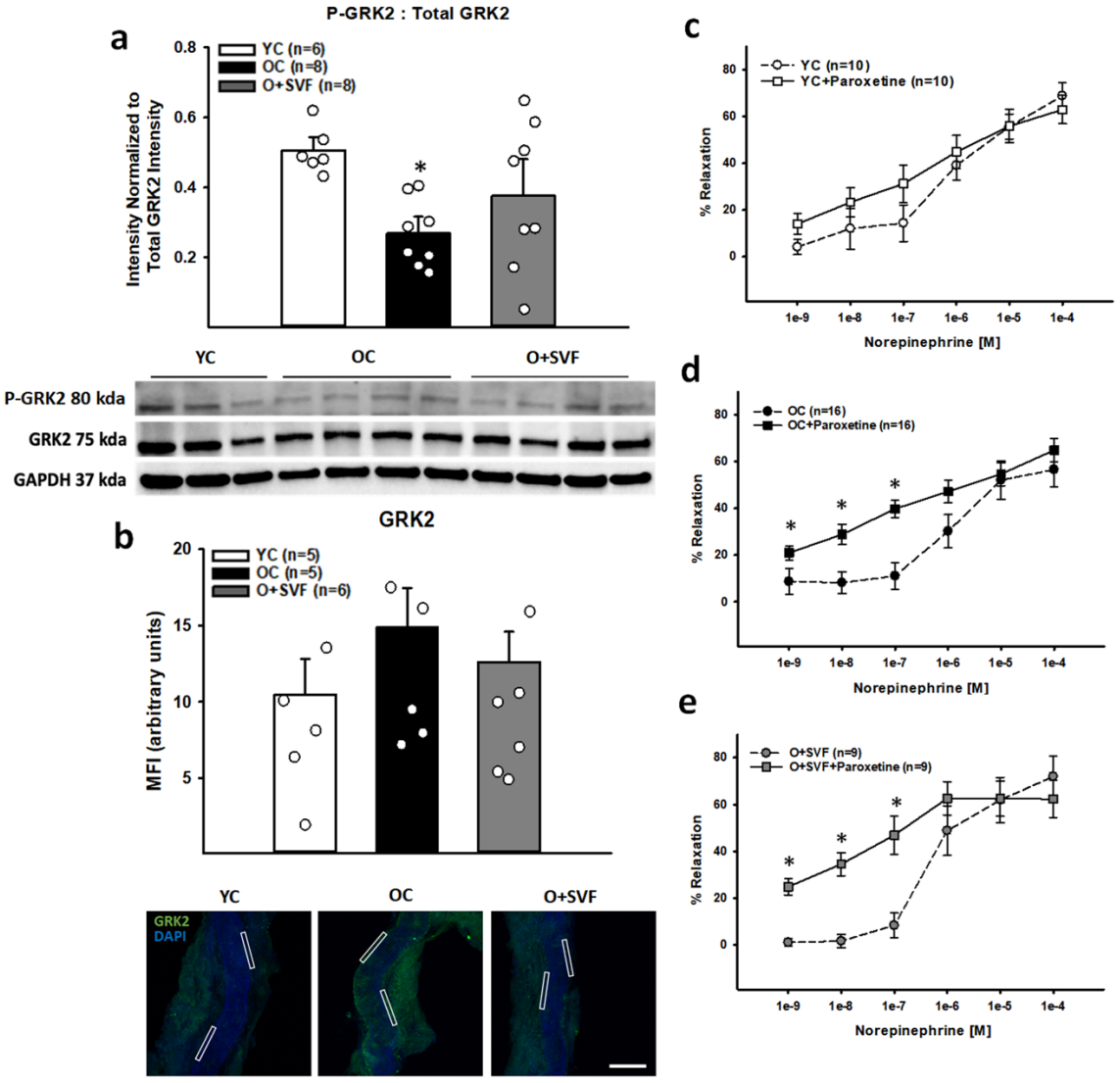

Figure 3.4: Phosphorylation status and function of GRK2 in cardiac tissues.

Western blots of phosphorylated and total GRK2 protein expression, immunofluorescent detection of GRK2 protein, and pressure myography with NE-mediated vasorelaxation before and after exogenous inhibition of GRK2 with Paroxetine HCl. The ratio of phosphorylated (naturally inhibited) GRK2 to total GRK2 is significantly higher in YC when compared to OC myocardial samples, but there is no difference in either group compared to O+SVF as measured by western blotting (**A**). Mean fluorescent intensities of

GRK2 (green) expression as measured by immunofluorescence; representative images from each group are shown with no significant difference between the groups (**B**). NE-mediated vasorelaxation is improved by GRK2 inhibition with Paroxetine HCl in OC ($1e^{-8}$ to $1e^{-6}$ [M]) (**D**) and O+SVF ($1e^{-9}$ to $1e^{-7}$ [M]) **(e)** while vessels from YC are unaffected (**C**). Data are presented as means±SEM. Significance defined by Kruskal-Wallis One-way ANOVA (**A, B**) and paired pre- to post-inhibition for analysis using Two-way Repeated Measures ANOVA with Bonferroni *post hoc* testing (**C-E**). $p < 0.05$ when vs. YC (*) (**A, B**) and pre- vs. post-inhibition (*) (**C-E**). ROI boxes are 5x100 μm. Scale bar represents 100 μm (**B**).

Figure 3.5

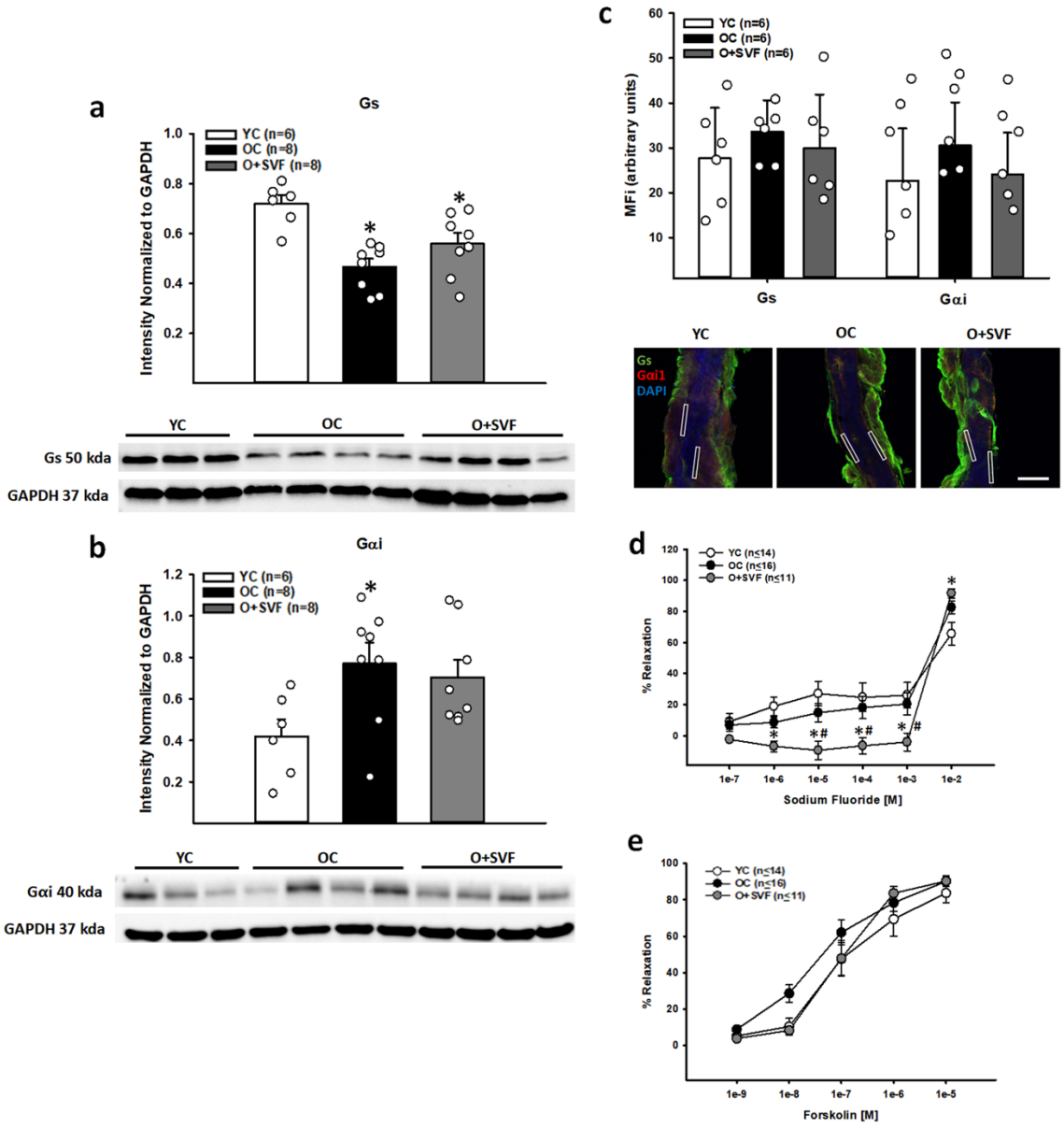

Figure 3.5: Intracellular G-proteins and AC contribution to adrenergic signaling. Western blots and immunofluorescent detection of Gs and Gαi protein expression as well as pressure myography with Gs and AC-mediated vasorelaxation. Myocardial Gs is significantly reduced in OC and O+SVF treated groups when compared to YC (**A**). Myocardial Gαi is significantly increased in OC as shown by western blot analysis (**B**).

Isolated coronary arterioles from YC, OC, and O+SVF treated groups were immunofluorescently stained for Gs (green), Gαi (red), and DAPI (blue) to measure mean fluorescent intensities; no differences between the groups were uncovered for either protein, with representative images shown (**C**). Activation of Gs with sodium fluoride leads to vasorelaxation in a dose-dependent manner which is significantly different in O+SVF treated vessels compared to YC ($1e^{-6}$ to $1e^{-2}$ [M] (*)) and OC ($1e^{-5}$ to $1e^{-3}$ [M] (#)) (**D**). Activation of AC with forskolin leads to concentration-dependent vasodilation that is similar between all groups (**E**). Data presented as means±SEM. Significance determined as $p < 0.05$ when vs. YC (*) and vs. OC (#) utilizing One-way ANOVA with Holm-Sidak *post hoc* analysis (**A-C**) or Two-way Repeated Measures ANOVA with Bonferroni *post hoc* analysis (**D, E**). ROI boxes are 5x100 μm. Scale bar represents 100 μm (**C**).

Figure 3.6

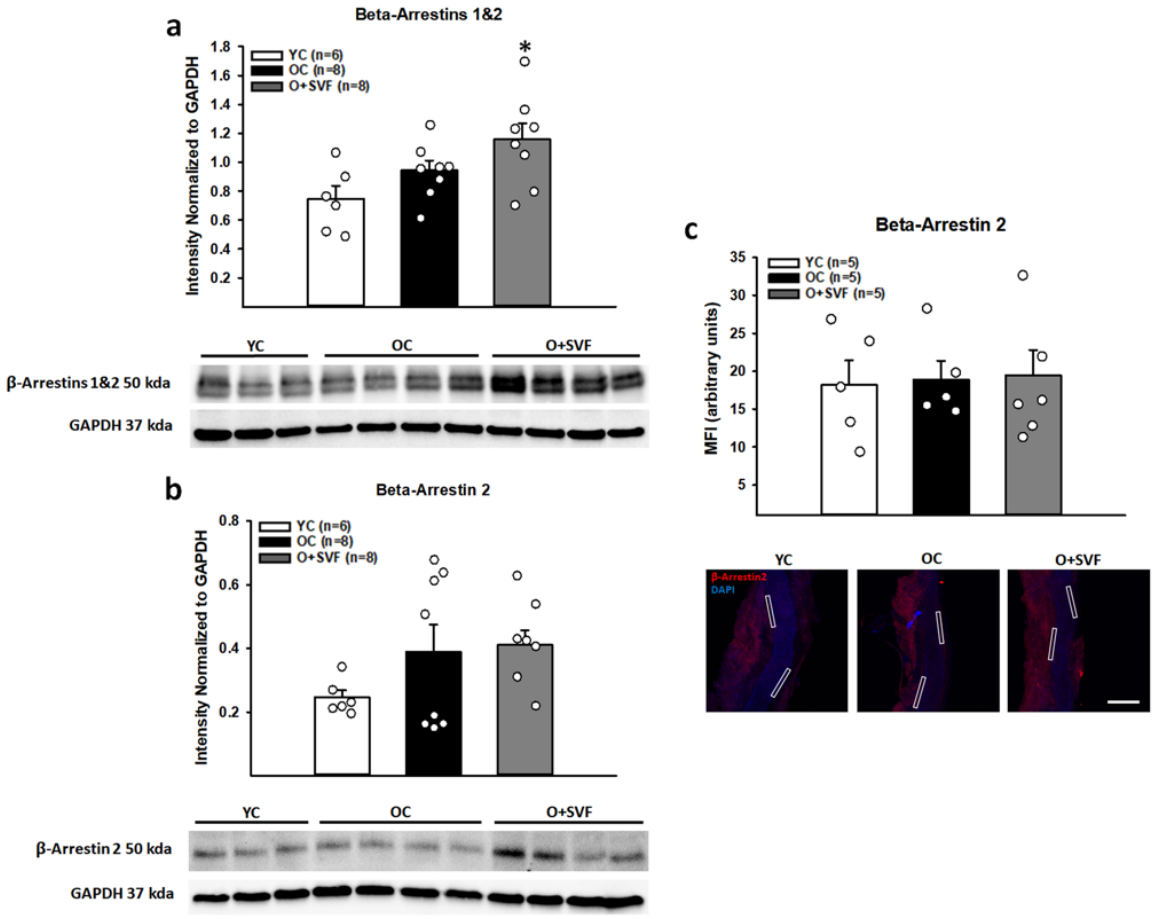

Figure 3.6: Cardiac expression of β-arrestins in youth, aging and SVF therapy. Western blotting and immunofluorescent detection of beta-arrestin proteins in myocardium and isolated coronary microvessels. Internalization proteins beta-arrestins 1&2 are marginally increased with age (OC) and significantly increased in the O+SVF relative to YC (**A**). Probing for beta-arrestin 2 showed no difference between the groups (**B**). Immunofluorescently staining isolated coronary arterioles from each group for beta-arrestin 2 (red) produced no significant differences between the groups and representative images are shown below (**C**). Western blot expression reported relative to GAPDH, and all data presented as means±SEM. Significance defined as $p < 0.05$ when vs. YC (*)

determined by One-way ANOVA with Holm-Sidak *post hoc* analysis (**A-C**). ROI boxes are 5x100 μm. Scale bar represents 100 μm (**C**).

Figure 3.7

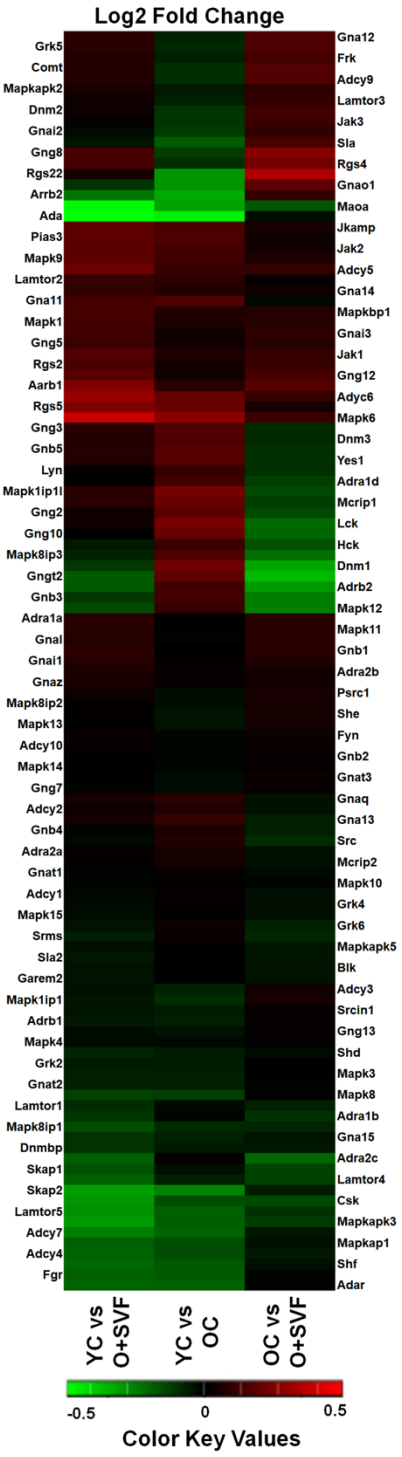

Fig. 7:RNA heat map.

Heat map representing color-coded RNA expression levels of differentially expressed genes involved in adrenergic signaling and receptor recycling in isolated coronary microvessels from YC, OC, and O+SVF samples. In total, 119 genes are listed. Significance defined as cuffdiff and DESeq2 for cutoff $p < 0.05$.

Figure 3.8

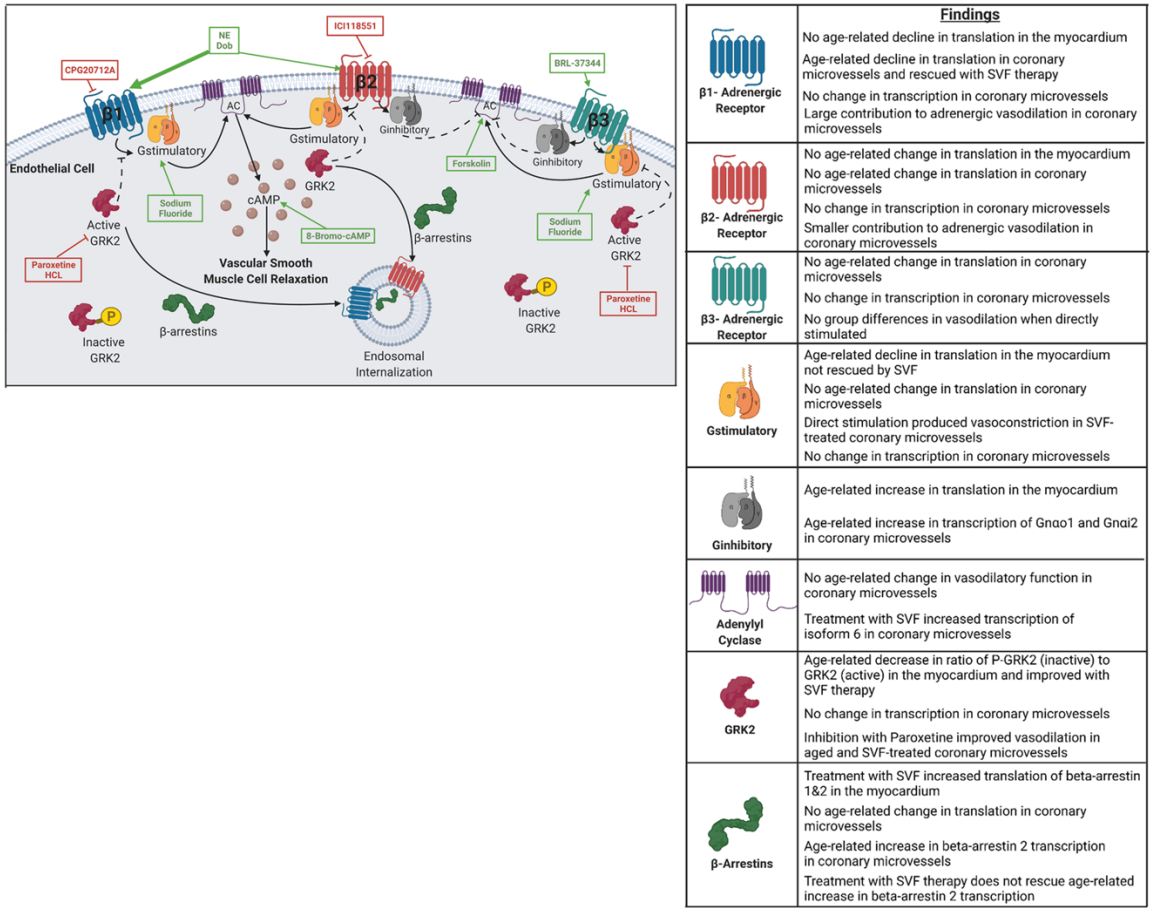

Figure 3.8: Summary of adrenergic signaling with alterations due to aging and SVF therapy.

In an aged coronary microvessel, there is a decrease in the β1-AR populations and vasodilation to β1-AR agonists is reduced. Adrenergic signaling is inhibited through GRK2 and Gαi proteins which are significantly increased in the aged myocardium and marginally increased in coronary microvessels. SVF cell therapy restores some vasodilatory capacity via rescuing β1-AR populations through post-translational modifications of GRK2 and the receptor recycling proteins beta-arrestins, as well as diminution in Gαi proteins. Green text represents activators whereas red text represents inhibitors. The thicker arrow pointing from NE to the β-ARs indicates higher antagonism

toward β1-AR compared to β2-AR. Solid black arrows indicate positive effects of cell signaling while dashed lines indicate negative or inhibitory effects. A key and a summary of findings are shown to the right. Image created with BioRender.com.

Supplemental Figure 3.1

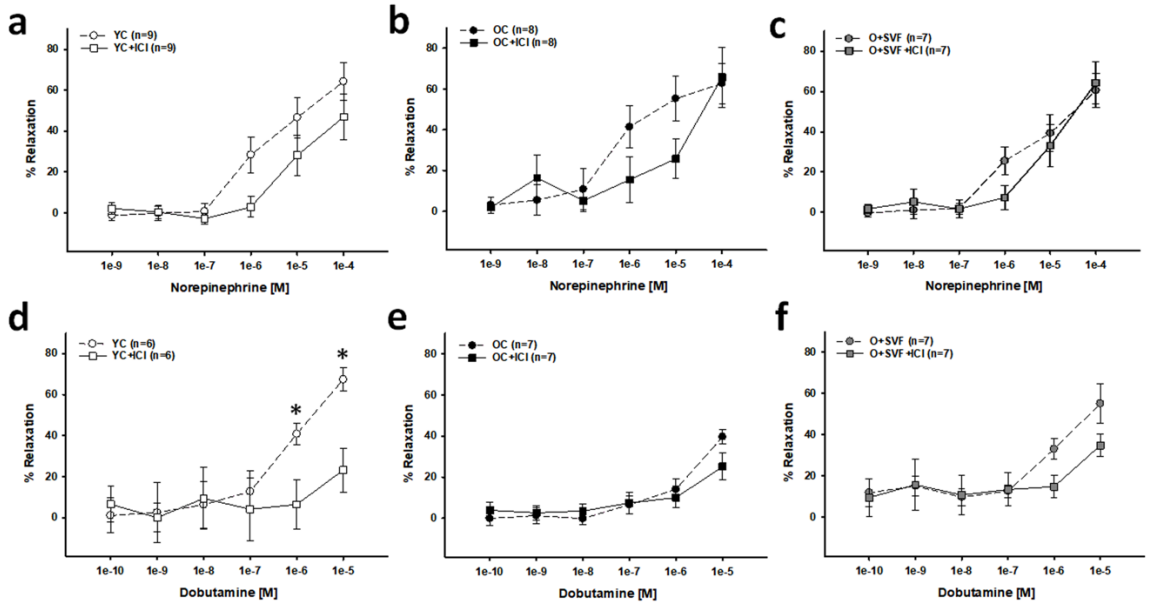

Supplemental Figure 3.1: Contribution of the β2- adrenergic receptor to adrenergic-dependent vasodilation.

Using pressure myography, isolated coronary microvessels from YC, OC, and O+SVF animals were subjected to β-AR agonism with NE with and without the β2-AR inhibitor ICI118551 (**A-C**) or dobutamine with and without the β2-AR inhibitor ICI118551 (**D-F**). Data are presented as means±SEM. Significance defined by paired pre- to post-inhibition for analysis using Two-way Repeated Measures ANOVA with Bonferroni *post hoc* testing. $p < 0.05$ when pre- vs. post-inhibition (*).

Supplemental Figure 3.2

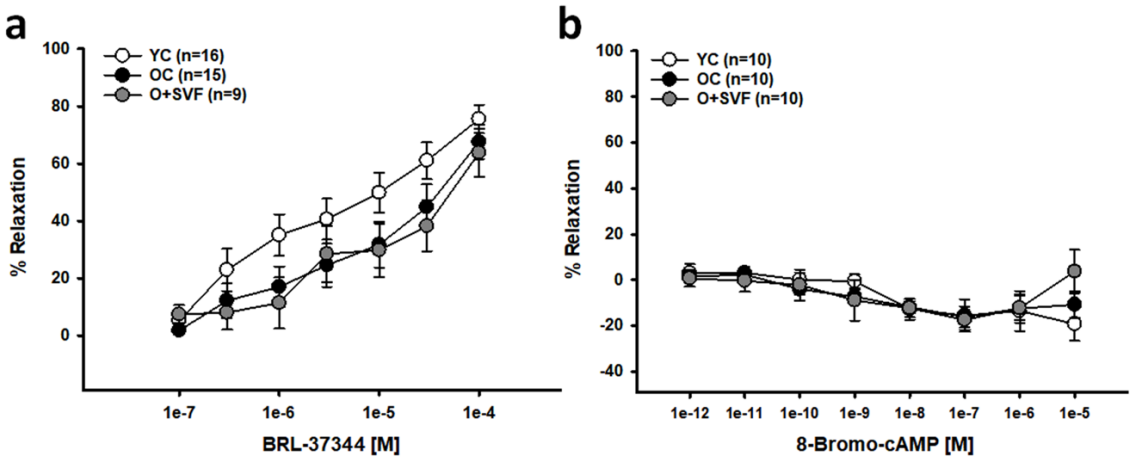

Supplemental Figure 3.2: Contribution of the β3- adrenergic receptor and cAMP to adrenergic-dependent vasodilation.

BRL-37344, a β3-AR agonist (**A**), and 8-Bromo-cAMP, a cAMP donor (**B**), were added in a dose-dependent manor to isolated coronary microvessels from YC, OC, and O+SVF animals via pressure myography. Data presented as means±SEM. Significance determined as $p < 0.05$ utilizing Two-way Repeated Measures ANOVA with Bonferroni *post hoc* analysis.

Discussion

In this study we hypothesized that SVF restored β1-AR function by blunting downstream negative regulatory factors i.e. GRK2, Gαi, and β-arrestin and promoting positive regulatory factors i.e. Gs that are altered by aging. Although aging significantly reduced positive and enhanced negative regulatory factors, SVF only partially restored these to youthful levels. The major finding of this study is that i.v. administered SVF restored the population of β1-AR in coronary microvessels compared to old controls. Advancing age desensitized the β1-AR through increased GRK2-dependent phosphorylation of the adrenergic receptor and increased Gαi levels. Furthermore, when AC was directly activated, neither age nor SVF treatment showed any difference from young vessels, suggesting age-related microvascular dysfunction is above the level of AC in the adrenergic signaling cascade. Additional findings are summarized in **Figure 3.8**.

This study assessed the functionality of the microvasculature in female rats. Our rationale for this is that as age progresses in humans, coronary vascular disease (CVD) and coronary microvascular disease (CMD) manifests in the sexes differently. Unlike men who predominately present with large vessel-CVD, as many as 50% of women referred for cardiac evaluation do not have obstructive coronary disease but present with coronary microvascular dysfunction/ischemia [114]. Impairment in endothelial function can begin developing as early as 40 years with most clinical manifestations apparent around 50 years of age followed by a steep decline in endothelial function after menopause [47]. The ages and strain of rat were chosen because the varying stages of estrous have no effect on vasodilatory capacity in coronary arterioles from young female Fisher 344 rats, but rather, advancing age and eventual loss of circulating estrogen

impairs the coronary microvasculature in an endothelial-dependent fashion [260], mimicking the clinical scenario. Since the small resistance arterioles of the microvasculature govern the blood flow through an organ, impairment and/or improper augmentation of blood flow to meet organ oxygen demand can result in tissue ischemia which can progress to organ failure [39, 45].

The traditional pharmaceuticals currently available for HF and vascular diseases are targeted at mitigating one aspect of multifactorial pathologies, which contrasts with the multi-faceted gains seen in cell-based therapies [126]. The current paradigm is that cell-based treatments provide therapeutic gains through the release of paracrine factors [141], like exosome release [142], and/or cellular engraftment into the host tissues [143]. SVF administered via tail vein injection can disseminate and engraft into the myocardium improving left ventricular function [42], while exosomes from mesenchymal cells have also been shown to preserve cardiac function following a myocardial infarction (MI) [261]. One possible mechanism for the therapeutic gains seen by mesenchymal-derived exosomes is through mitigation of oxidative stress [262]. In recent years, studies have demonstrated equal efficacy for SVF and bone marrow mesenchymal cells in treating myocardial ischemia [192, 193], promoting angiogenesis [194], and reducing inflammation [195]. SVF is inherently a heterogeneous cell population comprised of mostly endothelial cells, smooth muscle cells, pericytes, hematopoietic cells such as macrophages and T-cells, and a small number of mesenchymal stem cells (MSC) [176]. These various cell types are theorized to be an optimal milieu of environmental cues to stimulate SVF engraftment or release of paracrine factors within a tissue [186]. Ease of isolation and the availability of autologous SVF sources confer inherently minimal risk of

rejection [177]. Despite these benefits of cell-based therapies, there are few studies conducted using advanced age as the model of pathology as utilized in the current study.

An increase in sympathoadrenal catecholamines in response to HF correlates not only with the severity of HF [219] but also with the severity of β-AR desensitization in the myocardium with age [263]. We have shown that the catecholamine NE is increased with age when measured in the urine (**Table 3.1**) as well as in the plasma [39]. While initially protective against a declining cardiac output [84], chronic adrenergic stimulation can cause desensitization of the vascular β-ARs [85]. Using immunofluorescence, we measured a decline in β1-ARs with advancing age in isolated coronary microvessels when compared to YC (**Fig 3.2**). While helpful in preserving myocardial β-AR sensitivity, first-generation beta-blockers are non-specific [127] and little is known of their consequence to the vasodilatory function of coronary microvessels. Coronary microvessels are primarily dependent upon β1-AR contribution as shown by near complete abrogation of vasodilation after receptor inhibition with CPG20712A in all groups (**Fig 3.3 A-C**). In this study we show that SVF could be an ideal therapeutic for age-related coronary vascular dysfunction as it did not increase β1-AR populations in the myocardium (**Fig 3.1**) but did increase β1-AR populations in the coronary microvasculature (**Fig 3.2**). Even though SVF was associated with restoring the β1-AR population (**Fig 3.2**) and increasing coronary perfusion to adrenergic agonists [39], the therapeutic action of SVF does not appear to be due to increased transcription of the adrenergic receptors in a rat model (**Fig 3.7**). While β2- and 3-ARs are present in the coronary microvasculature (**Fig 3.2**), we measured no age or group differences in

vasodilation to β2-AR (**Supplemental Fig 3.1**) or β3-AR (**Supplemental Fig 3.2 A**) agonists.

Following ligand binding to the β-AR, signal transduction is regulated first by GRK2, which phosphorylates the internal tail of the receptor, initiating endocytosis [264]. GRK2 has different affinities for the β1- and β2-ARs, phosphorylating differing locations on the receptor tail [265]. Ungerer and colleagues measured an increase in transcription of GRK2 in myocardial samples from patients with HF averaging 50 years of age [251], but this does not match our own assessments of mRNA transcripts of GRK2 in the coronary microvasculature (**Fig 3.7**), highlighting the possible difference in expression between myocardium versus microvessel tissues. Over the course of two studies, Schutzer et. al showed that GRK2 increased activity in the aorta of aged rats [266], and this was directly related to a decline in β-AR functionality in aged rat coronaries [249]. GRK2 phosphorylation of the β-AR initiates receptor endocytosis through beta-arrestin-mediated binding and scaffolding, but the sequence differences between the β1- and β2-AR result in the β2-AR having higher affinity for GRK2 and thus higher recruitment of beta-arrestins when compared to the β1-AR [267]. In this study, we showed that SVF treatment increased protein expression of both beta-arrestins 1&2 in the myocardium (**Fig 3.6 A**), and transcription of beta-arrestin 2 mRNA is higher in coronary microvessels in OC (**Fig 3.7**). As previously described, the sequence differences in the adrenergic receptors lead to the beta-arrestins binding at different affinities, with beta-arrestin 2 having a higher affinity for the β1-AR [268]. Once internalized, Liang and colleagues showed that the β-ARs are sorted into different endosomal compartments where the β2-AR is dephosphorylated and redistributed back to the membrane while β1-AR

redistribution was not comparable [265]. Building off the literature as well as data currently presented, one possible mechanism for the restoration of the β1-AR population and gain in vasodilatory function following SVF therapy could be a redistribution of this receptor through the beta-arrestin - receptor recycling axis.

The role of GRK2 in β-AR desensitization has led to study of its inhibition as a potential therapeutic, both for treating HF [269] and for directing favorable myocardial remodeling following MI [270]. Paroxetine HCl is a small molecule that binds and stabilizes the active site of GRK2, leading to inhibition of kinase activity [271]. Utilizing pressure myography, we showed an improvement in vasorelaxation to NE following GRK2 inhibition with Paroxetine in our aged groups (OC and O+SVF) but not in YC (**Fig 3.4 C-E**), as well as a reduction in the ratio of phosphorylated GRK2 (naturally inhibited) to total GRK2 levels in the myocardium of OC vs. YC rats (**Fig 3.4 A**). Further, we showed that SVF therapy shifted the naturally inhibited (P-GRK2) to active (total) GRK2 ratio, resulting in levels returning to YC (**Fig 3.4 A**). It is interesting to note that a study conducted by Eckhart and colleagues using a transgenic mouse model of GRK2 overexpression led to increased vascular wall thickness and depleted vasorelaxation to isoproterenol [272]. Similarly, we observed an increased wall thickness in our aged groups (**Table 3.2**). Taken together these data suggest that with advancing age there is an increase in GRK2 activity in coronary microvessels that SVF does not reverse, but instead possibly alters the kinase activity via phosphorylation status of GRK2.

The G-proteins associated with the adrenergic receptors elicit vasodilation or vasoconstriction through the specificity of the associated G-proteins [273]. Unlike the β2-

AR which is associated with a Gs and a Gαi protein, the β1-AR is only directly associated with a Gs [7]. We used the small molecule, NaF, to directly activate the Gs protein in pressurized isolated coronary microvessels and observed significantly reduced relaxation in vessels from SVF-treated rats compared to YC and OC throughout the lower doses, but significantly higher relaxation compared to YC at the last dose (**Fig 3.5 D**). This data fits into a mixed field as Weber and colleagues reported NaF promoting a vasoconstriction response in mesenteric arteries from old rats [274] but is contrary to Cushing and colleagues reporting NaF vasodilation as an endothelial-dependent mechanism in porcine, bovine, canine, and human coronary arteries [275]. When examining Gs levels in isolated coronary microvessels, there was no difference due to age or SVF treatment (**Fig 3.5 C**). Yet in the myocardium, the Gs protein was reduced in both the OC and the O+SVF treated groups (**Fig 3.5 A**). Even though the Gs protein initiates the signaling cascade for vasodilation following β1-AR activation, crosstalk between Gs and Gαi can occur [276, 277], and both govern AC activity [278]. As previously mentioned, the activity and levels of Gαi have been shown to increase in the myocardium with HF [244, 245]; furthermore, a study conducted by Janssen and colleagues showed that adenovirus-directed overexpression of Gαi2 attenuated β-AR signaling in rabbit myocytes [279]. We measured an increase in Gαi1 in the myocardium of OC rats that is not reversed following SVF therapy (**Fig 3.5 B**). When we examined mRNA expression of inhibitory G-proteins in isolated coronary microvessels, we found an increase in Gnαo1 and Gnαi2 with age compared to young (**Fig 3.7**). While many studies have examined the effect of age or HF on Gαi levels in the myocardium and the ability of Gαi to cross-inhibit β1-AR mediated contractile response [280], few studies have examined

the effect of age on Gαi in the coronary microvasculature. It is important to note that vasodilation is not only adrenergic-dependent, but can also be elicited through nitric oxide (NO) production, which is more commonly associated with youth [281], and endothelial-derived hyperpolarizing factors, which are more commonly associated with age [282]. Gαi and Gnαo proteins can prompt vasodilation through the two alternative aforementioned pathways [283]. These data lend consideration that SVF works to restore microvascular health through shifting the vasodilatory mechanism back from hyperpolarization and more toward NO in conjunction with increased β-AR sensitivity, but future studies are needed to address this possibility.

Not only is cAMP production by AC the convergent point in β-AR and α2-AR signaling [284], but it is a common second messenger in other intracellular signaling cascades. Studies have shown that the myocardium expresses two main isoforms of AC, isoforms 5 and 6 [285]. Disruption of the AC isoform 5 led to prolonged life and increased resilience to apoptosis following MI [285], indicating its native deleterious effects. On the other hand, AC6 has been shown to be cardio-protective [286]. Compellingly, we have shown that there is a significant age-related reduction in mRNA transcription of AC6 in the coronary microvasculature, although SVF does not restore AC6 transcription back to levels seen in YC (**Fig 3.7**). To examine the functionality of AC in prompting vasorelaxation, we used forskolin to directly activate AC in isolated and pressurized microvessels, but no differences between the groups were found (**Fig 3.6 C**). While transcription of the cardio-protective AC isoform 6 may be reduced with age, functionality is intact (**Supplemental Fig 3.2 B**), conveying that age-related

microvascular dysfunction and improvement following SVF administration occur above the level of AC.

Conclusion

Coronary vascular function is compromised by as much as 43% with advancing age which can contribute to the prevalence of cardiovascular diseases (CVDs) and coronary microvascular disease (CMD) [52]. Our previous studies have shown that i.v. injected SVF incorporate into the cardiac and vascular spaces [42], improve vasodilation to adrenergic agonists as measured by coronary flow reserve, and remain detectable in aged rats four weeks post-injection [39]. At the present time, the field of cellular therapeutics is still exploring if benefits of injected cell therapies are a result of secreted factors through exosomes, the cells themselves engrafting into the tissues, or a combination of these [287]. While the mechanisms of cell therapy, SVF in particular, are still being evaluated, age-related beta-adrenergic desensitization has been targeted for pharmacological therapeutics to treat declining function in the myocardium. The data presented here investigated the effect of age on beta-adrenergic desensitization throughout the signaling cascade in cardiac tissues. We examined the differences between myocardial tissues and the microvascular tissue, and the effect age has on each signaling component. To our knowledge, this is the first time that coronary arterioles isolated from an aged rodent model have undergone RNAseq analysis to compare transcriptional changes to youth and cell therapy regime. Furthermore, we provide exciting evidence that SVF works to improve adrenergic-mediated vasodilation through re-establishing the β1 receptor population and reducing the aged effect of signal transduction inhibitors, GRK2

and Gαi, thereby improving vasodilation. These results lay significant groundwork for future studies on cell therapy and resultant sympathoadrenal and β-AR signaling.

Limitations and Future Directions

It is important to consider the limitations of the present study: 1) All of the rats in this study were females. Our rationale for this is that as age progresses, women more often present with microvascular dysfunction. Specifically, as many as 50% of women referred for evaluation of MI present with coronary microvascular dysfunction/ischemia rather than obstructive coronary disease, like most men, due to the loss of the protective effects of estrogen [114]. The males of the Fisher 344 strain have also been shown to develop coronary microvascular reactivity impairments with age [288], but we do not know if the findings in the current study persist in the male sex. 2) Data presented in this study sought to examine age-and SVF-related changes of beta-adrenergic signaling proteins in myocardial and microvascular tissues. Future studies will be needed to explore both sides of the cell therapy paradigms, i.e. paracrine versus engraftment, to elucidate the therapeutic mechanism of the SVF-mediated increase in beta-1 adrenergic receptor population. 3) Myocardial tissue samples were used for western blotting due to the anatomical limitations of the coronary microvasculature. Nonetheless, Next Gen sequencing of mRNA isolated from the pooled coronary microvessels yielded an extensive library of data (**Supplemental Table 3.1**) and immunofluorescence of specific adrenergic signaling targets were used in place of western blotting. Further examination of the RNA sequencing data and current literature could provide insight into SVF-mediated changes to transcription factors for genes involved in regulating the beta-

adrenergic receptor as part of SVF's therapeutic mechanism. 4) Future studies will use pertussis toxin to inhibit the Gαi protein to examine its contribution in microvascular functionality. 5) Furthermore, we also plan to inhibit beta-arrestin pharmacologically in isolated coronary microvessels to examine if there is an improved adrenergic vasodilation response in the OC group. The heterogeneous properties of the various cell populations within the SVF provide more than one outlet for improving vascular function and health within an aged microvascular network which the authors will continue to investigate in subsequent studies.

CHAPTER 4

REVERSAL OF AGING-RELATED IMPAIRMENT IN REVASCULARIZATION FOLLOWING INJURY BY ADIPOSE-DERIVED STROMAL VASCULAR FRACTION IS NOT WHOLLY T CELL MEDIATED.

Overview

Advancing age drives a decline in vascular function i.e. angiogenic potential increasing ischemic risk and impairing revascularization following an ischemic injury. Adipose-derived stromal vascular fraction (SVF) has emerged as a potential regenerative therapeutic following injury, but few studies have been conducted in the setting of advanced age. Importantly, which specific cell type(s) in SVF are responsible for therapeutic gains are still unknown. We hypothesized that aging would alter the composition of cell populations present in SVF and its ability to promote angiogenesis following injury, a mechanism that is T cell mediated. SVF isolated from young (4-9 mo) and old (24 mo) GFP+ Fischer-344 rats were examined with flow cytometry for cell composition. Mesenteric windows from old rats were isolated with or without exteriorization-induced (EI) hypoxic injury; upon surgical closure, animals received intravenous injection of one of four cell therapies: SVF from young or old donors, and SVF from old donors depleted or enriched of T cells. Three days later, mesenteric windows were removed and cultured for up to 5 days. Advancing age increased the SVF T cell population but reduced revascularization following injury. Both young and aged SVF engrafted throughout the host mesenteric microvessels but only young SVF

significantly increased vascular area following EI. T cell depletion did not affect the angiogenic potential of SVF. This study highlights the effect of donor age on SVF angiogenic efficacy and demonstrates how the *ex vivo* mesenteric window model can be used in conjunction with SVF therapy to investigate its contribution to angiogenesis.

This chapter is from the published work referenced as follows:

Rowe, G., et al., *Reversal of Aging-Related Impairment in Revascularization Following Injury by Adipose-Derived Stromal Vascular Fraction is not Wholly T cell Mediated.* J Vas Res, 2022. *in peer review*

Introduction

The microvasculature primarily control and regulate blood flow through an organ, but impairment of blood flow can result in tissue ischemia [39, 40, 45]. As aging progresses, aberrant physiological remodeling responses can serve as the foundation that eventually limit tissue plasticity during pathophysiological remodeling following injury [43]. The increase in systemic oxidative stress [58], cellular senescence [59], and chronic inflammation [60] that are characteristics of advancing age have been linked to endothelial cell dysfunction and a decline in the capacity of a microvascular network to sprout new vessels via angiogenesis and collateralization.

Current medications and surgical interventions utilized after an ischemic event act by decreasing organ workload, mitigating inflammation, or grafting of large vessels to redirect blood flow, but none target the multifactorial pathology of endothelial cell dysfunction to promote growth of the microvasculature [69]. These treatments stand in contrast to the gains observed in cell-based therapies [126]. Adipose tissue contains an abundant source of multipotent cell populations such as mesenchymal stem cells (MSCs), endothelial cells, pericytes, and hematopoietic cells including macrophages, T cells, and other cells of the perivascular niche [176, 185]. Of note, T cells have been shown to play a role in stimulating angiogenesis in ischemic areas [289] due to migration to the area of injury [290, 291] and collateralization specifically by homing to sites of active angiogenesis [292]. In recent years, studies have demonstrated equal efficacy for SVF and bone marrow MSCs in treating myocardial ischemia [192, 193], promoting angiogenesis [194], and reducing inflammation [195]. Availability of autologous and allogenic SVF sources confer inherently minimal risk of rejection [177], offering an ideal

candidate in vascular therapeutics due to the ability to leverage an easy-to-harvest, real-time, point-of-care therapeutic approach [178]. Despite these benefits of cell-based therapies, there are few studies conducted using advanced age as the model of pathology and examining the impact of donor age on the vasculogenic properties of cell therapy as utilized in the current study.

To investigate the effect of age on SVF cell populations as well the potential to increase angiogenesis in an aged microvasculature, we utilized an *ex vivo* model comprised of connective tissues located along the intestinal mesentery termed mesenteric windows [293]. The *ex vivo* mesentery culture model developed by the Murfee laboratory was utilized in this study for ease of access, time-lapse imaging capabilities, and survivability in culture [294]. This model has shown the functional effect of pericytes on tip cell formation and maintenance of *in vivo*-like endothelial cell phenotypes along capillary sprouts during active angiogenesis [295-298]. Furthermore, exteriorization injury (EI) of the tissue has been shown to be a reproducible model to induce acute hypoxia and stimulate angiogenesis [299, 300], but has not been previously used in a setting of advanced age. Prior studies from our laboratory have shown that systemically delivered SVF from young donors can improve coronary microvascular perfusion in aged rats [42]. Furthermore, a single intravenous (i.v.) injection of SVF from young donors resulted in a biodistribution of cellular engraftment across various organs and blood vessels [42]. However, the therapeutic potential of SVF from aged donors on tissue perfusion was not studied nor were changes in vascular density as a result of cell administration examined. This study aimed to leverage the benefits of the mesenteric *ex vivo* prep to investigate the impact of donor age on vasculogenic potential in a setting of

advanced age and injury with intravenously administered SVF therapy. We hypothesized that SVF from aged rats would exhibit increased inflammatory cell populations (M1 macrophages and T cells), limit the ability of the microvasculature to collateralize following hypoxic injury and reduce the angiogenic potential which is T cell mediated compared to SVF isolated from young rats.

Materials and Methods

Animal model.

The Institutional Animal Care and Use Committees of the University of Florida and the University of Louisville approved this study, and all procedures followed the NIH *Guide for the Care and Use of Laboratory Animals* [254]. Young (3-9 months) and aged (23-24 months) of male and female Fischer 344 rats (Harlan Laboratories, Indianapolis, IN, USA and National Institute of Aging, Bethesda, MD, USA, respectively) were group housed with free access to food and water and maintained on regular 12-hour light/dark cycles. Green fluorescent positive (GFP+) transgenic Fisher 344 male and female rats, maintained in house (Louisville), aged 3-9 and 24 mo were utilized as SVF donors. All rats were acclimated to facility conditions for a minimum of one week then randomly divided into the experimental groups described in detail below and depicted in **Figure 4.1**.

SVF isolation and experimental groups.

SVF cells were isolated as previously described [40, 298]. Briefly, epididymal/ovarian fat pads from young (4-9 mo) or aged (24 mo) Fischer 344 donor rats were harvested, mechanically homogenized and digested with a collagenase and deoxyribonuclease-1 enzymatic solution. Following centrifugation, the buoyant adipocyte

layer was removed. SVF cells were washed, filtered through a 20 μm nylon screen to remove large cell or tissue aggregates, then prepared for flow cytometry analysis, treatment of cultured mesenteric windows (Experimental Group 1), intravenous (i.v.) tail vein injection into experimental animals (Experimental Groups 2 and 3), or modification using magnetic antibody cell sorting prior to i.v. injection into experimental animals (Experimental Group 4).

Flow cytometry.

Following isolation, the fresh SVF from young and aged donors was incubated in rat Fc Block Mix (BD Biosciences 550271) at 4°C for 20 min protected from light. Cells were then stained for cell surface markers with the appropriate monoclonal antibodies at 4°C for 30 min also protected from light. **Supplemental Table 4.1** contains the antibodies included in each staining panel used in this study along with dilations. During the incubation, anti-mouse IgG kappa compensation beads and negative control beads (BD Biosciences 552843) were added to each compensation tube; antibodies (positive compensation) or fluorophore-conjugated IgG (negative compensation) were added to the appropriate tubes. Following antibody incubation, red blood cells were lysed with diluted Lyse buffer (BD Bioscience 5558999) and tubes were vortexed, incubated for 3 min at 37°C, spun at 350 g for 5 min, then cells washed twice with wash buffer. For the tubes requiring CD68 staining, cells were fixed and stained with MACS Inside Stain Kit (Miltenyi Biotec 130-090-477) according to manufacturer's instructions. Data was collected on an LSR II cytometer (BD Biosciences) and analyzed with FlowJo 7.6 software (Tree Star, Ashland, OR, USA).

Experimental group 1.

SVF was isolated as described [40, 298]. Young or aged Fisher-344 rats were anesthetized with an intramuscular injection of ketamine (80 mg/kg body weight) and xylazine (8 mg/kg body weight). Rat mesenteric tissues were harvested and cultured according to a previously established protocol [301-303]. Briefly, an incision was made along the linea alba, and the mesentery was placed onto a sterile plastic stage using cotton tip applicators to first remove the cecum and subsequently the ileum and jejunum. The rat was euthanized with an intracardiac injection of 0.2 ml Beuthanasia. Vascularized mesenteric tissues were excised and rinsed once in sterile saline (Baxter 2B1324X) and immersed in minimum essential media (MEM; Gibco 11095-072) containing 1% Penicillin-Streptomycin (PenStrep; Gibco 15140122) at 37°C.

To determine the effects of age on SVF transplantation therapy the following groups were utilized: young SVF + young tissue, young SVF + aged tissue, aged SVF + young tissue, and aged SVF + aged tissue (n=8 tissues per group; tissues per group were harvested from 2 rats). Freshly isolated SVF cells were suspended in 10% FBS + MEM solution at a concentration of 10 million cells/mL. Tissues were the spread onto a polycarbonate filter membrane (pore size = 5 μm) on a cell crown insert (Millipore Z681792-3EA) where 100 μL of SVF cell solution was transferred to the surface of each mesenteric window. Windows and cells were incubated for 20 min to allow attachment of SVF cells to the tissue. Cell crowns were then inverted into 6-well culture dishes (Cellstar 657 160) with the fat of the tissue pressing against the bottom surface. Three milliliters of culture medium composed of 10% FBS + MEM was added to each well on

top of the filter. Tissues were cultured in standard incubation conditions (5% CO_2, 37°C) for 3 days.

After 3 days in culture, tissues were spread on glass slides before being rinsed 3 times for 10 minutes in PBS +0.1% saponin (Sigma Aldrich S7900). Fat around window was removed and a hydrophobic marker was applied around the tissue. The tissue was then labeled with PECAM at 1:200 (BD Pharmigen555026) and cover slipped.

Images were acquired using 4x (dry, NA = 0.1), 10x (dry, NA = 0.3), and 20x (oil, NA = 0.8) objectives on an inverted microscope (Nikon Eclipse Ti2) coupled with an Andor Zyla sCMOS camera. Image analysis and quantification were done using ImageJ 2.0.0-rc-54 (U.S. National Institutes of Health, Bethesda, MD). Images were quantified as percent vascularized area for each tissue in order to evaluate angiogenic effect of SVF transplantation on networks. Vascularized areas were measured by drawing the perimeter along the edge of the vascular networks. Avascular regions within the network smaller than 130 μm^2 were subtracted from the vascularized area metric. The final vascularized area was divided by the total tissue area.

Two-way ANOVA with pairwise Tukey's multiple comparisons *post-hoc* tests with interactions were used to test for statistical significance between the groups *($p < 0.05$)*. Statistical analysis was performed using SigmaStat ver. 3.5 (Systat Software, San Jose, CA, USA). Values are presented as means±SEM.

Experimental group 2.

Previously isolated frozen GFP+ SVF cells were reconstituted 10 million/mL in 1 mL Lactated Ringer's solution (warmed to 37°C) as previously described [39, 40]. Aged

female rats were injected i.v. via tail vein with SVF from young donors (O+YSVF, n=4) or SVF from aged donors (O+OSVF, n=4). Three days after injection, aged rats treated with SVF were anesthetized with inhaled 5% isoflurane with 1.5-2.0 L/min oxygen flow through an induction chamber. After confirmation of a lack of a tactile reflex, the thoracic cavity was opened, and rat euthanized via cardiac removal. Mesenteric windows were isolated (6 tissues per animal) and placed individually in a 6 well dish on a crown insert with membrane as previously described [301-303]. Windows were then cultured in MEM media + 1% Penicillin-Streptomycin (Sigma-Aldrich PO7881) and cultured for up to 5 days at 5% CO_2 and 37°C.

After 1 or 3 days in culture, the windows were affixed to glass slides, fixed in 4% paraformaldehyde overnight, then rinsed in 1xPBS before being dried and stored at -20°C. Windows were washed x3 with PBS before being permeabilized in 0.5% Triton X-100/0.1 M glycine at room temperature (RT) for 30 minutes. After rinsing x3 in PBS slides were blocked with 5% normal donkey serum (Jackson ImmunoResearch 017-000-121) and 1.5% bovine serum albumin in 1xPBS at RT for 1 hour. Rabbit anti-rat CD3 (1:200, Abcam ab16669), and the fluorescent probe Griffonia (Bandeiraea) Simplicifolia Lectin 1 (GS-1) rhodamine (1:100, Vector Laboratories RL-1102) were diluted in 1.5% BSA-PBS to be incubated on the tissue at 4°C overnight. After x3 washes in PBS, the slides were incubated in secondary antibody solutions made in 1.5% BSA-PBS containing donkey anti-mouse IgG Alexa Fluor 647 (1:400, Abcam ab150111) or donkey anti-rabbit IgG Alexa Fluor 647 (1:400, Abcam ab150063) for 1 hour at RT. Slides were then washed, incubated with DAPI (Invitrogen P36962) and coverslipped using Fluoromount-G (SouthernBiotech 0100-01).

Image stacks were acquired using a Nikon C2+ confocal microscope (Melville, NY) with 20x objective + Nyquist resolution (final magnification ~70x), and 0.85 μm Z-step size with 10 slices/stack. GFP signal was excited with 488 laser alone rather than antibody detection. One mesenteric window from an old control (no cell injection) was utilized as a negative control. Visualization of co-localization of GFP+, CD3+, and DAPI (nuclei) was done using ImageJ (n=1/group).

Experimental group 3.

The methods for this surgical procedure have been adapted from the protocol described by Yang et al. [299]. Aged female Fisher 344 rats were anesthetized with inhaled 5% isoflurane with 1.5-2.0 L/min oxygen flow through an induction chamber. The animal's abdomen was prepped by shaving and then sterilized with 70% isopropyl alcohol and animal placed on heating pad. Under sterile conditions, a 3-cm opening was made through abdominal skin and muscle. Gently, a section containing 8-10 mesenteric windows was removed from the body cavity and placed onto a sterile plastic stage placed on top of the abdomen. This action exteriorizes the windows from the abdominal cavity but leaves all blood flow to the intestines and mesentery intact, resulting in an exteriorization injury (EI). The windows were bathed in sterile physiological salt solution warmed to 37°C throughout the 20-minute exteriorization procedure. The borders around the exteriorized zone were marked with 5-0 silk loops to ensure proper identification at explant, then the intestines and windows were placed back into the abdominal cavity and the incision closed with 5-0 silk sutures. A subset of animals was randomly allocated to a no cell control (NCC) group (n=4). Previously frozen SVF cells were thawed and

prepared as described above and injected via tail vein, at 10 million cells/mL in warmed Lactated Ringer's solution (O+YSVF and O+OSVF, n=4/group). The animals were subcutaneously injected on-time with a 1.2 mg/kg body weight buprenorphine slow release and monitored daily to evaluate post-operative recovery.

Three days after EI, mesenteric windows were isolated as described above both from EI regions and non-exteriorized (NEI) regions of the mesentery (6 tissues per condition per animal). Isolated windows were cultured individually in a 6 well dish on a crown insert with membrane as previously described [301-303]. During the mesenteric window culture, at days 0, 3, and 5, MEM + 1% PenStrep media was supplemented with 3mL of GSL-I Rhodamine (1:40 dilution) in MEM. Windows were incubated at 37°C for 20 minutes, rinsed with MEM media, then 3mL of fresh MEM+1% PenStrep was replaced. The 6 well plates were imaged on a Zeiss Z.1 Axio Observer with a sterile heated incubation chamber; 10x images were acquired in the same location for each mesenteric window over time. Images were processed in ImageJ by thresholding and conversion to binaries. Extraneous cells not a part of the microvascular network was excluded based upon circularity. Percent vascular area, or the area the microvessels occupy in the image, was measured via analysis of mean area. Conversion of the binary to a skeleton allowed for pruning of false branches. Analysis of the pruned skeleton images yielded total vessel length, average vessel length per segment, number of segments, and number of branches. Image analysis protocol modified from Strobel et al. [304]. Data are represented as box and whisker plots. Statistical analyses were performed in SigmaPlot 14.0 (Systat, San Jose, California, USA) with $p < 0.05$ as the significance level. Multiple Two-way repeated measures ANOVAs with Bonferroni pairwise

comparisons allowed for comparison of group, day, and injury model on the following angiogenic metrics: percent vascular area, total vessel length, average vessel length per segment, number of segments, and number of branches.

Experimental group 4.

The methods for this cell sorting have been adapted from the protocol provided by Miltenyi Biotec and as previously described in [200]. Previously frozen GFP+ SVF was thawed, washed, counted, and resuspended in chilled MACS buffer with rabbit anti-rat CD3 (1:500, Abcam ab16669) to incubate at 4°C for 30 min. The cell solution was then washed and resuspended in MACS buffer with anti-rabbit IgG microbeads (1:10, Miltenyi Biotec 130-048-602) and incubated at 4°C for 15 min. The cell solution was then washed and added to MS columns (Miltenyi Biotec 130-042-201) which were placed in the magnetic stand (Miltenyi 130-042-108). Once the flow through CD3 depleted fraction was collected, the magnetic column was washed with MACS buffer. To collect the CD3 enriched fraction, the column was removed from the magnetic field, 500 uL MACs buffer added to the column, then the solution gently expelled using the plunger. Once sorted, final cell counts of depleted and enriched populations were performed.

Exteriorization injury and SVF injection was done as described above (Experimental group 3). Sorted cells were reconstituted at 1.1 million cells/mL in 1 mL Lactated Ringer's solution (warmed to 37°C) as previously described [39, 40]. Aged female rats were injected i.v., via tail vein with the CD3+ depleted SVF from aged donors

(O+OSVF CD3-, n=4) or with the CD3+ enriched, 1.1 million CD3+ SVF cells, from aged donors (O+OSVF CD3+, n=4).

Three days after EI, mesenteric windows were isolated as described above both from EI regions and non-exteriorized (NEI) regions of the mesentery (6 tissues per condition per animal). Isolated windows were cultured individually as previously described [301-303]. During the culture on days 0, 3, and 5 the media was supplemented with GSL-1 Rhodamine in MEM and imaged as described above.

Statistical analyses were performed in SigmaPlot 14.0 (Systat, San Jose, California, USA) with $p \leq .05$ as the significance level. Multiple Two-way repeated measures ANOVAs with Bonferroni pairwise comparisons allowed for comparison of group, day, and injury model on the following angiogenic metrics: percent vascular area, total vessel length, average vessel length per segment, number of segments, and number of branches.

Results

Effect of donor age on SVF cell composition.

SVF isolated from young donors has a significantly higher percentage of hematopoietic stem cells (CD34+) and mesenchymal stem cells (CD45-/CD34-/CD90+) **(Fig 4.2 A)**. Young SVF had a significantly higher stromal fraction which can be comprised of fibroblasts, pericytes, and pre-adipocytes **(Fig 4.2 A)**. SVF from young donors contained significantly larger populations of total macrophages, as well as immature and transitional macrophages **(Fig 4.2 B)**. SVF from old donors had a higher percentage of lymphocytes **(Fig 4.2 A)** and M1 inflammatory macrophages **(Fig 4.2 B)**.

Young SVF shows a marked increase in thymocytes compared to SVF from aged rats (approaches significance, p=.057) **(Fig 4.2 A)**. SVF isolated from old donors has a significantly higher percentage of CD3+ T cells , as well as helper and CD4+ memory T cells compared to young SVF. Activated and CD8+ memory T cells are higher in aged SVF compared to young SVF (approaches significance, p=.057) **(Fig 4.2 C).**

Effect of SVF donor age on vascular area.

The varying combinations of host and donor ages resulted in a significant increase between young SVF on young mesenteric tissue compared to all other combinations when seeded and co-cultured (**Figs. 4.3 A and 4.3 E**). There was a reduced level of vascularized area in both aged SVF and aged tissue groups, but regardless of SVF age and tissue age, no one group had strikingly lower vascularized area after three days in culture (**Figs. 4.3 B-D** and **4.3 E**).

Cellular engraftment of SVF into the vasculature of mesenteric windows.

Following i.v. injection of GFP+ SVF, engrafted cells from both donor groups could be detected in and around the mesenteric microvasculature six days after administration **(Fig 4.4 A)**. Previously frozen SVF nor age of donor alters the ability of SVF to engraft into host tissues. Furthermore, some engrafted SVF cells were co-positive for the T cell marker CD3.

Effect of injury and SVF therapy on angiogenesis.

To examine the effect of advanced age on vascular area following injury and the angiogenic therapeutic effect of SVF, mesenteric windows subjected to EI from NCC, O+YSVF, and O+OSVF treated animals were cultured and imaged for up to 5 days. Representative images are shown in **Figure 4.5 A**. In the NEI control windows of the NCC group, the aged and untreated tissue showed a significant increase in vascular area by day 5 compared to day 0. By day 3 in the NEI windows of aged rats treated with young SVF (O+YSVF), there was a significant increase in vascular area compared to day 0. However, in the EI windows of the NCC there is no change in vascular area between any of the days. EI windows of aged rats treated with young SVF (O+YSVF) had a significantly higher vascularized area compared to the NCC. While the O+OSVF treated group showed a modest increase in vascular area in response to injury, it was not significantly different compared to the other EI groups; however, the O+OSVF day 0 EI was significantly higher than its NEI counterpart (*) **(Fig 4.5 B)**. **Supplemental Figure 4.2** displays further angiogenic metrics such as total vessel length **(A-B)** and average vessel length per segment **(C-D)**, number of vessel segments **(E-F)** and number of branch points **(G-H)** in non-injured (NEI) and injured (EI) mesenteric microvascular networks.

Effect of modification of CD3+ cell population on SVF's angiogenic potential.

The implication of modifying the T cell populations in SVF therapy was examined by administering depleted or enriched CD3+ SVF to aged rats following injury, and mesenteric windows were cultured and imaged for up to 5 days (**Fig 4.6 A)**. In the NEI condition CD3 depleted (CD3-) SVF had significantly higher vascular area compared to day 0 at days 3 and 5 **(Fig 4.6 B)**. Further, the CD3 depleted group at days 3 and 5 also had significantly higher vascular area than the CD3 enriched (CD3+) group at

the same time points **(Fig 4.6 B)**. Treatment with CD3 depleted or CD3 enriched SVF in the setting of injury (EI) did not produce differences between the groups at any time points. The CD3+ enriched group in the EI condition at day 5 had significantly higher percent vascular area compared to day 0. This is in contrast to no difference in vascular area observed in the CD3 depleted group for day 5 vs day 0 comparison (p=.126) **(Fig 4.6 B)**. **Supplemental Figure 4.3** displays further angiogenic metrics such as total vessel length **(A-B)** and average vessel length per segment **(C-D)**, number of vessel segments **(E-F)** and number of branch points **(G-H)** in non-injured (NEI) and injured (EI) mesenteric microvascular networks.

Figure 4.1

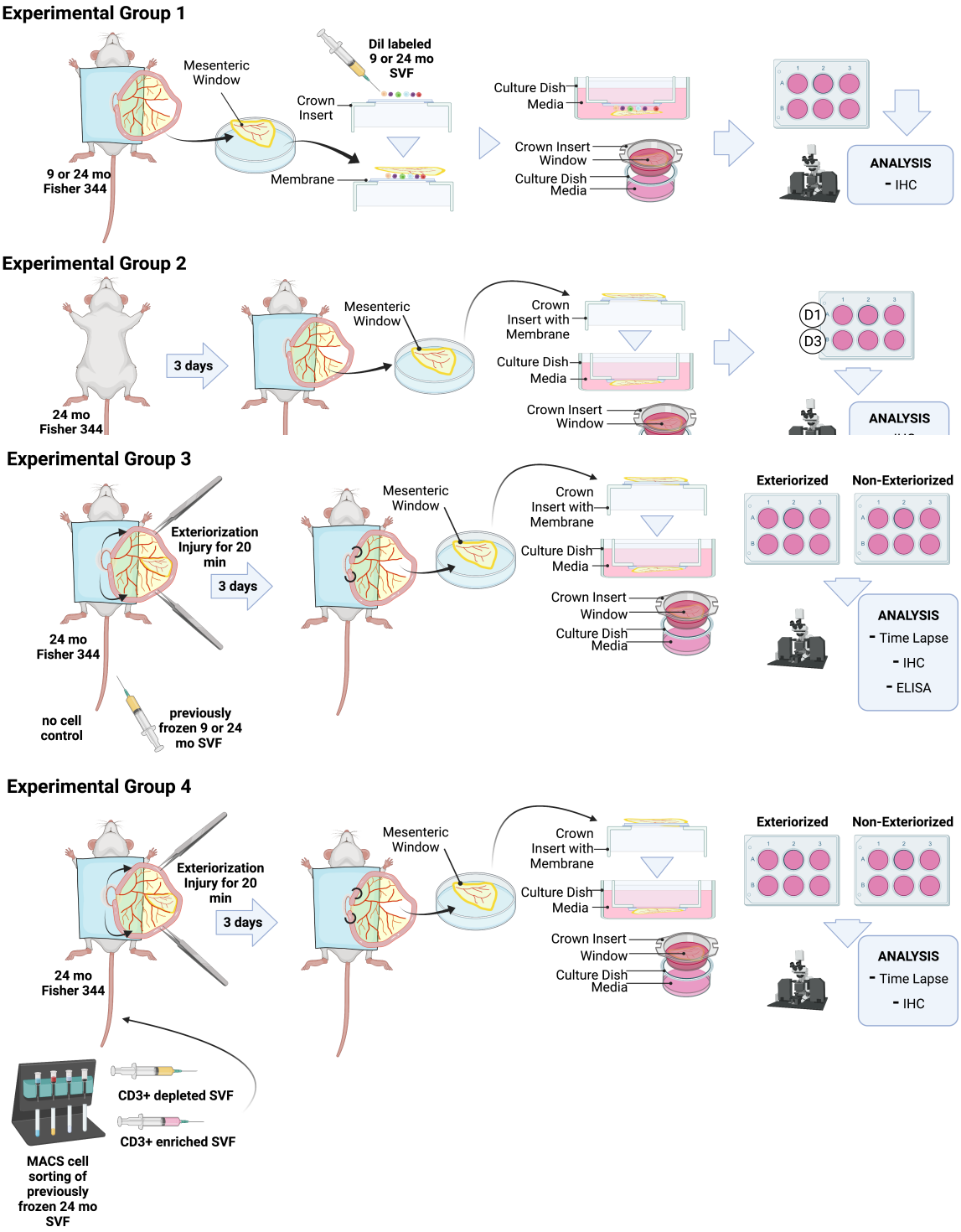

Figure 4.1: Summary of methodology.

Combinations of young or aged SVF cells seeded onto young or aged mesenteric windows was utilized to assess SVF's angiogenic properties influenced by age of donor and/or host **(Group 1)**. Young or aged SVF was administered to aged hosts via systemic administration to assess SVF's engraftment into the host mesenteric microvascular network **(Group 2)**. Exteriorization of the mesentery was utilized to induce injury in aged rats treated with no cells or SVF from either young or aged donors. The microvascular networks of injured windows and non-injured controls were imaged over time to quantify angiogenic growth **(Group 3)**. SVF from aged donors was subjected to magnetic antibody cell sorting to generate CD3 depleted and CD3 enriched SVF fractions. The modified SVF was then systemically administered following exteriorization injury **(Group 4)**. Angiogenic growth in the microvascular networks of injured and non-injured windows was analyzed. Adipose-derived stromal vascular fraction (SVF), CD3+ (T cell marker), cell membrane stain (Dil), exteriorization injury (EI), immunohistochemistry (IHC), magnetic antibody cell sorting (MACS), months old (mo), non-exteriorized/non-injured (NEI). Aged rats treated with SVF from young donors (O+Y SVF), aged rats treated with SVF from aged donors (O+O SVF), aged rats treated with SVF from aged donors depleted of CD3+ T cells (O+O SVF CD3-), aged rats treated with SVF from aged donors containing only CD3+ T cells (O+O SVF CD3+). Image created with BioRender.com.

Figure 4.2

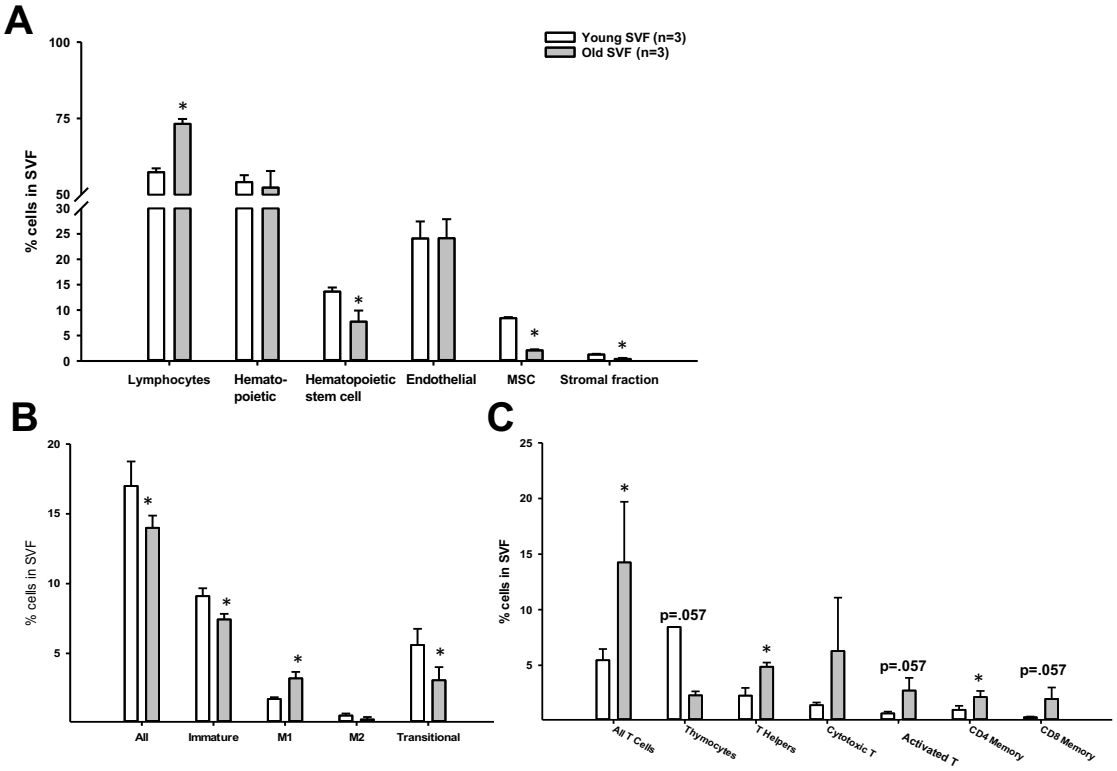

Figure 4.2: Cell composition of SVF from young or aged donors.

Flow cytometry analysis of cell composition for SVF isolated from young or aged donors **(A-C)**. **A)** Lymphocytes (forward and side scatter), hematopoietic (CD45+/CD11b+), hematopoietic stem cell (CD45+/CD34+), endothelial (CD31+), MSC (CD90+/CD45-/CD34-), and stromal fraction (CD45-/CD31-/CD34+). **B)** All macrophages (CD45+/CD11b+/CD68+), immature (CD45+/CD11b+/CD68+/CD86-/CD163-), M1 (CD45+/CD11b+/CD68+/CD86+/CD163-), M2 (CD45+/CD11b+/CD68+/CD86-/CD163+) and transitional (CD45+/CD11b+/CD68+/CD86+/CD163+). **C)** All T cells (CD3+), thymocytes (CD45-/CD90+), helper (CD3+/CD4+), cytotoxic (CD3+/CD8+), activated (CD3+/CD25+), CD4 memory (CD3+/CD4+/CD44+), and CD8 memory

(CD3+/CD8+/CD44+). Data are represented as percentage of cells in SVF mean+SEM, n=3/group. $p < 0.05$ when vs young SVF (*).

Figure 4.3

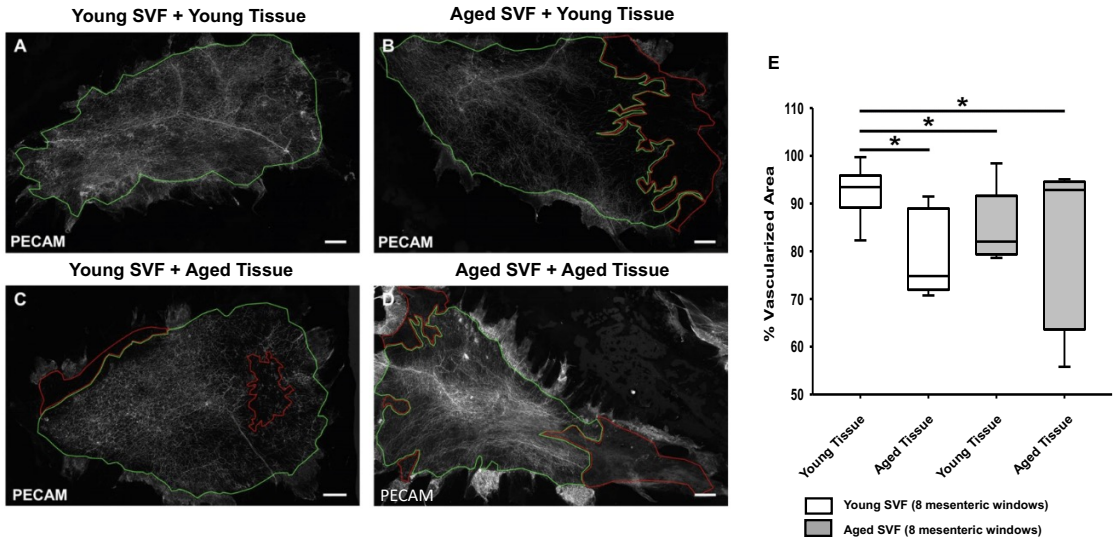

Figure 4.3: Aging effects between donor SVF and host tissue on vascularized area. Vascular coverage is greatest in young SVF + young tissue pairing **(A)** compared to aged SVF on young tissue **(B)**, young SVF on aged tissue **(C)** and aged SVF on aged tissue **(D)**. Quantitative analysis of percent vascularized area **(E)**. Green outline indicates vascularized area while red outline indicates avascular area. Scale bar = 2 mm. 8 mesenteric windows from 2 rats per group, $p < 0.05$ (*); values are shown as box and whisker plots.

Figure 4.4

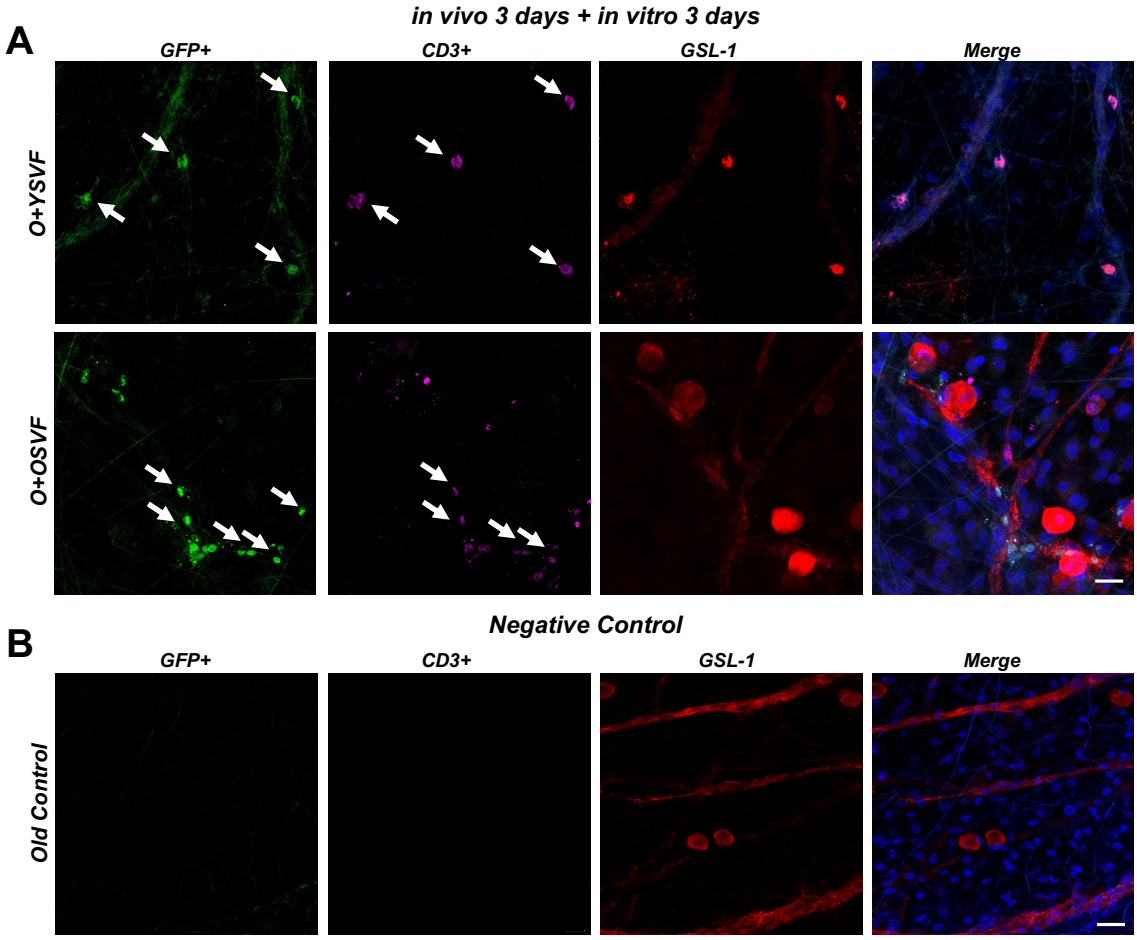

Figure 4.4: GFP positive SVF engrafted into mesenteric microvasculature following intravenous injection.

GFP+ SVF (green) cells from young or aged donors were found in the perivascular space and microvasculature (GSL-1 - red) of young host mesenteric windows six **(A)** days following i.v. injection. GFP is co-localized (arrows) with CD3+ (T cell marker, pink), and DAPI (blue). An old control animal not treated with SVF was used as a negative control for GFP signal and secondary antibody control for CD3 **(B)**. Scale bar = 20 μm.

Figure 4.5

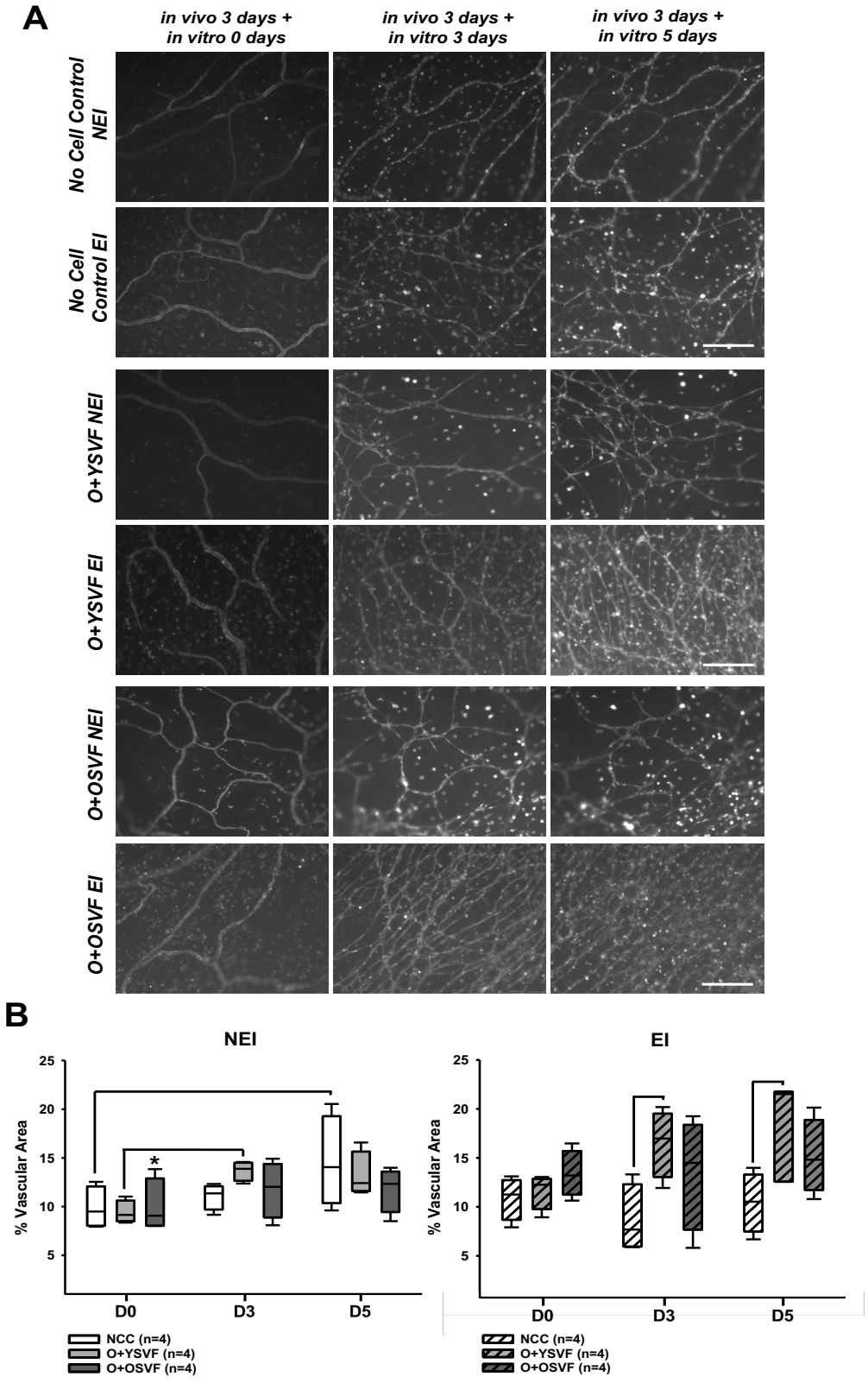
A
in vivo 3 days + in vitro 0 days
in vivo 3 days + in vitro 3 days
in vivo 3 days + in vitro 5 days
No Cell Control NEI
No Cell Control EI
O+YSVF NEI
O+YSVF EI
O+OSVF NEI
O+OSVF EI
B
NEI
EI
% Vascular Area
25
20
15
10
5
D0
D3
D5
*
NCC (n=4)
O+YSVF (n=4)
O+OSVF (n=4)

Figure 4.5: SVF rescues age-related impairment in revascularization following injury.

Representative images of injured (EI) and non-injured (NEI) mesenteric windows from NCC, O+YSVF, and O+OSVF groups at days 0, 3, and 5 of culture. Vascular networks stained with GSL-1 and scale bar = 200 μm **(A)**. Quantitative analysis of percent vascular area **(B)**. Data are shown as box and whisker plots (n=4/group), brackets indicate $p < 0.05$ when comparisons are between days or groups. $p < 0.05$ when EI vs NEI within group comparison (*).

Figure 4.6

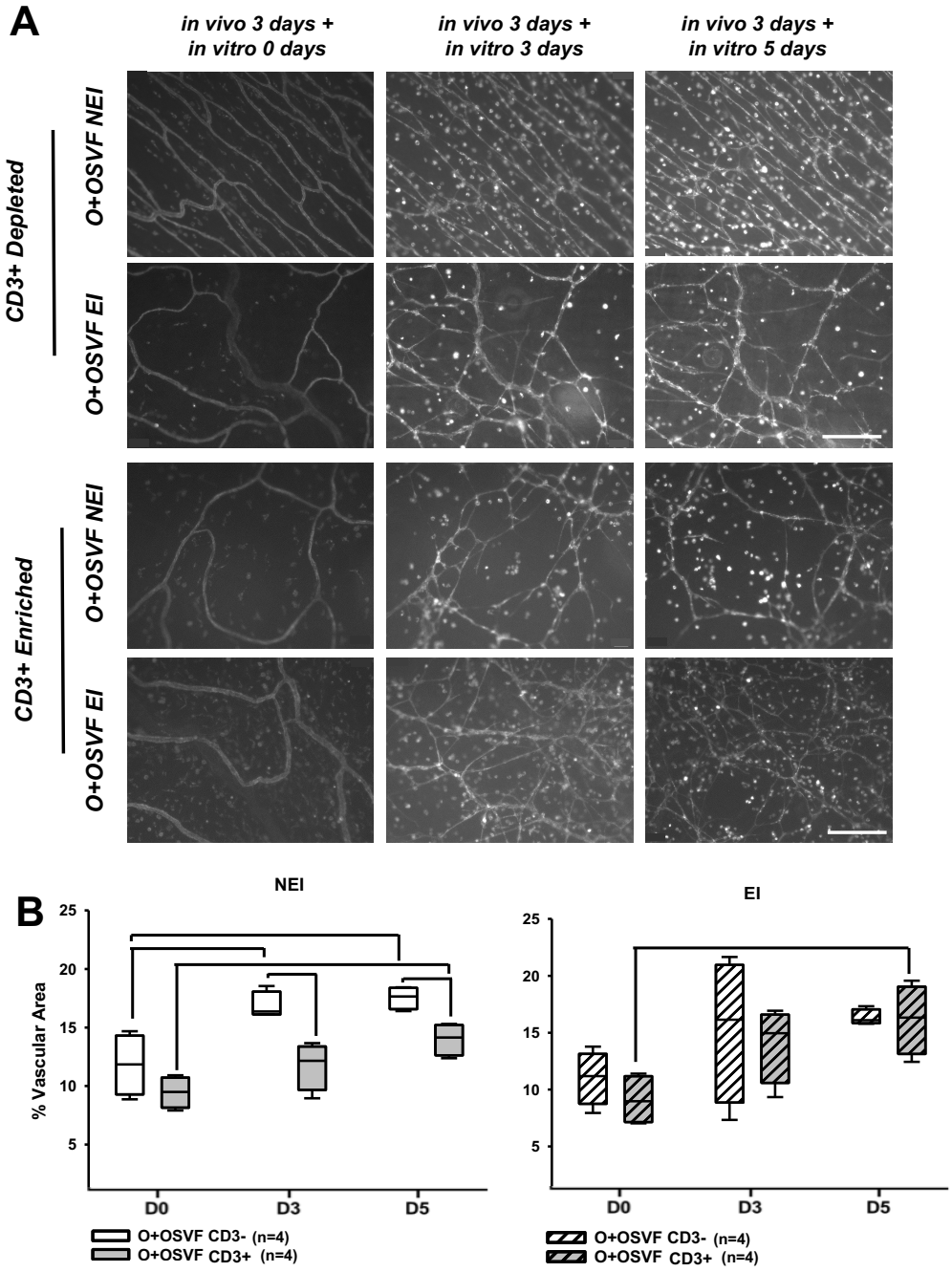

Figure 4.6: Modification of T cell population in SVF does not alter angiogenic potential following injury.

Representative images of injured (EI) and non-injured (NEI) mesenteric windows from O+OSVF animals that received CD3 depleted (CD3-) SVF or CD3 enriched (CD3+) SVF at days 0, 3, and 5 of culture. Vascular networks stained with GSL-1 and scale bar = 200 μm **(A)**. Quantitative analysis of percent vascular area **(B)**. Data are shown as box and whisker plots (n=4/group), brackets indicate $p < 0.05$ when comparisons are between days or groups.

Supplemental Table 4.1

Stromal and Mesenchymal Stem Cell					
Marker	*Vendor*	*Catalog #*	*Clone*	*Fluorophore*	*Dilution*
CD90	Novus Biologicals	NB100-65543V	OX-7	Dylight405	1:200
CD146	Novus Biologicals	FAB3250G	404722	Alexa488	1:100
CD34	Abcam	ab187284	ICO115	PE	1:20
CD31	BioRad	MCA1334A647	TLD-3A12	Alexa647	1:50
CD45	eBioscience	47-0461-82	OX1	APC-eFluor780	1:40
Immune Cells					
Marker	*Vendor*	*Catalog #*	*Clone*	*Fluorophore*	*Dilution*
CD45	BioRad	MCA43A488	OX-1	Alexa488	1:10
CD163	BioRad	MCA342PE	ED2	PE	1:10
CD86	Miltenyi Biotec	130-109-178	24F	PE-Vio770	1:20
CD3	eBioscience	46-0030-82	eBioG4.18	PerCP-eFluor710	1:40
CD11b	BioRad	MCA275A647	OX-42	Alexa647	1:200
CD68	Miltenyi Biotec	130-103-366	REA237	APC-Vio770	1:5
CD8	BD Biosciences	561614	OX-8	V450	1:100
CD44	BioRad	MCA643FA	OX-50	FITC	1:20
CD25	BioRad	MCA273PE	OX-39	PE	1:20
CD4	BD Biosciences	561578	OX-35	PE-Cy7	1:200
CD3	eBioscience	46-0030-82	eBioG4.18	PerCP-eFluor710	1:40

Supplemental Table 4.1: Complete list of all antibodies utilized in this study for flow cytometry.

Supplemental Figure 4.1

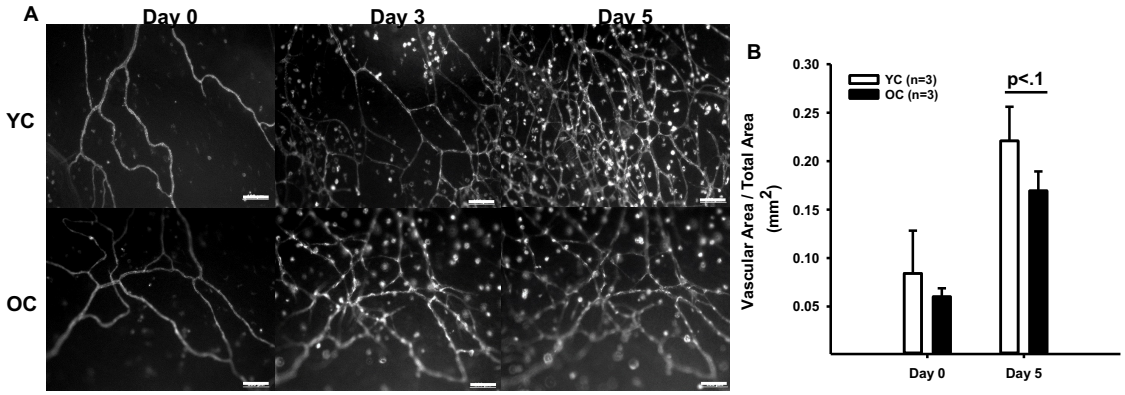

Supplemental Figure 4.1: The mesenteric microvasculature from aged animals exhibits impaired angiogenesis to serum stimulation.

Mesenteric windows were harvested from young (YC) and aged (OC) Fisher 344 animals to be cultured for 5 days. The media was supplemented with 10% fetal bovine serum to stimulate angiogenesis. The vasculature was stained for time-lapse images for vascular areas measurements. Representative images of mesenteric microvascular networks **(A)**. Vascular areas were measured and normalized to total area for days 0 and 5 **(B)**. Scale bar = 100 μm. Data are mean±STDEV. YC vs OC at $p < 0.1$.

Supplemental Figure 4.2

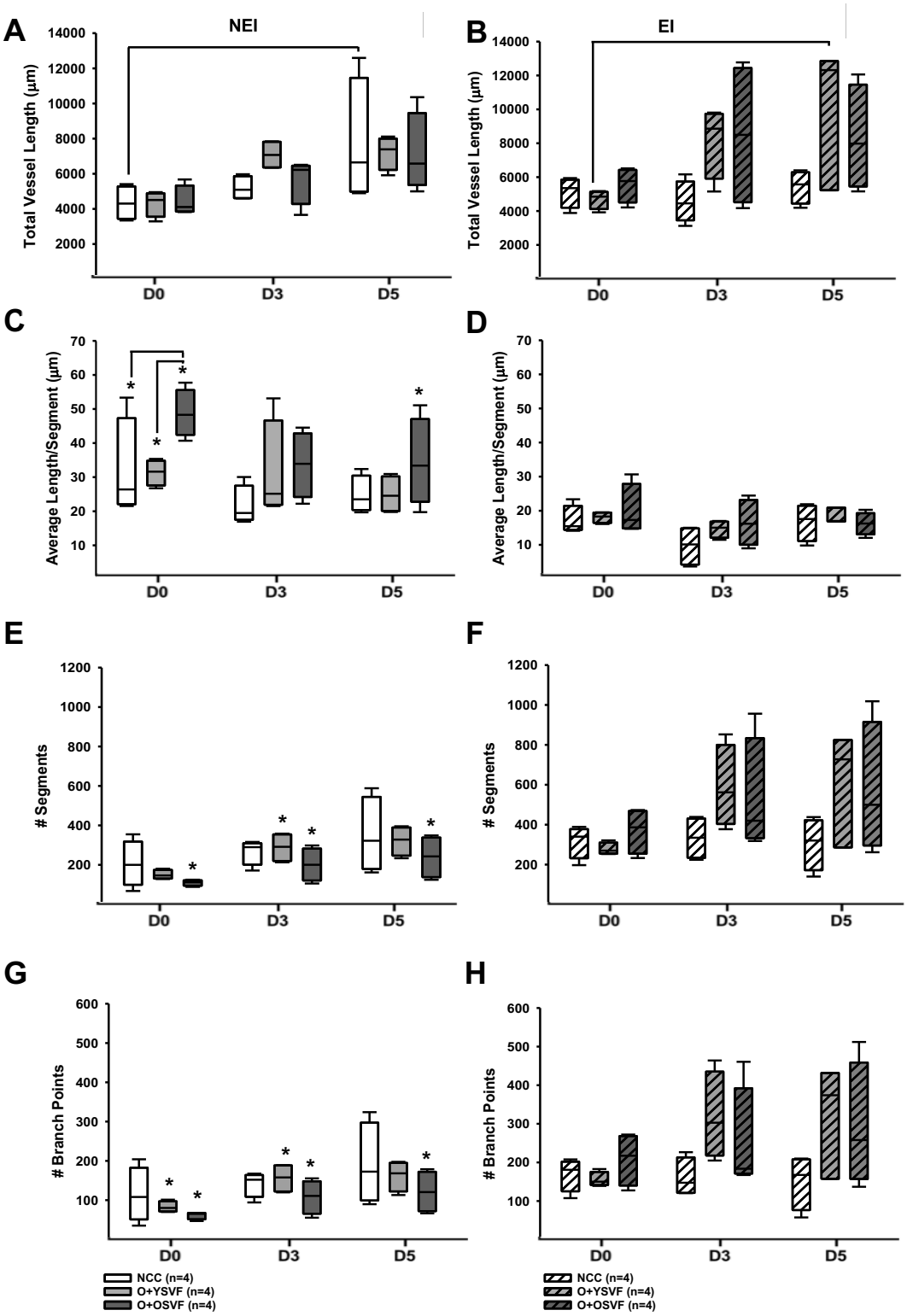

Supplemental Figure 4.2: Quantification of vascular morphology in response to injury and SVF therapy.

Quantitative analysis of total vessel length **(A-B)** and average vessel length per segment **(C-D)**, number of vessel segments **(E-F)** and number of branch points **(G-H)** in non-injured (NEI) and injured (EI) mesenteric microvascular networks. Data are shown as box and whisker plots (n=4/group), brackets indicate $p < 0.05$ when comparisons are between days or groups. $p < 0.05$ when EI vs NEI within group comparison (*).

Supplemental Figure 4.3

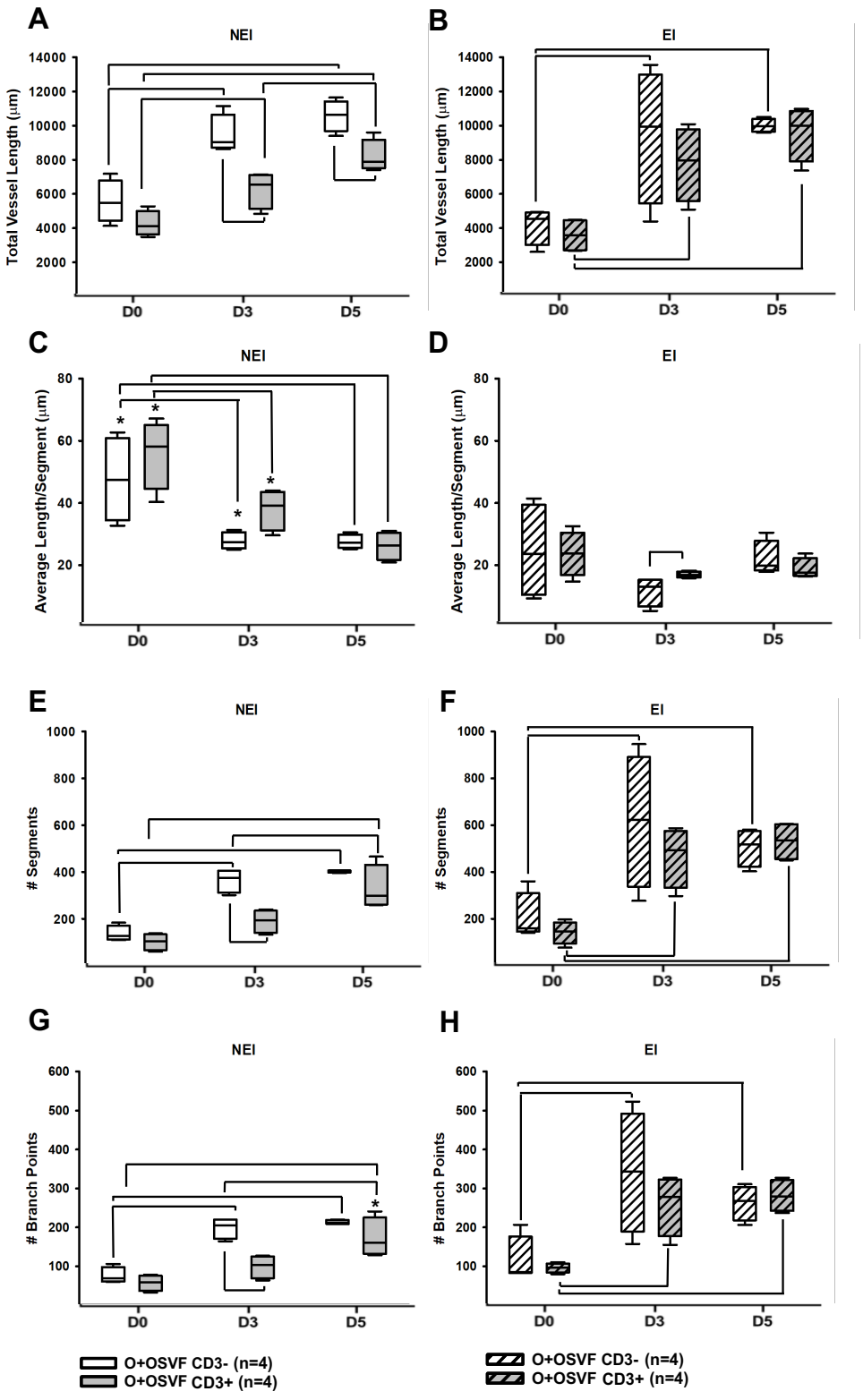

Supplemental Figure 4.3: Quantification of vascular morphology in response to injury and T cell modification of SVF therapy. Quantitative analysis of total vessel length **(A-B)** and average vessel length per segment **(C-D)**, number of vessel segments **(E-F)** and number of branch points **(G-H)** in non-injured (NEI) and injured (EI) mesenteric microvascular networks. Data are shown as box and whisker plots (n=4/group), brackets indicate $p < 0.05$ when comparisons are between days or groups. $p < 0.05$ when EI vs NEI within group comparison (*).

Supplemental Figure 4.4

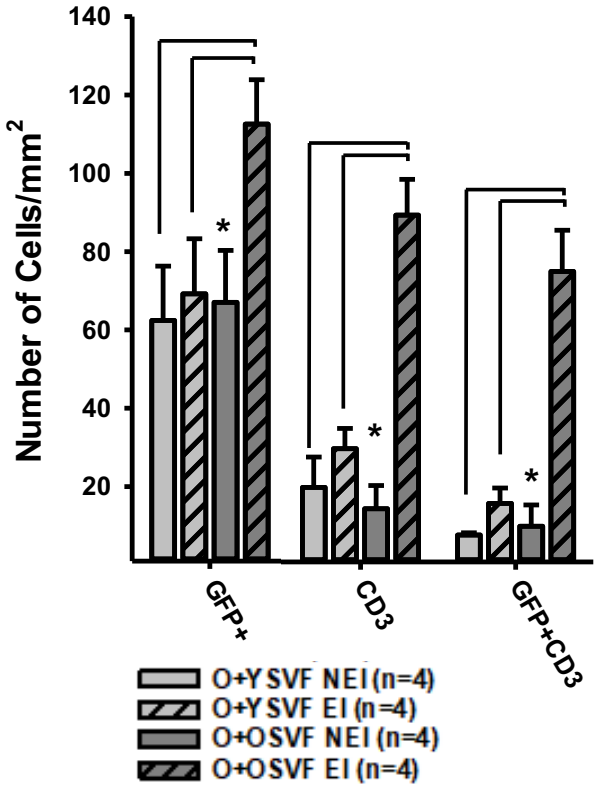

Supplemental Figure 4.4: Injury promotes homing of T cells in aged SVF.

Quantitative analysis of GFP+, CD3+ or co-localization of both GFP+ and CD3+ cells in NEI and EI windows 6 days post-injury and administration of SVF therapy from young and aged donors. Data is represented as cell counts normalized to micrometers^2 and plotted as means±SEM (n=4/group). Brackets indicate $p < 0.05$ when comparisons are between groups. $p < 0.05$ when EI vs NEI within group comparison (*).

Supplemental Figure 4.5

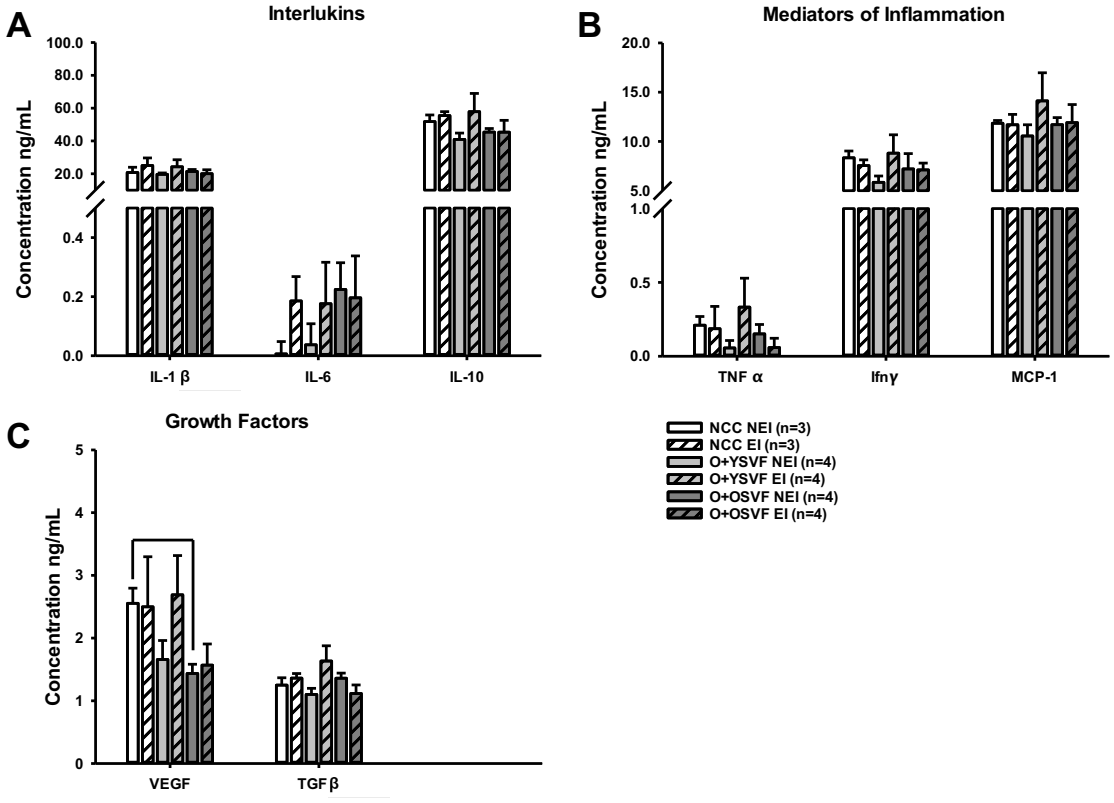

Supplemental Figure 4.5: Levels of inflammatory markers and growth factors as a result of injury or SVF therapy.

Concentrations of pro- and anti-inflammatory cytokines as well as mediators of inflammation and growth factors as measured from media. Data is shown as means+SEM in ng/mL (n=4/group), brackets indicate $p < 0.05$ when comparisons are between groups. Interleukin (IL), tumor necrosis factor alpha (TNFα), Interferon gamma (IFγ), monocyte chemoattractant protein-1 (MCP-1), vascular endothelial growth factor (VEGF), transforming growth factor beta (TGFβ).

Discussion

The first major finding from this study is that aging affects the cellular composition of SVF in adipose tissue, leading to increased T cell and decreased mesenchymal stem cell populations in older animals. Secondly, SVF can increase the vascular area of the mesenteric microvasculature via *in vitro* co-culture as well as *in vivo* when i.v. injected; in both conditions, SVF cells can engraft into these networks. Lastly, there is an age-related impairment in revascularization following injury; i.v. SVF therapy from young SVF donors improves angiogenic potential over non-cell-treated controls. While SVF from aged donors showed a gain in percentage of vascularized area compared to non-cell-treated controls, this was not significant. Contrasting our initial hypothesis, SVF increases revascularization following injury, but this therapeutic potential is not lost when T cells are removed from the fraction. In fact, there appears to be a T cell-mediated impedance on *in vitro* angiogenesis in the non-injured windows, as the CD3- group exhibited increased vascular area compared to the CD3+ group.

The overall goal of this study was to examine how composition in cell populations of SVF is altered with age of donor, it's impact on angiogenic potential in an aged vasculature, and to determine whether T cells contribute to this regenerative effect as part of a broader effort to elucidate which cell population is responsible for the therapeutic gains seen in SVF treatment. The cell(s) of most interest in the field of adipose-derived cellular-therapeutics remains a mystery, albeit this study provides evidence against T-cell mediated recovery. Importantly, this study utilized the *ex vivo* mesenteric window prep in a novel way to elucidate cell therapy testing in conjunction with injury and advancing age to visualize changes in the microvasculature as a response

over time. The applications of this model with differing cell populations and conditions represents an avenue towards further narrowing of candidate cells and/or cellular products responsible for vascular regenerative effect of SVF and other regenerative cell populations.

A novel strategy that can holistically mend the pathologic microvessels themselves or promote new growth, rather than merely treating the symptomatic consequence, is of significant clinical interest which parallels the multi-faceted gains seen in cell-based therapies [126]. Being easily isolated from lipo-aspirate, SVF therapy offers the ability to leverage a real-time autologous point-of-care therapy with inherently minimal risk of rejection, suggesting it is an ideal candidate in vascular therapeutics [177, 178, 305]. The heterogenous cell population containing both immune cell and vascular cell components is thought to be an optimal milieu of environmental cues to enhance vascular function [186-188]. Adipose-derived SVF is comprised of an array of cell populations including a small number of mesenchymal stem cells (MSC), endothelial cells, pericytes, and hematopoietic cells such as macrophages and T cells [176, 306]. While a few studies have examined how age of the SVF donor [154] or the culturing of SVF to confluency [307] affected cell surface markers, these studies did not examine cell populations. We show age-related changes to the cellular composition of SVF such as age-related decreases in the mesenchymal stem cell and stromal cell populations with increases in lymphocytes, M1 macrophages, and various T cells **(Fig 4.2)**. Our results from young SVF donors are congruent with current literature in total macrophage [308] and total T cell percentages [309] with the current data showing the breakdown of the constituents

(Fig 4.2). The-age related changes to cell populations within SVF are important to consider for use as an autologous cell therapy or its application in an aged setting.

The *ex vivo* mesenteric window model was selected for its ease of access, comprisal of an intricate microvascular network, and sustainability in culture. While the mesenteric window model is not an established model for studying vascular diseases, it has demonstrated age-related decreased angiogenesis [310] **(Supp Fig 4.1)** and impairments in vascular function [311] indicating that this model can be beneficial to studying an intact, aged, microvascular network. Previously, it has been shown that SVF from young donors, when seeded and co-cultured with mesenteric windows from young hosts, forms aggregates and demonstrates the beginnings of vasculogenesis within 36 hours of plating [191]. Furthermore, the SVF formed vessels indicating the presence of endothelial cells and vascular pericytes and integrated into the mesenteric tissue *in vitro* (Hodges et al. 2022, *Microcirculation*). The presence of young SVF on a young window stimulated angiogenesis compared to a window without SVF (Hodges et al. 2022, *Microcirculation*). Here we show co-culture with SVF from young and aged donors has similar angiogenic potential resulting in comparable vascularized areas of aged microvascular networks **(Fig 4.3)**. This is in contrast to our previous study which examined angiogenic potential of young vs. old SVF-laden collagen gels and reported decreased vessel formation and host perfusion after subdermal implantation with those containing aged SVF [154]. However, it is important to note that these age variable SVF constructs were both implanted into young mice, emphasizing that the age of the environment primarily determines angiogenic capability of SVF.

With clinical applications of cell therapies typically involving systemic administration, it is important to examine the biodistribution and engraftment potential of the therapy. Our previous study showed that four weeks following a one-time i.v. injection of 10 million young SVF cells into an aged rat resulted in the largest percentage of SVF being retained in the aorta and carotid arteries (50% and 40 % respectively) [42]. However, the microcirculation was not examined for SVF retention nor was the engrafting cell type. Scherberich et al. showed that SVF injected subcutaneously was able to physically contribute to the vasculature as endothelial cells [312] and were further supported by SVF-derived pericytes [313], but these experiments were not conducted in an aging model. Here we show that i.v. injection of 10 million GFP+ SVF cells from young and aged donors resulted in engraftment into the microvasculature within and around vessels, and that T cells from the donor fraction can also be found in the microvasculature **(Fig 4.4)**. Understanding what cell types are retained in the host tissues could aid in improving efficacy of administered cell therapies. Similar studies with chronic cell therapies such as mesenchymal stem cells administered via i.v. injection demonstrated that incorporation is as low as 10%, but this cell type was not shown to aggregate and form new vessels [314, 315]. Future studies will be needed to quantify the percentage of integration per host vessel, the percentages of integration of the various cell types found in SVF, and what cytokines may be altered as a result of administering SVF.

In vitro studies have shown that SVF has an intrinsic angiogenic potential [191] which when added to mesenteric windows increases the host vasculature (Hodges et al. 2022, *Microcirculation*) **(Fig 4.3)**. While SVF therapy has been utilized in models of ischemic injury and showed functional improvements, few studies integrate ischemic

models with aged models [41]. Exteriorization of mesenteric windows has been shown to be a stimulus for angiogenesis in young rats [299]. We showed that exteriorization injury in aged rats produced little change in vascular area of the mesentery in aged control rats, but i.v. administration of young SVF therapy markedly increased vascular area, while aged SVF administration was non-significant **(Fig 4.5)**. Aging has long been considered an unmodifiable risk factor for the development of vascular pathologies [44, 45, 105]. In the periphery, microvascular dysfunction can lead to organ perfusion/demand mismatch and ultimately organ failure or loss of limb [50, 51]. Therefore, an autologous cell therapy that could be administered to increase angiogenesis in an area following an ischemic injury is of significance. Despite this, a better understanding of how cell therapies achieve their gains either through paracrine release or cell engraftment and which cell types are crucial to their function still needs to be explored further.

T cells have been implicated as crucial cells needed for tissue and vascular repair following injury, as they activate other cells such as macrophages and fibroblasts, stimulate apoptosis and clearance of dead cells, and are responsible for switching from a pro-inflammatory state to a reparative state [316]. T cells have also been shown to migrate to the injured area [290], secrete factors that enhance angiogenesis [289] and be present at the angiogenic front following injury [291, 292]. In a knockout mouse model depleted of regulatory T cells, there was a marked reduction in angiogenesis following lung ischemia [317]. When we depleted aged SVF of the CD3+ T cells and administered during exteriorization injury, we measured no difference between T-cell depleted and T-cell enriched SVF at increasing vascular area following injury **(Fig 4.6)**. Interestingly, we did see differences between the T-cell depleted and enriched groups in the non-injured

windows with the SVF depleted of T cells having higher vascular area at days 3 and 5 of culture post-injury compared to the enriched group **(Fig 4.6)**. These data suggest that while T cells may not be responsible for the increase in angiogenesis following injury, a lack of T cells in SVF appears to be beneficial in a non-injury setting via increased microvascular angiogenesis. This is especially applicable to aging populations whose density of microvascular networks is decreased with age [318, 319]. Whether T-cell depleted SVF might preserve organ function after an ischemic insult is an important future direction. Of note, CD11b+ macrophages from young SVF donors administered systemically can engraft into large conducting arteries, reduce the vasomotor tone, and promote dilation following insult [200], albeit this was not in the microcirculation of an aged model and revascularization following insult was not analyzed.

We hypothesized that T cells may mediate the regenerative effect of SVF. On the contrary, our results show that vascular regeneration occurs steadily over 5 days with SVF even when depleted of CD3 cells. In fact, CD3 depleted SVF outperformed CD3 enriched SVF for vascular recovery in non-injurious settings. It is possible that a multitude of cells confer vascular regenerative properties to SVF (MSCs, fibroblasts, pericytes, other immune cells, etc.), which would explain why vascular regeneration still occurred in the CD3- SVF group during EI. Interestingly, with onset of injury, the ability to achieve significant vascular regeneration is lost in the CD3- group but is preserved in the CD3+ enriched group. This could signify that CD3+ T cells are a contributing component of SVF-mediated vascular regenerative response to injury. Correspondingly, potential angiogenic contributions of other SVF cells cannot preserve significant angiogenic response after injury. Contrasting this notion, we found that aged SVF has a

significantly greater proportion of T cells than young SVF, yet this increased T cell population did not confer significant vascular regenerative ability to aged SVF donation. Aged SVF yielded less stem cells, fibroblasts, and pericytes. Therefore, also examining changes in these cell populations would be warranted. It is possible that synergy between regenerative potential of multiple heterogenous cell types is required for optimal angiogenic response to SVF. Further elucidating this complex symphony of cells within SVF represents an important future direction. Additionally, future studies could employ the methods detailed in this study to isolate other cell populations in SVF to assess their contribution to SVF's angiogenic potential by measuring vascular changes over time in conjunction with cell tracking. Taken together this study presents novel insight into age-related changes to cell populations isolated from the adipose-derived stromal fraction, visualization of immune cells in SVF present in and around the microcirculation after i.v. injection, effects of SVF therapy from young and aged donors on microvasculature after ischemic injury, and evidence that the angiogenic effects of SVF cell therapy are not wholly T-cell mediated.

Conclusion and Future Directions

The aging population are at greater risk of ischemic injury with less capacity for vascular repair following injury. Therefore, the elderly stands to benefit greatly from cell therapies as a remedy for vascular dysfunction. The field of cellular therapeutics is in its relative infancy with current emphasis on optimization. In the context of this study, SVF represents a heterologous cell population shown to increase angiogenic regeneration in our novel aged mesenteric injury model. This study provides others with a new tool for

tracking vascular recovery and can be used in conjunction with study of cell therapies or pharmacologics in a setting of advanced age. Furthermore, we show how age of the donor should be considered not only for cellular differences but functionality as a vascular therapeutic. Age-related changes to cell dynamics and function in providing therapeutic gains - i.e., secretion of anti-inflammatory cytokines, increasing sensitivity to VEGF, increasing migration of injected cells, and endothelial cell division - are further avenues to be explored in cellular therapeutics that could be done using the aged mesenteric model.

CHAPTER 5

DISCUSSION

The idea of stem cells was first proposed back in the 1860s by Dr. Ernest Heckle, but stem cells did not enter into the realm of therapeutics until the 1950s [320]. Since then, their use has soared with over 5,000 registered clinical trials today (based on a search on clinicaltrials.gov in 2022). While almost every organ in the body contains a type of stem cell, mesenchymal cell sources have proven to be a better cell therapy in treating ischemic injury compared to hematopoietic stem cells, despite their longer history [321]. Within their organ niche, mesenchymal stem cell sources provide functional and structural support to the parenchymal cells of the organ by differentiating into connective cell types such as endothelial cells, pericytes, fibroblasts, etc. Their connective lineage also allows for harvesting from many regions throughout the body and their sustainability in culture [322]. One source of mesenchymal cells that has eclipsed the others is the stromal vascular fraction, found in adipose tissue - SVF. Recent studies have shown that SVF has equal efficacy in improving cardiac function following MI, reducing inflammation, differentiating into vascular elements, and promoting angiogenesis compared to BM-MSCs [189-195]. Our results echo these findings in that i.v. administration of BM-MSCs only partially rescued coronary flow reserve (CFR), left ventricular (LV) diastolic dysfunction, and vasoreactivity to beta-adrenergic agonists in

an aged rat model while SVF showed restorations in all of the metrics listed (**Chapter 2**). SVF contains mesenchymal stem cells (MSCs), endothelial cells, pericytes, and hematopoietic cells including macrophages, T-cells, and other cells of the perivascular niche [176, 185] (**Chapter 4**). The ease of harvest, real-time use, and low immunogenicity confer SVF either as an autologous or allogeneic cell therapy [159-162, 177, 178].

Therapeutic gains seen following SVF administration are thought to be due to cellular engraftment and incorporation of the donor cells into the host tissues, however, pre-clinical studies have shown that there is a markedly rapid decline in retained cells in as little as 24 hours, 1 week, and 30 days after administration [323-327]. Further, administration of exosomes harvested from mesenchymal cells can increase endothelial cell density following a dermal wound and preserve cardiac function following an MI, all of which support the current paracrine hypothesis of cell therapy mechanisms [261, 328]. However, long term studies have shown that SVF cell therapy can provide long term sustained improvements as measured at a few months, 3-years, and even a 6-year follow up even though cellular engraftment at the site of injury is low [329-332]. Intravenous administration of cell therapies results in a wide biodistribution of cells being retained in other non-target organs such as the spleen, where they were they may play a role in modulation of the hosts' immune cells [42, 329]. While the generally accepted paradigm is that cell therapies work via paracrine secretion, long term improvements suggest that engraftment of donor cells, while perhaps not in the organ of interest, cannot be wholly discounted. Therefore, increasing the degree and/or duration of cell engraftment and thus increasing exposure time to paracrine benefits would improve the efficacy of the cell

therapy and would be a value to the cell therapies field [330]. However, to do this, greater understanding of how cell therapy, specifically SVF, achieves its therapeutic gains is needed.

The safety and efficacy of SVF as a therapeutic for osteoarthritis [181], inflammatory bowel disease [180], idiopathic pulmonary fibrosis [182], chronic ischemic cardiomyopathy [183], and coronary artery disease [332] have been vigorously scrutinized. Ongoing studies exploring the long-term benefits and mechanism behind the efficacy of SVF have yet to examine SVF's therapeutic benefit or use as preventative measure in the microvasculature highlighting future directions for investigation.

Clinical trials employing SVF therapy in combination with transplantation during reconstruction, as well as preclinical trials showing SVF mitigating improvement in wound healing following diabetic or ischemic injury emphasizes SVF as a therapeutic approach to increase blood flow to a tissue via angiogenesis [333-335]. However, preclinical trials do not often use models of advancing age, and while some clinical trials do have populations of older patients, they are restricted in obtainable measurements such as organ function at set time points which can overlook the mechanism behind the improvement. The aged population is ever increasing and would benefit the most from cell-based therapies. The Women's Ischemia Syndrome Evaluation found that post-menopausal women are at greater risk for coronary microvascular dysfunction (CMD), presenting with angina, compared to their male counter parts [47, 57, 114]. Impairment in vascular dysfunction can begin developing as early as 40 years, with most clinical manifestations apparent around 50 years of age followed by a steep decline in function after menopause [47]. Previous studies have shown an age-related impairment in flow-

mediated dilation (FMD), an endothelial-dependent mechanism, in brachial, [47, 336], mesenteric [337], and coronary [260] arteries demonstrating that age-related vascular impairment occurs in the resistance arterioles of the microcirculation. We utilized a female rat model of advanced age, the Fisher 344 strain from the National Institute of Aging colony. Aging coupled with the eventual loss of circulating estrogen in these rats impair the coronary microvasculature in an endothelial-dependent fashion [260], mimicking the clinical scenario. Utilizing this rodent model, we showed an age-related decrease in CFR which is a functional and structural measure of the health of the coronary vasculature and subsequent LV diastolic dysfunction (**Chapter 2**). Second, we showed an age-related impairment in the vasodilatory capacity of coronary microvessels to response to β-AR agonist, NE, due to a reduced β-AR population (**Chapter 2** and **3**). Lastly, we found reduced capacity of the microvessels to undergo angiogenesis in response to hypoxic injury with advanced age (**Chapter 4**). Since the small resistance arterioles of the microvasculature govern the blood flow through an organ, impairment and/or improper augmentation of blood flow to meet organ oxygen demand can result in tissue ischemia which can progress to organ failure in a setting of advanced age with further impairment of revascularization in an ischemic area [39, 45]. As previously discussed, SVF could be a potential vascular therapeutic and be applicable to the aged population working to increase function and growth of the vessels through its anti-inflammatory, anti-oxidative, and angiogenic properties. However, the mechanism by which SVF achieve these gains in an aged vascular bed is an area that still needs to be explored.

Our studies conducted in aged vascular beds in combination with SVF therapy sought to explore several facets of its therapeutic paradigm. We administered SVF via the tail vein, as an intravenous injection would be the most clinically applicable administration route. Furthermore, we administered 10 million SVF cells systemically, as clinical trials have shown 10-20 million cells was found to be the beneficial range while preclinical trials have shown 3-250 million is beneficial with as little as 1 million exuding a vasculogenic effect in culture [320, 338]. Because improper blood flow to meet/match organ demand is most apparent in the coronary circulation, we used coronary microvessels from aged rats with and without i.v. SVF therapy. With this methodology we observed SVF rescuing CFR when stressed with a β-AR agonist, as well as improved LV diastolic dysfunction. Upon isolating coronary microvessels, we showed SVF increased vasodilatory sensitivity to a β-AR agonist compared to untreated age-matched controls. Interestingly, we also showed that the coronary microcirculation is heavily dependent upon β1-AR stimulated dilation, as inhibition of this receptor ablates vasodilation to NE in all groups including young controls (**Chapter 2**). Upon further exploration of how SVF improved β1-AR sensitivity, we probed coronary microvessels from SVF and age-matched control rats to show that SVF therapy reversed the age-related reduction in the β1-AR population back to young control levels. This therapeutic gain was in part due to modest reduction in the negative regulatory inhibitors of the β-AR signaling cascade, GRK2 and Gαi (**Chapter 3**). Systemic inhibition of GRK2 with paroxetine improved cardiac contractility and heart function in advanced age as well as improved myocardial repair following MI [270, 271, 339]. However, GRK2 knock down was shown to lead to hypertension and altered adrenergic signaling [340]. Inhibition of

GRK2 in aged-isolated coronary microvessels significantly improved vascular dilation of NE compared to an un-inhibited dose response in the same aged vessels. This effect also occurred in aged rats treated with SVF therapy. When expression of active and phosphorylated GRK2 were probed in myocardial samples, SVF improved the ratio of phospho : active GRK2 to levels seen in young control hearts. Transcription of GRK2 was not altered with age, therefore this data suggests that SVF therapy modulated GRK2's activation status in coronary microvessels. GRK2 being the first step in β-AR recycling, reduced activity of this kinase as a result of SVF therapy would increase β-AR dilation sensitivity (**Chapter 3**). Gαi is another β-AR regulator but is more commonly associated with the β2−3-ARs. Overexpression of Gαi in the myocardium leads to decreased β2-AR sensitivity and heart function [279, 341]. We showed that advancing age increases Gαi myocardial expression. Furthermore, subtypes Gnαo1 and Gnαi2 were significantly and markedly higher in aged coronary microvessels compared to young control (**Chapter 3**) contrary to Shimokawa et als. findings [342]. While extended β2-AR stimulation can lead to G-protein switching, stimulatory to inhibitory [343], the effect of extended β1-AR stimulation and subsequent inhibition by Gαi has not been explored in the microcirculation.

Potential mechanisms that are supported by findings presented in this manuscript and current literature in the field suggest that SVF-mediated gains are multifaceted and would employ multiple mechanisms. One theory of aging is that reactive oxygen species (ROS) increases as age advances, reducing protein function and impairing vasodilation in resistance vessels [32]. Coronary microvessels from aged rats were shown to have increased ROS which resulted in impaired β-AR mediated dilation and reduced the

bioavailability of NO. In a youthful setting, plentiful NO levels naturally inhibit GRK2s action to begin internalization of the β-AR. Incubating OC vessels with a NO donor, sodium nitroprusside, returned vessel function to YC levels. Furthermore, inhibiting a protein needed for internalization of the β-AR also improved vasodilation in OC vessels (**Appendix 3**). With SVF therapy, although NO bioavailability is not restored, ROS levels are reduced to alleviate β-AR thiol oxidation-mediated desensitization/internalization and restored receptor recycling back to the plasma membrane (**Appendix 3**). Secondly, while initially protective against failing cardiac output, increased levels of systemic catecholamines can lead to decreased β-AR sensitivity [94, 204, 205]. In measuring systemic plasma catecholamine levels, we showed an age-related increase in NE with some reduction following SVF therapy (**Chapter 2**). However, when measuring urine catecholamine levels, SVF did not reduce the level of NE present (**Chapter 3**). This may be in part due to SVF having catabolic action against catecholamines [344]. We measured a significant reduction in transcription of catechol-o-methyltransferase and modest reduction in catecholamine degradation enzyme monoamine oxidase A due to SVF therapy compared to aged-controls (**Chapter 3**). SVF therapy may contribute to the metabolism of catecholamines that begin the β-AR desensitization [345]. Thirdly, microvessels isolated from animals with inflammatory diseases such as irritable bowel and obesity exhibit impaired dilation to endothelium-dependent agonist acetylcholine compared to control animals [346, 347]. Chronic inflammation impairing endothelial function has been linked to advancing age [348]. Aged patients that received an NF-κB inhibitor demonstrated improved brachial artery FMD (+74%) compared to the age-matched placebo control group [348] and inhibition of

TNFα improved FMD in aged female mesenteric arteries [337]. Both NF-κB and TNFα are mediators of inflammation. Examining the transcriptome in young, aged, and SVF treated coronary microvessels we showed an age-related increased in transcription of inflammatory activators such as caspase 12, the IL-1 receptor kinase, and TNFα induced protein. SVF therapy was shown to increase a NF-κB inhibitor to levels comparable to YC (**Chapter 3**). The studies presented in this manuscript examine SVF's therapeutic mechanism to reverse age-related β1-AR desensitization and subsequent development of LV diastolic dysfunction by decreasing the presence of negative regulators, GRK2 and Gαi, and alleviating ROS induced internalization, thereby promoting receptor recycling back to the cell membrane and restoring the β1-AR population, improving sensitivity to vasodilators (**Chapter 2-3** and **Appendix 3**). While these findings represent a novel therapeutic pathway to be targeted in patients advanced in age, it also presents a novel mechanism by which SVF can be a promising microvascular therapeutic. However, it is still unknown which cells constitute this improvement, what cell fractions such as RNA, cytokines or exosomes may be released from SVF to drive these changes, and if this gain is only in the existing vasculature or if SVF therapy promotes angiogenesis through active integration and proliferation promoting increased tissue perfusion in an aged vascular bed.

With aged patients being more susceptible to ischemic injury with reduced revascularization following injury, we used a model of the mesentery to visualize angiogenesis in the vasculature and SVF's potential for integration into this vasculature. Mesenteric windows are clear connective like tissues located along the length of the small intestines which constitute a complete microcirculation and supporting divisions

such as lymphatics and nerves that are capable of being taken out for culture over 7 days [349]. While the *ex vivo* mesenteric window model is not an established model for studying microvascular disease, it has demonstrated age-related decreased angiogenesis [310] (**Chapter 4**) and age-related impairments in vascular function [311], mimicking the clinical scenario. Additionally, this model is beneficial to studying an intact microvascular network in combination with SVF therapy and it's been shown that brief exteriorization of a section of mesentery results in a hypoxic-like injury that can stimulate angiogenesis in young rats [293]. We utilized the *ex vivo* mesenteric window model in combination with SVF co-culture to examine the spatial-temporal interactions of SVF with an aged microvascular network. When SVF from young donors is seeded onto and co-cultured with a mesenteric window, SVF can form central hubs with endothelial cell markers and active branching by day 3 (**Appendix 4**) [298]. The presence of SVF on the window can increase the total vascularized area compared to an untreated control and form connections with the host microvasculature (**Appendix 4**). Pivoting to a more clinically relevant delivery, we showed that i.v. administration of SVF can disseminate and engraft into the mesenteric microvasculature 3 days after injection (**Chapter 4**). SVF's inherent ability to form microvascular constructs was utilized in a left anterior artery ligation MI model where SVF - Matrigel constructs were sutured and implanted over the ischemic area, leading to improved scar healing, vascularization, and perfusion of the SVF construct [41, 350]. While these studies show the angiogenic potential of SVF in a young model and even following injury, we wanted to examine the impact of age and injury in the mesenteric microvasculature.

Inducing a hypoxic-like exteriorization injury in aged rats resulted in an angiogenic impairment which was not present in non-injured aged control windows. Intravenous SVF therapy reversed this angiogenic impairment, significantly increasing vascular area following injury (**Chapter 4**). Unlike pharmaceuticals typically affecting only one therapeutic target; cell therapies can exert an influence on the multifaceted pathology seen in aging and vascular dysfunction. The caveat being autologous cell sources may not be more advantageous therapy due to their "aged nature". When SVF from young or aged donors was integrated into a Matrigel construct placed over the infarcted area of a young heart, the aged SVF construct had lower microvascular formation and less perfusion compared to the young SVF [154]. SVF taken from aged human donors has a reduced capacity to restore cutaneous blood flow in a mouse hindlimb ischemia model, reduced capacity for endothelial cell differentiation, and reduced secretion of pro-angiogenic factors. The age-related angiogenic discrepancy could be mitigated with pre-conditioning in hypoxic conditions [351]. We sought to examine the effect of the donor's age on SVF angiogenic potential in the mesentery and in combination with injury compared to age-matched no cell controls. We showed that when young SVF is co-cultured with a mesenteric window harvested from a young rat, it resulted in the highest vascularized area compared to other young/aged combinations of SVF donor and tissue. Interestingly, SVF from a young donor and an aged SVF donor resulted in comparable vascularized areas of aged tissues following co-culture. This highlights the equal efficacy in SVF either as an allogeneic or autologous vascular therapy. In response to injury, i.v. injected SVF from young donors did significantly

increase vascularized area of aged tissues while aged SVF only had a modest improvement compared to the non-treated group (**Chapter 4**).

During the course of these studies, we also examined the impact that freezing/thawing has on SVF's angiogenic potential. Freshly isolated SVF fractions were utilized in the vascular function experiments showing improvements in coronary flow (**Chapter 2-3**) and the co-culture experiments showing improvements in vascular area in aged tissues (**Chapter 4** and **Appendix 4**) [298]. When SVF is cultured to confluency (P0) then added to a construct that was implanted subdermally, the cultured SVF, while not cultured to senescence, showed a reduced capacity to be perfused by the host [307]. Although in the last decade there have been developments in medical equipment to take freshly isolated lipo-aspirate and automate the SVF isolation process so that it can be done within the operating suite for immediate use or to be frozen and stored for later use or as a potential allogeneic use [176]. A comparison between freshly isolated and frozen SVF in bone healing revealed that both therapies promoted bone healing through angiogenesis and osteogenesis with no difference between the groups [352]. Our results showed similar findings in that fresh and frozen SVF, from either young or aged donors, can increase angiogenesis in co-culture or following i.v. injection, but SVF from young donor's fares better compared to the aged SVF in increasing vascularized area following injury (**Chapter 4** and **Appendix 4**).

Exploring why SVF's angiogenic potential may be lower when harvested from aged patients, we examined the cell populations within SVF and their characteristics. Using flow cytometry with multiple staining and gating steps, we have identified 18 populations of cells in SVF and measured their percentage within the fraction. Most

notably, lymphocytes, M1 macrophages, CD3+ T cells, helper, activated, and memory T cells are all found in higher concentrations in aged SVF compared to young. However, in aged SVF there are fewer hematopoietic progenitor cells, mesenchymal stem cells, and total, immature, and transitional macrophages (**Chapter 4**). Our findings are consistent with the field where one study measured transcriptomic changes in SVF taken from pre- and post- menopausal patients; differences were found in the fertility-, sex hormone-, immune-, aging-, and angiogenesis-related terms and pathways. Additionally, SVF from post-menopausal donors could induce M1 polarization of macrophages, while their pre-menopausal counterparts facilitate T cell proliferation [353], although we found both of these cell populations to be higher in our aged female rat model. A potential rationale for SVF's age-related impairment in angiogenesis is that it contains fewer mesenchymal stem cells (**Chapter 4**). Furthermore, MSCs taken from aged patients were significantly compromised in their ability to support vascular network formation *in vitro,* with impaired migration and an inability to rescue age-associated impairments in cutaneous wound healing *in vivo* [354, 355]. Regardless of processing and administration, SVF's mechanism to promote angiogenesis in the mesentery, and following injury, needed to be explored.

Intravenous administration of a cell therapy can lead to a wide distribution throughout all the body's systems. It has been shown that an i.v. injection of 6 million SVF cells results in a majority being retained in the carotid, aorta, lungs, and spleen 4-weeks after injection [42]. We confirmed that i.v. injection of SVF can also result in retention of these cells in the mesenteric microvasculature, resulting in cells within and around microvessels (**Chapter 4**). Mounting evidence suggests that despite a wide

biodistribution from intravenous cell injection, there is a beneficial effect on organs with low engraftment, possibly due to cell therapy regulating the host's immune cells via homing in lymphoid organs such as the spleen; this observation needs to be explored further [356-358]. Following injury, immune cells migrate out from lymphoid organs and travel to the site of repair. When injury occurs in an aged patient, there is less infiltration of the immune cells compared to young leading to diminutive repair [359]. In 2007 it was reported that the i.v. administered MSCs homed to the infarcted region of the myocardium [360]. Six days after exteriorization injury and SVF injection in our mesenteric windows, we examined windows for GFP+ SVF engraftment and showed that injury significantly increases homing of aged SVF in an injured aged window compared to a non-injured control and an aged window treated with young SVF (**Chapter 4**). This evidence suggests that the increased angiogenesis seen following SVF therapy may be due to different effects depending on age of SVF donor, which cells are contributing to this effect needs to be explored.

Age-related endothelial dysfunction can impair microvascular functionality as well as angiogenesis. SVF contains a large population of endothelial cells which can physically contribute to a host's subdermal vasculature [312]. Although, injecting only endothelial cells is not a sufficient therapy in improving poor age-related microvascular perfusion, as we have previously shown [42]. Despite SVF's promising potential to form its own microvascular networks or contribute as endothelial cells, unprotected capillaries are subject to rarefaction (pruning) if not surrounded by pericytes. SVF is an abundant source of pericytes. When SVF is co-cultured with mesenteric window, SVF can form vascular hubs expressing endothelial cell pericytes markers (**Appendix 4**). Additionally,

MSCs within the SVF are capable of differentiating into pericytes, and SVF-derived pericytes have been found around mature vessels [313, 314, 361]. While important in protecting the endothelium, their use as a homogenous cell therapy is unknown. Although age decreases the macrophage population found in SVF, macrophages are the major contributors to the secretome [362] and host macrophages have been shown to be heavily involved in vascular formation in an ischemic tissue [363]. In a model of hindlimb ischemia, depletion of macrophages from SVF resulted in little change to revascularization but depletion of host macrophages resulted in impaired revascularization of the limb [364]. Contrary to this, administration of CD11b+ macrophages isolated from SVF improved vasomotor tone in a mouse model of hind limb ischemia [200]. The two distinct subpopulations of macrophages present in SVF, M1 and M2, can drive T cell function to either a pro-inflammatory state or a pro-regenerative state, respectively [365]. The polarization of macrophages and subsequent T cell implication has been shown to occur in aged tissues with macrophages being predominantly M1 (**Chapter 4**) leading to an inflammatory environment [366]. However, SVF therapy has been shown to promote tissue regeneration via M2 polarization of the macrophages [367, 368]. T cells are a critical part of the immune system, bridging the adaptive and innate divisions [369], activated via macrophages through the CD40 ligand/receptor axis [370], and have been shown to be crucial for the success/survival of a bone marrow graft. Furthermore, T cells also play a role in stimulating angiogenesis in ischemic areas [289] due to migration to the area of injury [290, 291] and collateralization specifically by homing to sites of active angiogenesis [292]. Upon probing for T cells in 6-day post injured mesenteric windows after SVF therapy, we

found that the injured group treated with aged SVF had a significantly higher number of donor GFP+ T cells (**Chapter 4**) consistent with others findings that T cell populations do increase around post-infarct days 6-7 [371] concurrently when we measured an increase in angiogenesis (**Chapter 4**). When T cells are depleted from SVF and intravenously injected following injury, the T cell depletion does not affect SVF's revascularization potential. Interestingly, the depletion of T cells from the fraction significantly increases the vascularized area in non-injured windows compared to treatment with only T cells. Taken together this data suggests that SVF's angiogenic potential does not solely lie in one cell type, despite being a large portion, and rather modification of SVF may be necessary in regard to when treatment is occurring. Our data suggests that SVF with the T cells removed T cell depleted SVF could be utilized as a preventative therapy to increase angiogenesis in a tissue prior to an ischemic event. Whereas utilizing only the T cells from SVF or even unmodified SVF would be more beneficial therapeutic following injury (**Chapter 4**). Nonetheless, many researchers still examine the mesenchymal stem cell contribution to angiogenic repair despite the low numbers found in SVF. While MSCs can differentiate into endothelial, pericytes, fibroblasts and other supporting cells of the stromal fraction [372, 373], they only comprise 5-10% of the SVF population; the percentage of MSCs is even lower when harvested from an aged patient (**Chapter 4**). Each cell type described above has been shown to have a promising therapeutic potential in one niche, but the amalgamation of all of these cell types within SVF lend to a superior therapeutic potential. A heterogeneous cell population may be more beneficial than the homogenous cell preparations, providing

the unknown optimal milieu of environmental cues, in which the environmental cues have yet to be examined [186, 374].

During embryogenesis, vascular endothelial growth factor (VEGF) is the predominant factor in the regulation of new blood vessel formation, stimulating new blood vessels to sprout from existing vasculature via angiogenesis. Hypoxic regions of a given tissue generate VEGF gradients to stimulate the differentiation of an endothelial cell into a tip cell which forms a stalk, ultimately leading to the generation of a capillary [34]. Together, the process of angiogenesis (growth of new vessels from existing ones) and vasculogenesis (single cells coming together to form a vessel) lead to a mature, perfused microvessel network. When exogenous VEGF is added onto mesenteric windows it stimulates angiogenesis in culture [301]. In a collagen matrix interface, SVF was placed in the core and microvascular migration, crosslinking, and density was examined in response to exogenous VEGF-A in the culture media. Exogenous VEGF-A promoted angiogenesis, increasing vascular density, but not neovessel guidance out from the core. Interestingly, when microvascular fragments were within the collagen core and SVF in the surrounding outer field, microvessels formed towards the SVF compared to when both the microvessels and SVF were located within the core. This data suggests a diffusion gradience cue exists due to SVF in directing microvascular growth [304]. A study utilizing several genetic and pharmacologic gain and loss of function models demonstrated that VEGF-A distribution in the extra cellular space guides tip cell migration (VEGF gradient) and cell proliferation (VEGF concentration) [375]. SVF cells appear to secrete VEGF in optimal spatiotemporal gradients to promote angiogenesis in microvessels.

Advancing age has been shown to reduce the circulating levels of VEGF [75]. Furthermore, advancing age reduces VEGF expression and reduces its dilation potential in the coronary microcirculation [288]. SVF has been shown to secrete growth factors such as VEGF and TGFβ *in vitro* [197]. In our aged-injury model, we measured various levels of cytokines in the media on day 3 of culture, 6 days post-injury. There were few changes in the levels of inflammatory markers between any of the groups. Interestingly, non-SVF-treated non-injured aged windows had comparable levels of VEGF to young SVF-injured windows which showed a significant increase in vascularized area at this time point. The non-treated non-injured aged windows had significantly higher levels of VEGF compared to the aged SVF non-injured windows (**Chapter 4**). Another group measured serum levels of VEGF in aged control, young control, aged treated with young SVF, and young to young. The aged group had higher levels of serum VEGF compared to the other groups [376]. Application of SVF following endometrial injury was associated with a 29% reduction in endometrial vascular endothelial growth factor (VEGF) expression 4-weeks after administration [377]. Our results fall between those of the two studies presented. We propose that young SVF, with greater angiogenic potential, improves endothelial sensitivity to VEGF while aged SVF increases angiogenesis through engraftment of immunomodulatory cells such as T cells following injury. To further support this, an *in vitro* study using HUVEC cells showed that mitochondrial ROS, hydrogen peroxide, increases in the presence of VEGF [378]. Studies from our lab showed that advancing age increases levels of hydrogen peroxide within coronary microvessels but FMD is impaired. Four weeks following an i.v. administration of young SVF, FMD was restored by switching the acute signaling mediator from hydrogen

peroxide to peroxynitrite, a molecule similar to the nitric oxide used in young vessels (**Appendix 3**). Overexpression of a mitochondrial enzyme catalases which converts ROS to hydrogen peroxide inhibits the effects of VEGF [378]. SVF therapy was shown to relatively decrease catalase levels compared to aged controls despite higher gene expression compared to young controls, this would shunt more ROS to become the peroxynitrite rather than hydrogen peroxide (**Appendix 3**). Although SVF from young donors reduces hydrogen peroxide in coronary vessels, we measured moderately high levels of VEGF being produced in response to injury and increase angiogenesis, suggesting SVF may increase vascular sensitivity to VEGF albeit through angiogenic or vasoreactivity mechanisms needs to be explored (**Chapter 4**). Further changes in how the secretome and transcriptome are altered in an aged vascular bed and following SVF therapy are future directions.

In summary, advancing age is an unmodifiable risk factor for the development of vascular pathologies developing in a complex and multifactorial manor [44, 45]. The findings presented in this study demonstrated that age decreases coronary perfusion and correlates with left ventricular diastolic dysfunction. Second, we showed that coronary microvessels are dependent upon the β1-AR to produce an adequate vasodilatory response but as chronological age advances the sensitivity of this receptor decreases (**Chapter 2**). A decrease in the β1-AR was due to a decline in the receptor population with age. Further exploration into why the β1-AR levels on coronary microvessels was decreased with age is due to increased activity of the negative regulator GRK2, which initiates receptor internalization following substrate binding, (**Chapter 3**) and increased ROS which correlated with impaired β-AR dilation (**Appendix 3**). In young control

animals, GRK2 can be both phosphorylated and nitrosolated, both contributing to natural inhibition of GRK2 [379]. With age and a decline in nitric oxide bioavailability, GRK2 becomes more active (**Chapter 3** and **Appendix 3**). A decline in nitric oxide with age only adds to a decreased vascular dilative function (**Appendix 3**), and this effectively puts aged patients at increased risk for an ischemic injury. Third, we showed advancing age decreases the angiogenic potential to revascularize following an ischemic injury. SVF has been an emerging therapeutic due to its ease of access, autologous and allogeneic potential, angiogenic, immune modulatory, and anti-oxidative properties. A caveat being we have shown that age can alter the cellular composition of SVF, lending more to a pro-inflammatory cellular phenotype. While aged SVF can increase angiogenesis following ischemic injury, it does not significantly perform better like SVF from young donors (**Chapter 4**). SVF from young donors was shown to improve all of the age-related alterations previously described above. Briefly, SVF therapy improved coronary perfusion and LV diastolic function, β1-AR sensitivity via restoring receptor population, modulating dilatory inhibitors, receptor recycling, and also by increasing angiogenesis in hypoxic areas of an aged vascular bed via engraftment and possible improvement in sensitivity to VEGF (**Chapter 2-4** and **Appendices 1-2**). Taken together this data provides substantial support for SVF's use as a therapeutic for the aged patient population whilst exploring mechanisms behind the therapeutic benefit.

Further age-related alterations driving the decline in vascular health with advancing age need to be explored. Current therapeutics aimed at preserving heart functionality e.g., paroxetine or beta-blockers do not consider the impact on the microvasculature often reliant on similar signaling cascades. Therapeutic targets

following an injury, e.g., non-steroidal anti-inflammatories, do not consider that a spike in inflammation is crucial for temporal control of healing and revascularization. The impact of how age affects cells involved in vascular function and healing following injury are future directions in the field of gerontology and biomedical sciences [35]. More studies utilizing SVF and examining its constituent's contribution to its therapeutic potential will only advance SVF's application in more disease states beyond advanced age.

Specifically, if I could continue within this field of research I would further examine SVF's impact on catecholamine metabolism in improving dilation in the resistance vessels [345]. The anti-oxidative properties of SVF warrant much further investigation as it ties into dilation, angiogenesis, immune, and cell survival pathways. The vascular hierarchy expresses many other receptors contributing to vasodilation and constriction, being stimulated by other bioactive molecules. Some examples of receptors to examine the impact of age, SVF therapy, and contribution to dilation are prostaglandin, estrogen, and bradykinin receptors. If drugs such as BEZ235 or okadaic acid are used systemically to inhibit β1-AR internalization and increase vasodilation; then the impact on the β-AR populations in the heart and increase in inotropy needs to be considered [121]. Interestingly we showed that SVF increased translation of the adenylyl isoform 6 in the coronary microvessels, albeit they were not completely free of myocytes. Isoform 6 is cardioprotective and has a role in the PKA/STAT3 pathway [285, 286]. During myocardial ischemia, an increase in IL-6 activates STAT3 which has a protective role in infarct size [380] and regulates transcription of VEGF [381]. Aberrant activation of STAT3, such as in a chronic inflammatory state like advanced age, contributed to the

development of atherosclerosis [382]. I believe the AC6/IL6 to STAT3 pathways in the myocardium and microvasculature needs further research as potential pathways SVF further provides therapeutic gains. I would also like to examine the potential of the Gαi subunit, normally associated with the β2-3-ARs, to cross-inhibit the Gs unit of the β1-AR after prolonged stimulation, like seen with the age-related increase in catecholamines. Lastly, I would continue utilization of the *ex vivo* mesenteric window model to assess what cell types in SVF persist infiltrate during the remolding process; what changes to the secretome correlate to this? How does remodeling of the vasculature look different to that of young animals?

SVF's contribution to angiogenesis and active vascular remodeling have unanswered questions. For example, of SVF's many cell types, which are the most beneficial? Can SVF therapy be altered, say from an aged patient, to be a better therapeutic i.e., pre-conditioning with growth factors or increasing one cellular component over another? The area of SVF research with the least knowledge is how advanced age of the donor modifies its therapeutic mechanism; the difference in cytokines being released, the functionality of the cells being administered, and its overall potential to be an effective therapeutic. How long can the therapeutic benefit of either an autologous or allogeneic therapy last as it is being introduced into a potential "hostile" aged environment? It would be pertinent if trials utilizing SVF as a therapeutic, when measuring organ function, also examined vascular functionality and density, as the health of the vasculature would only support the health of the organ. The data presented within this study add to the discussion of how SVF can be used as a vascular therapeutic,

potential mechanisms, reason for inclusion of aged subjects, and introduction to models that can be employed for further investigation to SVF's therapeutic gains.

The future of the cell therapies field is exploring these questions and more to bring cell therapies, specifically SVF, to the front as a valuable vascular therapeutic to a population that currently has little clinical remedies. Trending topics in the cell therapies field, beyond the vasculature, include CRISPER Cas 9 modification of human leukocyte antigens for reduced rejection, cellular reprograming to a more pluripotent state, 3-D bio-constructs with stem cells to bridge ischemic regions, further investigation into dosing strategies, and organ regeneration from tissue scaffolds [320]. The pace the scientific field is moving is an exceptional rate, only hindered by innovation, need, and technology.

REFERENCES

1. Townsend, R.R., et al., *Recommendations for Improving and Standardizing Vascular Research on Arterial Stiffness: A Scientific Statement From the American Heart Association.* Hypertension, 2015. **66**(3): p. 698-722.
2. Jain, R.K., *Molecular regulation of vessel maturation.* Nat Med, 2003. **9**(6): p. 685-93.
3. Schoneberg, J., et al., *Engineering biofunctional in vitro vessel models using a multilayer bioprinting technique.* Sci Rep, 2018. **8**(1): p. 10430.
4. Tucker, W.D., Y. Arora, and K. Mahajan, *Anatomy, Blood Vessels*, in *StatPearls*. 2021: Treasure Island (FL).
5. Guven, G., M.P. Hilty, and C. Ince, *Microcirculation: Physiology, Pathophysiology, and Clinical Application.* Blood Purif, 2020. **49**(1-2): p. 143-150.
6. Muller-Delp, J.M., *Heterogeneous ageing of skeletal muscle microvascular function.* J Physiol, 2016. **594**(8): p. 2285-95.
7. Fleming, J.W., P.L. Wisler, and A.M. Watanabe, *Signal transduction by G proteins in cardiac tissues.* Circulation, 1992. **85**(2): p. 420-33.
8. Wachter, S.B. and E.M. Gilbert, *Beta-adrenergic receptors, from their discovery and characterization through their manipulation to beneficial clinical application.* Cardiology, 2012. **122**(2): p. 104-12.
9. Barbato, E., *Role of adrenergic receptors in human coronary vasomotion.* Heart, 2009. **95**(7): p. 603-8.
10. Bristow, M.R., et al., *Beta 1- and beta 2-adrenergic-receptor subpopulations in nonfailing and failing human ventricular myocardium: coupling of both receptor subtypes to muscle contraction and selective beta 1-receptor down-regulation in heart failure.* Circ Res, 1986. **59**(3): p. 297-309.
11. Moniotte, S., et al., *Upregulation of beta(3)-adrenoceptors and altered contractile response to inotropic amines in human failing myocardium.* Circulation, 2001. **103**(12): p. 1649-55.
12. Murphree, S.S. and J.E. Saffitz, *Delineation of the distribution of beta-adrenergic receptor subtypes in canine myocardium.* Circ Res, 1988. **63**(1): p. 117-25.
13. Liggett, S.B., *Update on current concepts of the molecular basis of beta2-adrenergic receptor signaling.* J Allergy Clin Immunol, 2002. **110**(6 Suppl): p. S223-7.
14. Myagmar, B.E., et al., *Adrenergic Receptors in Individual Ventricular Myocytes: The Beta-1 and Alpha-1B Are in All Cells, the Alpha-1A Is in a Subpopulation, and the Beta-2 and Beta-3 Are Mostly Absent.* Circ Res, 2017. **120**(7): p. 1103-1115.

15. Gauthier, C., et al., *Beta-3 adrenoceptors as new therapeutic targets for cardiovascular pathologies.* Curr Heart Fail Rep, 2011. **8**(3): p. 184-92.
16. Collins, S., W. Cao, and J. Robidoux, *Learning new tricks from old dogs: beta-adrenergic receptors teach new lessons on firing up adipose tissue metabolism.* Mol Endocrinol, 2004. **18**(9): p. 2123-31.
17. Lefkowitz, R.J., et al., *Mechanisms of beta-adrenergic receptor desensitization and resensitization.* Adv Pharmacol, 1998. **42**: p. 416-20.
18. Kohout, T.A., et al., *Augmentation of cardiac contractility mediated by the human beta(3)-adrenergic receptor overexpressed in the hearts of transgenic mice.* Circulation, 2001. **104**(20): p. 2485-91.
19. de Lucia, C., A. Eguchi, and W.J. Koch, *New Insights in Cardiac beta-Adrenergic Signaling During Heart Failure and Aging.* Front Pharmacol, 2018. **9**: p. 904.
20. Vasudevan, N.T., et al., *Regulation of beta-adrenergic receptor function: an emphasis on receptor resensitization.* Cell Cycle, 2011. **10**(21): p. 3684-91.
21. Benovic, J.L., et al., *Phosphorylation of the mammalian beta-adrenergic receptor by cyclic AMP-dependent protein kinase. Regulation of the rate of receptor phosphorylation and dephosphorylation by agonist occupancy and effects on coupling of the receptor to the stimulatory guanine nucleotide regulatory protein.* J Biol Chem, 1985. **260**(11): p. 7094-101.
22. Magalhaes, A.C., H. Dunn, and S.S. Ferguson, *Regulation of GPCR activity, trafficking and localization by GPCR-interacting proteins.* Br J Pharmacol, 2012. **165**(6): p. 1717-1736.
23. Lefkowitz, R.J., *G protein-coupled receptors. III. New roles for receptor kinases and beta-arrestins in receptor signaling and desensitization.* J Biol Chem, 1998. **273**(30): p. 18677-80.
24. Drake, M.T., S.K. Shenoy, and R.J. Lefkowitz, *Trafficking of G protein-coupled receptors.* Circ Res, 2006. **99**(6): p. 570-82.
25. Ferguson, S.S., et al., *Role of phosphorylation in agonist-promoted beta 2-adrenergic receptor sequestration. Rescue of a sequestration-defective mutant receptor by beta ARK1.* J Biol Chem, 1995. **270**(42): p. 24782-9.
26. Sibley, D.R., et al., *Phosphorylation/dephosphorylation of the beta-adrenergic receptor regulates its functional coupling to adenylate cyclase and subcellular distribution.* Proc Natl Acad Sci U S A, 1986. **83**(24): p. 9408-12.
27. Yu, S.S., R.J. Lefkowitz, and W.P. Hausdorff, *Beta-adrenergic receptor sequestration. A potential mechanism of receptor resensitization.* J Biol Chem, 1993. **268**(1): p. 337-41.
28. Zhang, J., et al., *A central role for beta-arrestins and clathrin-coated vesicle-mediated endocytosis in beta2-adrenergic receptor resensitization. Differential regulation of receptor resensitization in two distinct cell types.* J Biol Chem, 1997. **272**(43): p. 27005-14.
29. Zhang, J., et al., *Cellular trafficking of G protein-coupled receptor/beta-arrestin endocytic complexes.* J Biol Chem, 1999. **274**(16): p. 10999-1006.
30. Krueger, K.M., et al., *The role of sequestration in G protein-coupled receptor resensitization. Regulation of beta2-adrenergic receptor dephosphorylation by vesicular acidification.* J Biol Chem, 1997. **272**(1): p. 5-8.

31. Spadari, R.C., et al., *Role of Beta-adrenergic Receptors and Sirtuin Signaling in the Heart During Aging, Heart Failure, and Adaptation to Stress.* Cell Mol Neurobiol, 2018. **38**(1): p. 109-120.
32. Kang, L.S., et al., *Aging and estrogen alter endothelial reactivity to reactive oxygen species in coronary arterioles.* Am J Physiol Heart Circ Physiol, 2011. **300**(6): p. H2105-15.
33. Garland, C.J. and K.A. Dora, *EDH: endothelium-dependent hyperpolarization and microvascular signalling.* Acta Physiol (Oxf), 2017. **219**(1): p. 152-161.
34. Adair, T.H. and J.P. Montani, in *Angiogenesis*. 2010: San Rafael (CA).
35. LeBlanc, A.J., et al., *Microvascular repair: post-angiogenesis vascular dynamics.* Microcirculation, 2012. **19**(8): p. 676-95.
36. Secomb, T.W. and A.R. Pries, *The microcirculation: physiology at the mesoscale.* J Physiol, 2011. **589**(Pt 5): p. 1047-52.
37. Aghazadeh, Y., et al., *Cell-based therapies for vascular regeneration: Past, present and future.* Pharmacol Ther, 2021: p. 107976.
38. Pries, A.R. and T.W. Secomb, *Making microvascular networks work: angiogenesis, remodeling, and pruning.* Physiology (Bethesda), 2014. **29**(6): p. 446-55.
39. Rowe, G., et al., *Enhanced beta-1 adrenergic receptor responsiveness in coronary arterioles following intravenous stromal vascular fraction therapy in aged rats.* Aging (Albany NY), 2019. **11**(13): p. 4561-4578.
40. Rowe, G., et al., *Cell therapy rescues aging-induced beta-1 adrenergic receptor and GRK2 dysfunction in the coronary microcirculation.* Geroscience, 2021.
41. Leblanc, A.J., et al., *Adipose stromal vascular fraction cell construct sustains coronary microvascular function after acute myocardial infarction.* Am J Physiol Heart Circ Physiol, 2012. **302**(4): p. H973-82.
42. Kelm, N.Q., et al., *Adipose-derived cells improve left ventricular diastolic function and increase microvascular perfusion in advanced age.* PLoS One, 2018. **13**(8): p. e0202934.
43. Tracy, E., G. Rowe, and A.J. LeBlanc, *Cardiac Tissue Remodeling in Healthy Aging: The Road to Pathology.* Am J Physiol Cell Physiol, 2020.
44. Aviv, A., *Chronology versus biology: telomeres, essential hypertension, and vascular aging.* Hypertension, 2002. **40**(3): p. 229-32.
45. Beckman, J.A., et al., *Microvascular Disease, Peripheral Artery Disease, and Amputation.* Circulation, 2019. **140**(6): p. 449-458.
46. Sabayan, B., et al., *Markers of endothelial dysfunction and cerebral blood flow in older adults.* Neurobiol Aging, 2014. **35**(2): p. 373-7.
47. Celermajer, D.S., et al., *Aging is associated with endothelial dysfunction in healthy men years before the age-related decline in women.* J Am Coll Cardiol, 1994. **24**(2): p. 471-6.
48. Houben, A., R.J.H. Martens, and C.D.A. Stehouwer, *Assessing Microvascular Function in Humans from a Chronic Disease Perspective.* J Am Soc Nephrol, 2017. **28**(12): p. 3461-3472.
49. Shabani Varaki, E., et al., *Peripheral vascular disease assessment in the lower limb: a review of current and emerging non-invasive diagnostic methods.* Biomed Eng Online, 2018. **17**(1): p. 61.

50. Donato, A.J., et al., *Direct evidence of endothelial oxidative stress with aging in humans: relation to impaired endothelium-dependent dilation and upregulation of nuclear factor-kappaB.* Circ Res, 2007. **100**(11): p. 1659-66.
51. Behroozian, A. and J.A. Beckman, *Microvascular Disease Increases Amputation in Patients With Peripheral Artery Disease.* Arterioscler Thromb Vasc Biol, 2020. **40**(3): p. 534-540.
52. Hachamovitch, R., et al., *Alterations of coronary blood flow and reserve with aging in Fischer 344 rats.* Am J Physiol, 1989. **256**(1 Pt 2): p. H66-73.
53. Czernin, J., et al., *Influence of age and hemodynamics on myocardial blood flow and flow reserve.* Circulation, 1993. **88**(1): p. 62-9.
54. Passmore, J.C., et al., *Reduced alpha adrenergic mediated contraction of renal preglomerular blood vessels as a function of gender and aging.* J Cell Biochem, 2005. **96**(4): p. 672-81.
55. Jagathesan, R., et al., *Comparison of myocardial blood flow and coronary flow reserve during dobutamine and adenosine stress: Implications for pharmacologic stress testing in coronary artery disease.* J Nucl Cardiol, 2006. **13**(3): p. 324-32.
56. Anderson, R.D., et al., *Prevalence of Coronary Endothelial and Microvascular Dysfunction in Women with Symptoms of Ischemia and No Obstructive Coronary Artery Disease Is Confirmed by a New Cohort: The NHLBI-Sponsored Women's Ischemia Syndrome Evaluation-Coronary Vascular Dysfunction (WISE-CVD).* J Interv Cardiol, 2019. **2019**: p. 7169275.
57. Shaw, L.J., et al., *The economic burden of angina in women with suspected ischemic heart disease: results from the National Institutes of Health--National Heart, Lung, and Blood Institute--sponsored Women's Ischemia Syndrome Evaluation.* Circulation, 2006. **114**(9): p. 894-904.
58. Lopez, M.J. and N.D. Spencer, *In vitro adult rat adipose tissue-derived stromal cell isolation and differentiation.* Methods Mol Biol, 2011. **702**: p. 37-46.
59. Durik, M., et al., *Nucleotide excision DNA repair is associated with age-related vascular dysfunction.* Circulation, 2012. **126**(4): p. 468-78.
60. Ungvari, Z., et al., *Mechanisms of Vascular Aging.* Circ Res, 2018. **123**(7): p. 849-867.
61. Abdulhannan, P., D.A. Russell, and S. Homer-Vanniasinkam, *Peripheral arterial disease: a literature review.* Br Med Bull, 2012. **104**: p. 21-39.
62. Bachschmid, M.M., et al., *Vascular aging: chronic oxidative stress and impairment of redox signaling-consequences for vascular homeostasis and disease.* Ann Med, 2013. **45**(1): p. 17-36.
63. Yoon, H.J., et al., *Alterations in the activity and expression of endothelial NO synthase in aged human endothelial cells.* Mech Ageing Dev, 2010. **131**(2): p. 119-23.
64. Ungvari, Z., et al., *Mechanisms of vascular aging: new perspectives.* J Gerontol A Biol Sci Med Sci, 2010. **65**(10): p. 1028-41.
65. Ferrucci, L. and E. Fabbri, *Inflammageing: chronic inflammation in ageing, cardiovascular disease, and frailty.* Nat Rev Cardiol, 2018. **15**(9): p. 505-522.
66. d'Adda di Fagagna, F., et al., *A DNA damage checkpoint response in telomere-initiated senescence.* Nature, 2003. **426**(6963): p. 194-8.

67. Swift, M.E., H.K. Kleinman, and L.A. DiPietro, *Impaired wound repair and delayed angiogenesis in aged mice.* Lab Invest, 1999. **79**(12): p. 1479-87.
68. Yang, J., et al., *Human endothelial cell life extension by telomerase expression.* J Biol Chem, 1999. **274**(37): p. 26141-8.
69. Cheng, S., et al., *Correlates of echocardiographic indices of cardiac remodeling over the adult life course: longitudinal observations from the Framingham Heart Study.* Circulation, 2010. **122**(6): p. 570-8.
70. Franceschi, C., et al., *Inflamm-aging. An evolutionary perspective on immunosenescence.* Ann N Y Acad Sci, 2000. **908**: p. 244-54.
71. van der Feen, D.E., et al., *Cellular senescence impairs the reversibility of pulmonary arterial hypertension.* Sci Transl Med, 2020. **12**(554).
72. Wang, Y., M. Boerma, and D. Zhou, *Ionizing Radiation-Induced Endothelial Cell Senescence and Cardiovascular Diseases.* Radiat Res, 2016. **186**(2): p. 153-61.
73. Chen, W. and N.G. Frangogiannis, *The role of inflammatory and fibrogenic pathways in heart failure associated with aging.* Heart Fail Rev, 2010. **15**(5): p. 415-22.
74. Duvall, W.L., *Cardiovascular disease in women.* Mt Sinai J Med, 2003. **70**(5): p. 293-305.
75. Sadoun, E. and M.J. Reed, *Impaired angiogenesis in aging is associated with alterations in vessel density, matrix composition, inflammatory response, and growth factor expression.* J Histochem Cytochem, 2003. **51**(9): p. 1119-30.
76. Boyle, M., et al., *Chronic inflammation and angiogenic signaling axis impairs differentiation of dental-pulp stem cells.* PLoS One, 2014. **9**(11): p. e113419.
77. Xia, S., et al., *An Update on Inflamm-Aging: Mechanisms, Prevention, and Treatment.* J Immunol Res, 2016. **2016**: p. 8426874.
78. Ferrucci, L., et al., *The origins of age-related proinflammatory state.* Blood, 2005. **105**(6): p. 2294-9.
79. Gerli, R., et al., *Chemokines, sTNF-Rs and sCD30 serum levels in healthy aged people and centenarians.* Mech Ageing Dev, 2000. **121**(1-3): p. 37-46.
80. Newman, A.B., et al., *Trajectories of function and biomarkers with age: the CHS All Stars Study.* Int J Epidemiol, 2016. **45**(4): p. 1135-1145.
81. Cohen, H.J., et al., *The association of plasma IL-6 levels with functional disability in community-dwelling elderly.* J Gerontol A Biol Sci Med Sci, 1997. **52**(4): p. M201-8.
82. Sorriento, D., B. Trimarco, and G. Iaccarino, *Adrenergic mechanism in the control of endothelial function.* Transl Med UniSa, 2011. **1**: p. 213-28.
83. Mendzef, S.D. and J.R. Slovinski, *Neurohormones and heart failure.* Nurs Clin North Am, 2004. **39**(4): p. 845-61.
84. Parmley, W.W., *Pathophysiology of congestive heart failure.* Am J Cardiol, 1985. **56**(2): p. 7A-11A.
85. Ferro, A., A.J. Kaumann, and M.J. Brown, *Beta-adrenoceptor subtypes in human coronary artery: desensitization of beta 2-adrenergic vasorelaxation by chronic beta 1-adrenergic stimulation in vitro.* J Cardiovasc Pharmacol, 1995. **25**(1): p. 134-41.

86. Xiao, R.P., et al., *Age-associated reductions in cardiac beta1- and beta2-adrenergic responses without changes in inhibitory G proteins or receptor kinases.* J Clin Invest, 1998. **101**(6): p. 1273-82.
87. Xiao, R.P. and E.G. Lakatta, *Deterioration of beta-adrenergic modulation of cardiovascular function with aging.* Ann N Y Acad Sci, 1992. **673**: p. 293-310.
88. Mader, S.L., *Influence of animal age on the beta-adrenergic system in cultured rat aortic and mesenteric artery smooth muscle cells.* J Gerontol, 1992. **47**(2): p. B32-6.
89. Fujii, K., et al., *Age-related changes in endothelium-dependent hyperpolarization in the rat mesenteric artery.* Am J Physiol, 1993. **265**(2 Pt 2): p. H509-16.
90. Fujii, K., et al., *Impaired isoproterenol-induced hyperpolarization in isolated mesenteric arteries of aged rats.* Hypertension, 1999. **34**(2): p. 222-8.
91. Rockman, H.A., W.J. Koch, and R.J. Lefkowitz, *Seven-transmembrane-spanning receptors and heart function.* Nature, 2002. **415**(6868): p. 206-12.
92. Bristow, M.R., *Mechanism of action of beta-blocking agents in heart failure.* Am J Cardiol, 1997. **80**(11A): p. 26L-40L.
93. Bristow, M.R., et al., *Decreased catecholamine sensitivity and beta-adrenergic-receptor density in failing human hearts.* N Engl J Med, 1982. **307**(4): p. 205-11.
94. Pan, H.Y., et al., *Decline in beta adrenergic receptor-mediated vascular relaxation with aging in man.* J Pharmacol Exp Ther, 1986. **239**(3): p. 802-7.
95. Dinenno, F.A. and M.J. Joyner, *Alpha-adrenergic control of skeletal muscle circulation at rest and during exercise in aging humans.* Microcirculation, 2006. **13**(4): p. 329-41.
96. Gurdal, H., et al., *The expression of alpha 1 adrenoceptor subtypes changes with age in the rat aorta.* J Pharmacol Exp Ther, 1995. **275**(3): p. 1656-62.
97. Arbab-Zadeh, A., et al., *Effect of aging and physical activity on left ventricular compliance.* Circulation, 2004. **110**(13): p. 1799-805.
98. Tracy, E., G. Rowe, and A.J. LeBlanc, *Cardiac tissue remodeling in healthy aging: the road to pathology.* Am J Physiol Cell Physiol, 2020. **319**(1): p. C166-C182.
99. Carmeliet, P., *Angiogenesis in life, disease and medicine.* Nature, 2005. **438**(7070): p. 932-6.
100. Lahteenvuo, J. and A. Rosenzweig, *Effects of aging on angiogenesis.* Circ Res, 2012. **110**(9): p. 1252-64.
101. Nakae, I., et al., *Age-dependent impairment of coronary collateral development in humans.* Heart Vessels, 2000. **15**(4): p. 176-80.
102. Jia, G., et al., *Endothelial cell senescence in aging-related vascular dysfunction.* Biochim Biophys Acta Mol Basis Dis, 2019. **1865**(7): p. 1802-1809.
103. Rivard, A., et al., *Age-dependent impairment of angiogenesis.* Circulation, 1999. **99**(1): p. 111-20.
104. Holt, D.R., et al., *Effect of age on wound healing in healthy human beings.* Surgery, 1992. **112**(2): p. 293-7; discussion 297-8.
105. Kim, D.J., T. Mustoe, and R.A. Clark, *Cutaneous wound healing in aging small mammals: a systematic review.* Wound Repair Regen, 2015. **23**(3): p. 318-39.

106. Kurotobi, T., et al., *Reduced collateral circulation to the infarct-related artery in elderly patients with acute myocardial infarction.* J Am Coll Cardiol, 2004. **44**(1): p. 28-34.
107. Kourembanas, S., R.L. Hannan, and D.V. Faller, *Oxygen tension regulates the expression of the platelet-derived growth factor-B chain gene in human endothelial cells.* J Clin Invest, 1990. **86**(2): p. 670-4.
108. Pollman, M.J., L. Naumovski, and G.H. Gibbons, *Endothelial cell apoptosis in capillary network remodeling.* J Cell Physiol, 1999. **178**(3): p. 359-70.
109. Mohammed, S.F., et al., *Coronary microvascular rarefaction and myocardial fibrosis in heart failure with preserved ejection fraction.* Circulation, 2015. **131**(6): p. 550-9.
110. Frangogiannis, N.G., *The immune system and cardiac repair.* Pharmacol Res, 2008. **58**(2): p. 88-111.
111. Evanson, J.R., et al., *Gender and age differences in growth factor concentrations from platelet-rich plasma in adults.* Mil Med, 2014. **179**(7): p. 799-805.
112. Campisi, J., et al., *From discoveries in ageing research to therapeutics for healthy ageing.* Nature, 2019. **571**(7764): p. 183-192.
113. Moyer, A.M., et al., *Influence of SULT1A1 genetic variation on age at menopause, estrogen levels, and response to hormone therapy in recently postmenopausal white women.* Menopause, 2016. **23**(8): p. 863-9.
114. Marinescu, M.A., et al., *Coronary microvascular dysfunction, microvascular angina, and treatment strategies.* JACC Cardiovasc Imaging, 2015. **8**(2): p. 210-20.
115. Cocco, G. and P. Jerie, *Angina pectoris in patients without flow-limiting coronary artery disease (cardiac syndrome X). A forest of a variety of trees.* Cardiol J, 2015. **22**(6): p. 605-12.
116. Beale, A.L., et al., *Sex Differences in Cardiovascular Pathophysiology: Why Women Are Overrepresented in Heart Failure With Preserved Ejection Fraction.* Circulation, 2018. **138**(2): p. 198-205.
117. Wang, H., et al., *Activation of GPR30 attenuates diastolic dysfunction and left ventricle remodelling in oophorectomized mRen2.Lewis rats.* Cardiovasc Res, 2012. **94**(1): p. 96-104.
118. Nicholson, C.J., et al., *Estrogenic vascular effects are diminished by chronological aging.* Sci Rep, 2017. **7**(1): p. 12153.
119. Reis, S.E., et al., *Coronary microvascular dysfunction is highly prevalent in women with chest pain in the absence of coronary artery disease: results from the NHLBI WISE study.* Am Heart J, 2001. **141**(5): p. 735-41.
120. Buteau-Lozano, H., et al., *Transcriptional regulation of vascular endothelial growth factor by estradiol and tamoxifen in breast cancer cells: a complex interplay between estrogen receptors alpha and beta.* Cancer Res, 2002. **62**(17): p. 4977-84.
121. Tracy, E.P., et al., *Aging Induced Impairment of Vascular Function - Mitochondrial Redox Contributions and Physiological/Clinical Implications.* Antioxid Redox Signal, 2021.
122. Chao, C.Y. and G.L. Cheing, *Microvascular dysfunction in diabetic foot disease and ulceration.* Diabetes Metab Res Rev, 2009. **25**(7): p. 604-14.

123. Roustit, M., et al., *Microvascular Changes in the Diabetic Foot*, in *The Diabetic Foot*, V. A., G. J., and G. R., Editors. 2018, Humana, Cham. p. 173-188.
124. Bolognese, L., et al., *Impact of microvascular dysfunction on left ventricular remodeling and long-term clinical outcome after primary coronary angioplasty for acute myocardial infarction.* Circulation, 2004. **109**(9): p. 1121-6.
125. Wei, J., S. Cheng, and C.N. Bairey Merz, *Coronary Microvascular Dysfunction Causing Cardiac Ischemia in Women.* JAMA, 2019. **322**(23): p. 2334-2335.
126. Nguyen, P.K., J.W. Rhee, and J.C. Wu, *Adult Stem Cell Therapy and Heart Failure, 2000 to 2016: A Systematic Review.* JAMA Cardiol, 2016. **1**(7): p. 831-841.
127. Satwani, S., G.W. Dec, and J. Narula, *Beta-adrenergic blockers in heart failure: review of mechanisms of action and clinical outcomes.* J Cardiovasc Pharmacol Ther, 2004. **9**(4): p. 243-55.
128. Colucci, W.S., *Positive inotropic/vasodilator agents.* Cardiol Clin, 1989. **7**(1): p. 131-44.
129. Gori, T. and J.D. Parker, *Long-term therapy with organic nitrates: the pros and cons of nitric oxide replacement therapy.* J Am Coll Cardiol, 2004. **44**(3): p. 632-4.
130. Takahashi, J., et al., *Prognostic impact of chronic nitrate therapy in patients with vasospastic angina: multicentre registry study of the Japanese coronary spasm association.* Eur Heart J, 2015. **36**(4): p. 228-37.
131. Task Force, M., et al., *2013 ESC guidelines on the management of stable coronary artery disease: the Task Force on the management of stable coronary artery disease of the European Society of Cardiology.* Eur Heart J, 2013. **34**(38): p. 2949-3003.
132. Santos-Parker, J.R., et al., *Habitual aerobic exercise does not protect against micro- or macrovascular endothelial dysfunction in healthy estrogen-deficient postmenopausal women.* J Appl Physiol (1985), 2017. **122**(1): p. 11-19.
133. Tarnawski, A.S. and M.K. Jones, *Inhibition of angiogenesis by NSAIDs: molecular mechanisms and clinical implications.* J Mol Med (Berl), 2003. **81**(10): p. 627-36.
134. Seropian, I.M., et al., *Anti-inflammatory strategies for ventricular remodeling following ST-segment elevation acute myocardial infarction.* J Am Coll Cardiol, 2014. **63**(16): p. 1593-603.
135. Khalil, R.A., *Estrogen, vascular estrogen receptor and hormone therapy in postmenopausal vascular disease.* Biochem Pharmacol, 2013. **86**(12): p. 1627-42.
136. Aly, R.M., *Current state of stem cell-based therapies: an overview.* Stem Cell Investig, 2020. **7**: p. 8.
137. Williams, A.R. and J.M. Hare, *Mesenchymal stem cells: biology, pathophysiology, translational findings, and therapeutic implications for cardiac disease.* Circ Res, 2011. **109**(8): p. 923-40.
138. Patel, K.M., et al., *Mesenchymal stem cells attenuate hypoxic pulmonary vasoconstriction by a paracrine mechanism.* J Surg Res, 2007. **143**(2): p. 281-5.
139. Hong, S.J., D.O. Traktuev, and K.L. March, *Therapeutic potential of adipose-derived stem cells in vascular growth and tissue repair.* Curr.Opin.Organ Transplant., 2010. **15**(1): p. 86-91.

140. Rehman, J., et al., *Secretion of angiogenic and antiapoptotic factors by human adipose stromal cells.* Circulation, 2004. **109**(10): p. 1292-8.
141. Dubey, N.K., et al., *Revisiting the Advances in Isolation, Characterization and Secretome of Adipose-Derived Stromal/Stem Cells.* Int J Mol Sci, 2018. **19**(8).
142. Stavely, R. and K. Nurgali, *The emerging antioxidant paradigm of mesenchymal stem cell therapy.* Stem Cells Transl Med, 2020. **9**(9): p. 985-1006.
143. Zhu, M., et al., *[Effects of different human adipose-derived cells in promoting human adipose tissue engraftment in nude mice].* Nan Fang Yi Ke Da Xue Xue Bao, 2012. **32**(9): p. 1265-9.
144. Johnson, T.K., et al., *Exosomes derived from induced vascular progenitor cells promote angiogenesis in vitro and in an in vivo rat hindlimb ischemia model.* Am J Physiol Heart Circ Physiol, 2019. **317**(4): p. H765-H776.
145. Ge, Q., et al., *VEGF secreted by mesenchymal stem cells mediates the differentiation of endothelial progenitor cells into endothelial cells via paracrine mechanisms.* Mol Med Rep, 2018. **17**(1): p. 1667-1675.
146. Zhang, B., et al., *Co-culture of mesenchymal stem cells with umbilical vein endothelial cells under hypoxic condition.* J Huazhong Univ Sci Technolog Med Sci, 2012. **32**(2): p. 173-180.
147. Phan, J., et al., *Engineering mesenchymal stem cells to improve their exosome efficacy and yield for cell-free therapy.* J Extracell Vesicles, 2018. **7**(1): p. 1522236.
148. Pegtel, D.M. and S.J. Gould, *Exosomes.* Annu Rev Biochem, 2019. **88**: p. 487-514.
149. Aghazadeh, Y., et al., *Microvessels support engraftment and functionality of human islets and hESC-derived pancreatic progenitors in diabetes models.* Cell Stem Cell, 2021.
150. Xue, C., et al., *Exosomes Derived from Hypoxia-Treated Human Adipose Mesenchymal Stem Cells Enhance Angiogenesis Through the PKA Signaling Pathway.* Stem Cells Dev, 2018. **27**(7): p. 456-465.
151. Wang, N., et al., *Vascular endothelial growth factor stimulates endothelial differentiation from mesenchymal stem cells via Rho/myocardin-related transcription factor--a signaling pathway.* Int J Biochem Cell Biol, 2013. **45**(7): p. 1447-56.
152. Scheiner, Z.S., S. Talib, and E.G. Feigal, *The potential for immunogenicity of autologous induced pluripotent stem cell-derived therapies.* J Biol Chem, 2014. **289**(8): p. 4571-7.
153. Khorraminejad-Shirazi, M., et al., *Aging: A cell source limiting factor in tissue engineering.* World J Stem Cells, 2019. **11**(10): p. 787-802.
154. Aird, A.L., et al., *Adipose-derived stromal vascular fraction cells isolated from old animals exhibit reduced capacity to support the formation of microvascular networks.* Exp Gerontol, 2015. **63**: p. 18-26.
155. Dos-Anjos Vilaboa, S., M. Navarro-Palou, and R. Llull, *Age influence on stromal vascular fraction cell yield obtained from human lipoaspirates.* Cytotherapy, 2014. **16**(8): p. 1092-7.

156. Sanchez-Diaz, M., et al., *Biodistribution of Mesenchymal Stromal Cells after Administration in Animal Models and Humans: A Systematic Review.* J Clin Med, 2021. **10**(13).
157. Li, M., et al., *Mesenchymal stem cell-derived exosomes ameliorate dermal fibrosis in a murine model of bleomycin-induced scleroderma.* Stem Cells Dev, 2021.
158. Kabat, M., et al., *Trends in mesenchymal stem cell clinical trials 2004-2018: Is efficacy optimal in a narrow dose range?* Stem Cells Transl Med, 2020. **9**(1): p. 17-27.
159. Stagg, J., et al., *Interferon-gamma-stimulated marrow stromal cells: a new type of nonhematopoietic antigen-presenting cell.* Blood, 2006. **107**(6): p. 2570-7.
160. Uccelli, A., L. Moretta, and V. Pistoia, *Mesenchymal stem cells in health and disease.* Nat Rev Immunol, 2008. **8**(9): p. 726-36.
161. Bartholomew, A., et al., *Mesenchymal stem cells suppress lymphocyte proliferation in vitro and prolong skin graft survival in vivo.* Exp Hematol, 2002. **30**(1): p. 42-8.
162. Di Nicola, M., et al., *Human bone marrow stromal cells suppress T-lymphocyte proliferation induced by cellular or nonspecific mitogenic stimuli.* Blood, 2002. **99**(10): p. 3838-43.
163. Hamamoto, H., et al., *Allogeneic mesenchymal precursor cell therapy to limit remodeling after myocardial infarction: the effect of cell dosage.* Ann Thorac Surg, 2009. **87**(3): p. 794-801.
164. Hashemi, S.M., et al., *A placebo controlled, dose-ranging, safety study of allogenic mesenchymal stem cells injected by endomyocardial delivery after an acute myocardial infarction.* Eur Heart J, 2008. **29**(2): p. 251-9.
165. Schuleri, K.H., et al., *Autologous mesenchymal stem cells produce reverse remodelling in chronic ischaemic cardiomyopathy.* Eur Heart J, 2009. **30**(22): p. 2722-32.
166. Hu, X., et al., *Transplantation of hypoxia-preconditioned mesenchymal stem cells improves infarcted heart function via enhanced survival of implanted cells and angiogenesis.* J Thorac Cardiovasc Surg, 2008. **135**(4): p. 799-808.
167. Zhou, T., C.C. Chuang, and L. Zuo, *Molecular Characterization of Reactive Oxygen Species in Myocardial Ischemia-Reperfusion Injury.* Biomed Res Int, 2015. **2015**: p. 864946.
168. Duong Van Huyen, J.P., et al., *Bone marrow-derived mononuclear cell therapy induces distal angiogenesis after local injection in critical leg ischemia.* Mod Pathol, 2008. **21**(7): p. 837-46.
169. Nagaya, N., et al., *Intravenous administration of mesenchymal stem cells improves cardiac function in rats with acute myocardial infarction through angiogenesis and myogenesis.* Am J Physiol Heart Circ Physiol, 2004. **287**(6): p. H2670-6.
170. Halkos, M.E., et al., *Intravenous infusion of mesenchymal stem cells enhances regional perfusion and improves ventricular function in a porcine model of myocardial infarction.* Basic Res Cardiol, 2008. **103**(6): p. 525-36.

171. Lee, J.W., et al., *A randomized, open-label, multicenter trial for the safety and efficacy of adult mesenchymal stem cells after acute myocardial infarction.* J Korean Med Sci, 2014. **29**(1): p. 23-31.
172. Carmona, M.D., et al., *Intramyocardial bone marrow mononuclear cells versus bone marrow-derived and adipose mesenchymal cells in a rat model of dilated cardiomyopathy.* Cytotherapy, 2017. **19**(8): p. 947-961.
173. Charbord, P., *Bone marrow mesenchymal stem cells: historical overview and concepts.* Hum Gene Ther, 2010. **21**(9): p. 1045-56.
174. Gorjipour, F., et al., *Mesenchymal stem cells from human amniotic membrane differentiate into cardiomyocytes and endothelial-like cells without improving cardiac function after surgical administration in rat model of chronic heart failure.* J Cardiovasc Thorac Res, 2019. **11**(1): p. 35-42.
175. Tiryaki, T., et al., *A 3-step Mechanical Digestion Method to Harvest Adipose-derived Stromal Vascular Fraction.* Plast Reconstr Surg Glob Open, 2020. **8**(2): p. e2652.
176. Bora, P. and A.S. Majumdar, *Adipose tissue-derived stromal vascular fraction in regenerative medicine: a brief review on biology and translation.* Stem Cell Res Ther, 2017. **8**(1): p. 145.
177. Stivers, K.B., et al., *Adipose-derived cellular therapies in solid organ and vascularized-composite allotransplantation.* Curr Opin Organ Transplant, 2017. **22**(5): p. 490-498.
178. Zimmerlin, L., et al., *Stromal vascular progenitors in adult human adipose tissue.* Cytometry A, 2010. **77**(1): p. 22-30.
179. Zuk, P.A., et al., *Multilineage cells from human adipose tissue: implications for cell-based therapies.* Tissue Eng, 2001. **7**(2): p. 211-28.
180. Mao, F., et al., *Mesenchymal stem cells and their therapeutic applications in inflammatory bowel disease.* Oncotarget, 2017. **8**(23): p. 38008-38021.
181. Fodor, P.B. and S.G. Paulseth, *Adipose Derived Stromal Cell (ADSC) Injections for Pain Management of Osteoarthritis in the Human Knee Joint.* Aesthet Surg J, 2016. **36**(2): p. 229-36.
182. Ntolios, P., et al., *Longitudinal outcomes of patients enrolled in a phase Ib clinical trial of the adipose-derived stromal cells-stromal vascular fraction in idiopathic pulmonary fibrosis.* Clin Respir J, 2018. **12**(6): p. 2084-2089.
183. Comella, K., et al., *Effects of the intramyocardial implantation of stromal vascular fraction in patients with chronic ischemic cardiomyopathy.* J Transl Med, 2016. **14**(1): p. 158.
184. Laloze, J., L. Fievet, and A. Desmouliere, *Adipose-Derived Mesenchymal Stromal Cells in Regenerative Medicine: State of Play, Current Clinical Trials, and Future Prospects.* Adv Wound Care (New Rochelle), 2021. **10**(1): p. 24-48.
185. Ullah, I., R.B. Subbarao, and G.J. Rho, *Human mesenchymal stem cells - current trends and future prospective.* Biosci Rep, 2015. **35**(2).
186. Wilson, A., et al., *Multiplicity of Mesenchymal Stromal Cells: Finding the Right Route to Therapy.* Front Immunol, 2019. **10**: p. 1112.
187. Nguyen, A., et al., *Stromal vascular fraction: A regenerative reality? Part 1: Current concepts and review of the literature.* J Plast Reconstr Aesthet Surg, 2016. **69**(2): p. 170-9.

188. Jones, V.M., et al., *A clinical perspective on adipose-derived cell therapy for enhancing microvascular health and function: Implications and applications for reconstructive surgery.* Microcirculation, 2021. **28**(3): p. e12672.
189. Sheu, J.J., et al., *Therapeutic effects of adipose derived fresh stromal vascular fraction-containing stem cells versus cultured adipose derived mesenchymal stem cells on rescuing heart function in rat after acute myocardial infarction.* Am J Transl Res, 2019. **11**(1): p. 67-86.
190. Yang, G., et al., *Obtaining spontaneously beating cardiomyocyte-like cells from adipose-derived stromal vascular fractions cultured on enzyme-crosslinked gelatin hydrogels.* Sci Rep, 2017. **7**: p. 41781.
191. Zakhari, J.S., et al., *Vasculogenic and angiogenic potential of adipose stromal vascular fraction cell populations in vitro.* In Vitro Cell Dev Biol Anim, 2018. **54**(1): p. 32-40.
192. Paul, A., et al., *Functional assessment of adipose stem cells for xenotransplantation using myocardial infarction immunocompetent models: comparison with bone marrow stem cells.* Cell Biochem Biophys, 2013. **67**(2): p. 263-73.
193. Rasmussen, J.G., et al., *Comparison of human adipose-derived stem cells and bone marrow-derived stem cells in a myocardial infarction model.* Cell Transplant, 2014. **23**(2): p. 195-206.
194. Kim, Y., et al., *Direct comparison of human mesenchymal stem cells derived from adipose tissues and bone marrow in mediating neovascularization in response to vascular ischemia.* Cell Physiol Biochem, 2007. **20**(6): p. 867-76.
195. Elman, J.S., et al., *A comparison of adipose and bone marrow-derived mesenchymal stromal cell secreted factors in the treatment of systemic inflammation.* J Inflamm (Lond), 2014. **11**(1): p. 1.
196. Bacakova, L., et al., *Stem cells: their source, potency and use in regenerative therapies with focus on adipose-derived stem cells - a review.* Biotechnol Adv, 2018. **36**(4): p. 1111-1126.
197. Li, X., et al., *Harnessing the secretome of adipose-derived stem cells in the treatment of ischemic heart diseases.* Stem Cell Res Ther, 2019. **10**(1): p. 196.
198. Feisst, V., S. Meidinger, and M.B. Locke, *From bench to bedside: use of human adipose-derived stem cells.* Stem Cells Cloning, 2015. **8**: p. 149-62.
199. Savvatis, K., et al., *Mesenchymal stromal cells but not cardiac fibroblasts exert beneficial systemic immunomodulatory effects in experimental myocarditis.* PLoS One, 2012. **7**(7): p. e41047.
200. Morris, M.E., et al., *Systemically delivered adipose stromal vascular fraction cells disseminate to peripheral artery walls and reduce vasomotor tone through a CD11b+ cell-dependent mechanism.* Stem Cells Transl Med, 2015. **4**(4): p. 369-80.
201. Morris, M.E., et al., *Systemically Delivered Adipose Stromal Vascular Fraction Cells Disseminate to Peripheral Artery Walls and Reduce Vasomotor Tone Through a CD11b+ Cell-Dependent Mechanism.* Stem Cells Transl Med, 2015.
202. Ferrara, N., et al., *beta-adrenergic receptor responsiveness in aging heart and clinical implications.* Front Physiol, 2014. **4**: p. 396.

203. Davies, C.H., N. Ferrara, and S.E. Harding, *Beta-adrenoceptor function changes with age of subject in myocytes from non-failing human ventricle.* Cardiovasc Res, 1996. **31**(1): p. 152-6.
204. Ford, G.A., et al., *Age-related changes in adenosine and beta-adrenoceptor responsiveness of vascular smooth muscle in man.* Br J Clin Pharmacol, 1992. **33**(1): p. 83-7.
205. Schutzer, W.E. and S.L. Mader, *Age-related changes in vascular adrenergic signaling: clinical and mechanistic implications.* Ageing Res Rev, 2003. **2**(2): p. 169-90.
206. White, M., et al., *Age-related changes in beta-adrenergic neuroeffector systems in the human heart.* Circulation, 1994. **90**(3): p. 1225-38.
207. Dhein, S., et al., *Effects of autologous bone marrow stem cell transplantation on beta-adrenoceptor density and electrical activation pattern in a rabbit model of non-ischemic heart failure.* J Cardiothorac Surg, 2006. **1**: p. 17.
208. Monnerat-Cahli, G., et al., *Bone marrow mesenchymal stromal cells rescue cardiac function in streptozotocin-induced diabetic rats.* Int J Cardiol, 2014. **171**(2): p. 199-208.
209. in *Guide for the Care and Use of Laboratory Animals, 9th edition*. 2011: Washington (DC).
210. Barbash, I.M., et al., *Systemic delivery of bone marrow-derived mesenchymal stem cells to the infarcted myocardium: feasibility, cell migration, and body distribution.* Circulation, 2003. **108**(7): p. 863-8.
211. Lennon, D.P., et al., *A chemically defined medium supports in vitro proliferation and maintains the osteochondral potential of rat marrow-derived mesenchymal stem cells.* Exp Cell Res, 1995. **219**(1): p. 211-22.
212. Au - Kelm, N.Q., J.E. Au - Beare, and A.J. Au - LeBlanc, *Evaluation of Coronary Flow Reserve after Myocardial Ischemia Reperfusion in Rats.* JoVE: p. e59406.
213. Chilian, W.M., C.L. Eastham, and M.L. Marcus, *Microvascular distribution of coronary vascular resistance in beating left ventricle.* Am J Physiol, 1986. **251**(4 Pt 2): p. H779-88.
214. LeBlanc, A.J., et al., *Nanoparticle inhalation impairs coronary microvascular reactivity via a local reactive oxygen species-dependent mechanism.* Cardiovasc Toxicol, 2010. **10**(1): p. 27-36.
215. Wessler, B., et al., *Short-term effects of ketamine and isoflurane on left ventricular ejection fraction in an experimental Swine model.* ISRN Cardiol, 2011. **2011**: p. 582658.
216. Banerjee, M.N., R. Bolli, and J.M. Hare, *Clinical Studies of Cell Therapy in Cardiovascular Medicine: Recent Developments and Future Directions.* Circ Res, 2018. **123**(2): p. 266-287.
217. Besedovsky, H.O. and A. del Rey, *Immune-neuro-endocrine interactions: facts and hypotheses.* Endocr Rev, 1996. **17**(1): p. 64-102.
218. Brodde, O.E., M. Khamssi, and H.R. Zerkowski, *Beta-adrenoceptors in the transplanted human heart: unaltered beta-adrenoceptor density, but increased proportion of beta 2-adrenoceptors with increasing posttransplant time.* Naunyn Schmiedebergs Arch Pharmacol, 1991. **344**(4): p. 430-6.

219. Engelhardt, S., et al., *Analysis of beta-adrenergic receptor mRNA levels in human ventricular biopsy specimens by quantitative polymerase chain reactions: progressive reduction of beta 1-adrenergic receptor mRNA in heart failure.* J Am Coll Cardiol, 1996. **27**(1): p. 146-54.
220. Gayen, J.R., et al., *Role of reactive oxygen species in hyperadrenergic hypertension: biochemical, physiological, and pharmacological evidence from targeted ablation of the chromogranin a (Chga) gene.* Circ Cardiovasc Genet, 2010. **3**(5): p. 414-25.
221. Kaplon, R.E., A.E. Walker, and D.R. Seals, *Plasma norepinephrine is an independent predictor of vascular endothelial function with aging in healthy women.* J Appl Physiol (1985), 2011. **111**(5): p. 1416-21.
222. Deisher, T.A., S. Mankani, and B.B. Hoffman, *Role of cyclic AMP-dependent protein kinase in the diminished beta adrenergic responsiveness of vascular smooth muscle with increasing age.* J Pharmacol Exp Ther, 1989. **249**(3): p. 812-9.
223. Mader, S.L. and P.A. Alley, *Age-related changes in adenylyl cyclase activity in rat aorta membranes.* Mech Ageing Dev, 1998. **101**(1-2): p. 111-8.
224. Ross, A.J., et al., *beta-Adrenergic receptor blockade impairs coronary exercise hyperemia in young men but not older men.* Am J Physiol Heart Circ Physiol, 2014. **307**(10): p. H1497-503.
225. Williams, R.S. and T. Bishop, *Selectivity of dobutamine for adrenergic receptor subtypes: in vitro analysis by radioligand binding.* J Clin Invest, 1981. **67**(6): p. 1703-11.
226. Abdelkrim, M.A., et al., *Antibodies against the second extracellular loop of beta(1)-adrenergic receptors induce endothelial dysfunction in conductance and resistance arteries of the Wistar rat.* Int Immunopharmacol, 2014. **19**(2): p. 308-16.
227. Sun, D., et al., *Norepinephrine elicits beta2-receptor-mediated dilation of isolated human coronary arterioles.* Circulation, 2002. **106**(5): p. 550-5.
228. Moura, A.L., et al., *Functional beta2-adrenoceptors in rat left atria: effect of foot-shock stress.* Can J Physiol Pharmacol, 2017. **95**(9): p. 999-1008.
229. Ziegler, M.G., C.R. Lake, and I.J. Kopin, *Plasma noradrenaline increases with age.* Nature, 1976. **261**(5558): p. 333-5.
230. Schutzer, W.E., et al., *Effect of age on vascular beta2-adrenergic receptor desensitization is not mediated by the receptor coupling to Galphai proteins.* J Gerontol A Biol Sci Med Sci, 2006. **61**(9): p. 899-906.
231. Sun, Y., et al., *Prevention of cardiac events caused by surgical stress in aged rats: simultaneously activating beta2-adrenoceptor and inhibiting beta1-adrenoceptor.* Stress, 2014. **17**(4): p. 373-81.
232. Brodde, O.E., M.C. Michel, and H.R. Zerkowski, *Signal transduction mechanisms controlling cardiac contractility and their alterations in chronic heart failure.* Cardiovasc Res, 1995. **30**(4): p. 570-84.
233. Bohm, M., et al., *Cardiac adenylyl cyclase, beta-adrenergic receptors, and G proteins in salt-sensitive hypertension.* Hypertension, 1993. **22**(5): p. 715-27.

234. Ferrara, N., et al., *The role of Gi-proteins and beta-adrenoceptors in the age-related decline of contraction in guinea-pig ventricular myocytes.* J Mol Cell Cardiol, 1997. **29**(2): p. 439-48.
235. Hoffman, W.E., et al., *Ketamine decreases plasma catecholamines and improves outcome from incomplete cerebral ischemia in rats.* Anesthesiology, 1992. **76**(5): p. 755-62.
236. Marinescu, M.A., et al., *Coronary Microvascular Dysfunction, Microvascular Angina, and Treatment Strategies.* JACC Cardiovasc Imaging, 2015. **8**(2): p. 210-220.
237. Pepine, C.J., et al., *Coronary microvascular reactivity to adenosine predicts adverse outcome in women evaluated for suspected ischemia results from the National Heart, Lung and Blood Institute WISE (Women's Ischemia Syndrome Evaluation) study.* J Am Coll Cardiol, 2010. **55**(25): p. 2825-32.
238. Aird, A.L., et al., *Adipose-derived stromal vascular fraction cells isolated from old animals exhibit reduced capacity to support the formation of microvascular networks.* Exp Gerontol, 2015. **63C**: p. 18-26.
239. Chen, H.T., et al., *Proliferation and differentiation potential of human adipose-derived mesenchymal stem cells isolated from elderly patients with osteoporotic fractures.* J Cell Mol Med, 2012. **16**(3): p. 582-93.
240. Stolzing, A., et al., *Age-related changes in human bone marrow-derived mesenchymal stem cells: consequences for cell therapies.* Mech Ageing Dev, 2008. **129**(3): p. 163-73.
241. Yang, W., et al., *Depletion of beta3-adrenergic receptor induces left ventricular diastolic dysfunction via potential regulation of energy metabolism and cardiac contraction.* Gene, 2019. **697**: p. 1-10.
242. LeBlanc, A.J. and S. Uchida, *A step closer to improving cardiac homing of adipose-derived mesenchymal stem cells.* Am J Physiol Heart Circ Physiol, 2018.
243. Velasco, A., et al., *Differential effects of nebivolol vs. metoprolol on microvascular function in hypertensive humans.* Am J Physiol Heart Circ Physiol, 2016. **311**(1): p. H118-24.
244. Neumann, J., et al., *Increase in myocardial Gi-proteins in heart failure.* Lancet, 1988. **2**(8617): p. 936-7.
245. Feldman, A.M., et al., *Increase of the 40,000-mol wt pertussis toxin substrate (G protein) in the failing human heart.* J Clin Invest, 1988. **82**(1): p. 189-97.
246. Narayanan, N. and L. Tucker, *Autonomic interactions in the aging heart: age-associated decrease in muscarinic cholinergic receptor mediated inhibition of beta-adrenergic activation of adenylate cyclase.* Mech Ageing Dev, 1986. **34**(3): p. 249-59.
247. Lamba, S. and W.T. Abraham, *Alterations in adrenergic receptor signaling in heart failure.* Heart Fail Rev, 2000. **5**(1): p. 7-16.
248. Hall, S.A., et al., *Time course of improvement in left ventricular function, mass and geometry in patients with congestive heart failure treated with beta-adrenergic blockade.* J Am Coll Cardiol, 1995. **25**(5): p. 1154-61.
249. Schutzer, W.E., et al., *Age-related beta-adrenergic receptor-mediated vasorelaxation is changed by altering G protein receptor kinase 2 expression.* Vascul Pharmacol, 2011. **55**(5-6): p. 178-88.

250. El-Armouche, A., et al., *Inhibitory G-proteins and their role in desensitization of the adenylyl cyclase pathway in heart failure.* Cardiovasc Res, 2003. **60**(3): p. 478-87.
251. Ungerer, M., et al., *Altered expression of beta-adrenergic receptor kinase and beta 1-adrenergic receptors in the failing human heart.* Circulation, 1993. **87**(2): p. 454-63.
252. Johnson, M.D., et al., *Expression of G protein alpha subunits in the aging cardiovascular system.* J Gerontol A Biol Sci Med Sci, 1995. **50A**(1): p. B14-9.
253. Nash, C.A., et al., *Differential regulation of beta2-adrenoceptor and adenosine A2B receptor signalling by GRK and arrestin proteins in arterial smooth muscle.* Cell Signal, 2018. **51**: p. 86-98.
254. Council, N.R., *Guide for the Care and Use of Laboratory Animals: Eighth Edition*. 2011, Washington, DC: The National Academies Press. 246.
255. Turturro, A., et al., *Growth curves and survival characteristics of the animals used in the Biomarkers of Aging Program.* J Gerontol A Biol Sci Med Sci, 1999. **54**(11): p. B492-501.
256. Xie, Z., et al., *Comprehensive, robust, and sensitive UPLC-MS/MS analysis of free biogenic monoamines and their metabolites in urine.* J Chromatogr B Analyt Technol Biomed Life Sci, 2018. **1099**: p. 83-91.
257. Mboge, M.Y., et al., *A non-catalytic function of carbonic anhydrase IX contributes to the glycolytic phenotype and pH regulation in human breast cancer cells.* Biochem J, 2019. **476**(10): p. 1497-1513.
258. Lanceta, L., et al., *Transcriptomic Profiling Identifies Differentially Expressed Genes in Palbociclib-Resistant ER+ MCF7 Breast Cancer Cells.* Genes (Basel), 2020. **11**(4).
259. Miralda, I., et al., *Whole Transcriptome Analysis Reveals That Filifactor alocis Modulates TNFalpha-Stimulated MAPK Activation in Human Neutrophils.* Front Immunol, 2020. **11**: p. 497.
260. LeBlanc, A.J., et al., *Estrogen replacement restores flow-induced vasodilation in coronary arterioles of aged and ovariectomized rats.* Am J Physiol Regul Integr Comp Physiol, 2009. **297**(6): p. R1713-23.
261. Kore, R.A., et al., *MSC exosome-mediated cardioprotection in ischemic mouse heart comparative proteomics of infarct and peri-infarct areas.* Mol Cell Biochem, 2021. **476**(4): p. 1691-1704.
262. Cheng, L., et al., *Focus on Mesenchymal Stem Cell-Derived Exosomes: Opportunities and Challenges in Cell-Free Therapy.* Stem Cells Int, 2017. **2017**: p. 6305295.
263. Tsujimoto, G. and B.B. Hoffman, *Desensitization of beta-adrenergic receptor-mediated vascular smooth muscle relaxation.* Mol Pharmacol, 1985. **27**(2): p. 210-7.
264. Penela, P., C. Ribas, and F. Mayor, Jr., *Mechanisms of regulation of the expression and function of G protein-coupled receptor kinases.* Cell Signal, 2003. **15**(11): p. 973-81.
265. Liang, W., et al., *Differences in endosomal targeting of human (beta)1- and (beta)2-adrenergic receptors following clathrin-mediated endocytosis.* J Cell Sci, 2004. **117**(Pt 5): p. 723-34.

266. Schutzer, W.E., et al., *Upregulation of G protein-linked receptor kinases with advancing age in rat aorta.* Am J Physiol Regul Integr Comp Physiol, 2001. **280**(3): p. R897-903.
267. Shiina, T., et al., *Interaction with beta-arrestin determines the difference in internalization behavor between beta1- and beta2-adrenergic receptors.* J Biol Chem, 2000. **275**(37): p. 29082-90.
268. Noor, N., C.B. Patel, and H.A. Rockman, *Beta-arrestin: a signaling molecule and potential therapeutic target for heart failure.* J Mol Cell Cardiol, 2011. **51**(4): p. 534-41.
269. Rengo, G., et al., *GRK2 as a novel gene therapy target in heart failure.* J Mol Cell Cardiol, 2011. **50**(5): p. 785-92.
270. Schumacher, S.M., et al., *Paroxetine-mediated GRK2 inhibition reverses cardiac dysfunction and remodeling after myocardial infarction.* Sci Transl Med, 2015. **7**(277): p. 277ra31.
271. Thal, D.M., et al., *Paroxetine is a direct inhibitor of g protein-coupled receptor kinase 2 and increases myocardial contractility.* ACS Chem Biol, 2012. **7**(11): p. 1830-9.
272. Eckhart, A.D., et al., *Vascular-targeted overexpression of G protein-coupled receptor kinase-2 in transgenic mice attenuates beta-adrenergic receptor signaling and increases resting blood pressure.* Mol Pharmacol, 2002. **61**(4): p. 749-58.
273. Molinoff, P.B., *Alpha- and beta-adrenergic receptor subtypes properties, distribution and regulation.* Drugs, 1984. **28 Suppl 2**: p. 1-15.
274. Weber, L.P., et al., *Enhanced contractile responses of arteries from streptozotocin diabetic rats to sodium fluoride.* Br J Pharmacol, 1996. **118**(1): p. 115-22.
275. Cushing, D.J., et al., *Fluoride produces endothelium-dependent relaxation and endothelium-independent contraction in coronary artery.* J Pharmacol Exp Ther, 1990. **254**(1): p. 28-32.
276. Hippe, H.J., et al., *Competition for Gbetagamma dimers mediates a specific cross-talk between stimulatory and inhibitory G protein alpha subunits of the adenylyl cyclase in cardiomyocytes.* Naunyn Schmiedebergs Arch Pharmacol, 2013. **386**(6): p. 459-69.
277. Navarro, G., et al., *Cross-communication between Gi and Gs in a G-protein-coupled receptor heterotetramer guided by a receptor C-terminal domain.* BMC Biol, 2018. **16**(1): p. 24.
278. Cabrera-Vera, T.M., et al., *Insights into G protein structure, function, and regulation.* Endocr Rev, 2003. **24**(6): p. 765-81.
279. Janssen, P.M., et al., *Intracellular beta-blockade: overexpression of Galpha(i2) depresses the beta-adrenergic response in intact myocardium.* Cardiovasc Res, 2002. **55**(2): p. 300-8.
280. Zhu, W., et al., *Gi-biased beta2AR signaling links GRK2 upregulation to heart failure.* Circ Res, 2012. **110**(2): p. 265-74.
281. Lyons, D., *Impairment and restoration of nitric oxide-dependent vasodilation in cardiovascular disease.* Int J Cardiol, 1997. **62 Suppl 2**: p. S101-9.

282. Mokhtar, S.S., et al., *Endothelium dependent hyperpolarization-type relaxation compensates for attenuated nitric oxide-mediated responses in subcutaneous arteries of diabetic patients.* Nitric Oxide, 2016. **53**: p. 35-44.
283. Hendriks-Balk, M.C., et al., *Regulation of G protein-coupled receptor signalling: focus on the cardiovascular system and regulator of G protein signalling proteins.* Eur J Pharmacol, 2008. **585**(2-3): p. 278-91.
284. Stiles, G.L. and R.J. Lefkowitz, *Cardiac adrenergic receptors.* Annu Rev Med, 1984. **35**: p. 149-64.
285. Ho, D., et al., *Modulation of beta-adrenergic receptor signaling in heart failure and longevity: targeting adenylyl cyclase type 5.* Heart Fail Rev, 2010. **15**(5): p. 495-512.
286. Wu, Y.S., et al., *The type VI adenylyl cyclase protects cardiomyocytes from beta-adrenergic stress by a PKA/STAT3-dependent pathway.* J Biomed Sci, 2017. **24**(1): p. 68.
287. LeBlanc, A.J. and S. Uchida, *A step closer to improving cardiac homing of adipose-derived mesenchymal stem cells.* Am J Physiol Heart Circ Physiol, 2019. **316**(2): p. H260-H261.
288. LeBlanc, A.J., et al., *Age impairs Flk-1 signaling and NO-mediated vasodilation in coronary arterioles.* Am J Physiol Heart Circ Physiol, 2008. **295**(6): p. H2280-8.
289. Kwee, B.J., et al., *CD4 T-cells regulate angiogenesis and myogenesis.* Biomaterials, 2018. **178**: p. 109-121.
290. Wang, H., et al., *Regulatory T cells in ischemic stroke.* CNS Neurosci Ther, 2021. **27**(6): p. 643-651.
291. Nossent, A.Y., et al., *CCR7-CCL19/CCL21 Axis is Essential for Effective Arteriogenesis in a Murine Model of Hindlimb Ischemia.* J Am Heart Assoc, 2017. **6**(3).
292. Zhong, Q., et al., *Effector T Cells and Ischemia-Induced Systemic Angiogenesis in the Lung.* Am J Respir Cell Mol Biol, 2016. **54**(3): p. 394-401.
293. Azimi, M.S., J.M. Motherwell, and W.L. Murfee, *An Ex Vivo Method for Time-Lapse Imaging of Cultured Rat Mesenteric Microvascular Networks.* J Vis Exp, 2017(120).
294. Stapor, P.C., et al., *An angiogenesis model for investigating multicellular interactions across intact microvascular networks.* Am J Physiol Heart Circ Physiol, 2013. **304**(2): p. H235-45.
295. Sweat, R.S., P.C. Stapor, and W.L. Murfee, *Relationships between lymphangiogenesis and angiogenesis during inflammation in rat mesentery microvascular networks.* Lymphat Res Biol, 2012. **10**(4): p. 198-207.
296. Motherwell, J.M., C.R. Anderson, and W.L. Murfee, *Endothelial Cell Phenotypes are Maintained During Angiogenesis in Cultured Microvascular Networks.* Sci Rep, 2018. **8**(1): p. 5887.
297. Motherwell, J.M., et al., *Bioreactor System to Perfuse Mesentery Microvascular Networks and Study Flow Effects During Angiogenesis.* Tissue Eng Part C Methods, 2019. **25**(8): p. 447-458.

298. Majbour, D., et al., *An Ex Vivo Tissue Culture Method for Discovering Cell Dynamics Involved in Stromal Vascular Fraction Vasculogenesis Using the Mouse Mesentery.* Methods Mol Biol, 2022. **2441**: p. 157-170.
299. Yang, M., et al., *Rat mesentery exteriorization: a model for investigating the cellular dynamics involved in angiogenesis.* J Vis Exp, 2012(63): p. e3954.
300. Yang, M., M. Aragon, and W.L. Murfee, *Angiogenesis in mesenteric microvascular networks from spontaneously hypertensive versus normotensive rats.* Microcirculation, 2011. **18**(7): p. 574-82.
301. Sweat, R.S., D.C. Sloas, and W.L. Murfee, *VEGF-C induces lymphangiogenesis and angiogenesis in the rat mesentery culture model.* Microcirculation, 2014. **21**(6): p. 532-40.
302. Azimi, M.S., et al., *An Ex Vivo Tissue Culture Model for Anti-angiogenic Drug Testing.* Methods Mol Biol, 2016. **1464**: p. 85-95.
303. Yang, M. and W.L. Murfee, *The effect of microvascular pattern alterations on network resistance in spontaneously hypertensive rats.* Med Biol Eng Comput, 2012. **50**(6): p. 585-93.
304. Strobel, H.A., et al., *Stromal Cells Promote Neovascular Invasion Across Tissue Interfaces.* Front Physiol, 2020. **11**: p. 1026.
305. Kastrup, J., et al., *Cryopreserved Off-the-Shelf Allogeneic Adipose-Derived Stromal Cells for Therapy in Patients with Ischemic Heart Disease and Heart Failure-A Safety Study.* Stem Cells Transl Med, 2017. **6**(11): p. 1963-1971.
306. Bourin, P., et al., *Stromal cells from the adipose tissue-derived stromal vascular fraction and culture expanded adipose tissue-derived stromal/stem cells: a joint statement of the International Federation for Adipose Therapeutics and Science (IFATS) and the International Society for Cellular Therapy (ISCT).* Cytotherapy, 2013. **15**(6): p. 641-8.
307. Nunes, S.S., et al., *Generation of a functional liver tissue mimic using adipose stromal vascular fraction cell-derived vasculatures.* Sci Rep, 2013. **3**: p. 2141.
308. Ramakrishnan, V.M. and N.L. Boyd, *The Adipose Stromal Vascular Fraction as a Complex Cellular Source for Tissue Engineering Applications.* Tissue Eng Part B Rev, 2018. **24**(4): p. 289-299.
309. Dykstra, J.A., et al., *Concise Review: Fat and Furious: Harnessing the Full Potential of Adipose-Derived Stromal Vascular Fraction.* Stem Cells Transl Med, 2017. **6**(4): p. 1096-1108.
310. Sweat, R.S., et al., *Aging is associated with impaired angiogenesis, but normal microvascular network structure, in the rat mesentery.* Am J Physiol Heart Circ Physiol, 2017. **312**(2): p. H275-H284.
311. Gocmez, S.S., et al., *Age Impaired endothelium-dependent vasodilation is improved by resveratrol in rat mesenteric arteries.* J Exerc Nutrition Biochem, 2016. **20**(1): p. 41-8.
312. Scherberich, A., et al., *Adipose tissue-derived progenitors for engineering osteogenic and vasculogenic grafts.* J Cell Physiol, 2010. **225**(2): p. 348-53.
313. Doi, R., et al., *Transplantation of bioengineered rat lungs recellularized with endothelial and adipose-derived stromal cells.* Sci Rep, 2017. **7**(1): p. 8447.
314. Mendel, T.A., et al., *Pericytes derived from adipose-derived stem cells protect against retinal vasculopathy.* PLoS One, 2013. **8**(5): p. e65691.

315. Cronk, S.M., et al., *Adipose-derived stem cells from diabetic mice show impaired vascular stabilization in a murine model of diabetic retinopathy.* Stem Cells Transl Med, 2015. **4**(5): p. 459-67.
316. Kino, T., M. Khan, and S. Mohsin, *The Regulatory Role of T Cell Responses in Cardiac Remodeling Following Myocardial Infarction.* Int J Mol Sci, 2020. **21**(14).
317. D'Alessio, F.R., et al., *Lung Angiogenesis Requires CD4(+) Forkhead Homeobox Protein-3(+) Regulatory T Cells.* Am J Respir Cell Mol Biol, 2015. **52**(5): p. 603-10.
318. Urbieta-Caceres, V.H., et al., *Age-dependent renal cortical microvascular loss in female mice.* Am J Physiol Endocrinol Metab, 2012. **302**(8): p. E979-86.
319. Park, S.H., et al., *Changes in the Retinal Microvasculature Measured Using Optical Coherence Tomography Angiography According to Age.* J Clin Med, 2020. **9**(3).
320. Tracy, E.P., et al., *State of the Field: Cellular Therapy Approaches in Microvascular Regeneration.* Am J Physiol Heart Circ Physiol, 2022.
321. Arminan, A., et al., *Mesenchymal stem cells provide better results than hematopoietic precursors for the treatment of myocardial infarction.* J Am Coll Cardiol, 2010. **55**(20): p. 2244-53.
322. Han, Y., et al., *Mesenchymal Stem Cells for Regenerative Medicine.* Cells, 2019. **8**(8).
323. Mikami, S., et al., *Autologous bone-marrow mesenchymal stem cell implantation and endothelial function in a rabbit ischemic limb model.* PLoS One, 2013. **8**(7): p. e67739.
324. Hong, K.U., et al., *A highly sensitive and accurate method to quantify absolute numbers of c-kit+ cardiac stem cells following transplantation in mice.* Basic Res Cardiol, 2013. **108**(3): p. 346.
325. Luger, D., et al., *Intravenously Delivered Mesenchymal Stem Cells: Systemic Anti-Inflammatory Effects Improve Left Ventricular Dysfunction in Acute Myocardial Infarction and Ischemic Cardiomyopathy.* Circ Res, 2017. **120**(10): p. 1598-1613.
326. Guo, J., et al., *Anti-inflammation role for mesenchymal stem cells transplantation in myocardial infarction.* Inflammation, 2007. **30**(3-4): p. 97-104.
327. Wang, W., et al., *Intravenous administration of bone marrow mesenchymal stromal cells is safe for the lung in a chronic myocardial infarction model.* Regen Med, 2011. **6**(2): p. 179-90.
328. Park, S.R., et al., *Stem Cell Secretome and Its Effect on Cellular Mechanisms Relevant to Wound Healing.* Mol Ther, 2018. **26**(2): p. 606-617.
329. Wysoczynski, M., A. Khan, and R. Bolli, *New Paradigms in Cell Therapy: Repeated Dosing, Intravenous Delivery, Immunomodulatory Actions, and New Cell Types.* Circ Res, 2018. **123**(2): p. 138-158.
330. Spees, J.L., R.H. Lee, and C.A. Gregory, *Mechanisms of mesenchymal stem/stromal cell function.* Stem Cell Res Ther, 2016. **7**(1): p. 125.
331. Carstens, M.H., et al., *Adipose-derived stromal vascular fraction (SVF) cells for the treatment of non-reconstructable peripheral vascular disease in patients with*

critical limb ischemia: A 6-year follow-up showing durable effects. Stem Cell Res, 2020. **49**: p. 102071.
332. Mathiasen, A.B., et al., *Autotransplantation of mesenchymal stromal cells from bone-marrow to heart in patients with severe stable coronary artery disease and refractory angina--final 3-year follow-up.* Int J Cardiol, 2013. **170**(2): p. 246-51.
333. Zhu, M., et al., *Anti-inflammatory effect of stromal vascular fraction cells in fat transplantation.* Exp Ther Med, 2019. **17**(2): p. 1435-1439.
334. Yin, Y., et al., *Autologous fat graft assisted by stromal vascular fraction improves facial skin quality: A randomized controlled trial.* J Plast Reconstr Aesthet Surg, 2020. **73**(6): p. 1166-1173.
335. Nilforoushzadeh, M.A., et al., *Engineered skin graft with stromal vascular fraction cells encapsulated in fibrin-collagen hydrogel: A clinical study for diabetic wound healing.* J Tissue Eng Regen Med, 2020. **14**(3): p. 424-440.
336. Parker, B.A., S.J. Ridout, and D.N. Proctor, *Age and flow-mediated dilation: a comparison of dilatory responsiveness in the brachial and popliteal arteries.* Am J Physiol Heart Circ Physiol, 2006. **291**(6): p. H3043-9.
337. Arenas, I.A., Y. Xu, and S.T. Davidge, *Age-associated impairment in vasorelaxation to fluid shear stress in the female vasculature is improved by TNF-alpha antagonism.* Am J Physiol Heart Circ Physiol, 2006. **290**(3): p. H1259-63.
338. Maijub, J.G., et al., *Concentration-Dependent Vascularization of Adipose Stromal Vascular Fraction Cells.* Cell Transplant, 2015. **24**(10): p. 2029-39.
339. Cannavo, A., D. Liccardo, and W.J. Koch, *Targeting cardiac beta-adrenergic signaling via GRK2 inhibition for heart failure therapy.* Front Physiol, 2013. **4**: p. 264.
340. Tutunea-Fatan, E., et al., *GRK2 targeted knock-down results in spontaneous hypertension, and altered vascular GPCR signaling.* J Biol Chem, 2016. **291**(39): p. 20822.
341. Rau, T., et al., *Overexpression of wild-type Galpha(i)-2 suppresses beta-adrenergic signaling in cardiac myocytes.* FASEB J, 2003. **17**(3): p. 523-5.
342. Shimokawa, H., et al., *Endothelial Gi protein expression is markedly low in human coronary microvessels.* J Cardiovasc Pharmacol, 1996. **27**(2): p. 297-302.
343. Hill, S.J. and J.G. Baker, *The ups and downs of Gs- to Gi-protein switching.* Br J Pharmacol, 2003. **138**(7): p. 1188-9.
344. Ayala-Lopez, N. and S.W. Watts, *New actions of an old friend: perivascular adipose tissue's adrenergic mechanisms.* Br J Pharmacol, 2017. **174**(20): p. 3454-3465.
345. Ayala-Lopez, N., J.M. Thompson, and S.W. Watts, *Perivascular Adipose Tissue's Impact on Norepinephrine-Induced Contraction of Mesenteric Resistance Arteries.* Front Physiol, 2017. **8**: p. 37.
346. Hatoum, O.A., et al., *Acquired microvascular dysfunction in inflammatory bowel disease: Loss of nitric oxide-mediated vasodilation.* Gastroenterology, 2003. **125**(1): p. 58-69.
347. Nguyen-Tu, M.S., et al., *Inflammation-linked adaptations in dermal microvascular reactivity accompany the development of obesity and type 2 diabetes.* Int J Obes (Lond), 2019. **43**(3): p. 556-566.

348. Pierce, G.L., et al., *Nuclear factor-{kappa}B activation contributes to vascular endothelial dysfunction via oxidative stress in overweight/obese middle-aged and older humans.* Circulation, 2009. **119**(9): p. 1284-92.
349. Suarez-Martinez, A.D., et al., *A Novel ex vivo Mouse Mesometrium Culture Model for Investigating Angiogenesis in Microvascular Networks.* J Vasc Res, 2018. **55**(3): p. 125-135.
350. Leblanc, A.J., et al., *Adipose-derived cell construct stabilizes heart function and increases microvascular perfusion in an established infarct.* Stem Cells Transl Med, 2013. **2**(11): p. 896-905.
351. De Barros, S., et al., *Aging-related decrease of human ASC angiogenic potential is reversed by hypoxia preconditioning through ROS production.* Mol Ther, 2013. **21**(2): p. 399-408.
352. Kamenaga, T., et al., *Cryopreserved human adipose-derived stromal vascular fraction maintains fracture healing potential via angiogenesis and osteogenesis in an immunodeficient rat model.* Stem Cell Res Ther, 2021. **12**(1): p. 110.
353. Xie, Y., et al., *Transcriptome differences in adipose stromal cells derived from pre- and postmenopausal women.* Stem Cell Res Ther, 2020. **11**(1): p. 92.
354. Duscher, D., et al., *Aging disrupts cell subpopulation dynamics and diminishes the function of mesenchymal stem cells.* Sci Rep, 2014. **4**: p. 7144.
355. Liu, M., et al., *Adipose-Derived Mesenchymal Stem Cells from the Elderly Exhibit Decreased Migration and Differentiation Abilities with Senescent Properties.* Cell Transplant, 2017. **26**(9): p. 1505-1519.
356. Swirski, F.K., et al., *Identification of splenic reservoir monocytes and their deployment to inflammatory sites.* Science, 2009. **325**(5940): p. 612-6.
357. Horckmans, M., et al., *Neutrophils orchestrate post-myocardial infarction healing by polarizing macrophages towards a reparative phenotype.* Eur Heart J, 2017. **38**(3): p. 187-197.
358. Dayan, V., et al., *Mesenchymal stromal cells mediate a switch to alternatively activated monocytes/macrophages after acute myocardial infarction.* Basic Res Cardiol, 2011. **106**(6): p. 1299-310.
359. Strong, A.L., et al., *Adipose stromal cells repair pressure ulcers in both young and elderly mice: potential role of adipogenesis in skin repair.* Stem Cells Transl Med, 2015. **4**(6): p. 632-42.
360. Boomsma, R.A., P.D. Swaminathan, and D.L. Geenen, *Intravenously injected mesenchymal stem cells home to viable myocardium after coronary occlusion and preserve systolic function without altering infarct size.* Int J Cardiol, 2007. **122**(1): p. 17-28.
361. Azimi, M.S., et al., *A novel tissue culture model for evaluating the effect of aging on stem cell fate in adult microvascular networks.* Geroscience, 2020. **42**(2): p. 515-526.
362. Carelli, S., et al., *Mechanical Activation of Adipose Tissue and Derived Mesenchymal Stem Cells: Novel Anti-Inflammatory Properties.* Int J Mol Sci, 2018. **19**(1).
363. Czapla, J., et al., *Adipose tissue-derived stromal cells stimulated macrophages-endothelial cells interactions promote effective ischemic muscle neovascularization.* Eur J Pharmacol, 2020. **883**: p. 173354.

364. Koh, Y.J., et al., *Stromal vascular fraction from adipose tissue forms profound vascular network through the dynamic reassembly of blood endothelial cells.* Arterioscler Thromb Vasc Biol, 2011. **31**(5): p. 1141-50.
365. Di Benedetto, P., et al., *Macrophages with regulatory functions, a possible new therapeutic perspective in autoimmune diseases.* Autoimmun Rev, 2019. **18**(10): p. 102369.
366. Costantini, A., et al., *Age-related M1/M2 phenotype changes in circulating monocytes from healthy/unhealthy individuals.* Aging (Albany NY), 2018. **10**(6): p. 1268-1280.
367. Bowles, A.C., et al., *Immunomodulatory Effects of Adipose Stromal Vascular Fraction Cells Promote Alternative Activation Macrophages to Repair Tissue Damage.* Stem Cells, 2017. **35**(10): p. 2198-2207.
368. Riccobono, D., et al., *First Insights Into the M2 Inflammatory Response After Adipose-Tissue-Derived Stem Cell Injections in Radiation-Injured Muscles.* Health Phys, 2018. **115**(1): p. 37-48.
369. Rabb, H., *The T cell as a bridge between innate and adaptive immune systems: implications for the kidney.* Kidney Int, 2002. **61**(6): p. 1935-46.
370. Stout, R.D., et al., *Impaired T cell-mediated macrophage activation in CD40 ligand-deficient mice.* J Immunol, 1996. **156**(1): p. 8-11.
371. Leoni, G. and O. Soehnlein, *(Re) Solving Repair After Myocardial Infarction.* Front Pharmacol, 2018. **9**: p. 1342.
372. Strioga, M., et al., *Same or not the same? Comparison of adipose tissue-derived versus bone marrow-derived mesenchymal stem and stromal cells.* Stem Cells Dev, 2012. **21**(14): p. 2724-52.
373. Ikegame, Y., et al., *Comparison of mesenchymal stem cells from adipose tissue and bone marrow for ischemic stroke therapy.* Cytotherapy, 2011. **13**(6): p. 675-85.
374. Sun, Y., et al., *Significance of Cellular Cross-Talk in Stromal Vascular Fraction of Adipose Tissue in Neovascularization.* Arterioscler Thromb Vasc Biol, 2019. **39**(6): p. 1034-1044.
375. Gerhardt, H., et al., *VEGF guides angiogenic sprouting utilizing endothelial tip cell filopodia.* J Cell Biol, 2003. **161**(6): p. 1163-77.
376. Wu, Q., et al., *Antiobesity Effects of Adipose-Derived Stromal/Stem Cells in a Naturally Aged Mouse Model.* Obesity (Silver Spring), 2021. **29**(1): p. 133-142.
377. Hunter, R.K., 2nd, et al., *Adipose-Derived Stromal Vascular Fraction Cell Effects on a Rodent Model of Thin Endometrium.* PLoS One, 2015. **10**(12): p. e0144823.
378. Wang, Y., et al., *Regulation of VEGF-induced endothelial cell migration by mitochondrial reactive oxygen species.* Am J Physiol Cell Physiol, 2011. **301**(3): p. C695-704.
379. Whalen, E.J., et al., *Regulation of beta-adrenergic receptor signaling by S-nitrosylation of G-protein-coupled receptor kinase 2.* Cell, 2007. **129**(3): p. 511-22.
380. Boengler, K., et al., *The myocardial JAK/STAT pathway: from protection to failure.* Pharmacol Ther, 2008. **120**(2): p. 172-85.
381. Chen, Z. and Z.C. Han, *STAT3: a critical transcription activator in angiogenesis.* Med Res Rev, 2008. **28**(2): p. 185-200.

382. Chen, Q., et al., *Targeted inhibition of STAT3 as a potential treatment strategy for atherosclerosis.* Theranostics, 2019. **9**(22): p. 6424-6442.
383. Lin, K.C., et al., *Combination of adipose-derived mesenchymal stem cells (ADMSC) and ADMSC-derived exosomes for protecting kidney from acute ischemia-reperfusion injury.* Int J Cardiol, 2016. **216**: p. 173-85.
384. Liu, Z., et al., *Exosomes from adipose-derived mesenchymal stem cells prevent cardiomyocyte apoptosis induced by oxidative stress.* Cell Death Discov, 2019. **5**: p. 79.
385. Yurdakul, S., et al., *Oxidative DNA damage is significantly correlated with flow-mediated dilation in patients with coronary artery disease.* J Investig Med, 2008. **56**(7): p. 925-30.
386. Gurovich, A.N., et al., *Flow-mediated dilation is associated with endothelial oxidative stress in human venous endothelial cells.* Vasc Med, 2014. **19**(4): p. 251-256.
387. Beyer, A.M., et al., *Transition in the mechanism of flow-mediated dilation with aging and development of coronary artery disease.* Basic Res Cardiol, 2017. **112**(1): p. 5.
388. Gaballa, M.A., et al., *Vascular beta-adrenergic receptor adenylyl cyclase system in maturation and aging.* J Mol Cell Cardiol, 2000. **32**(9): p. 1745-55.
389. Guo, M.Y., et al., *Thiol-oxidation reduces the release of amylase induced by beta-adrenergic receptor activation in rat parotid acinar cells.* Biomed Res, 2010. **31**(5): p. 293-9.
390. Lewis, S.J., et al., *Peroxynitrite elicits dysfunction of stereoselective s-nitrosocysteine recognition sites.* J Cardiovasc Pharmacol, 2005. **46**(5): p. 637-45.
391. Lewis, S.J., et al., *Potential role of nitration and oxidation reactions in the effects of peroxynitrite on the function of beta-adrenoceptor sub-types in the rat.* Eur J Pharmacol, 2005. **518**(2-3): p. 187-94.
392. Frame, M.D., et al., *Nitrosative stress uncovers potent beta2-adrenergic receptor-linked vasodilation further enhanced by blockade of clathrin endosome formation.* Am J Physiol Heart Circ Physiol, 2018. **314**(6): p. H1298-H1308.
393. Gioscia-Ryan, R.A., et al., *Mitochondria-targeted antioxidant (MitoQ) ameliorates age-related arterial endothelial dysfunction in mice.* J Physiol, 2014. **592**(12): p. 2549-61.
394. Rossman, M.J., et al., *Chronic Supplementation With a Mitochondrial Antioxidant (MitoQ) Improves Vascular Function in Healthy Older Adults.* Hypertension, 2018. **71**(6): p. 1056-1063.
395. in *Guide for the Care and Use of Laboratory Animals*, th, Editor. 2011: Washington (DC).
396. Rowe, G., et al., *Cell therapy rescues aging-induced beta-1 adrenergic receptor and GRK2 dysfunction in the coronary microcirculation.* Geroscience, 2021. **in-press**.
397. Fukai, T. and M. Ushio-Fukai, *Cross-Talk between NADPH Oxidase and Mitochondria: Role in ROS Signaling and Angiogenesis.* Cells, 2020. **9**(8).
398. Guo, J., et al., *p66Shc links alpha1-adrenergic receptors to a reactive oxygen species-dependent AKT-FOXO3A phosphorylation pathway in cardiomyocytes.* Circ Res, 2009. **104**(5): p. 660-9.

399. Yamamori, T., et al., *P66shc regulates endothelial NO production and endothelium-dependent vasorelaxation: implications for age-associated vascular dysfunction.* J Mol Cell Cardiol, 2005. **39**(6): p. 992-5.
400. Francia, P., et al., *Deletion of p66shc gene protects against age-related endothelial dysfunction.* Circulation, 2004. **110**(18): p. 2889-95.
401. Camici, G.G., et al., *The role of p66Shc deletion in age-associated arterial dysfunction and disease states.* J Appl Physiol (1985), 2008. **105**(5): p. 1628-31.
402. MacMillan-Crow, L.A., J.P. Crow, and J.A. Thompson, *Peroxynitrite-mediated inactivation of manganese superoxide dismutase involves nitration and oxidation of critical tyrosine residues.* Biochemistry, 1998. **37**(6): p. 1613-22.
403. Rhee, S.G., et al., *Controlled elimination of intracellular H(2)O(2): regulation of peroxiredoxin, catalase, and glutathione peroxidase via post-translational modification.* Antioxid Redox Signal, 2005. **7**(5-6): p. 619-26.
404. Beyer, A.M., et al., *Critical Role for Telomerase in the Mechanism of Flow-Mediated Dilation in the Human Microcirculation.* Circ Res, 2016. **118**(5): p. 856-66.
405. Muller-Delp, J.M., et al., *Redox balance in the aging microcirculation: new friends, new foes, and new clinical directions.* Microcirculation, 2012. **19**(1): p. 19-28.
406. Vasudevan, N.T., et al., *Inhibition of protein phosphatase 2A activity by PI3Kgamma regulates beta-adrenergic receptor function.* Mol Cell, 2011. **41**(6): p. 636-48.
407. Bubnell, J., et al., *beta2 adrenergic receptor fluorescent protein fusions traffic to the plasma membrane and retain functionality.* PLoS One, 2013. **8**(9): p. e74941.
408. Mazor, R., et al., *Toll-like Receptor 4 Contributes to Vasodilalatory Shock via Alpha Adrenergic Receptor Internalization.* Critical Care Medicine, 2020. **48**(1): p. 841.
409. Ren, K., *Exosomes in perspective: a potential surrogate for stem cell therapy.* Odontology, 2019. **107**(3): p. 271-284.
410. Hogan, S.E., et al., *Mesenchymal stromal cell-derived exosomes improve mitochondrial health in pulmonary arterial hypertension.* Am J Physiol Lung Cell Mol Physiol, 2019. **316**(5): p. L723-L737.
411. Teng, X., et al., *Mesenchymal Stem Cell-Derived Exosomes Improve the Microenvironment of Infarcted Myocardium Contributing to Angiogenesis and Anti-Inflammation.* Cell Physiol Biochem, 2015. **37**(6): p. 2415-24.
412. Rohrich, R.J. and D. Wan, *Making Sense of Stem Cells and Fat Grafting in Plastic Surgery: The Hype, Evidence, and Evolving U.S. Food and Drug Administration Regulations.* Plast Reconstr Surg, 2019. **143**(2): p. 417e-424e.
413. van Dongen, J.A., M.C. Harmsen, and H.P. Stevens, *Isolation of Stromal Vascular Fraction by Fractionation of Adipose Tissue.* Methods Mol Biol, 2019. **1993**: p. 91-103.
414. Qayyum, A.A., et al., *Autologous adipose-derived stromal cell treatment for patients with refractory angina (MyStromalCell Trial): 3-years follow-up results.* J Transl Med, 2019. **17**(1): p. 360.

415. Biel, N.M., et al., *Limitations of the dorsal skinfold window chamber model in evaluating anti-angiogenic therapy during early phase of angiogenesis.* Vasc Cell, 2014. **6**: p. 17.
416. Seynhaeve, A.L. and T.L. Ten Hagen, *High-Resolution Intravital Microscopy of Tumor Angiogenesis.* Methods Mol Biol, 2016. **1464**: p. 115-127.
417. Prunier, C., et al., *Procedures and applications of long-term intravital microscopy.* Methods, 2017. **128**: p. 52-64.
418. Azimi, M.S., et al., *An ex vivo model for anti-angiogenic drug testing on intact microvascular networks.* PLoS One, 2015. **10**(3): p. e0119227.
419. Azimi, M.S., et al., *Lymphatic-to-blood vessel transition in adult microvascular networks: A discovery made possible by a top-down approach to biomimetic model development.* Microcirculation, 2020. **27**(2): p. e12595.
420. Motherwell, J.M., et al., *Evaluation of Arteriolar Smooth Muscle Cell Function in an Ex Vivo Microvascular Network Model.* Sci Rep, 2017. **7**(1): p. 2195.
421. Karagergou, E., et al., *Adipose-derived stromal vascular fraction aids epithelialisation and angiogenesis in an animal model.* J Wound Care, 2018. **27**(10): p. 637-644.
422. Lu, L.Y., et al., *Effects of Local Application of Adipose-Derived Stromal Vascular Fraction on Tendon-Bone Healing after Rotator Cuff Tear in Rabbits.* Chin Med J (Engl), 2018. **131**(21): p. 2620-2622.
423. Mohammadi, R., et al., *Stromal vascular fraction combined with silicone rubber chamber improves sciatic nerve regeneration in diabetes.* Chin J Traumatol, 2015. **18**(4): p. 212-8.
424. Hodges, N.A., R.W. Barr, and W.L. Murfee, *The maintenance of adult peripheral adult nerve and microvascular networks in the rat mesentery culture model.* J Neurosci Methods, 2020. **346**: p. 108923.
425. Suarez-Martinez, A.D., et al., *Induction of microvascular network growth in the mouse mesentery.* Microcirculation, 2018. **25**(8): p. e12502.

APPENDIX 1

LIST OF ABBREVIATIONS

α1-AR	alpha-1 adrenergic receptor
α2-AR	alpha-2 adrenergic receptor
β1-AR	beta-1 adrenergic receptor
β2-AR	beta-2 adrenergic receptor
β3-AR	beta-3 adrenergic receptor
5-HIAA	metabolite of serotonin
5HT	serotonin
AC	adenylyl cyclase
AR	adrenergic receptor
BF	blood flow
BM-MSC	bone-marrow mesenchymal stem cells
BW	body weight
cAMP	cyclic adenosine monophosphate
CFR	coronary flow reserve
CMD	coronary microvascular disease
CO	cardiac output
CPG	CPG20712A
CVD	cardiovascular disease
DA	dopamine
Dmax	maximum diameter
Dob	dobutamine
EF	ejection fraction
EI	exteriorization-induced hypoxic-like injury
Epi	epinephrine
FS	fractional shortening
Gαi	inhibitory G-protein
GFP+	green fluorescent protein
GRK	G-protein receptor kinase
Gs	stimulatory G-protein
GSL-1	griffonia (bandeiraea) simplicifolia lectin 1
HF	heart failure
i.v.	intravenous
ICI	ICI118551
IVC	inferior vena cava
IVRT	isovolumic relaxation time

LAD	left anterior descending
LV	left ventricle
LVDP	left ventricular diastolic pressure
LVDs/d	left ventricular dimensions systolic or diast
LVVs/d	left ventricular volume systolic or diastolic
MFI	mean fluorescence intensity
MI	myocardial infraction
MSC	mesenchymal stem cell
NaF	sodium fluoride
NE	norepinephrine
NEI	non-exteriorized control
NO	nitric oxide
P-GRK2	phosphorylated G-protein receptor kinase 2 (inhibited)
Parox	paroxetine HCl
PRSW	preload recruitable stroke work
PSS	physiological salt solution
PV	pressure-volume
RNS	reactive nitrogen species
ROI	region of interest
ROS	reactive oxygen species
RT	room temperature
SNO	S-nitrosolation
SNP	sodium nitroprusside
SV	stroke volume
SVF	adipose-derived stromal vascular fraction
VSMC	vascular smooth muscle

APPENDIX 2

LIST OF GROUPS

NCC	no cell control
O+BM	old i.v. injected with 5 mil GFP+ bone-marrow mesenchymal stem cells
O+OSVF	old i.v. injected with 10 mil GFP+ adipose-derived stromal vascular fraction from old donors
O+OSVF CD3-	old i.v. injected with 1.1 mil GFP+ adipose-derived stromal vascular fraction from old donors depleted of CD3+ T cells
O+OSVF CD3+	old i.v. injected with 1.1 mil GFP+ adipose-derived stromal vascular fraction from old donors consisting of only CD3+ T cells
O+SVF	old i.v. injected with 10 mil GFP+ adipose-derived stromal vascular fraction
O+YSVF	old i.v. injected with 10 mil GFP+ adipose-derived stromal vascular fraction from young donors
OC	old control
YC	young control

APPENDIX 3

STROMAL VASCULAR FRACTION RESTORES VASODILATORY FUNCTION BY REDUCING OXIDATIVE STRESS IN AGING-INDUCED CORONARY MICROVASCULAR DISEASE

Overview

The objective is to identify mechanisms for stromal vascular fraction's (SVF) previously reported restorative effects on vasodilative function in aging-induced coronary microvascular disease (CMD). We hypothesize that aging-induced reactive oxygen species (ROS) diminishes flow-mediated dilation (FMD) and β1-adrenergic receptor (β1-AR) dilation in coronary arterioles of aged female rats, reversible by SVF-mediated reduction in oxidative stress. SVF attenuates aging-induced chronic accumulation of ROS and prooxidant gene and protein expression with concomitant enhancement of antioxidant gene and protein expression and glutathione, but not nitric oxide. FMD and β1-AR-mediated dilation were diminished in aging, restored with SVF. FMD was restored by a switch in the acute signaling mediator from hydrogen peroxide in aging to peroxynitrite with SVF therapy. Vasorelaxation to β1-AR-agonism was mechanistically linked to ROS and nitric oxide levels in an age-dependent manner via their effects on desensitization and internalization. Exogenous ROS eliminates isoproterenol-mediated dilation that is blocked by inhibition of pro-desensitization and internalization proteins

GRK2 and dynamin (via paroxetine and dynasore). Exogenous nitrosylation, paroxetine, and dynasore restore β1-AR-mediated dilation in aged vessels. We introduce a novel mechanism by which ROS impacts β1-AR receptor trafficking; the ROS/RNS-β1-AR Desensitization and Internalization Axis (**Fig A3.1**). Aging induces oxidative stress that shunts β1-AR trafficking from the plasma membrane into endosomes. SVF reduces oxidative burden in this axis, restoring functional β1-AR. SVF reduces oxidative stress and restores flow- and β1-AR-mediated vasodilation with aging. SVF represents a promising alternative therapeutic strategy for CMD by addressing root cause of pathology i.e., oxidative stress-mediated hyperconstriction.

This chapter is from the published work referenced as follows:

Tracy, E.P., M. Dukes, G. Rowe, J.E. Beare, A.J. LeBlanc, *Stromal Vascular fraction Restores Vasodilatory Function by Reducing Oxidative Stress in Aging-Induced Coroanry Microvascular Disease.* Antioxid Redox Signal, 2022. *in revsion*

Introduction

Coronary microvascular disease (CMD) presents in a majority of post-menopausal, aging women with chronic angina due to microvascular hyperconstriction, as opposed to atherosclerotic blockage seen typically in men [56]. Clinically, CMD is defined as a coronary flow reserve (CFR) ≤ 2.5, endothelial dysfunction with constriction to acetylcholine, and <20% coronary dilation to nitroglycerin [56]. Coronary perfusion is compromised by ~43% in advanced age with a negative correlation between advancing age and myocardial flow reserve, exacerbating CMD severity [52, 53]. Current treatments are known to be minimally effective. Beta blockers may be utilized to preserve oxygen consumption by reducing the workload of the myocardium but may inhibit vascular dilative beta-adrenergic receptor (β-AR) function [128]. Conversely, beta agonists would lead to habituation over time and would increase inotropic myocardial workload [128]. Although nitrates may provide acute relief of symptoms, there is little evidence of reduced major adverse cardiac events (MACE) or mortality [129, 130]. Further, nitrates cause rebound angina and increase oxidative stress, and are difficult to manage.

A novel strategy that can holistically treat each facet of CMD pathophysiology by mending the pathologic microvessels themselves, rather than merely treating their symptomatic consequences, is of significant clinical interest. Adipose-derived stromal vascular fraction (SVF) represents a heterogenous population of cells with regenerative potential, including mesenchymal and hematopoietic stem cells, microvascular endothelial cells, pericytes, fibroblasts, B and T cells, natural killer cells, dendritic cells, and macrophages [39]. We have previously shown that injected SVF incorporates into carotid arteries and aorta, and to a lesser extent the myocardium, lung, and brain [39, 42].

SVF therapy reverses aging-mediated reduction in CFR and perfusion (a clinical determinant of CMD), improves maximal cardiac output one-week post-injection, and reverses markers of diastolic dysfunction typical of aging [39, 42]. One possible mechanism for the regenerative effects of SVF could be due to antioxidant effects [383, 384].

A cornerstone aspect of vascular aging is increased oxidative stress [50]. We recently reviewed how aging-associated oxidative stress impacts mitochondrial dynamics, FMD and β-AR function [121]. There is a known correlation between aging-associated oxidative stress and decline in functional vasodilation [50, 205, 385, 386], although uncertainty remains as to whether this relationship is purely correlational or if there is a causal link. If there is causality, then targeting oxidative stress in age-related CMD may provide new therapeutic avenues to restore vascular function. In this study, we examine the interplays of oxidative stress in aging and two mechanisms for maintenance of microvascular patency: flow- and β-adrenergic-mediated dilation.

Increasing intraluminal flow causes shear stress that in youth activates endothelial nitric oxide synthase (eNOS) to produce nitric oxide, leading to vasorelaxation [33]. During aging, this instead leads to production of hydrogen peroxide resulting in hyperpolarization-mediated vasorelaxation [387]. Overall, it is thought that the hyperpolarization-mediated pathways in aging are less efficient than nitric oxide-mediated during youth. Indeed, reductions in FMD are correlated with advancing age, which starts earlier in men but becomes more severe (steeper correlation) in postmenopausal women [47]. Therefore, therapeutically restoring nitric oxide bioavailability in aging vessels may restore effective FMD signaling.

We previously showed decreased vasodilative β1-AR protein in aged coronary microvessels, but not β2-3 AR or constrictive alpha 1-2 adrenergic receptor (α1-2 AR) [39, 40]. Furthermore, β1-AR is rescued to young control levels by the SVF therapy in aging female rats [40]. Aging leads to an overload of catecholamines, with compensatory receptor degradation. Upon catecholamine-receptor binding, G-protein receptor kinase 2 (GRK2) causes desensitization by phosphorylation of β-AR, reducing dilation efficacy. Beta-arrestin associates with the phosphorylated receptor, which initiates dynamin-mediated internalization of the β-AR into endosomes for storage, eventual degradation, or recycling back at the membrane. The protein expression of GRK2 and beta-arrestin are known to increase in aging Fischer 344 rat aortas [266, 388], and we have recently shown an age-related increase in myocardial and coronary microvascular protein expression of GRK2 [40]. Intravenous SVF was not able to fully reverse this age-related discrepancy, although it partially increased naturally inhibited GRK2 (phospho-GRK2) [40]. Since SVF did not reduce expression of pro-desensitization and internalization proteins, yet restored dilative βADR function, perhaps regulation of these proteins is altered with SVF therapy.

Post-translational modification may also be in play, as S-nitrosylation sterically inhibits GRK2 to block desensitization [20]. It is thought that thiol oxidation by ROS of the βADR facilitates desensitization and/or internalization [389-391]. ROS activates phosphatidylinositol 3-kinase gamma (PI3kγ) signaling, causing inhibition of protein phosphatase 2A (PP2A)-mediated recycling of the β-AR back to the plasma membrane [20]. Therefore, it may be possible to influence β-AR function by therapeutically modulating oxidative stress and nitrosative potential. Frame *et al.* found that nitrosative

exposure with sodium nitroprusside (SNP) can "uncover" β2-AR pools that increase isoproterenol potency (albeit with reduced efficacy) through GRK2 nitrosylation/inhibition, leaving functional β2-AR at the plasma membrane [392]. Mitochondrial antioxidant therapy with mitoQ can improve endothelium-dependent dilation and FMD [393, 394]. The role of mitochondrial redox dysfunction in aging coronary microvascular β-AR- and FMD with therapeutic potential of antioxidative strategies has yet to be elucidated.

We hypothesized that flow- and β1 adrenergic-mediated dilation are reduced with aging, reversed by SVF therapy by attenuating oxidative stress and restoring protective nitrosative signaling. Specifically, we predicted FMD will be restored in aging with SVF via restored nitric oxide production (as well as reduced ROS that siphons nitric oxide). Reduced ROS and enhanced nitrosative signaling will alleviate β1-AR desensitization and internalization of the receptor according to our conceptually novel ROS/RNS β1-AR Desensitization & Internalization Axis (**Fig A3.1 Graphic Summary**). The ability to therapeutically modulate vasodilative mechanisms through manipulating redox dynamics as shown in this study will provide exciting new avenues for addressing management of diseases such as CMD.

Materials and Methods

Animal model, groups, and endpoint procedures.

Surgeries for all animals were carried out in accordance with approved protocols from the University of Louisville Institutional Animal Care and Use Committee and the NIH Guide for the Care and Use of Laboratory Animals [395]. Female Fisher 344 young

control (YC, 3–6-month-old, Harlan Laboratories, Indianapolis, IN, USA) and aged (23-24-month-old, National Institute on Aging, Bethesda, MA, USA) rats were housed in pairs and allowed free access to food and water. Rats were accustomed to a regular 12-hour light/dark cycle and acclimated to facility environment for at least one week prior to endpoint procedures. Aged rats were randomly divided into two groups, old control (OC, 24 months) or old treated with SVF (OSVF). SVF was injected at 23 months of age, with sacrifice at 24 months of age. Euthanasia was achieved by removal of the heart under deep anesthesia (lack of tactile toe reflex and lower respiratory rate) consisting of 5% inhaled isoflurane with 1.5-2.0 L/min O2 flow in an induction chamber.

SVF isolation and injection.

Young (3-6 mo) rats from a green fluorescent positive (GFP+) Fischer-344 colony (original breeders obtained from University of Missouri RRRC, strain #307, colony maintained in house) were utilized to obtain SVF cells as described before [39, 41, 42]. In short, a 1:1 mixture of male epididymal and female ovarian fat pads was isolated. The fat was harvested, washed, and finely minced with subsequent digestion in 0.75 mg/mL Type 1 collagenase solution (Vitacyte, Indianapolis, IN, 011-1030) and 1 mg/mL DNAse (Sigma, Burlington, MA 9003-96-9) in 0.1% BSA-PBS. Two centrifugation cycles at 400 rpm for 4 minutes were performed to separate and then remove buoyant adipocytes. The SVF cell pellet was resuspended in 0.1% BSA-PBS followed by a second centrifugation cycle for 5 minutes and removal of remaining supernatant. The cell pellet was resuspended in 0.1% BSA-PBS once more, followed by gravity filtration through 20 μm mesh. The final SVF solution was collected, and cells counted by hemocytometer, followed by a final centrifugation, removal of supernatant, and resuspension in normal

saline to allow for 1 mL injections with 10 million SVF cells. The SVF-saline solution was warmed to 37°C and injected in the tail vein of rats under isoflurane anesthesia.

Heart and subepicardial arteriole isolation.

Hearts were isolated from each euthanized rat and coronary arterioles were dissected and transferred to a vessel chamber pressure myography system. Each end of the vessel was attached to a glass pipette and subjected to physiologic temperature (37°C) and pressure (45 mmHg) as shown in **Figure A3.2**. Vessels were allowed to achieve spontaneous tone of >20% constriction from initial diameter [39, 41, 42]. Whole heart, left ventricle, total body weight, initial tone achieved, and maximum dilation were acquired for each animal (**Table A3.1**).

Pressure myography with concentration or flow response.

The following experiments were randomized to each vessel. Baseline concentration-response curves were generated for each group for dobutamine at 10^{-10}-10^{-5} [M] (primary β1-AR agonist, partial β2-AR agonist, Sigma-Aldrich, Burlington, MA D0676), isoproterenol 10^{-14}-10^{-4} [M] (non-specific βADR, Sigma-Aldrich, Burlington, MA I6504), and norepinephrine at 10^{-9}-10^{-4} [M] (primary β1-AR, β2-AR, α1-AR, and α2-AR agonist, Sigma-Aldrich, Burlington, MA A9512). Vessels were monitored for two minutes at each concentration and diameter recorded manually using video calipers. Percent dilation was calculated as ([intraluminal diameter at specific concentration – diameter at baseline]/[maximal diameter – diameter at baseline]) x 100. Percent dilation responses for norepinephrine and dobutamine were plotted against mean fluorescence intensity (MFI) values for hydrogen peroxide, peroxynitrite, superoxide, nitric oxide, and glutathione (described further later). Once experiments were concluded, vessels were

washed with calcium-free physiologic salt solution twice for fifteen minutes each time, followed by sodium nitroprusside (SNP, 10^{-4} [M] Sigma-Aldrich, Burlington, MA, 13451, 2 minutes) to achieve maximum dilation. Tone was calculated as 1-(initial diameter/maximum diameter) x 100.

Isoproterenol concentration-response curves were also generated for vessels from YC and OSVF vessels pre-incubated for 1 hour with exogenous hydrogen peroxide (10^{-4} [M] Sigma-Aldrich, Burlington, MA, 7722841) plus menadione (superoxide donor, 10^{-5} [M], Sigma-Aldrich, Burlington, MA, 130-37-0) plus or minus dynasore (inhibits dynamin-mediated internalization, 1.6 μM Abcam, Cambridge, United Kingdom, 120192) and paroxetine (GRK2 antagonist, 5 μM, VWR, Radnor, PA, 89160-896). Additional isoproterenol concentration-response curves were generated for OC vessels with either incubation of dynasore, paroxetine, or SNP pre-treatment. Vessels were incubated with SNP (10^{-4} [M]) for one minute, followed by a fifteen-minute wash without SNP, followed by isoproterenol concentration-response generation plus low-dose SNP (10^{-9} [M]).

In a separate cohort, vessels from each group were incubated with inhibitors of β1-AR recycling including okadaic acid (PP2A inhibitor, 10^{-9} [M], APeX Bio A4540) and BEZ235 (PI3Kγ inhibitor, 10^{-6} [M] MedChemExpress, Monmoth Junction, NJ, HY-50673), and concentration curves for isoproterenol were generated. In separate YC and OSVF vessels, concentration curves for isoproterenol were generated with exogenous hydrogen peroxide and menadione plus or minus BEZ235 co-incubation. A detailed pathway of βADR desensitization, internalization, and recycling with inhibitors utilized in this manuscript are illustrated in **Figure A1.1**, adapted from Tracy *et al.* [121].

Percent dilation to varied flow rates (0, 5, 10, 15, 20, 25 μL/min, 2 minutes each) were assessed in separate vessels from each group. Following baseline FMD, flow rates were re-assessed with addition of uric acid (peroxynitrite scavenger, 1 mM Sigma-Aldrich, Burlington, MA, 69-93-2 for 20 min), catalase (hydrogen peroxide scavenger, 500 U/ mL, Sigma-Aldrich, Burlington, MA, C4963, 1 hour), and L-NAME (eNOS inhibitor, 10^{-5} [M] Sigma-Aldrich, Burlington, MA, N5751 for 20 min), separately.

Pressure myography with fluorescence imaging.

Isolated coronary arterioles from each group were infused with fluorescent dyes for superoxide (Mitosox, 0.1 μM, Invitrogen, Waltham, MA, m36008, 30 min), peroxynitrite (Biotracker 515, 20 μM Sigma-Aldrich, Burlington, MA, SCT035, 30 min), hydrogen peroxide (Mitopy1, 10^{-5} [M], Tocris, Bristol, United Kingdom, 1041634-69-8, 1 hour), nitric oxide (2,3-diaminonapthalene (DAN), 10^{-4} [M], Alfa Aesar, Haverhill, MA, 771-97-1, 10 minutes), and glutathione (DSSQ SEMKUR-IM, 250 μM, ProteinMods, Waunakee, WI, 1 hour). Experiments were carried out in physiologic salt solution without albumin. Flow (10 and 25 μm/min) was applied to infused vessels plus or minus either Diethyldithiocarbamic acid (DETC, 1 mM, Fisher, Hampton, NH 140-61-7, 1 hour) or 3-amino-1,2,4-triazole (AMT, 100 μM, Sigma-Aldrich, Burlington, MA, A8506, 1 hour) with images taken after 2 minutes at each flow rate. Mean fluorescence intensity (MFI) for each image was calculated from the average of two regions of interest (ROI) of consistent size (20 x 100 μm) applied over the left and right vessel walls using NIS Elements AR Analysis software (Nikon Instruments, Melville, NY, USA). For Mitosox, cobalt chloride (generates superoxide through hypoxia-inducible factor 1, 0.5 mM, Sigma-Aldrich, Burlington, MA, 15862, 1 hour) represented positive control

whereas Tiron (superoxide scavenger, 10 mM, Acros Organics, Geel, Belgium, 174140250, 1 hour) represented a negative control. For Biotracker 515, menadione (10^{-5} [M], Sigma-Aldrich, Burlington, MA, 130-37-0) + SNP (10^{-4} [M]) for 1 hour represented positive control, whereas Tiron (10 mM) + catalase (10 mM, 500 U/mL) for 1 hour represented a negative control. For Mytopy1, exogenous hydrogen peroxide (10-4 [M], 20 minutes) represented positive control whereas catalase (500 U/mL, 1 hour) represented a negative control. For DAN, exogenous SNP (10^{-4} [M], 2 minutes) represented positive control whereas CPTiO flow (1 mM, Sigma-Aldrich, Burlington, MA, C221, 20 minutes) represented a negative control. Simplified illustration of ROS and the fluorescent labels, enzyme activator/donors, and inhibitors/scavengers are summarized in **Figure A3.3**.

Immunofluorescence staining.

Vessel immunofluorescence staining was performed as previously described [39, 396]. Briefly, coronary arterioles measuring 750-1000 μm in length and <250 μm in diameter were isolated and fixed in 2% paraformaldehyde for one hour. After fixation, vessels were washed 2 x 15 minutes in DCF-PBS followed by 20 minutes in 0.5% Triton-X/DCF-PBS, all at room temperature with mild rotation. Next, vessels were placed in blocking solution containing 5% donkey serum, 0.5% BSA, and 0.5% triton X/DCF-PBS for one hour followed by incubation with primary antibodies including manganese superoxide dismutase (mSOD, 1:100, Novus Biologicals, Littleton, CO, NB100-1992SS), catalase (1:100 dilution, Bioss, Woburn, MA, 980693W), NOX4 (1:100 Novus, Littleton, CO NB110), heat shock protein 70 (1:100 Abcam, Cambridge, United Kingdom, 2787), glutathione synthetase (1:100 Novus Biologicals, Littleton, CO NBP2-

75513), S-nitrosocysteine (1:100 Abcam, Cambridge, United Kingdom, 268288), PP2A (1:100 Abcam, Cambridge, United Kingdom, 81G5), I2PP2A (1:100 Santa Cruz Biotechnologies, Dallas, TX, sc-133138), and PI3ky (1:100 Arigo Biolaboratories, Hsinchu City, Taiwan, ARG43246) rotating at 4°C overnight. Normal rabbit serum replaced primary antibody for negative control vessels. The following day, the vessels were washed x3 times in DCF-PBS, followed by one-hour incubation in donkey anti-rabbit IgG Alexa Fluor 594 (1:300 Invitrogen, Waltham, MA, A21207) or goat anti-mouse IgG Alexa Fluor 488 (1:300 Abcam, Cambridge, United Kingdom, 150113) in blocking solution. Nuclei were stained with DAPI (Life Technologies, Carlsbad, CA, R37606). Vessels were placed on slides with mounting media and coverslip, then imaged with Olympus FV1000 confocal microscope system (Olympus America, Center Valley, PA, USA) with a 405 and 562 nm laser. The pixel density set for image capture was 1024x1024 with 2 μm Z-step with 20X magnification, with ~12 slices stacked together post-image capture. Immunofluorescence intensity for each antibody were quantified using the Nikon NIS Elements AR Analysis software using 20 μm x 100 μm area. ROI boxes were placed on the right and left vascular walls (endothelial + smooth muscle) excluding cardiomyocytes with MFI averaged.

RNA sequencing.

Additional coronary arterioles were allocated for RNA sequencing via flash freezing; samples were stored at -80°C until samples from all groups were collected as done previously [396]. Six isolated vessels were pooled from two animals in the same group for n=3 biological replicates/group. RNA was harvested with RNAqueous Micro kit (Invitrogen, Waltham, MA, AM1931) and quantified on a NanoDrop (ThermoFisher,

Waltham MA, USA). Samples were sent to the University of Louisville Genomics Core for quality control analysis using the Agilent Bioanalyzer 2100 system (Agilent Technologies, Santa Clara, CA) and quantified using a Qubit fluorometric assay (Thermo Fisher Scientific, Waltham, MA) as previously described [257]. Poly-A enrichments, barcoding, and Illumina Next-Gen sequencing for library preparation were performed as previously described [257, 258]. Gene transcripts were analyzed by the University of Louisville Bioinformatics Core for differential expression analysis between group comparisons as previously described [259].

Statistical analysis.

SigmaPlot 14 (Systat) was utilized for statistical analyses, with significance level set at $p \leq 0.05$ for all analysis. Concentration- and flow-response curves as well as MFI evaluations were analyzed with Two-way Repeated Measures ANOVA with Bonferroni or Holm-Sidak *post hoc* testing as appropriate. Data are presented as means plus or minus standard error of the means as indicated. For pressure myographic fluorescence analysis, 20% of the data was re-analyzed by blinded inter- and intraobservers. Linear regression and Bland-Altman Plots were generated to assess for bias in interpretation of data (**Supplemental Fig A1.3**). For confocal images, the images were coded and analyzed in a blind fashion with the code being broken only after all MFI quantifications were acquired. Electronic laboratory notebooks were not used for this study.

Results

Animal characteristics.

Animal groups and experimental setup are illustrated in **Figure A3.2**. There was a significant increase in body weight and total ventricular weight between young control (YC) vs old control (OC) and YC vs old treated with SVF (OSVF) ($p < 0.001$ for all) (**Table A3.1**). LV weight increased significantly with aging ($p < 0.001$) and was reduced with SVF therapy ($p = 0.026$), albeit not to YC levels ($p < 0.001$). There was no significant change in wall thickness, maximal diameter, or percent resting tone.

Stromal vascular fraction reduces aging-associated oxidative stress.

An illustrative guide for fluorescent dyes, inhibitors/scavengers, and activators of key ROS/RNS and their mediators used in this section are shown in **Figure A3.3**. There were significant increases in coronary microvascular hydrogen peroxide and peroxynitrite in coronary arterioles from aged rats ($p = 0.015$ and $p = 0.01$, respectively), but no significant increases in superoxide MFI at baseline (**Fig A3.4**). Hydrogen peroxide, peroxynitrite, and superoxide MFI were all significantly decreased in OSVF compared to OC ($p < 0.001$, $p = 0.024$, $p = 0.004$, respectively). Meanwhile, there were significant decreases in nitric oxide ($p = 0.024$) and glutathione ($p < 0.01$) MFI between youth and aging (**Fig A3.4 D-E**). SVF therapy was unable to significantly increase nitric oxide MFI, but did significantly increase glutathione MFI compared to OC, although not fully restored to YC levels ($p = 0.017$ vs. OC, $p = 0.014$ vs. YC). The validity of the fluorescent dyes was confirmed with positive and negative controls for each dye. Briefly, mytopy1, Biotracker 515, Mitosox, 2,3-diaminonapthalene (DAN), and SEMKUR-IM MFI were appropriately increased by exogenous hydrogen peroxide, cobalt chloride (CoCl2), SNP, and tiron + catalase, respectively. Mytopy1, Biotracker 515, Mitosox,

DAN, and SEMKUR-IM MFI were appropriately decreased by PEG-catalase, tiron, CPTiO, and hydrogen peroxide, respectively. Further, repeatability was confirmed via linear regression and Bland-Altman analysis with blinded inter- and intra-observer re-analysis of 20% of the data.

To elucidate the redox environments between youth, aging, and aging + SVF, we utilized RNA sequencing to study gene expression and fluorescence staining to extrapolate protein expression of various antioxidant and prooxidant enzymes (**Fig A3.5**). Among prooxidant enzymes, xanthine dehydrogenase was increased by 21% in OC vs. YC and 28% in SVF vs. YC ($p = 0.042$ and $p = 0.006$, respectively). Peroxisome proliferator-activated receptor gamma (coactivator-related), known to increase oxidative stress, was increased by 22% in OC vs. YC ($p = 0.042$). There were no significant differences between groups for suspected prooxidant enzyme NOX4. SHC adaptor protein 1 expression was 18.9% greater in OC vs. YC ($p = 0.018$).

Among antioxidant enzymes, there was significant increase in catalase by 19% ($p = 0.049$), (extracellular) SOD3 by 22% ($p = 0.007$), thioredoxin reductase 1 by 23% ($p = 0.014$), and glutathione-S-transferase mu 1 by 24% ($p = 0.019$) and pi 1 by 31% ($p = 0.025$) in OC vs. YC. Antioxidant enzyme expression increases in YC vs. OC included 26% more oxidation resistance protein 1 ($p = 0.035$), 40% more COX20 assembly factor ($p = 0.002$), and 15% and 21% more heat shock proteins 90 and 110 ($p = 0.037$ and $p = 0.034$, respectively). For OSVF vs. YC antioxidant enzymes, catalase was increased by 19% (approaching significance, $p = 0.057$), SOD3 by 20% ($p = 0.012$), glutathione peroxidase 3 and 4 by 24% and 18% ($p = 0.016$ and $p = 0.024$, respectively), sirtuin 5 by

20% (p = 0.038), thioredoxin reductase by 20% (p = 0.034), and peroxiredoxin 4 by 39% (p = 0.015) albeit with 40% decreased heat shock protein 110 (p = 0.003).

Comparing antioxidant enzyme expression between OSVF vs. OC, glutathione synthetase was increased by 28% (p = 0.018), thioredoxin-like protein 1 increased by 17.2% (p = 0.045), heat shock proteins 40 (member C7) and 70 increased by 21.4% and 22% (p = 0.01 and p = 0.07, respectively), and cytochrome oxidase assembly factor 3 increased by 21% (p = 0.032) in OSVF. A comprehensive listing of antioxidant and prooxidant proteins are illustrated in the heat map in **Figure A3.5 A**.

We selected gene targets of most interest and potential impact/relevance to evaluate protein expression utilizing fluorescence imaging of isolated coronary microvessels (**Fig A3.5 B-C**). Antioxidant enzymes catalase, glutathione synthetase, and heat shock protein 70 yielded no differences in MFI. mSOD MFI was reduced with aging (albeit not significantly) but was significantly increased with SVF therapy (p = 0.041). Prooxidant enzyme NOX4 was significantly increased with aging (p = 0.032) with significant reversal to YC levels by SVF (p = 0.037). S-nitrosylation of proteins was significantly reduced with aging (p = 0.012) but was not restored with SVF (p = 0.047 vs. YC).

Alterations of flow-mediated dilation signaling throughout the lifespan and with stromal vascular fraction.

Introduction of intraluminal flow into isolated coronary microvessels in pressure myography experiments elicited different signaling responses to induce FMD between YC vs. OC vs. OSVF. In youth, flow elicited an increase in nitric oxide MFI (significant

compared to OC at flow rate of 10 & 25 μL/min, $p = 0.015$ and $p = 0.046$, respectively) (**Fig A3.6 A**). There was minimal change in nitric oxide MFI with flow in OC and OSVF groups.

In all groups, flow induced an increase in hydrogen peroxide, but the increase was greatest in the OC group (significant vs. YC at flow rate of 25 μL/min, $p = 0.045$) (**Fig A3.6 B**). Inhibition of superoxide dismutase with diethyldithiocarbamic acid (DETC) led to overall reduced hydrogen peroxide production with flow in all groups, with greater reduction in OC than OSVF at 25 μL/min ($p = 0.041$) **(Supplemental Fig A3.1)**. Inhibition of catalase with 3-amino-1,2,4-triazole (AMT) without flow led to greater hydrogen peroxide MFI increases in OSVF vs. YC and OC ($p = 0.01$ and $p < 0.01$, respectively) **(Fig A3.6 B)**. With AMT + flow at 10 and 25 μL/min, OSVF hydrogen peroxide MFI was significantly greater than OC ($p < 0.001$ and $p < 0.001$, respectively) and nearly significant vs. YC ($p = 0.051$ and $p = 0.087$, respectively). OC was non-significantly reduced compared to YC at all flow rates. These results with AMT suggest significantly greater catalase function in OSVF vs. YC and OC.

Superoxide MFI decreased with intraluminal flow in all groups (**Fig A3.6 C**). Inhibition of superoxide dismutase with DETC led to significantly greater superoxide accumulation in YC and OSVF groups compared to OC at baseline ($p = 0.035$ and $p = 0.011$, respectively). With flow + DETC, OC exhibited less superoxide production at flow rates of 10 (vs. YC and OSVF, $p < 0.001$, $p = 0.008$, respectively) and 25 (vs. YC, $p = 0.029$) μL/min, suggesting greater SOD expression and/or function in youth than aging, and that SOD function was restored with SVF therapy. DETC inhibition of SOD with flow reduced hydrogen peroxide production in all groups as expected. Peroxynitrite MFI

was increased with intraluminal flow at 10 and 25 μL/min in young control and significantly so in OSVF compared to minimal peroxynitrite production in OC ($p = 0.027$ and $p = 0.01$, respectively) (**Fig A3.6 D**).

Glutathione is an essential antioxidant that reflects the redox balance of the cell, quenching ROS such as hydrogen peroxide, superoxide, and peroxynitrite. The SEMKUR-IM dye indirectly reports the ratio between reduced and oxidized glutathione, with increased fluorescence changes indicating reduced glutathione, and decreased changes indicating oxidized glutathione. At intraluminal flow rate of 10 μL/min, glutathione MFI was increased in YC but significantly decreased in OC ($p = 0.04$) (**Fig A3.6 E**). At intraluminal flow rate of 25 μL/min, there was a significant difference between YC ($p = 0.01$) and OSVF ($p = 0.013$) MFI vs. OC. These results are consistent with the results that flow in OC increased hydrogen peroxide (and superoxide transiently before it was converted to hydrogen peroxide by SOD).

These data indicate that the FMD signaling mediator is nitric oxide during youth, hydrogen peroxide in aging, and switching to peroxynitrite with SVF therapy. To complement and strengthen the validity of these findings, we used pressure myography with flow while recording percent vasorelaxation in each group with or without inhibitors/scavengers/enzymes of these redox signaling mediators. Overall, the effectiveness of FMD was significantly attenuated with aging at flow rates of 10, 15, 20, & 25 μL/min ($p < 0.01$, $p < 0.01$, $p = 0.024$, and $p < 0.01$, respectively) but rescued to YC levels in the SVF therapy group ($p = 0.011$, $p = 0.006$, $p = 0.04$, and $p = 0.002$, respectively) (**Fig A3.7 A**). In youth, FMD was significantly attenuated by pre-incubation with N-Nitro-L-arginine methylester (L-NAME), but not catalase or uric acid, at all flow

rates ($p = 0.005$, $p < 0.001$, $p < 0.001$, $p < 0.001$, and $p < 0.001$, respectively) (**Fig A3.7 B**). This signifies that nitric oxide production is responsible for FMD during youth, as L-NAME inhibits eNOS-mediated nitric oxide production. During aging, FMD was not further attenuated by L-NAME, uric acid, or catalase (**Fig A3.7 C**). OSVF's improvement in FMD was significantly abrogated by uric acid at all flow rates ($p = 0.04$, $p = 0.04$, $p = 0.04$, $p < 0.001$, and $p < 0.001$, respectively) and L-NAME at flow rates 15-25 μL/min ($p = 0.027$, $p = 0.014$, and $p = 0.012$, respectively) (**Fig A3.7 D**). This signifies that with SVF therapy, the FMD signaling mediator switches to peroxynitrite, at least partially dependent on nitric oxide production.

Baseline oxidative and nitrosative stress are mechanistically linked with β1-AR-mediated dilative function.

Consistent with our lab's previous reporting, β1-adrenergic-mediated vasorelaxation was reduced with aging and restored to YC levels in aging + SVF therapy. Specifically, there were significant differences between YC vs. OC NE concentration responses at 10^{-8}-10^{-4} [M] ($p = 0.022$, $p < 0.001$, $p < 0.001$, $p < 0.001$, and $p < 0.001$, respectively) and OSVF vs. OC at 10^{-8}-10^{-4} [M] ($p < 0.001$ for all) (**Fig A3.8 A**). Similarly, there were significant differences between YC vs. OC Dob dose responses at 10^{-9}-10^{-5} [M] ($p = 0.018$, $p < 0.001$, $p = 0.002$, $p = 0.001$, and $p < 0.001$, respectively) and OSVF vs. OC at 10^{-9}-10^{-7} and 10^{-5} [M] ($p = 0.043$, $p = 0.002$, $p = 0.004$, and $p < 0.001$, respectively) (**Fig A3.8 B**). Since aging is associated with both increased oxidative stress and reduced β-adrenergic function, we next endeavored to determine if there was a true correlation between them.

Using separate vessels from the same animal, we correlated percent relaxation to norepinephrine 10^{-4} [M] with ROS/RNS/glutathione MFI. There were negative correlations between percent vasorelaxation to NE and MFI of hydrogen peroxide and superoxide, but not peroxynitrite ($r(27) = -0.69$, $p < 0.001$; $r(15) = -0.505$, $p = 0.018$; $r(20) = -0.24$, $p = 0.297$, respectively) (**Fig A3.8 C-E**). There was a positive correlation between increasing nitric oxide and glutathione with percent vasorelaxation to NE ($r(19) = 0.50$, $p = 0.021$; $r(18) = 0.50$, $p = 0.028$, respectively) (**Fig A3.8 F-G**)

Exogenous ROS eliminates while RNS rescues β-AR vasodilation due to the ROS/RNS β-AR desensitization & internalization axis.

For isoproterenol, there were significant differences between YC vs. OC concentration responses at 10^{-8}-10^{-4} [M] ($p < 0.001$ for all doses) and OSVF vs. OC at 10^{-11}-10^{-4} [M] ($p = 0.002$, $p = 0.002$, $p < 0.001$, $p < 0.001$, $p < 0.001$, $p < 0.001$, $p < 0.001$, and $p < 0.001$, respectively) (**Fig A3.9 A**). Isoproterenol concentration response was significantly abrogated in YC from doses 10^{-8}-10^{-4} [M] ($p = 0.003$, $p < 0.001$, $p < 0.001$, $p < 0.001$, and $p < 0.001$, respectively) and OSVF at 10^{-8}-10^{-4} [M] ($p < 0.001$ for all doses) when pre-incubated with exogenous hydrogen peroxide and superoxide donation via menadione (**Fig A3.9 B** and **D**). Post-experimentation, exposure to calcium-free solution + SNP still facilitated dilation, indicating ROS-attenuated dilation is β-adrenergic specific (YC=78.39±9.76%; OSVF=88.88±6.37% dilation). In YC, the effect from ROS was nullified when co-incubating with dynasore at 10^{-8}-10^{-4} [M] ($p = 0.005$, $p < 0.001$, $p < 0.001$, $p < 0.001$, and $p < 0.001$, respectively), but not restored to YC levels at 10^{-6}-10^{-5} [M] ($p = 0.037$ and $p = 0.003$, respectively). Paroxetine also nullified the

ROS attenuation of dilation at doses 10^{-8}-10^{-4} [M] ($p = 0.02$, <.001, $p < 0.001$, $p = 0.001$, and $p = 0.001$, respectively), albeit not completely restored to baseline levels for doses 10^{-7}-10^{-4} [M] ($p = 0.047$, $p = 0.011$, $p = 0.01$, and $p = 0.004$, respectively). In OSVF + ROS, dynasore and paroxetine pre-incubation also rescued function from doses 10^{-7}-10^{-4} [M] (dynasore: $p = 0.009$, $p = 0.0033$, $p = 0.005$, and $p = 0.007$, respectively) and 10^{-5}-10^{-4} [M] (paroxetine, $p = 0.042$ and $p = 0.015$, respectively). These reversing effects to attenuate ROS-blunted adrenergic dilation were therefore the result of inhibiting GRK2-mediated desensitization and dynamin-mediated internalization, respectively. Response to isoproterenol in old control vessels was significantly rescued at doses 10^{-7}-10^{-6} [M] by pre-incubation with a one-minute high-dose SNP preincubation followed by fifteen minutes of low-dose SNP and throughout the experiment ($p = 0.004$ and $p = 0.023$, respectively) (**Fig A3.9 C**). The response was also rescued by pre-incubation with dynasore at 10^{-8}-10^{-4} [M] ($p = 0.015$, $p < 0.001$, $p < 0.001$, $p < 0.001$, and $p = 0.004$, respectively) and paroxetine at 10^{-7}-10^{-4} [M] ($p < 0.001$, $p = 0.022$, $p = 0.019$, and $p = 0.004$, respectively).

β1-AR recycling is necessary in aging, but not youth or OSVF for maximal dilation to agonist.

To determine the contribution of β1-AR recycling (from endosome back to plasma membrane), we inhibited recycling regulatory proteins PP2A (pro-recycling) with okadaic acid, or PI3kγ (anti-recycling) with BEZ235 in a separate cohort of coronary arterioles from each group. Okadaic acid did not significantly reduce YC dilation to isoproterenol but did significantly reduce dilation in OC at 10^{-5}-10^{-4} [M] ($p = 0.01$, $p <$

0.001) and OSVF at 10^{-7}-10^{-6} [M] ($p = 0.005$, $p = 0.045$) (**Supplemental Fig A3.2 A-C**). Inhibition with BEZ235 did not alter aged dilation but did significantly reduce dilation in YC at 10^{-7}-10^{-4} [M] ($p = 0.011$, $p = 0.002$, $p < 0.001$, and $p = 0.004$, respectively) and OSVF at 10^{-6}-10^{-4} [M] ($p = 0.045$, $p = 0.008$, and $p = 0.017$, respectively). BEZ235 partially negated the effects of exogenous ROS incubation in YC at 10^{-5}-10^{-4} [M] ($p < 0.001$, $p = 0.004$), although differences were also significant against baseline at those doses ($p < 0.001$ for both) (**Supplemental Fig A3.2 D**). BEZ235 also negated the attenuation of dilation from exogenous ROS in OSVF at 10^{-6}-10^{-5} [M] (p=0.042, $p = 0.017$) (**Supplemental Fig A3.2 E**). There were no significant differences between groups for MFI of PP2A, protein phosphatase 2A inhibitor 2 (I2PP2A), or PI3kγ (**Supplemental Fig A3.3**).

Table A3.1

Animal & Vessel Characteristics	YC (n=66)	OC (n=58)	OSVF (n=55)
Age (Months)	3-6	24	24
Body Weight (g) (n)	181.25 +/- 2.5 (65) *#	249.97 +/- 3.795 (46)	246.82 +/- 2.99 (45)
Total Ventricular Weight (mg) (n)	502.66 +/- 6.64 (66) *#	651.47 +/- 16.31 (53)	653.89 +/- 6.74 (42)
LV Weight (mg) (n)	421.34 +/- 5.34 (66) *#	566.55 +/- 3.74 (53) ^	530.32 +/- 14.51 (43)
Vessel Wall Thickness (μm) (n)	12.58 +/- 0.4 (72)	16.22 +/- 1.68 (61)	15.39 +/- 1.75 (64)
Maximum Diameter (n)	138.55 +/- 3.33 (72)	148.42 +/- 3.93 (62)	147.45 +/- 3.29 (67)
Average % Tone (n)	30.65 +/- 1.52 (72)	29 +/- 1.62 (62)	32.71 +/- 1.81 (67)

Table A3.1: Rat anatomic, cardiac and vascular characteristics.

Significance set as $p < 0.05$ (* YC vs OC, # YC vs OSVF, ^ OC vs OSVF) via One-way ANOVA with Bonferroni post hoc analysis.

Figure A3.1

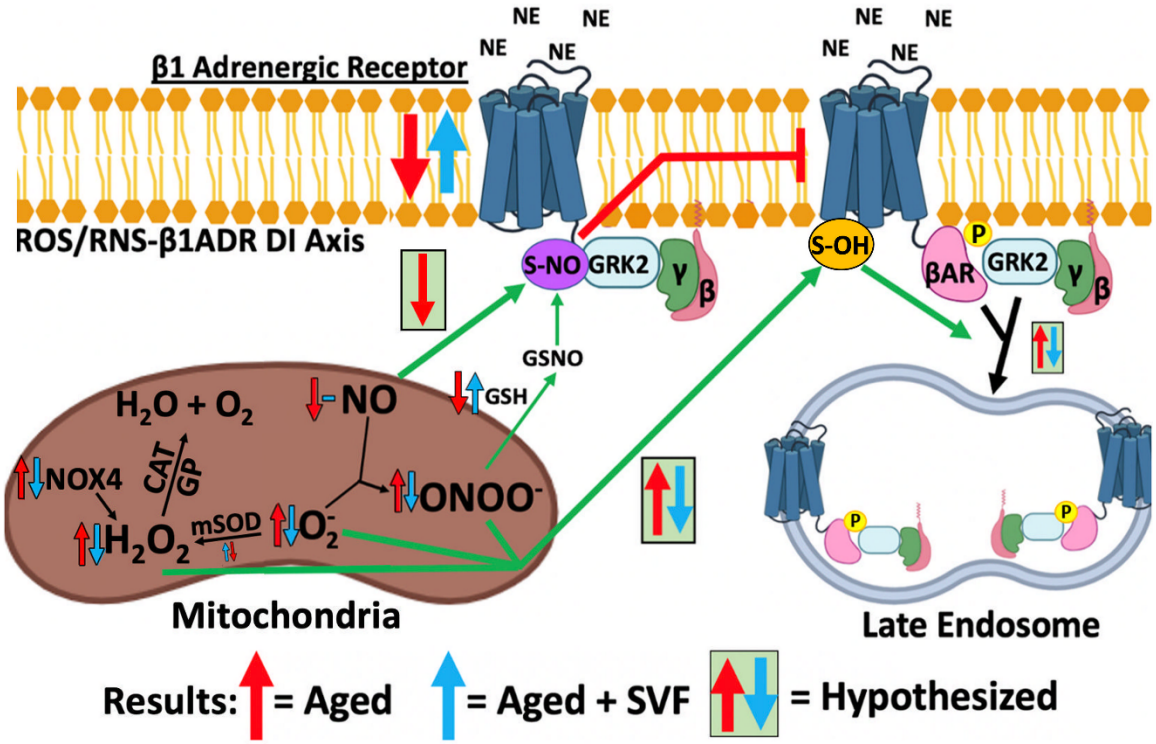

Figure A3.1: Simplified schematic model of ROS/RNS- β1-AR desensitization and internalization axis.

Age-dependent accumulation of mitochondrial ROS may oxidize the β1-AR and reduce nitric oxide-mediated nitrosylation of GRK2 to facilitate desensitization and internalization into endosomes. SVF restores β1-AR mediated dilation within this axis through antioxidation of mitochondrial ROS, which likely decreases β1-AR thiol oxidation. However, GRK2 nitrosylation is likely not restored to youthful levels as SVF does not restore nitric oxide or general protein SNO signaling. Overall, the results of this manuscript explain the therapeutic effects of SVF in CMD to reverse hyperconstriction by increased functional β1-AR at the plasma membrane in part due to antioxidative effects. βAR: Beta Arrestin, CAT: catalase, GRK-2: G-protein Receptor Kinase 2, GSH:

glutathione, GSNO: nitrosoglutathione, mSOD: manganese superoxide dismutase, NE: norepinephrine, OH, thiol oxidation, S-NO: S-nitrosylation

Figure A3.2

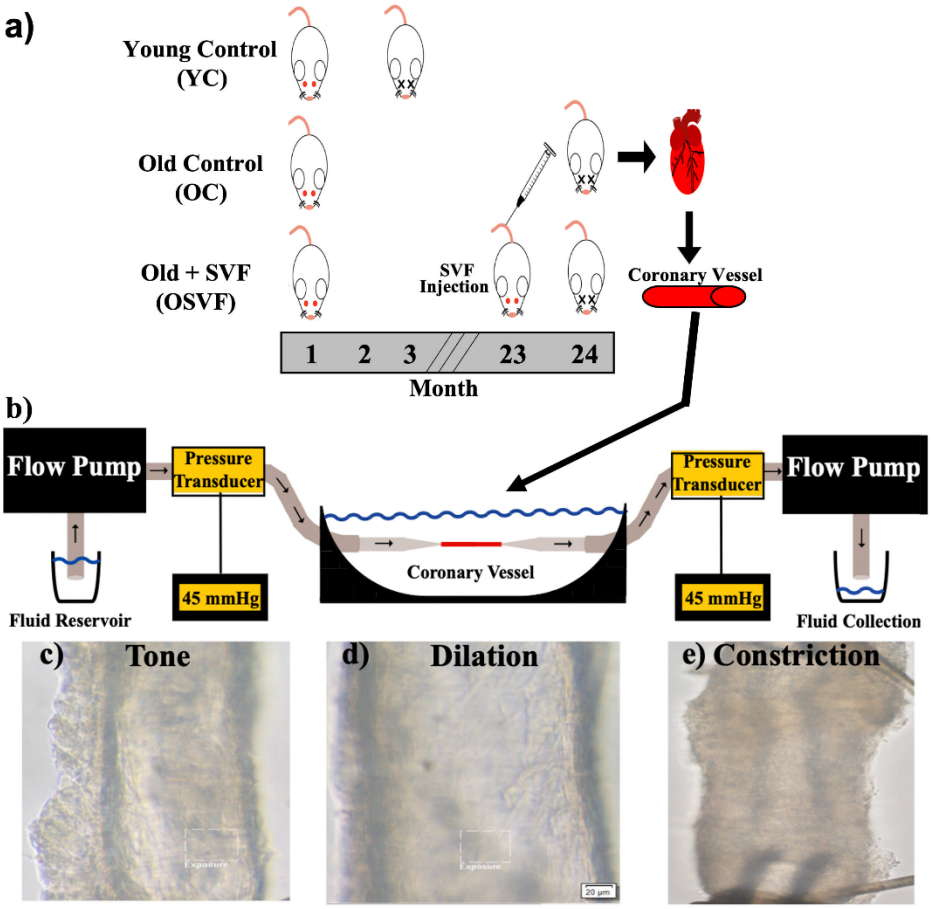

Figure A3.2: Outline of pressure myography methodology.

Female Fisher-344 rats in three experimental groups including young control (3-6 months old), old control (24 months old), and old + SVF (OSVF, 24 months old) with SVF tail vain injection (10 million cells) one month prior to sacrifice (**A**). At time of sacrifice, hearts are removed and microvessels (100-200 μm) dissected and attached to glass pipettes of a pressure myography rig allowing flow through the vessel via a flow pump at 0-25 μL/minute at 37°C and 45 mmHg (physiologic pressure) (**B**). Vessel fluorescence or intraluminal diameter can be tracked in real time with examples at tone (**C**), dilation (**D**) and constriction (**E**).

Figure A3.3

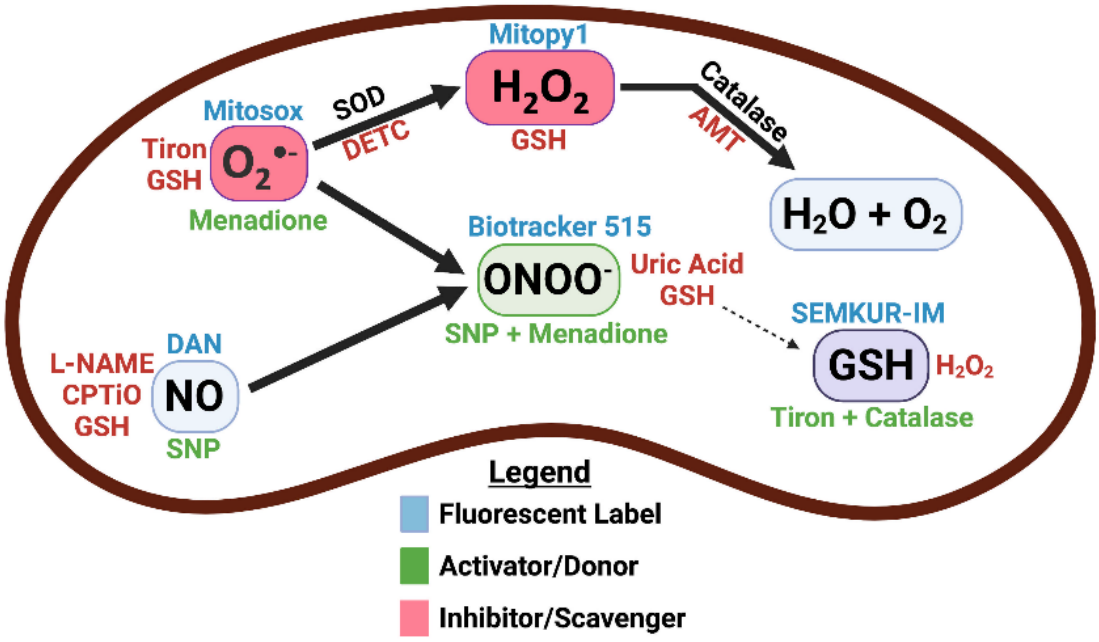

Figure A3.3: ROS map illustrating experimental fluorescent labels (blue), activators/donors (green) and inhibitors/scavengers (red).

Figure A3.4

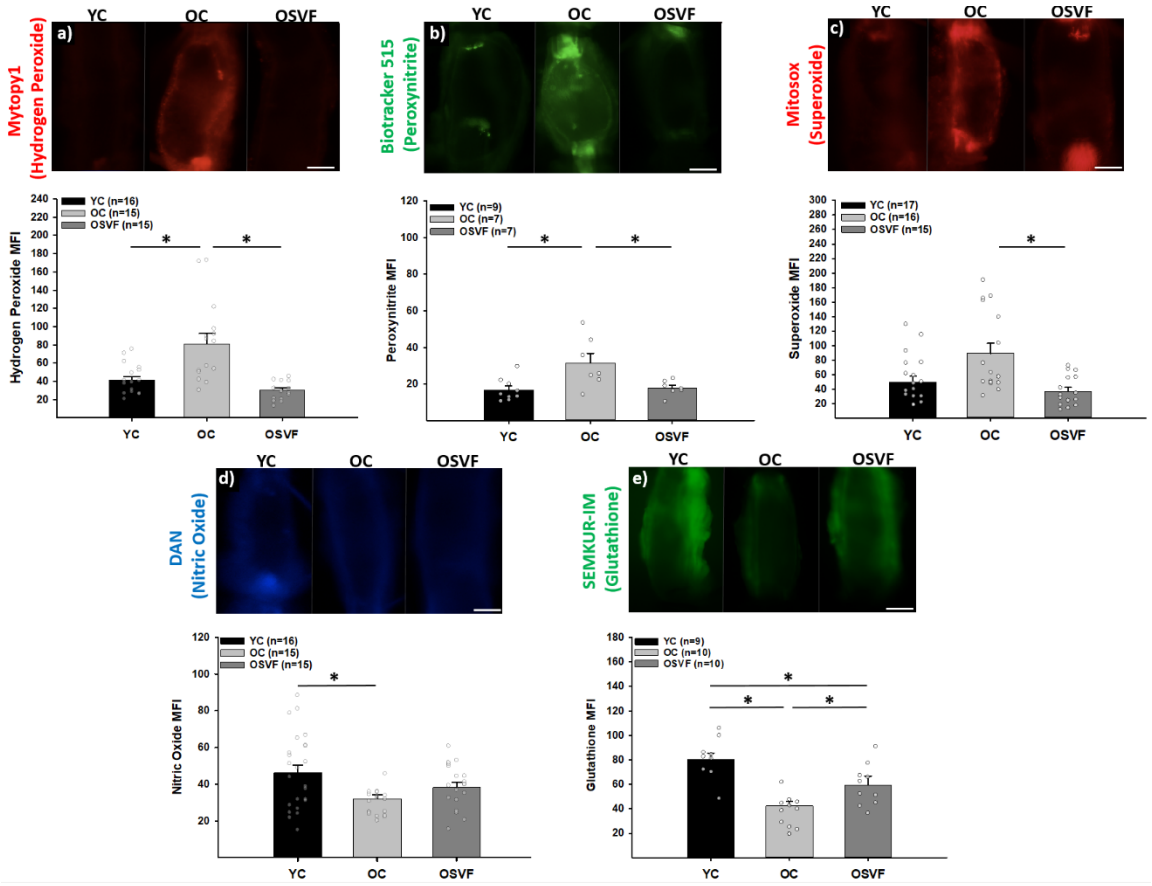

Figure A3.4: Changes in mitochondrial ROS, nitric oxide, and glutathione at baseline with aging and SVF therapy.

Hydrogen peroxide, peroxynitrite, and superoxide Mean Fluorescent Intensity (MFI, arbitrary units) are increased with aging, reversed by SVF (**A-C**). Nitric oxide and Glutathione MFI are decreased with aging, with SVF partially restoring glutathione, but not nitric oxide to youthful levels (**D-E**). Data presented as means±SEM. Significance determined as $p < 0.05$ with One-way ANOVA with Bonferroni *post-hoc* analysis. Scale bar represents 100 μm. OC: Old Control, OSVF: Old + Stromal Vascular Fraction, YC: Young Control.

Figure A3.5

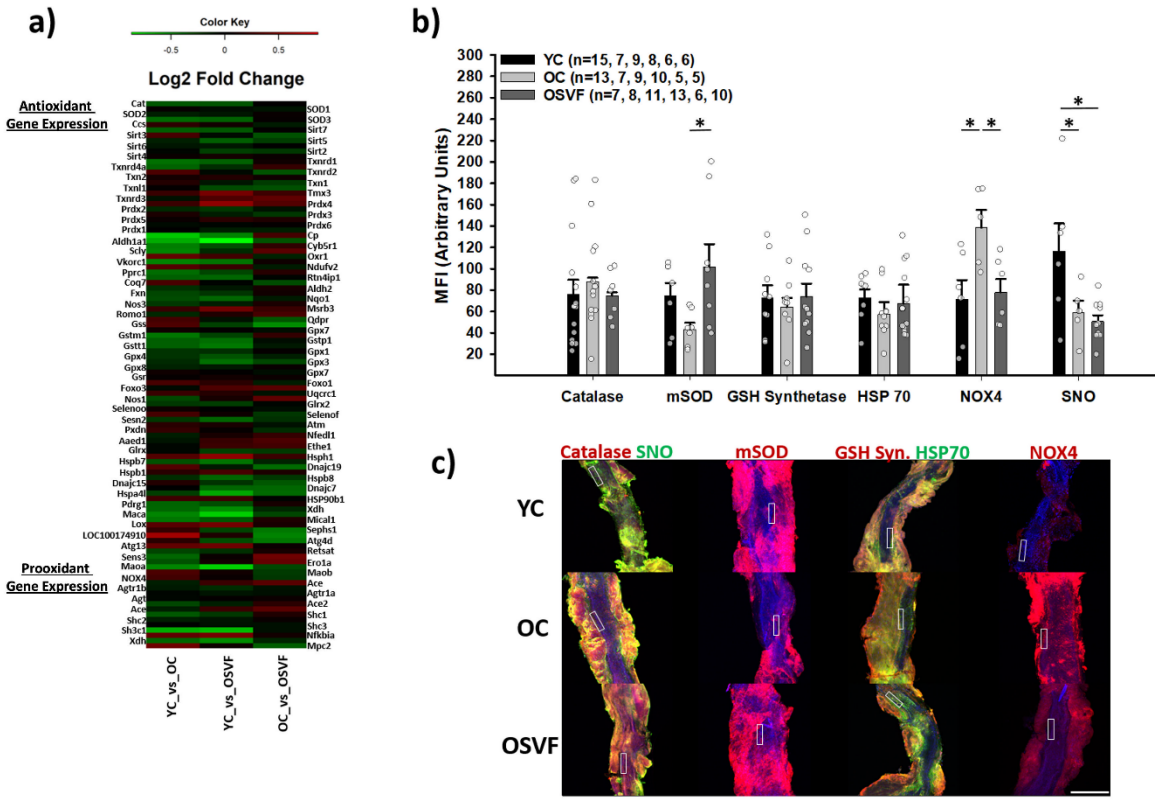

Figure A3.5: Antioxidant and pro-oxidant gene and protein expression in youth, aging, and SVF therapy.

RNA sequencing of isolated vessels with genes relevant to cellular and mitochondrial redox balance (**A**). Protein MFI of isolated vessels for catalase, mSOD, glutathione synthetase, HSP70, NOX4, and SNO (**B**) with representative confocal images (**C**). Nuclei signified by DAPI. Data presented as means±SEM. Significance determined as $p < 0.05$ with One-way ANOVA with Holm-Sidak *post-hoc* analysis. Scale bar represents 200 μm and ROI represents 20x100 μm with blue representing DAPI. GSH synth.: glutathione synthetase, HSP70: Heat Shock Protein 70 mSOD: manganese Superoxide Dismutase, NOX4: NADPH Oxidase 4, OC: Old Control, OSVF: Old + Stromal Vascular Fraction, SNO: S-nitrosylation, YC: Young Control.

Figure A3.6

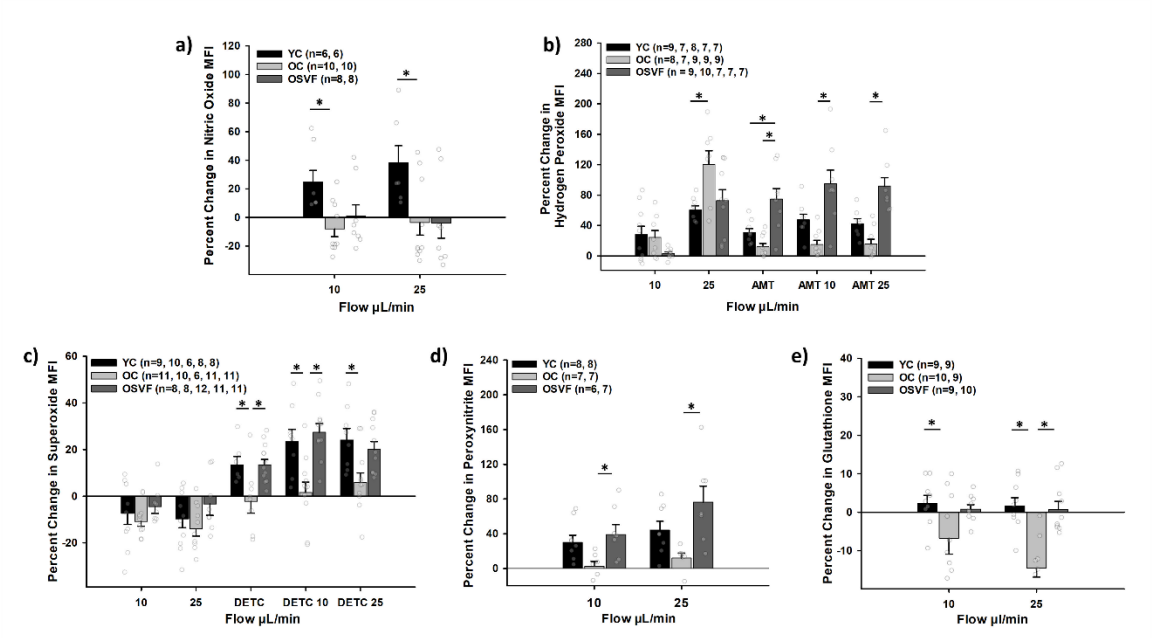

Figure A3.6: Effect of intraluminal flow on ROS/NO/GSH MFI with and without antioxidant enzyme inhibitors.

Nitric oxide signaling to flow is greatest with youth but minimal in aging and SVF therapy (**A**). Hydrogen peroxide accumulation to flow is greatest in aging (**B**). Further, blocking catalase with AMT yields greatest buildup of hydrogen peroxide in response to flow with SVF therapy, indicating greatest catalase function in OSVF. There is no age- or therapy-induced changes to superoxide response to flow at baseline, however, with DETC there is significantly less buildup of superoxide to flow in aging, indicating greater SOD function with youth/OSVF (**C**). OSVF has greater accumulation of peroxynitrite with flow than young or old control (**D**). Flow leads to a significant decrease in glutathione MFI in aging alone compared to youth or OSVF (**E**). Data presented as means±SEM. Significance determined as $p < 0.05$ with One-way ANOVA with Bonferroni *post-hoc* analysis. AMT: 3-amino-1,2,4-triazole, DETC:

Diethyldithiocarbamic acid, OC: Old Control, OSVF: Old + Stromal Vascular Fraction, YC: Young Control.

Figure A3.7

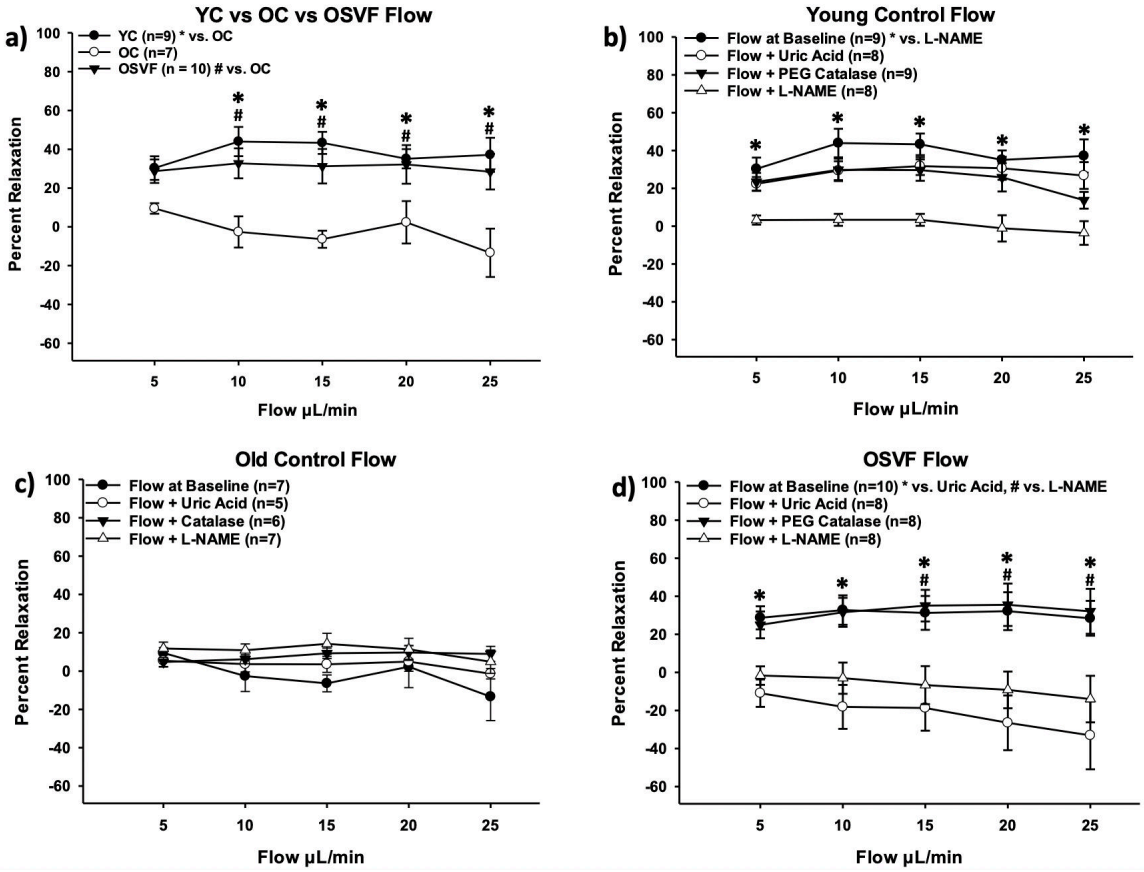

Figure A3.7: Flow-mediated dilation changes in response inhibitors/scavengers of ROS/RNS.

There is a significant decrease in FMD in aging, reversed by SVF therapy (**A**). During youth, FMD is inhibited by L-NAME inhibition of eNOS nitric oxide production, but not uric acid or catalase (**B**). During aging, there are no differences in FMD with preincubation of L-NAME, uric acid, or catalase (**C**). With SVF therapy, FMD is attenuated with L-NAME and uric acid scavenging of peroxynitrite (**D**). Data presented as means±SEM. Significance determined as $p < 0.05$ with Two-way Repeated Measures ANOVA with Bonferroni (**A**) or Holm-Sidak (**B-D**) *post-hoc* analysis. eNOS: endothelial nitric oxide synthase, FMD: flow mediated-dilation, L-NAME: N-Nitro-L-arginine

methylester, OC: Old Control, OSVF: Old + Stromal Vascular Fraction, YC: Young Control.

Figure A3.8

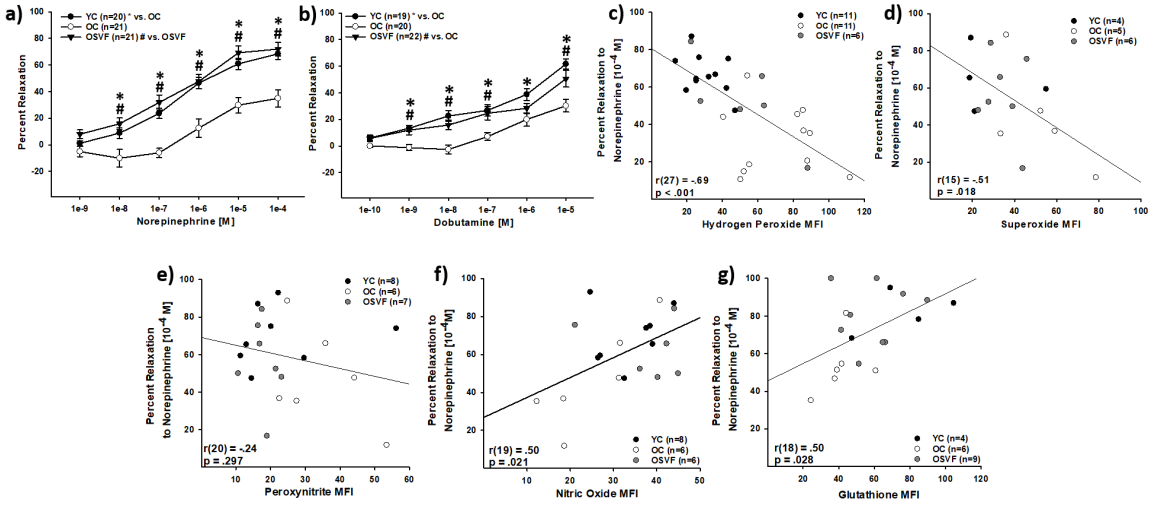

Figure A3.8: Link between β1-AR dysfunction and increased ROS and attenuated nitric oxide, and glutathione concentration in aging.

Aging reduces β1-AR dilative response to norepinephrine and dobutamine, restored to young control levels by SVF therapy (**A-B**). β1-AR dilation to norepinephrine (10^{-4} [M]) negatively and significantly correlates with hydrogen peroxide and superoxide, but not peroxynitrite, while positively and significantly correlating with nitric oxide and glutathione MFI (**C-G**). Data presented as means±SEM. Significance determined as $p < 0.05$ with Two-way Repeated Measures ANOVA with Bonferroni *post-hoc* analysis (**A-B**) and Linear Regression (**C-G**). OC: Old Control, OSVF: Old + Stromal Vascular Fraction, YC: Young Control.

Figure A3.9

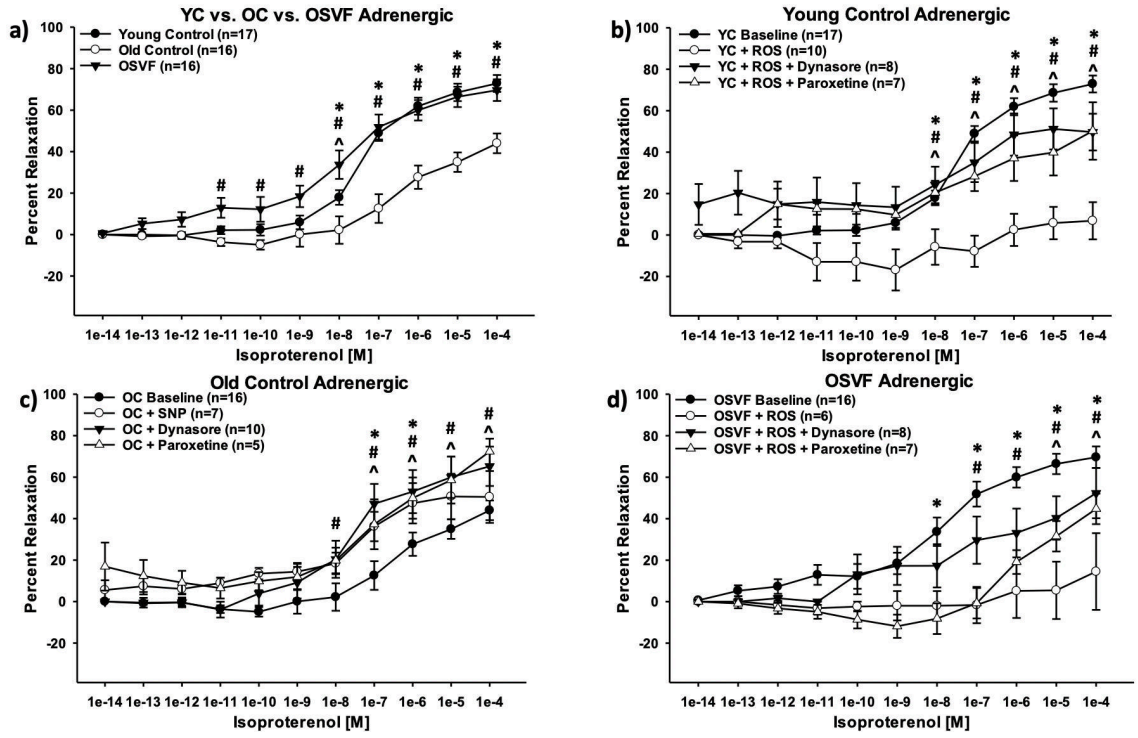

Figure A3.9: Effect of ROS/RNS on β1-AR desensitization & internalization in youth, aging, and SVF therapy.

With aging there is a significant decrease in dilation to isoproterenol, reversed by SVF (* = YC vs. OC, # = SVF vs. OC, ^ = YC vs. OSVF) (**A**). YC vessels exposed to exogenous ROS (hydrogen peroxide 10^{-4} [M] and menadione superoxide donor 10^{-5} [M]) have abrogated dilation reversed by paroxetine and dynasore inhibition of desensitization & internalization (* = baseline vs. ROS, # = dynasore vs. ROS, ^ = paroxetine vs. ROS) (**B**). OC vessels exposed to SNP, dynasore, and paroxetine have significantly improved percent relaxation (* = baseline vs. SNP, # = baseline vs. dynasore, ^ = baseline vs. paroxetine) (**C**). OSVF vessels exposed to exogenous ROS have ameliorated dilation reversed by paroxetine and dynasore (* = baseline vs. ROS, # = dynasore vs. ROS, ^ = paroxetine vs. ROS) (**D**). Data presented as means±SEM. Significance defined

as $p < 0.05$ utilizing two-way repeated measures ANOVA with Bonferroni (**A**) or Holm-Sidak (**B-D**) *post hoc* analysis. OC; Old Control, OSVF: Old + Stromal Vascular Fraction, ROS: Reactive Oxygen Species, SNP: Sodium Nitroprusside. YC: Young Control.

Supplemental Figure A3.1

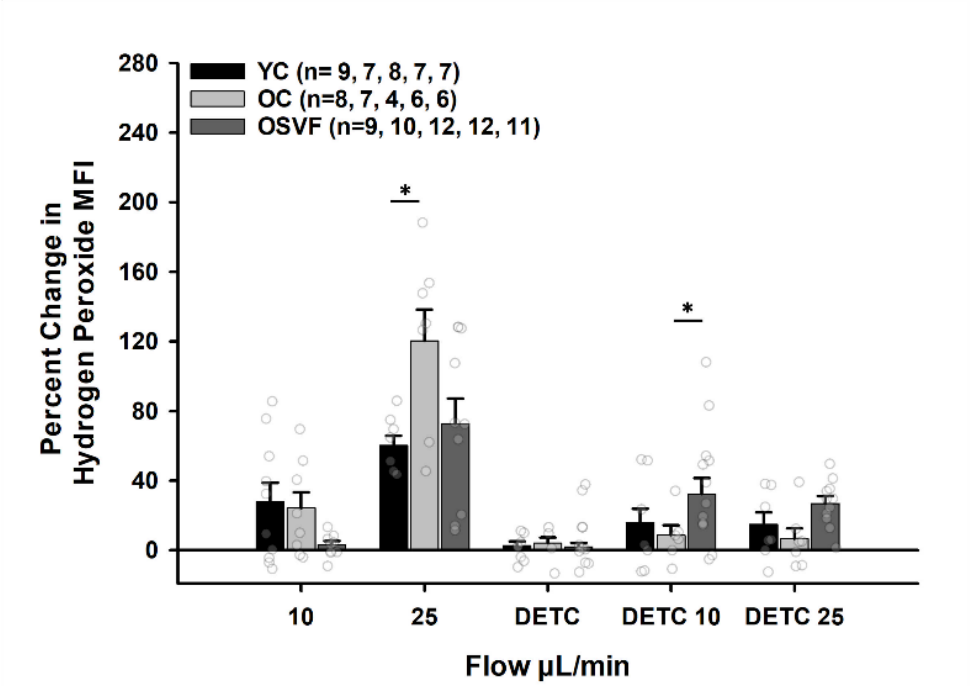

Supplemental Figure A3.1: Hydrogen peroxide production with DETC superoxide dismutase inhibition.

Data presented as means±SEM. Significance defined as $p < 0.05$ via One-way ANOVA with Bonferroni post hoc analysis. DETC: Diethyldithiocarbamic acid. Old Control, OSVF: Old + Stromal Vascular Fraction, YC: Young Control.

Supplemental Figure A3.2

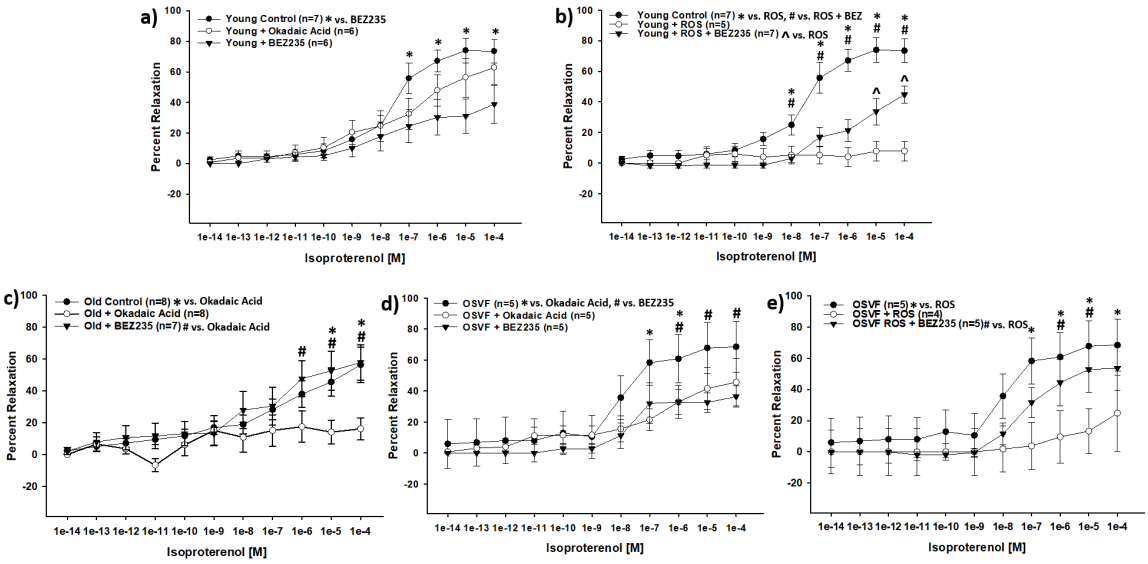

Supplemental Figure A3.2: Contribution of β1-AR recycling on dilative function between groups.

Incubation with BEZ235, but not okadaic acid, attenuates dilation to isoproterenol in YC (**A**). In YC, pre-incubation with ROS (hydrogen peroxide and menadione) leads to abrogation of dilation, partially prevented by co-incubation with BEZ235 (**B**). OC dilation to isoproterenol is significantly attenuated by okadaic acid, but not BEZ235 (**C**). In OSVF, dilation to isoproterenol is diminished with okadaic acid at lower respective doses and BEZ235 at higher respective doses (**D**). Pre-incubation of vessels with ROS attenuates dilation to isoproterenol in OSVF, partially prevented by co-incubation with BEZ235 (**E**). Data presented as means±SEM. Significance defined as $p < 0.05$ via two-way ANOVA with Bonferroni *post hoc* analysis.

Supplemental Figure A3.3

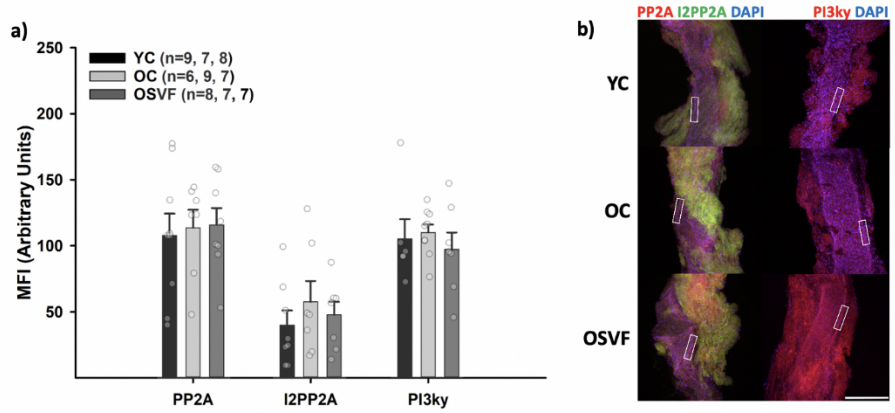

Supplemental Figure A3.3: Protein expression of β-AR recycling mediators is unchanged with aging or SVF therapy. There is no significant change in MFI of PP2A (activates recycling) or its inhibitors I2PP2A or PI3ky (**A**). Representative confocal images are shown (**B**). Data presented as means±SEM. Significance determined as $p < 0.05$ with one-way ANOVA. Scale bar represents 200 μm and ROI represents 20x100 μm. OC: Old Control, OSVF: Old + Stromal Vascular Fraction, YC: Young Control.

Discussion

Aging induces a redox shift in coronary microvessels towards oxidative stress, accompanied by a decrease in antioxidants glutathione and nitric oxide. Intravenous treatment with SVF four weeks prior to explant reverses these trends in old rats, except for nitric oxide. Oxidative stress occurs despite an age-related increase in gene expression of several antioxidant proteins including catalase, superoxide dismutase 3, and thioredoxin reductase. This likely indicates attempted compensatory regulation that cannot compete with prooxidant processes, including gene expression of xanthine dehydrogenase, monoamine oxidase A, and SHC1 (encodes p66SHC). These consequences with aging include abrogated vasodilation through reduced FMD and β1-AR signaling. We show for the first time that ROS levels negatively correlate whereas nitric oxide and glutathione positively correlates with β1-AR function. The major findings support that antioxidant effects of SVF cell therapy restores vasodilation in aging by switching the acute mediator of FMD from hydrogen peroxide to peroxynitrite, as well as by attenuating desensitization and internalization of the β1-AR.

Immunofluorescence staining found greater NOX4 protein MFI with aging albeit no increase in gene expression. NOX4-derived hydrogen peroxide can lead to ROS-induced ROS release in part through activation of p66SHC [397]. The MFI of mSOD was reduced with aging and reversed by SVF, despite no genetic expression changes. Interestingly, p66SHC (increased gene expression in OC) can inactivate FOXO3, causing mSOD downregulation [398]. p66SHC overexpression is also known to reduce dilation to acetylcholine and nitric oxide bioavailability, while the opposite is true in knockout models [399-401]. Therefore, greater NOX4 and p66SHC could be a major driver of

ROS production in aging coronary microvasculature. One explanation for SVF's antioxidant effects could be to reduce signaling from NOX4/p66SHC. NOX4 MFI was reduced to YC levels by SVF and there was no expressional difference in p66SHC between YC and OSVF. Moreover, SVF upregulated gene expression of additional antioxidant proteins such as glutathione synthetase, Sirt5, thioredoxin-like 1, glutaredoxin-like protein, selenophosphate synthetase 1, and several heat shock protein subunits compared to OC. Although there was no increase in glutathione synthetase protein MFI, glutathione itself was increased with SVF to YC levels.

It has previously been reported that the mediator of FMD shifts throughout the lifespan from prostaglandin during youth, to nitric oxide during young adulthood, to hydrogen peroxide in coronary artery disease [387]. Our data confirms this trend, as youth produced significant nitric oxide MFI and FMD was inhibited by L-NAME, whereas in aging hydrogen peroxide MFI was most significantly increased with flow. Catalase did not inhibit FMD in aged vessels because dilation was minimal to begin with. With flow plus DETC inhibition of superoxide dismutase, superoxide MFI was greater in YC and OSVF compared to OC. This suggests that there is reduced mSOD expression or function in aging, reversed by SVF therapy. Although RNAseq showed no difference in mSOD transcription, immunofluorescence showed increased mSOD availability in OSVF compared to OC. Other than expression changes in mSOD described above, function of mSOD in aging can be inhibited by peroxynitrite-mediated tyrosine nitration (and chronic baseline peroxynitrite MFI was increased in OC) [402]. Inhibiting catalase with AMT led to greater hydrogen peroxide in YC and OSVF compared to OC, indicating a reduction in catalase expression/function with aging that is restored by SVF. Interestingly, RNAseq

showed increased catalase gene expression in the aged groups, OC and OSVF, when compared to YC, while immunofluorescence showed no difference between groups. Catalase function can be activated by phosphorylation of catalase at tyrosine 231 and 386, and can be ubiquitin degraded, which may explain these findings [403].

With SVF there was increased peroxynitrite MFI in response to flow, and FMD was inhibited by uric acid scavenging of peroxynitrite as well as L-NAME. This goes against our initial hypothesis, as we believed nitric oxide would be restored to YC levels and would mediate FMD in OSVF vessels [404]. However, as nitric oxide is required to produce peroxynitrite (in combination with superoxide), and L-NAME inhibited FMD, it stands to reason that peroxynitrite FMD response is dependent on enough nitric oxide production to combine with superoxide resulting in significantly increased peroxynitrite. Although peroxynitrite is a ROS, it has been speculated to have functional significance in geriatric populations as a "new healthy vascular endothelium redox status" because peroxynitrite can donate nitric oxide, thereby acting as a reservoir and eliciting FMD, possibly without the pro-atherogenic effects of hydrogen peroxide [405]. To emphasize, the increase in OSVF peroxynitrite is acute, and limited to periods of FMD. During baseline (chronic status), aged vessels had greater peroxynitrite MFI than YC or OSVF. These acute vs. chronic redox signaling changes are likely of significance to cellular health.

β1-AR-mediated dilation with dobutamine, norepinephrine, and isoproterenol were reduced with aging, restored by SVF therapy. Using two vessels from the same animals, we determined there is negative correlation between oxidative stress and β1-AR dilative function (albeit not for peroxynitrite) and a significant positive correlation

between glutathione and nitric oxide with β1-AR function. Thus, oxidative stress reduces functional dilation with aging. Incubating vessels with exogenous hydrogen peroxide and superoxide (mimicking aging conditions) completely attenuated YC and OSVF β1-AR dilation to isoproterenol. This effect was diminished if co-incubating the ROS with dynasore (inhibiting dynamin i.e internalization) or paroxetine (inhibiting GRK2 i.e. desensitization). OC vessels pre-incubated with SNP (mimicking YC nitrosylation status), dynasore and paroxetine significantly improved β1-AR dilation to isoproterenol. These results indicate a role for ROS and RNS in β1-AR trafficking.

It has been speculated that the β1-AR can be influenced to internalize upon thiol oxidation, and receptor recycling from the endosome is known to be inhibited by ROS [20, 406]. We found that inhibition of PI3kγ (which activates I2PP2A to inhibit PP2A-mediated β1-AR recycling) with BEZ235 countered the poor dilatory effects produced by exogenous ROS YC and OSVF vessels. This is consistent with what others have found, specifically that ROS can influence β1-AR recycling [20, 406]. This did not translate to BEZ235 improving OC vessel dilation. Interestingly, inhibiting β1-AR recycling with okadaic acid led to significant reduction in isoproterenol-mediated dilation in OC but not in youth. This signifies that recycling is not necessary in youth for successful maximal response to agonist, likely due to plentiful receptor density at the plasma membrane. This is not the case in aging, indicating that greater density of receptor has been desensitized and internalized, and maximal dilative response to agonist depends in part on recycling. OSVF vessels exhibit partially attenuated dilation with okadaic acid, but at high doses of isoproterenol this is not significant. Overall, this indicates OC vessels are most reliant on recycling, followed by OSVF, then YC. Supporting these observations, we found that

protein levels (evaluated by MFI) of PP2A, I2PP2A, and PI3kγ were unchanged with aging or SVF therapy, indicating the mechanisms of recycling themselves are unchanged.

SNP-mediated improvement in β1-AR function has been attributed to nitrosylation and inhibition of GRK2 [392]. We analyzed general protein nitrosative status using a fluorescent S-nitrosocysteine antibody, believing SVF may restore β1-AR function by reducing ROS which would alleviate nitric oxide bioavailability to nitrosylate/inhibit GRK2. Instead, we found that S-nitrosylation status is significantly reduced in aging and OSVF compared to youth. This complements our findings that SVF does not restore nitric oxide bioavailability. Therefore, we conclude that in the ROS/RNS β1-AR Desensitization and Internalization Axis, young vessels experience limited ROS and plentiful nitric oxide bioavailability, resulting in functional β1-AR at the plasma membrane potentially via greater GRK2 nitrosylation, less β1-AR thiol oxidation, and less ROS-mediated blockade of receptor recycling. In aging, this axis shifts such that there is reduced nitric oxide bioavailability, allowing functional GRK2 to influence desensitization and internalization, and there is greater accumulation of ROS to oxidize β1-AR-thiols and inhibit recycling. With SVF therapy, although nitric oxide bioavailability is not restored, ROS are reduced to alleviate β1-AR thiol oxidation-mediated desensitization/internalization and restored receptor recycling.

Future directions should confirm these findings by studying β1-AR trafficking through qualitative and quantification studies. For example, in living vessels or in endothelial cells, fluorescently tracking the trafficking of the β1-AR in response to ROS, SNP, paroxetine, and dynasore in YC, OC, OSVF would qualitatively confirm and support our findings [392, 407]. β1-AR trafficking can also be quantified by western

blotting of plasma membrane and endosomal β1-AR [408]. Finally, the constituents of SVF that are responsible for restoration of redox balance, FMD, and adrenergic homeostasis should be determined. Differentiating between which cell type(s) and/or paracrine factors (exosomal or exocytosed proteins, miRNA, etc.) induce the observed changes would be of benefit for therapeutic development. It would be of interest if SVF-derived exosomes could be used in lieu of cells [409]. Indeed, adipose SVF-derived mesenchymal stem cell exosomes have antioxidant effects and protect against ischemia and apoptosis, encourage angiogenesis, and restore mitochondrial health [383, 384, 410, 411].

In conclusion, we hypothesized that flow- and β1-AR-mediated dilation are reduced with aging and reversed via SVF therapy by attenuating oxidative stress and restoring protective nitrosative signaling. FMD and β1-AR were significantly reduced in aging with reversal by SVF therapy. However, nitric oxide bioavailability was not restored by SVF cell therapy to YC levels; instead, peroxynitrite was the mediator of improved FMD. B1-adrenergic dilative function was restored in SVF correlating with reduced ROS and increased antioxidant glutathione. Our conceptual ROS/RNS β1-AR Desensitization and Internalization Axis is supported since exogenous SNP or blockade of desensitization/internalization restored β1-AR function in aging, and exogenous ROS attenuated β1-AR function in youth/OSVF unless simultaneously blocking desensitization/internalization. In conclusion, aging-mediated microvascular dysfunction and hyperconstriction can be ameliorated by targeting oxidative stress. SVF therefore has significant translational potential for patients with CMD and is theoretically superior over

current clinical standards (e.g., beta blockers) that treat symptoms but do not address the pathologic cause of microvascular dysfunction and hyperconstriction.

Innovation

Current therapeutic options for coronary microvascular disease are of limited effectiveness, however, SVF therapy in a female rodent model reverses hyperconstriction by restoring effectiveness of flow-mediated and β1ADR-mediated dilation. SVF's mechanism of action is to reduce chronic oxidative stress, which restores β1-AR function according to our novel conceptual ROS/RNS-β1-AR Desensitization and Internalization Axis (**Fig A3.1**). SVF also facilitates an acute substrate switch in response to intraluminal flow from pro-atherogenic hydrogen peroxide-mediated FMD in aging to peroxynitrite-mediated FMD with SVF. This switch of FMD mediator is associated with FMD restored to levels seen in young control animals.

APPENDIX 4

VIEWING STROMAL VASCULAR FRACTION *DE NOVO* VESSEL FORMATION AND INTEGRATION WITH HOST MICROVASCULATURE USING THE RAT MESENTERY CULTURE MODEL

Overview

The objective of the study is to demonstrate the innovation and utility of mesenteric tissue culture for discovering the microvascular growth dynamics associated with adipose-derived stromal vascular fraction (SVF) transplantation. Understanding how SVF cells contribute to *de novo* vessel growth (i.e., neovascularization) and host network angiogenesis motivates the need to make observations at single cell and network levels within a tissue. SVF was isolated from the inguinal adipose of adult male Wistar rats, labeled with DiI, and seeded onto adult Wistar rat mesentery tissues. Tissues were then cultured in MEM + 10% FBS for 3 days and labeled for BSI-lectin to identify vessels. Alternatively, SVF and tissues from green fluorescent positive (GFP) Sprague Dawley rats were used to track SVF derived versus host vasculature. SVF treated tissues displayed a dramatically increased vascularized area compared to untreated tissues. DiI and GFP+ tracking of SVF identified neovascularization involving initial segment formation, radial outgrowth from central hub-like structures, and connection of segments. Neovascularization was also supported by the formation of segments in previously

avascular areas. New segments characteristic of SVF neovessels contained endothelial cells and pericytes. Additionally, a subset of SVF cells displayed the ability to associate with host vessels and the presence of SVF increased host network angiogenesis. The results showcase the use of the rat mesentery culture model as a novel tool for elucidating SVF cell transplant dynamics and highlight the impact of model selection for visualization.

This chapter is from the published work referenced as follows:

Hodges, N.A., A.O. Lampejo, H. Shang, G. Rowe, A.J. LeBlanc, A.J. Katz, W.L. Murfee, *Viewing Stromal Vascular Fraction De Novo Vessel Formation and Integration with Host Microvasculature Using the Rat Mesentery Culture Model.* Microcirculaiton, 2022.

Introduction

The isolation of adipose stromal cells with multi-lineage differentiation potential was first reported in the peer-reviewed literature in 2001 [179]. In recent years, the use of stromal vascular fraction (SVF) has emerged as an alternative therapeutic strategy to form new vessels, with its use in clinical trials growing exponentially [184]. SVF has become an ideal candidate in vascular therapeutics due to the ability to leverage a real-time autologous point-of-care therapeutic approach, thereby avoiding excessive costs related to good manufacturing practice and logistical obstacles related to cell transport, storage, tracing, and inventory. SVF includes multiple cell types and can be thought of as a heterogeneous mixture of leukocytes, erythrocytes, stromal cells, progenitor cells, endothelial cells, endothelial progenitor cells, pericytes, and other cells of the perivascular niche [412, 413]. Though SVF as a therapeutic has entered into clinical testing for a variety of pathologies such as osteoarthritis [181], chronic heart ischemia [183], angina [414], and pulmonary fibrosis [182], none to date are approved by the Food and Drug Administration (FDA). While these clinical trials have shown beneficial effects of SVF administration, questions regarding treatment timing, cell dose, and duration remain. There is also a need to better understand how SVF cells spatially and temporally contribute to neovascularization and blood flow within a vascular bed. The ultimate goal is to deliver cells to influence and promote microvascular growth and function. Since microvascular remodeling is a complex process involving multiple cell types, a heterogeneous cell therapy such as the SVF may be more conducive to vascularization than single homogenous cell approaches. A heterogeneous cell composition might provide the unknown optimal milieu of environmental cues [186]. As of now, we know

that SVF can dramatically affect the presence of new vessels both *in vivo* and *in vitro* [191, 307], possibly due to engraftment into the host vasculature [42] or release of angiogenic growth factors.[13] This study will examine the former of the two paradigms and address the knowledge gaps concerning how SVF spatially and temporally incorporates within living tissues and promotes microvascular growth and remodeling.

The identification of SVF dynamics during neovessel formation and integration with host microvascular networks can be thought of as an imaging challenge. Meeting this challenge requires the ability 1) to view SVF cell populations in a real tissue environment at the single cell level and 2) to view changes of the existing vasculature over time. These experimental challenges thus require investigators to make decisions related to the imaging technology and the experimental model. Potential *in vivo* models include two-photon imaging of brain vasculature (cranial window) or the use of dorsal window chamber models via intravital microscopy [415, 416]. These models incorporate the necessary complexity of microvascular networks *in situ*, however these models have yet to be used for SVF characterization because of the technical difficulties associated with SVF transplantation, repeated imaging, and the need for invasive survival surgeries [417]. In comparison, *in vitro* studies involving culturing SVF in two-dimensional or three-dimensional substrates represent a simplified environment that allows for easier time-lapse imaging needed to track vessel formation dynamics. Such methods have also proven valuable for reductionist studies focused on concentration-dependent and matrix-dependent effects [191, 338]. However, *in vitro* methods do not offer a view of an intact host microvascular network and the impact of host-derived cell signaling factors is not considered.

Within the last decade, our laboratory has developed the rat mesentery *ex vivo* culture model to bridge the gap between in vitro and *in vivo* (**Fig A4.1**). Traditionally used for intravital microscopy because it is 20 – 40 μm thick, the rat mesentery is relatively easy to image with common epifluorescent microscopes. The thinness also makes it ideal for continued culturing and despite being excised, mesenteric windows survive up to at least 7 days [294]. We have shown that the culture model enables time-lapse investigation of cell-cell interactions at specific locations across blood and lymphatic microvascular networks [294, 418, 419]. The physiological relevance of the model is supported by demonstration of the functional effects of pericytes on endothelial cell sprouting, smooth muscle cell contraction along arterioles, and the maintenance of *in vivo*-like endothelial cell phenotypes along capillary sprouts during angiogenesis [294, 296, 420]. The objective of this study was to showcase the use of the rat mesentery culture model as a platform for visualizing SVF cell dynamics and effects on the host vasculature (**Fig A4.1**). Our results confirm that SVF can be translated onto the mesentery tissue and integrate into the networks when cultured for 3 days, thus offering a new view for SVF derived vasculogenesis and interactions with the host vasculature. The SVF formed unique networks that connected with the pre-existing host networks. In addition, SVF induced host microvascular network angiogenesis and examples of individual cells were observed to be integrated along individual host vessel segments. This study demonstrates the therapeutic potential of SVF and the importance of SVF interaction with the host microvascular network. The results further showcase the use of the rat mesentery culture model for visualizing SVF neovessel formation, time-lapse

dynamics, and SVF effects on a live tissue. The comprehensive readouts will serve to guide our understanding of SVF transplantation.

Materials and Methods

Animal model.

The University of Florida Animal Care and Use Committee approved all experimental protocols. Adult male Wistar rats were anesthetized via intramuscular injection with ketamine (80 mg/kg body weight) and xylazine (8 mg/kg body weight). Adult male Wistar rats were used to be consistent with previous published studies in our laboratory using the rat mesentery culture model. Sprague Dawley EGFP rats (Rat Resource and Research Center; 800-1000 g) were anesthetized via isoflurane. The specific strain and weight of Sprague Dawley EGFP rats were used because of availability through a collaboration at the time of the study. Adult Fischer 344 rats were used for immunolabelling for endothelial cells and pericytes; rats were anesthetized via intramuscular injection with ketamine (80 mg/kg body weight) and xylazine (8 mg/kg body weight). Post tissue harvesting and/or SVF isolation, all rats were euthanized by intracardiac injection of Beuthanasia (0.2 ml).

Rat mesentery tissue harvesting, SVF transplantation, and culture.

Rat mesenteric tissues were harvested and cultured according to a previously established protocol [301, 418]. To harvest mesenteric tissues, the abdominal region was shaved then sterilized with 70% isopropyl alcohol before an incision was made along the linea alba. The mesentery was exteriorized onto a sterile plastic stage using cotton tip

applicators to first remove the cecum and subsequently the ileum and jejunum. Vascularized mesenteric tissues were excised and rinsed once in sterile saline with 0.9% NaCl (Baxter; Deerfield, IL) and immersed in minimum essential media (MEM; Gibco; Grand Island, NY) containing 1% Penicillin-Streptomycin (PenStrep; Gibco; Grand Island, NY) at 37°C. Isolated SVF cells were suspended in 10% FBS + MEM solution at a concentration of 10 million cells/mL. Tissues were then spread onto a polycarbonate filter membrane (pore size = 5 μm) on a cell crown. 100 μL of SVF solution was transferred to the surface of each mesenteric window before incubating for 20 min so the SVF cells attached to the tissue (**Fig A4.1**). Cell crowns were then inverted into a 6-well plate with the fat of the tissue pressing against the bottom of the well. 3 mL of culture media composed of 10% FBS + MEM was then added to each well on top of the filter. Tissues were cultured in standard incubation conditions (5% CO_2, 37°C) for three days.

Adipose tissue harvest and SVF isolation.

A scalpel was used to make a Y shaped incision into the skin from the bottom of the previous incision of the linea alba to each of the inner thighs along the midline, stopping above the knee. The skin was carefully removed from the subcutaneous adipose and muscle layers using the scalpel and microscissors. Hemostats were used to hold the skin back as the separation was advanced to the coxal region. The center skin flap of pelvic region was removed in a similar fashion. The inguinal fat pad was removed in a continuous strip from one hip and leg to the other and placed in a 50 mL conical tube containing sterile saline at 37°C.

Fat was placed onto a large petri dish and diced into fine pieces before transfer into an empty 50 mL conical tube for weighing. Once weight was measured, a 0.15%

collagenase type 1 (Thermo Fisher; Waltham, MA) and DPBS solution heated to 37°C was prepared. Collagenase solution was pushed through a 0.22 µm filter with a syringe for sterilization at a ratio of 2 mL per 1 gram of fat. In the event that the fat weighed less than 3 grams, 5 mL was used to ensure enough volume was in the conical tube containing the diced adipose. The collagenase/adipose mixture was then transferred to a shaker set to 150 RPM and digested for 45 min at 37°C. After digestion, the mixture was centrifuged for 10 min at 600 G to separate the cells from the collagenase and the undigested fat. The top layer of undigested fat was transferred to a new conical tube containing the same volume of fresh filtered collagenase and transferred back to the incubator for a second digestion. The collagenase solution was then removed from the centrifuged tube and the bottom layer of cells was resuspended in 5 mL of 5% FBS + DPBS. The resuspended mixture was filtered through a 250 µm cytostrainer into a new 50 mL conical tube then centrifuged at 600 G for 5 min. Media was removed and 5 mL of ACK lysing buffer (Thermo Fisher; Waltham, MA) was added to the cells through a 0.22 µm filter for sterilization. The solution was then gently shaken in the dark at room temperature for 3 min. Immediately afterwards, 5 mL of 5% FBS + DPBS was added to the solution to neutralize the lysing buffer. This solution was filtered through a 70 µm filter into a new conical tube and the centrifuged for 5 min at 600 G. The media was removed, and the remaining SVF was resuspended with 1 mL of 5% FBS + DPBS. 10 µL of the SVF solution was added to 10 µL of trypan blue, mixed, and then added to a disposable slide for cell counting with a Countess™ II Automated Cell Counter (Thermo Fisher; Waltham, MA).

Immunohistochemistry.

Cultured tissues were fixed in methanol for thirty minutes at -20°C. Tissues were spread on glass slides before being rinsed 3 times for 10 minutes in PBS +0.1% saponin. Fat around window was removed and a hydrophobic barrier was applied around the tissue before being labeled for either platelet endothelial cell adhesion molecule (PECAM; endothelial cell marker) or PECAM plus Neuron-glial antigen 2 (NG2; pericyte marker): Tissues were incubated for 1 hour at room temperature with a primary antibody solution of 1:200 mouse monoclonal biotinylated anti-PECAM antibody (CD31 antibody, BD Pharmigen; San Diego, CA) with 1:100 rabbit polyclonal anti-NG2 antibody (Millipore/Chemicon, Billerica, MA). Tissues were then incubated for 1 hour at room temperature with a secondary antibody solution of 1:500 CY3-conjugated Streptavidin secondary (Jackson Immunoresearch Laboratories) and 1:100 goat anti-rabbit CY2-conjugated antibody (Jackson Immunoresearch Laboratories). Antibodies were diluted in antibody buffer solution comprised of phosphate-buffered solution (PBS; Sigma-Aldrich) + 0.1% saponin (Sigma-Aldrich) + 2% bovine serum albumin (BSA; Jackson Immunoresearch Laboratories) + 5% normal goat serum (Jackson Immunoresearch Laboratories). After each antibody incubation period, the tissues were submerged in PBS + 0.1% saponin for 3 x 10 min washes. The representative images shown in **Figure A4.2** were obtained from experiments involving tissues and SVF harvested from adult Fischer 344 rats.

Cell and vascular network tracking studies.

In order to investigate the fate of the stromal vascular fraction and the microvascular networks to which they were transplanted, cell tracking models were implemented. For the first experimental model, DiI solution was mixed with MEM to make a 5 μL/mL labeling solution. Isolated adult male Wistar SVF cell suspension was centrifuged, aspirated, and resuspended in the DiI solution. The SVF was then incubated for 5 min at 37°C followed by 10 min incubation at 4°C. The SVF suspension was centrifuged at 600 G for 5 min and the labeling media was replaced with suspension media. Cell were then centrifuged again and washed for 2 more times before being seeding onto Wistar tissues according to the protocol above. After 3 days, BSI-Lectin conjugated to FITC (Sigma-Aldrich; St. Louis, MO) was added to media in a 1:40 ratio, transferred to the well containing the seeded tissue, and incubated for 30 min at 37°C. After incubation, the supplemented media was removed, and the tissues were subsequently rinsed with label free media. To preserve DiI labeling, tissues were fixed in methanol-free 4% formaldehyde solution for 10 min at room temperature.

In another experiment, SVF from GFP rats was transplanted onto unlabeled Adult Wistar tissues. The 6-well plates containing these tissues were then placed into a culture chamber mounted on a microscope stage to maintain a temperature of 37 °C. Two to four microvascular networks were imaged per tissue every 24 hours using an inverted epifluorescent microscope. After 3 days, tissues were labeled with TRITC lectin according to the same protocol above and imaged again.

The third tracking experimental group used adult male Wistar SVF on GFP tissues. The time lapse was performed as described above. Following a 3-day culture,

TRITC lectin labeling of the whole tissue was performed as described above and imaged again.

Image acquisition.

Images were acquired using 4x (dry, NA = 0.1), 10x (dry, NA = 0.3), and 20x (oil, NA = 0.8) objectives on an inverted microscope (Nikon Eclipse Ti2) coupled with an Andor Zyla sCMOS camera. Image analysis and quantification were done using ImageJ 2.0.0-rc-54 (U.S. National Institutes of Health, Bethesda, MD).

Statistical analysis.

Two statistical comparisons were made in this study. In order to evaluate the effects of SVF on tissue vascular area, a comparison was made using a two-tailed Student's t-test between 2 experimental groups: FBS alone (control) and SVF + FBS. In order to evaluate the effects of SVF, a comparison was made using a paired t-test between the vascularized areas of native vessels in GFP tissues at day 0 and day 3. Results were considered statistically significant when $p < 0.05$. Statistical analysis was performed using SigmaStat ver. 3.5 (Systat Software, San Jose, CA, USA). Values are presented as mean ± standard error of the mean (SEM).

Results

SVF formation of new vessels via neovascularization.

Visualization of microvascular growth dynamics using the rat mesentery culture model enables identification of SVF derived neovascularization. Lectin labeling of tissues after

DiI positive SVF transplantation and culture for 3 days revealed clusters of vessels with a central hub and radial outgrowth (**Fig A4.2 A-C**). This unique pattern was unlike the typical branching hierarchy of mesenteric vessels and resembled the aggregation and sprouting dynamics reported for SVF vessel formation *in vitro* [191]. Positive DiI labeling identified the central hub structure and the radial spoke structures indicating SVF origin (**Fig A4.2 B**). Lectin co-labeling of the radially patterned segments isolated from nearby host networks characterized by hierarchical branching suggests that the segments were SVF derived. PECAM and NG2 labeling of the apparent hub and spoke patterned structures confirmed that vessel segments contained endothelial cells and vascular pericytes (**Fig A4.2 D-F**). NG2 labeling revealed pericytes along vessels extending from the central hub aggregates and the branching vessels that connected the hubs (**Fig A4.2 E**). After 3 days of culture, the SVF treated tissues displayed a dramatic increase in percentage of vascularized area, indicative of new vessel formation (**Fig A4.2 G-I**). The vascular coverage increased nearly two-fold compared to serum stimulation alone ((88.5 ± 2.2% vs. 45.9 ± 6.9%, $p = 0.0004$) (**Fig A4.2 G-I**). Lectin labeling of the networks in the SVF transplanted tissues identified an intact network with no apparent distinction between the host and SVF derived vessels. The apparent increased vascularized areas were also covered with branching capillary networks. SVF neovascularization is further supported by comparing the locations of host vessels versus host and SVF vessels. Such a comparison was made possible by transplantation of wild type SVF on GFP tissues. After 3 days in culture, areas void of GFP positive vessel segments were observed between GFP positive host networks. This same region contained GFP negative, lectin positive vessels, indicating SVF neovascularization had

formed connections between the networks (**Fig A4.3**). SVF derived neovascularization is also supported by time-lapse imaging of SVF from transgenic GFP rats which was used to track vasculogenesis over time (**Fig A4.4**). SVF tracking revealed 3 phases involved in initial vessel formation: initial segment formation, segment network formation, and the connection of branched segment networks (**Fig A4.4**). Segments were defined by the apparent elongation of individual cells and segment networks were classified as networks made up of two or more connected segments.

SVF association with host vessels and effect on angiogenesis.

The visualization of microvascular growth dynamics using the rat mesentery culture model also enables SVF association with host vessels and SVF effects on angiogenesis. In support of the potential for SVF association along host vessels, examples of DiI positive SVF cells were observed along lectin vessels (**Fig A4.5 A-C**). DiI positive cells were also observed in the interstitial space not associated with vessels. These cells associated with vessels were only observed to be present along capillaries and not observed along larger diameter arterioles, larger diameter venules, or initial lymphatic vessels (data not shown). The different vessel types were identified based on previously described characteristic morphologies and position within a network consistent[18,21]. Finally, to determine the effect of SVF on host tissue angiogenesis, vascularized area measurements were compared for GFP host tissues with wild type SVF versus no SVF transplantation control groups (**Fig A4.5 D-G**). For this experiment, GFP only identified the native, host derived networks and comparison of Day 0 versus Day 3 vascularized area per tissue allowed for the quantification of network expansion due to angiogenesis.

Day 3 tissues treated with SVF displayed a significant increase in vascular coverage compared to tissues treated with serum alone (25.3 ± 4.2% vs. 13.0 ± 3.2%, $p = 0.0017$) indicating a proangiogenic effect (**Fig A4.5 H**).

Figure A4.1

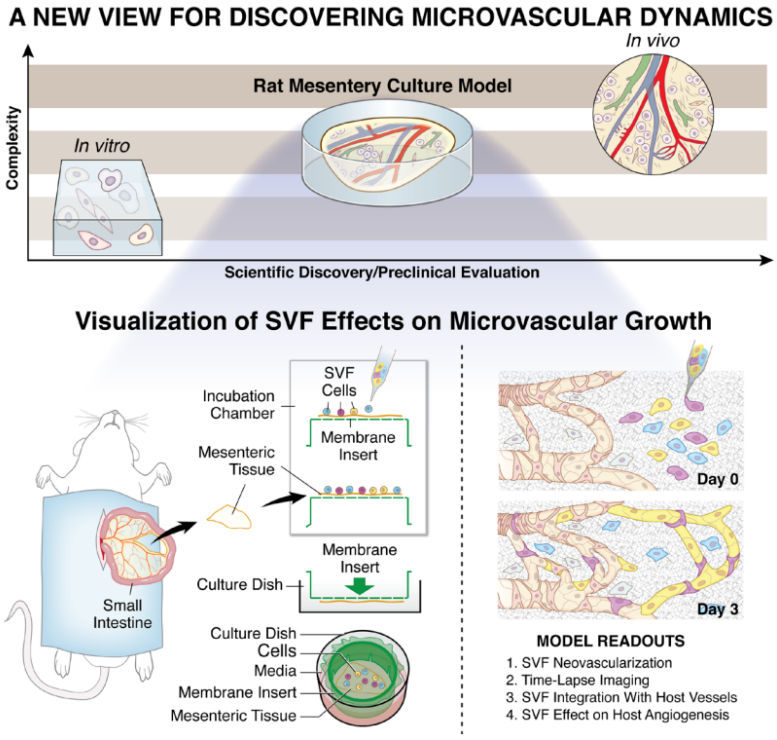

Figure A4.1: The rat mesentery culture model enables the visualization of SVF effects on microvascular growth.

A gap in complexity exists between common three-dimensional *in vitro* cell culture methods and *in vivo* systems. The rat mesentery culture model fills this gap by maintaining tissue complexity, while enabling observation over a short time course. For the visualization of SVF dynamics, SVF can be pipetted onto tissues prior to culture. Mesenteric tissues are surgically removed, rinsed in buffered saline, and placed in media. Post cell seeding, tissues are inverted into a culture well and covered with media. Readouts include SVF neovascularization, time-lapse imaging, SVF integration with host vessels, and effects on host network angiogenesis.

Figure A4.2

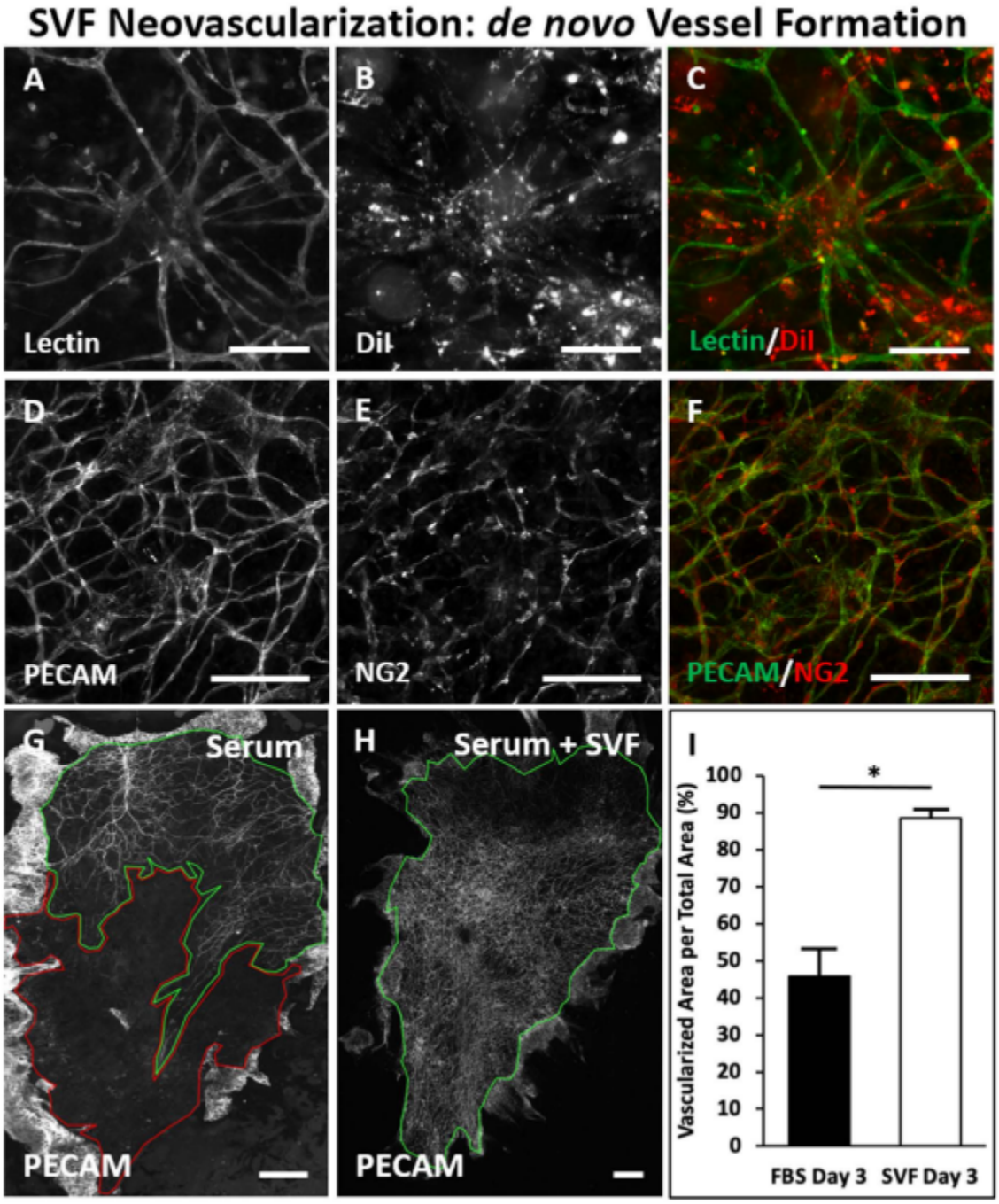

Figure A4.2: SVF formation of new vessels via neovascularization.

Example of cluster and outgrowth pattern of SVF derived cells after 3 days in culture. DiI labeled SVF cells identify lectin positive central hubs with spoked vascular branching (**A-**

C). PECAM and NG2 labeling of SVF formed vessels indicating the presence of endothelial cells and vascular pericytes (**D-F**). Images comparing the vascular area per tissue area for tissues cultured with serum and serum plus SVF. Green outline indicates vascularized area. Red outline indicates avascular area (**G-H**). Quantitative analysis of percent vascularized area was significantly higher in the SVF treated tissues compared to serum alone (n= 4 tissues from 2 rats per group) (**I**). * represents $p < 0.05$. Values are shown as mean ± SEM. Scale bars = 100 μm (**A-F**), 2 mm (**G-H**).

Figure A4.3

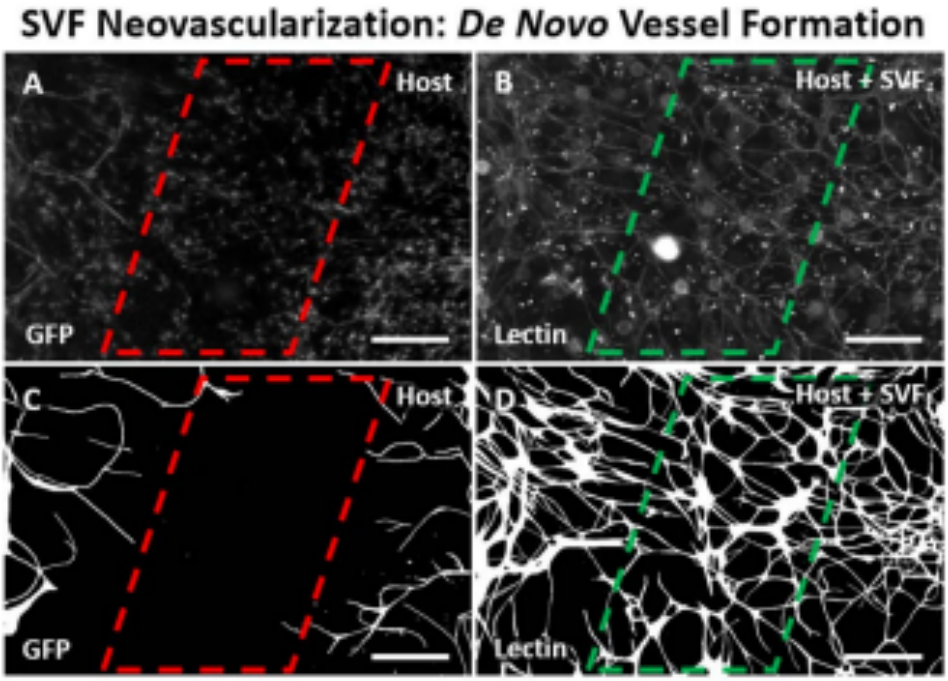

Figure A4.3: Observation of host microvasculature versus SVF derived vessels confirms neovascularization. Images of GFP positive host vessels and all vessels in the same tissue region after 3 days in culture. Tissues were harvested from GFP transgenic rats allowing for identification of host tissue vessel segments. Lectin labeling identifies all vessels including the host vessels and new SVF derived vessels. GFP negative, lectin positive segments indicate SVF origin (**A-B**). Corresponding processed images more clearly show connected vessel segments because lectin and GFP labeling also identifies non-vascular interstitial cells. Vessel segments were defined by continuous labeling and connection within a network. Observation of lectin positive segments spanning the gap between GFP positive vessel labeling supports the formation of SVF derived vessels (**C-D**). Scale bars = 100 μm.

Figure A4.4

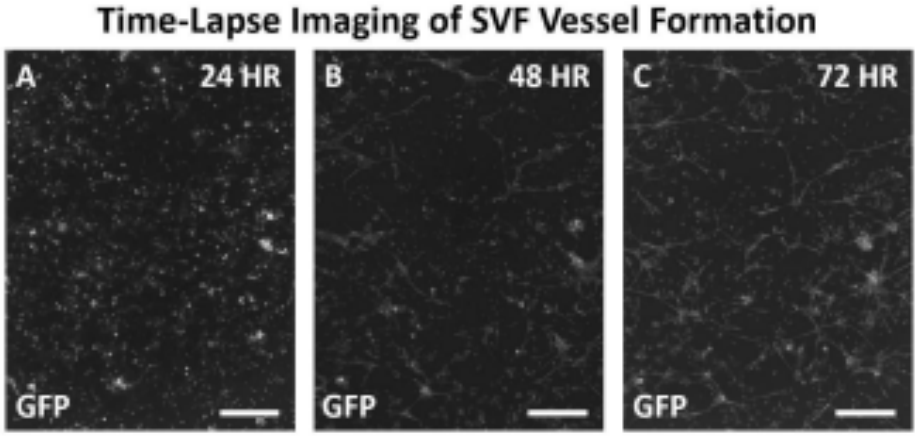

Figure A4.4: Time-lapse imaging of initial SVF vessel formation.

Example images of GFP positive SVF cells over the initial vessel development time course. GFP sourced SVF was seeded onto tissues at the start of the culture duration (**A-C**). At 24 hours the GFP cells appeared unassembled (**A**). By 48 hours GFP structures were observed in assembled segments (**B**). By 72 hours assembled segments formed connections. In some regions, a central hub with outward radial segment growth was identified (**C**). Scale bars = 250 μm.

Figure A4.5

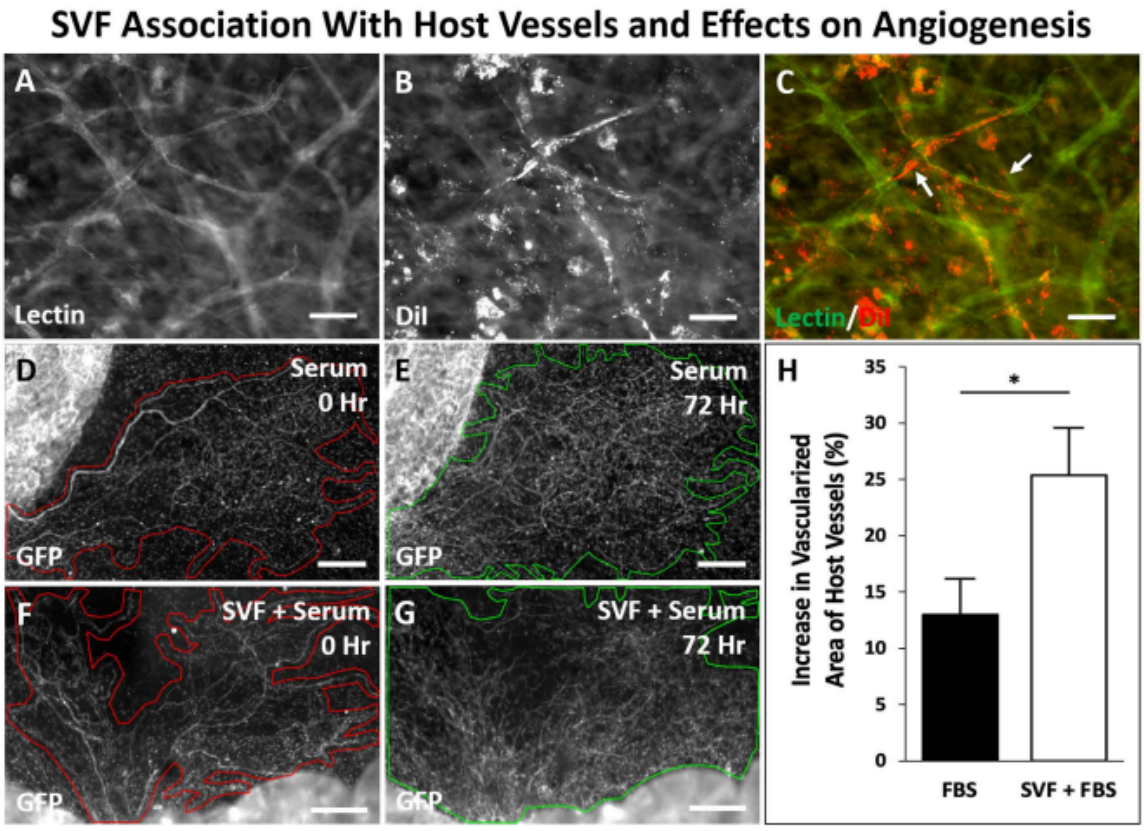

Figure A4.5: SVF can associate with host vessels and stimulate host network angiogenesis.

Example of DiI positive SVF derived cells along DiI negative, lectin positive vessel segments (A-C). Analysis of the effect of SVF on host network angiogenesis. DiI positive cells can also be observed not associated with vessels in the interstitial space. Representative network images of tissues harvested from GFP transgenic rats at 0 hours and 72 hours for 2 experimental groups: cultured with serum (FBS) and cultured with serum (FBS) + wild type SVF. Outlines identify circumscribed vascular areas per network (**D-H**). Quantification of the percent increase in the vascularized area of native GFP vessels after 3 days in culture with serum alone or serum plus SVF (n= 6 tissues

from 2 rats per group) (**H**). * represents $p < 0.05$; values are shown as mean ± SEM. Scale bar = 50 μm.

Figure A4.6

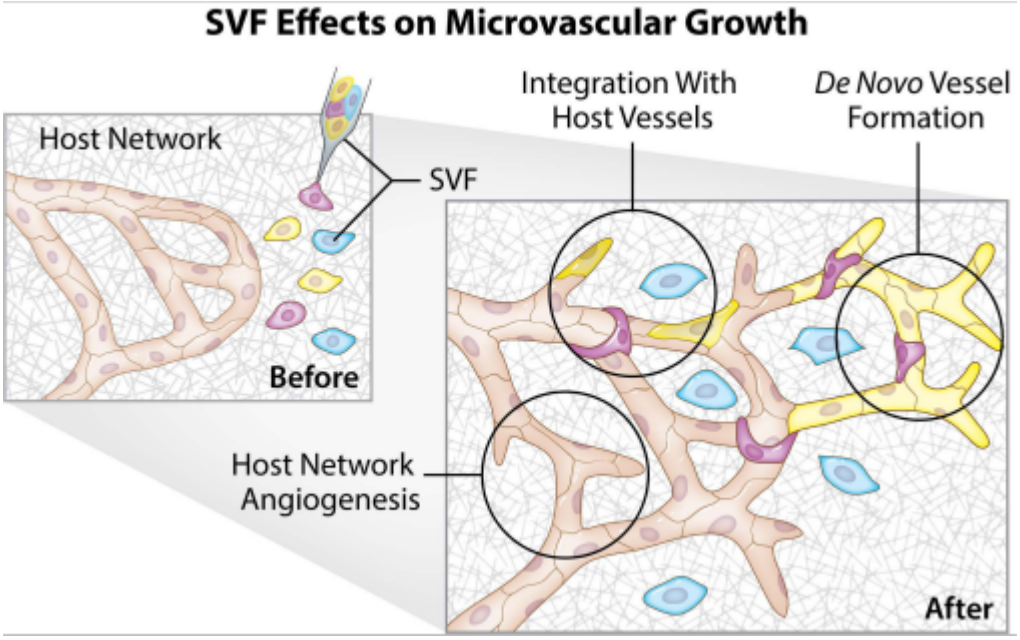

Figure A4.6: Summary schematic of observed SVF effects on microvascular network growth using the rat mesentery culture model.

On day 0, before SVF and host network remodeling, SVF cells were transplanted onto cultured tissues. The rat mesentery culture model enabled the viewing of SVF and host network cells over time. Characterization of cell, vessel, and network dynamics during culture supports that SVF can contribute to microvascular growth via 1) de novo vessel formation, 2) integration or association of individual cells along host vessels, and 3) stimulation of host network angiogenesis.

Discussion

SVF implantation *in vivo* has been shown to result in the formation of patent microvessels [41, 364, 421]. Yet current SVF therapies have not reached their full potential due to the lack of understanding concerning the processes related to how SVF contributes to the growth and remodeling of a vascular network. The infancy of SVF research and our lack of information surrounding the mechanisms of SVF function motivates the need to view the relative contributions of SVF effects on host network angiogenesis, host vessel integration, and neovessel formation. Discovery of SVF dynamics will guide new paradigms for research and therapeutic design.

Visualizing cell dynamics across temporal and spatial scales is a key challenge in advancing our understanding of the microvasculature. Imaging cellular *in vitro* systems does not accurately mimic the complexity of real vascular networks and imaging of *in vivo* systems is often limited to end time points. To this end, *in vitro* models are valuable for reductionist experiments investigating what players are important for vessel formation and *in vivo* models are essential for evaluating functional effects. For example, *in vitro* studies have shown the importance of the extracellular matrix environment; SVF cultured on collagen, gelatin, and laminin formed monolayers while SVF cultured on Matrigel formed microvascular networks [191]. As an *in vivo* example, a study by Koh et al. demonstrated that SVF injection can cause neovascularization via cell re-assembly and increase blood perfusion post hind limb ischemia [364]. Previous studies utilizing SVF therapy to improve tendon, cardiac, and nerve regeneration also emphasize the ability of SVF to form new vessels and integrate with nearby host vasculature [183, 422, 423].

Questions regarding how cell assembly dynamics and contributions of new vessel formation effect angiogenesis motivate the need to visualize SVF during these processes.

This study presents the rat mesentery culture model as a tool for visualizing SVF during microvascular growth in real, intact, multi-cellular microvascular networks over the time course of a few days. Advantages of the tissue culture model include the ability to view an entire microvascular network, the use of a standard epifluorescent microscope, the ease of adding SVF cells, and the use of multiple tissues per rat. As a thin (20 - 40 μm), translucent tissue, the mesentery provides an intact tissue ideal for observation at the whole tissue, network, and cellular levels. Observation of DiI and GFP labeled SVF identified segment formation and structures consisting of a central hub with segments projecting radially. These central aggregates of cells and their projections labeled positively for endothelial and pericyte markers. Important for the utility of the mesentery culture model, the process occurs over several days. SVF derived hubs interconnect with each other and establish branching capillary network. The characterization of the DiI and GFP derived segments as vessels is supported by cell 1) the formation of similar DiI positive SVF segments and structures in initially avascular areas, 2) the co-labeling of these structures for lectin and PECAM, and 3) similar evidence of SVF vessel segment formation dynamics observed in vitro [191].

Labeling of SVF versus the host microvasculature enabled the visualization of SVF neovasculogenesis. This is important because chronic *in vivo* cell therapy studies involving transplantation or injection of mesenchymal stem cells or circulating stem cell types have suggested cells incorporate into the existing vasculature at rates of ~ 0% – 10%, but do not assemble to form new vessels [188, 314, 315, 361].

In comparison, our results show that SVF derived vessels can cause a dramatic increase in vascular area in a tissue via cell assembly. We speculate that since SVF contains various stem cell populations, the dramatic differences in effects on microvascular growth might be attributed to SVF's mixture of multiple cell types. These differences motivate future studies to 1) compare the advantages between specific stem cell therapy approaches and 2) elucidate the roles of specific sub-cell populations [320].

Our results also support the ability of SVF cell to associate with host vessels, though future studies will be needed to quantify the percentage of integration per host vessel type and the percentages of integration of vascular pericytes or endothelial cells. Isolated GFP positive vessel segments derived from GFP SVF were observed interconnecting with lectin positive, GFP negative network regions (data not shown), suggesting that SVF cells can also integrate with host networks as pre-assembled endothelial segments. As support for integration as pericytes, examples of DiI positive SVF cells were observed wrapping and elongated along lectin positive vessels in characteristic pericyte locations. Interestingly, SVF cells were not observed on vessels with larger diameters (arterioles and venules) nor lymphatic vessels (data not shown). These findings were made possible by viewing the hierarchy of intact microvascular networks. Additional studies are needed to evaluate the percentages of integration and whether SVF preferably integrate as one cell type or another.

The SVF effects on microvascular growth observed in this study (**Fig A4.6**) further emphasize the need to also evaluate the relative contributions of neovascularization, vessel integration, or host network angiogenesis. Comparison of the quantification of SVF presence on vascularized tissue area (**Fig A4.2**) and host network

vascular area growth (**Fig A4.5**) suggests that neovascularization might be the most dramatic contributor to microvascular growth. However, questions regarding the relative dynamics remain. How does, for example, initial microvascular network size or the area of initial avascular regions influence SVF dynamics? Do SVF cells prefer to populate avascular regions? What are the paracrine mechanisms for interstitial residing SVF cells on host network angiogenesis? How far can SVF cells migrate? Our examples of visualizing SVF in the current study provide some information and highlight the utilization of the model for follow up studies focused on further characterization of cell dynamics.

The scope of this study focused on demonstrating the capability of the rat mesentery culture model for viewing the locations of SVF neovascularization, SVF time-lapse vessel segment assembly, and SVF effects on the host microvasculature. As SVF related areas of research are still in their early stages, these types of images are highly valuable. Novel findings reported herein show that SVF can assemble into new vessels that fill avascular tissue regions and connect to host networks. In vitro studies have suggested that SVF forms aggregates that develop into a central hub structure from which radial vessels sprouting occurs [191]. Our *ex vivo* results support these initial dynamics and subsequently show that these hubs can interconnect with other nearby hubs, form networks, and connect to the host microvasculature. Consequently, our view of SVFs effect on microvascular growth help link in vitro observations to an intact microvascular system. The results of the current study motivate follow-up evaluation of SVF derived vessel functionality, endothelial junctional structure, the size of SVF derived vessels, and additional microvascular remodeling metrics. Another advantage of the tissue culture

model is the presence of lymphatic vessels, immune cells, and nerves [294, 419, 424]. Additional follow up studies could also include investigation of SVF fate and functional relationships within these systems.

Use of the rat mesentery culture model allows for the incorporation of a variety of methods used to investigate the microvascular dynamics of SVF transplantation. Despite the unique view the mesentery culture model provides, there are still several challenges associated with the characterization of SVF dynamics. DiI labeling of cells is valuable for tracking the original transplanted cells but as a membrane marker, each new generation of cell has less vibrant labeling which makes long-term observation difficult. Other limitations are the lack of perfusion and the limited options for transgenic rats. In a recent study, we demonstrated the ability to perfuse the networks in culture, yet future studies are needed to incorporate perfusion with SVF transplantation. Model development can also include the culturing of SVF on mouse mesentery tissue. The mouse mesentery tissue is typically avascular, yet our laboratory has recently demonstrated a method to stimulate vascularization and the feasibility of culturing the tissues analogous to the rat mesentery culture model [425]. Finally, using cell specific lineage or knockout transgenic mice strains, studies could probe the roles of specific SVF cell populations. Future work can also adapt the model to investigate pathological conditions or the influence of aging. For example, whether in rat or mouse, tissues and/or SVF can be harvested from disease strains to evaluate cell versus host tissue effects. Regarding aging, a study by Aird et al. showed that SVF constructs from old donors had reduced perfused vascular networks compared to SVF taken from young donors following 4-week subdermal implantation [154]. Utilization of the multiple readouts made possible by the rat

mesentery culture model would allow for determination of what SVF effects might be compromised.

Perspective

SVF transplantation represents a promising microvascular growth platform and advancing our understanding of SVF effects requires the ability to visualize SVF integration during microvascular growth. The challenges associated with dynamically viewing multiple cell types across an intact network motivates the need for models that fill the gap created by *in vivo* and *in vitro* limitations. In this study, we demonstrate the ability to visualize SVF *de novo* vessel formation and integration with a host microvasculature via time-lapse observations of mesenteric tissues in an *ex vivo* setting.

CURRICULUM VITAE

Gabrielle (Rowe) Brown, MS.

Ph: (615) 478-8355
gnrowe01@louisville.edu

EDUCATION

2017-present Ph.D. in Physiology, University of Louisville, Louisville, KY (3.828 GPA)
2017-2019 M.S. in Physiology, University of Louisville, Louisville, KY (3.828 GPA)
2013-2016 B.A. in General Biology and Psychology (with honors), Carson-Newman University, Jefferson City, TN (3.56 GPA)

OTHER POSITIONS AND EMPLOYMENT

2019-present Tutor, University of Louisville School of Dentistry, Louisville, KY
2016-2017 Laboratory Technician, Absorption Systems LLC., Exton, PA
2015-2017 Tutor, Carson-Newman University Student Success, Jefferson City, TN
2014-2016 Librarian Assistant, Carson-Newman University Student Affairs, Jefferson City, TN
2013-2014 Chemistry Stockroom Technician, Carson-Newman University Chemistry Department, Jefferson City, TN

PROFESSIONAL MEMBERSHIP AND ACTIVITIES

Active
2019-present Microcirculatory Society
2017-present American Heart Association
2017-present American Physiological Society
Previous
2014-2016 Alpha Lambda Delta Honors Society
2015-2016 Psi Chi Honors Society
2019-2020 American Association for the Advancement of Science

Community Outreach
June 2016 American Physiological Society Invited Contributor to Physiology Blog, "The Fat Blocking Powers of Fiber" https://ispyphysiology.com/2018/06/06/the-fat-blocking-powers-of-fiber/
Aug 2013 Mossy Creek Restoration Project Participant, Carson-Newman University

HONORS AND AWARDS

2019 3rd Place Poster Presentation, Kentucky Chapter American Physiological Society, Northern Kentucky University

2013-2016 Dean's List Member (GPA 3.5+), Carson-Newman University

EDUCATIONAL ACTIVITIES

Teaching Activities

2022 University of Louisville PHZB 611 Advanced Human Cardiovascular Physiology Lecture, "*Stem Cells*", March 2022

2022 University of Louisville PHZB 611 Advanced Human Cardiovascular Physiology Lecture, "*The Microcirculation*", March 2022

2021 Certificate of Completion in the Graduate Teaching Academy, University of Louisville, KY

2021 University of Louisville PHZB 611 Advanced Human Cardiovascular Physiology Lecture, *"Myocardial Ischemia"*, Jan 2021

2019-present Tutor for BMSC 805, 4 students, University of Louisville School of Dentistry, Louisville, KY

2016-2017 Undergraduate Research Assistant for BIOL 207-208, BIOL 320, 10-30 students, Carson-Newman University, Jefferson City, TN

2016-2017 Undergraduate Teaching Assistant for BIOL 314, 402, 404, 407, 5-30 students, Carson-Newman University, Jefferson City, TN

Student Mentorship

May - Aug 2021: David S. Heng - Second Year University of Louisville School of Medicine Summer Research Scholar Program

LeBlanc Lab: Pallavi Katragadda (High School), Bailey Beery (University of Louisville) Samuel Oyeleve (University of Louisville), Michaela Dukes (University of Louisville), Rajeev Nair (University of Louisville), Virginia Steilberg (University of Louisville School of Medicine), Daniel Benson (University of Louisville J.B. Speed School of Bioengineering)

PRESENTATIONS

Invited Seminars/Presentations

1. University of Louisville Diabetes and Obesity Center Seminar Series, "*Elucidating the therapeutic mechanism of adipose derived cell therapy in improving age-related microvascular dysfunction."*, Feb 2022
2. University of Louisville Diabetes and Obesity Center Seminar Series, "*Elucidating the therapeutic mechanism of SVF in microvascular repair.*", May 2020
3. Carson-Newman University Department of Biology Seminar Series, "*Elucidating the mechanism of action for adipose-derived stromal vascular fraction medicated improvements in vascular function in an aged female."*, March 2020

Poster Abstracts

1. **Rowe G**, Heng D.S, Beare JE, Benson D, LeBlanc AJ. North American Vascular Biology Organization. Adipose-derived stromal vascular fractions rescue age-related impairment in angiogenesis within ex vivo mesenteric windows following injury. 2021

2. Heng D.S**, Rowe G**, LeBlanc AJ. Research!Louisville, Louisville, KY. Adipose-derived stromal vascular fractions rescue age-related impairment in angiogenesis within ex vivo mesenteric windows following injury. 2021
3. Tracy EP, **Rowe G**, Beare JE, LeBlanc AJ. Experimental Biology. Adipose stromal vascular fraction restores coronary microvascular flow-mediated dilation in aging female rats via enhanced peroxynitrite signaling. 2021
4. **Rowe G**, Beare JE, LeBlanc AJ. North American Vascular Biology Organization. Age-related impairment in angiogenesis within ex vivo mesenteric windows. 2020
5. Tracy EP, **Rowe G**, Toro LN, Beyer A, LeBlanc AJ. Experimental Biology. Telomerase reverse transcriptase mediates restoration of vasodilation in isolated coronary microvessels of aged female rats. 2020
6. **Rowe G**, Beare JE, Yuan FP, Tracy EP, Kem NQ, Steilberg V, LeBlanc AJ. Kentucky Chapter of the American Physiological Society, Kentucky State University, Frankfort, KY. Altered beta-1 adrenergic intracellular signaling in coronary arterioles following intravenous stromal vascular fraction therapy in aged female rats. 2020
7. Steilberg V, **Rowe G**, Yuan FP, Beare JE, LeBlanc AJ. Research!Louisville, Louisville, KY. Adipose derived stromal vascular fraction cells and vasodilation of aged coronary microvasculature. 2019
8. **Rowe G**, Beare JE, Yuan FP, Tracy EP, Kem NQ, Steilberg V, LeBlanc AJ. Research!Louisville, Louisville, KY. Altered beta-1 adrenergic receptor signaling in coronary arterioles following intravenous stromal vascular fraction therapy in aged female rats. 2019
9. **Rowe G,** Kelm NQ, Tracy EP, Beare JE, Yuan FP, and LeBlanc AJ. University of Louisville Cardiovascular Research Symposium, Louisville, KY. Stromal vascular fraction but not CD11b+ cells improve coronary microvascular dysfunction in aging. 2019
10. Kelm NQ, Beare JE, Yuan FP, **Rowe G**, and LeBlanc AJ. Experimental Biology, Orlando, FL. Novel role of Thbs-1/CD47-DRP-1 signaling following ischemia reperfusion in the aging heart. 2019
11. **Rowe G**, Kelm NQ, Yuan FP, Tracy EP, Beare JE, and LeBlanc AJ. Experimental Biology, Orlando, FL. Stromal vascular fraction but not CD11b+ cells improve coronary microvascular dysfunction in aging. 2019
12. **Rowe G**, Kelm NQ, Yuan FP, Tracy EP, Beare JE, and LeBlanc AJ. Kentucky Chapter of the American Physiological Society, Northern Kentucky University, Highland Heights, KY. Stromal vascular fraction but not CD11b+ cells improve coronary microvascular dysfunction in aging. 2019
13. **Rowe G**, Kelm NQ, Yuan FP, Beare JE, and LeBlanc AJ. Research!Louisville, Louisville, KY. Age-related changes in the microvascular vasoreactivity of the spinotrapezius. 2018

PUBLICATIONS

Articles Published in Peer Reviewed Journals (Original Research Articles):

1. **Rowe G**, Heng DS, Beare JE, Hodges NA, Tracy EP, Murfee WL, LeBlanc AJ. Reversal of aging-related impairment in revascularization following injury by

adipose-derived stromal vascular fraction is not wholly t-cell mediated, *Journal of Vascular Research*, 2022 March, *in peer review*

2. Hodges NA, Arinola LO, Hulan S, **Rowe G**, LeBlanc AJ, Kantz AJ, Murfee WL. Viewing stromal vascular fraction de novo vessel formation and integration with host microvasculature using the rat mesentery culture model. *Microcirculation*, 2022 April 12. PMID: 35466504
3. Tracy EP, Dukes M, **Rowe G**, Beare JE, LeBlanc AJ. Stromal vascular fraction restores vasodilatory function by reducing oxidative stress in aging-induced coronary microvascular disease, *Antioxid Redox Signal,* 2021 Dec, *in revision*
4. **Rowe G**, Tracy EP, Beare JE, LeBlanc AJ. Cell therapy rescues aging-induced beta-1 adrenergic receptor and GRK2 dysfunction in the coronary microcirculation. *Geroscience,* 2021 Oct 4. PMID: 34608562
5. **Rowe G**, Kelm NQ, Beare JE, Tracy EP, Yuan FP, and LeBlanc AJ. Enhanced beta-1 adrenergic receptor responsiveness in coronary arterioles following intravenous stromal vascular fraction therapy in aged rats. *Aging*, 2019 Jul 11. PMID: 32296794

Articles Published in Peer Reviewed Journals (Review Articles):

1. Tracy EP, Stielberg V, **Rowe G**, Benson D, Nunes SS, Hoying J, Murfee WL, LeBlanc AJ. State of the field: cellular and exosomal therapeutic approaches in microvascular regeneration. *Am J Physiol Heart and Circulation*, 2022 Feb 18, *online ahead of print.* PMID: 35179976
2. Tracy EP, Hughes W, Beare JE, **Rowe G**, Beyer A, LeBlanc AJ. Aging-Induced Impairment of Vascular Function: Mitochondrial Redox Contributions and Physiological/Clinical Implications. *Antioxid Redox Signal,* 2021 Sept 17. PMID: 34314229
3. Tracy EP*, **Rowe G***, LeBlanc AJ. Cardiac Tissue Remodeling in Healthy Aging: The Road to Pathology. *Am J Physiol Cell Physiol*, 2020 May 20. PMID 32432929
   * denotes equal authorship

SUMMARY OF TEACHING EXPERIENCES

Graduate Educational training, University of Louisville

I have actively pursued opportunities to learn new techniques in education and improve my teaching competency. Through the intense course education in the Graduate Teaching Academy, we learned how to align student assessments so the educators can accurately measure if learning has occurred, different types of assessments/rubrics, and how to ensure a positive classroom community with a focus on a safe learning environment and inclusivity. We also addressed the student writing crisis in higher education, how to maximize active learning, and how to translate learning theories into teaching strategies. To exercise the new education techniques I have learned I began guest lecturing for the Advanced Human Cardiovascular class and participating in research based presentations at the Diabetes and Obesity Center seminar series.

Undergraduate educational training with Drs. Stephen Wright, Matthew Wilkerson, and Patsy Boyce, Carson-Newman University

I was responsible for preparing lab materials and assisting students with lab protocols and equipment utilization for the general biology, cell biology, anatomy and physiology, mammalian, gross anatomy, kinesiology, and genetics class. Furthermore, I created lectures for graph design with statistical analysis, the cardiac cycle, and metabolism with nutrition. Lastly, I was responsible for preparing prosected areas on the anterior and posterior sides of the cadavers maintained at CNU and discussed aspects of anatomy with visiting A&P classes from high schools in the local area.

SUMMARY OF RSEARCH EXPERIENCES

Graduate research training with Dr. Amanda J. LeBlanc, University of Louisville, Department of Physiology

Our lab is focused on exploring the therapeutic potential of adipose-derived stomal vascular fraction (SVF) in the restoration of microvascular function in the aged female, which are a population understudied in the scientific community. First, I sought to ascertain the effects of SVF treatment on an aged coronary microvascular system in connection with beta-adrenergic-mediated dysfunction. The main findings from this initial study were that age reduces the beta-1-adrenergic vasodilatory potential of the coronary microvessels, and this dysfunction presents as impaired coronary flow reserve. We showed that a single treatment of SVF restores coronary flow and microvascular function back to levels seen in young animals (PMID: 32296794). I followed this study up by examining the contribution of intracellular signaling proteins and inhibitors involved in beta-1 adrenergic-mediated vasodilation. This recently published study found that SVF therapy can reverse the age-related decline of the beta-1 adrenergic receptor population in coronary microvessels and helps improve vasodilation through equilibrium of signal activators to signal inhibitors (PMID: 34608562). From these findings, I continued to explore the mechanism by which SVF improves vascular function in an aged model. I established and adapted an injury model of the mesenteric circulation in our laboratory to identify and track age-variable SVF. The major finding from this study are that SVF therapy improves an age-related impairment in revascularization following ischemic injury through homing and engraftment into the host microvasculature (manuscript in preparation).

Absorption systems LLC, Research Technician

My role at Absorption Systems was to establish a standard operating procedure for a colorimetric assay of enzyme kinetics for a membranous ATPase transporter (MRP2) and subsequent design of a commercial kit. For this, I maintained our lab's various cell cultures and successive vesicular membrane harvest for assay. MRP2 is in a class of membrane transporters responsible for the exclusion of drugs from mammalian cells and the development of drug resistance in some patients. Using a colorimetric change representing the amount of ATP used for transport, the kinetics of MRP2 could be examined on vesicles. The goal of marketing this assay was that inhibitors to MRP2, developed by independent labs, could be tested for deimmunization in transport speed, therefore making other drugs more effective. I was also successful in the procurement of two flow cytometers for the initialization of a core for use by faculty at Carson-Newman University and by other smaller universities in the east Tennessee area.

LABORATORY SKILLS

- Cadaver prosection and preservation
- Rat general surgery and animal handling
- Pressure myography
- Microdissection of coronary and mesenteric microvessels
- Adipose-derived stromal vascular fraction isolation
- Spinotrapezius and mesenteric intravital prep
- Ultrasound for echocardiography
- Pressure volume loops
- Mesenteric window exteriorization and culture
- Cell culture and maintenance
- Immunofluorescence
- Western blotting
- RNA isolation
- Magnetic antibody cell sorting
- Enzyme-linked immunoassay
- Nikon Elements and Olympus imaging software
- Fiji/Image analysis
- Statistical analysis (Sigma Plot)
- Biorender figure design